# Synthesis and Characterisation of Silver(I)-Bioglues and Assessment of Biological Activity of $AgNO_3$ Against *Staphylococcus aureus*

**Alanna Pauline Majella Smith, B.Sc.**

NUI MAYNOOTH

Ollscoil na hÉireann Má Nuad

A Thesis Submitted to the National University of Ireland

for the Degree of Doctor of Philosophy

**August 2012**

**Research Supervisors**

Dr. Kevin Kavanagh

Department of Biology

Dr. Malachy McCann

Department of Chemistry

**Head of Department**

Prof. Kay Ohlendieck

Department of Biology

Dr. John Stephens

Department of Chemistry

# Table of Contents

## Appendix

## Declaration of Authorship

I hereby certify that this thesis has not been submitted before, in whole or in part, to this or any other university for any degree and is, except were stated, the original work of the author.

Signed: _____ Date: _____

Alanna Smith, B.Sc.

# Acknowledgements

Firstly I would like to take this opportunity to sincerely thank my supervisors, Dr. Kevin Kavanagh and Dr. Malachy McCann for their guidance, advice and support over the last number of years and without which, the completion of this thesis would not have been possible. I would like to thank Dr. James Kennedy at Athlone Institute of Technology for all his time and help with the tensile testing, Dr. Johnny Colleran for his assistance with the electrochemistry, Dr. Denise Rooney for her help with the UV-Vis analysis and Conor McCarthy for the SEM images.

I would like to express my sincere gratitude to Prof. Kay Ohlendieck and Prof. John Lowry for giving me the opportunity to pursue my Ph.D.. Also, I would like to thank PRTLI strand IV for funding my research and to Monaghan County Council for funding my final year at NUI Maynooth.

I would like to thank the technicians in both Biology and Chemistry for all their help and assistance, usually at short notice, when it was needed. Special thanks must be said to Noel for making my first tensile testing set-up and for his unending help when my laptop seemed to give up the will to live in the last stages of writing up!

I would like to thank the members of my Chemistry research group both past and present; Marcia, Theresa, Rob, Trish, Pauraic and Kaijie, and to the members of the Medical Mycology lab, both past and present, Judy, John, Justyna, Karen, Niamh, Nessa, Matt, Ahmed, and Niall. Also, to all the postgrads and postdocs in both Biology and Chemistry (there are too many of you to name!), thank you for all the laughs, random conversations over lunch/tea and for all the great nights out over the last 4 years.

Special mention to ‘the girls’; Carol, Niamh, Trish, Louise and Niamh O’Reilly for their friendship, support and encouragement, especially in the last year when I needed it most. To my friends that I made when I first came to Maynooth all those years ago; Aine, Cathriona, Laura and my friends from home; Aine, Denise, Emma, Lucy and Maryann for all the laughs and distractions from Maynooth and for

understanding that it wasn't always possible to meet up as often as I would have liked. Hopefully, now I'll have more free time to catch up with you all.

To Joe, thank you for your unending support. For always having such practical advice, for talking sense into me with every drama that came my way and making me realise it's never as bad as it seems. To the Lynch's and granny Dollard, for making me so welcome down through the years, thank you.

Lastly, I'd like to thank my family from the bottom of my heart for their constant love, support and encouragement throughout the years. To my cousin Amanda, who despite the distance always kept in touch. To my niece Jenna thank you for always making me smile. To my sisters Louisa, Grainne and Maria thank you for all the laughs, for keeping me sane and dragging me for nights out when I didn't want to and always being glad you did. Despite the bickering and constant winding each other up (only sisters know how to do it best!), you are my best friends and I wouldn't have gotten through this without you. Hopefully I'll get you all to Maynooth for a night out before I leave so you can finally see what you've been missing!

To my parents Martin and Pauline, thank you for all your love, support and your words of encouragement especially in the tougher days when I didn't think I'd get through it ("Don't get despondent dear" became my favourite phrase!). I wouldn't be where I am today without all your help and to you I dedicate this thesis.

*To my parents*

**Peer Reviewed Publications**

**Alanna Smith**, Raymond Rowan, Malachy McCann & Kevin Kavanagh. Exposure of *Staphylococcus aureus* to silver(I) induces a short term protective response. *Biometals* **2012**, *25*, 611.

**Alanna Smith**, Malachy McCann & Kevin Kavanagh, (2012). Proteomic analysis of released proteins from *Staphylococcus aureus* following silver(I) exposure. Submitted to *Burns*.

**Oral Presentations**

Impregnating Surgical Bioglue with Silver(I) ions to inhibit microbial growth. CASH Research Day, Institute of Technology Tallaght, June 2009.

Synthesis of Silver(I) Bioglue Complexes and Assessment of Anti-Microbial Activity. Departmental Seminar, N.U.I Maynooth, May 2009.

Assessment of Antimicrobial Efficacy of Novel Silver(I)-Containing Bioglues. Irish Metal Based Drugs Symposium (IMBD), Dublin Institute of Technology, November 2009.

An Analysis of the Response of *Staphylococcus aureus* to Ag(I). Departmental Seminar, N.U.I Maynooth, June 2010.

An Investigation of the Interaction of Silver(I) with *Staphylococcus aureus.* Society of General Microbiology (SGM), Institute of Technology Tallaght, September 2011.

**Poster Presentations**

Impregnating Surgical Bioglue with Silver(I) ions to inhibit microbial growth. CASH Research Day, Institute of Technology Tallaght, June 2009.

Impregnating Surgical Bioglue with Silver(I) ions to inhibit microbial growth. Chemistry Colloquium, Dublin Institute of Technology, June 2009.

An Analysis of the Response of *Staphylococcus aureus* to Ag(I). Society of General Microbiology (SGM), N.U.I Galway, April 2010.

A proteomic Analysis of the Response of *Staphylococcus aureus* to Silver(I). Society of General Microbiology (SGM), N.U.I Maynooth, September 2010.

An Analysis of the Proteomic Response of *Staphylococcus aureus* to Silver(I). International Conference on Antimicrobial Research, Valladolid, Spain, November 2010.

Synthesis and Characterisation of Silver(I)-Containing Bioglue and Biological Assessment of $AgNO_3$. Irish Metal Based Drugs Symposium (IMBD), N.U.I Maynooth, September 2011.

# Abstract

Bioglue samples prepared in the absence and in the presence of Ag(I) ions (using $AgNO_3$ and $[Ag_2(3,6,9\text{-tdda})].2H_2O$ ($tddaH_2$ = trioxaundecanedioic acid)) were thermally stable and had the ability to swell in the presence of water. Generally, for the Ag(I)-Bioglues, as the amount of added Ag(I) ions decreased the degree of swelling increased. The surface morphology of the Bioglue without Ag(I) ions was very porous in comparison to the smooth surface of the Ag(I)-Bioglues. In tests using wood and pig skin, the adhesive properties of the Bioglues decreased with increasing amounts of added Ag(I) ions. The elasticity of the Bioglue also reduced upon incorporation of Ag(I) ions. Leaching of bioactive Ag(I) ions from $AgNO_3$-Bioglue samples increased over time and equilibrium was reached after 55 h. Ag(I)-Bioglues were reduced to Ag(0) using sodium borohydride and sodium citrate, but there was no evidence of Ag(0) nanoparticle formation.

Bioglue formulated without Ag(I) ions is readily colonized by microbes. The Ag(I)-Bioglues inhibit the growth of the fungal pathogen, *Candida albicans*, and are even more potent against the bacterial species, *Pseudomonas aeruginosa*, *Escherichia coli*, *Staphylococcus aureus* and *Methicillin-Resistant Staphylococcus aureus*. *S. aureus* cells exposed to $AgNO_3$ show a short-term increase in the activity of antioxidant enzymes, such as superoxide dismutase, catalase and, to a lesser extent, glutathione reductase, but this activity decreases as the cells lose viability. $AgNO_3$ also induces an increase in the amount of amino acid leakage from *S. aureus* cells, suggesting that Ag(I) ions affect membrane permeability. Proteomic analysis revealed that *S. aureus* cells were experiencing stress as a result of exposure to $AgNO_3$, which causes an increase in the expression of virulent and essential metabolic proteins.

These Ag(I)-Bioglues have the potential to offer significant antimicrobial protection if used in surgical wound closure.

# Abbreviation list

| | |
|---|---|
| α | Alpha |
| β | Beta |
| ε | Strain |
| σ | Stress |
| ΔG | Gibb's free energy |
| µg | Micro gram |
| µl | Micro litre |
| 1-D | One dimensional |
| 2-D | Two dimensional |
| AAS | Atomic Absorption Spectrometry |
| ABC | ATP binding cassette |
| ADP | Adenosine diphosphate |
| AI | Autoinducer |
| APS | Ammonium Persulphate |
| ATCC | American Type Culture Collection |
| ATCUN | Amino terminal Cu and Ni binding |
| ATP | Adenosine triphosphate |
| BSA | Bovine serum albumin |
| CAMP | Cationic antimicrobial peptide |
| CAT | Catalase |
| cDNA | Complementary DNA |
| CHAPS | 3-[(3-cholamidopropyl)dimethylammonio]-1-propanesulfonate |
| Cna | Collagen-binding protein |
| CXCL | Chemokine |
| DEPC | Diethyl pyrocarbonate |

| | |
|---|---|
| d.i. | Direct inhibition |
| DMSO | Dimethyl sulfoxide |
| DNA | Deoxyribonucleic acid |
| DNase | Deoxyribonuclease |
| dNTP | Deoxyribonucleotide triphosphate |
| DSC | Differential Scanning Calorimetry |
| DTT | Dithiothreitol |
| E | Young's modulus or the modulus of elasticity |
| EDTA | Ethylenediaminetetraacetic acid disodium salt dehydrate |
| EDX | Energy dispersive X-ray spectroscopy |
| FAD | Flavin adenine dinucleotide |
| FAK | Focal adhesion kinase |
| FDA | Food and Drug Administration |
| FnBp | Fibronectin-binding protein |
| GDP | Guanine diphosphate |
| GI tract | Gastro-intestinal tract |
| GLA | Glutaraldehyde |
| GLR | Glutathione reductase |
| GRF | Gelatin-resorcinol-formaldehyde |
| GSSG | Glutathione |
| GTP | Guanine triphosphate |
| IAA | Iodoacetamide |
| IEF | Iso-Electric Focusing |
| IL-1 | Interleukin-1 |
| IPG | Immobilised pH gradient |
| IR | Infrared |

| | |
|---|---|
| kDa | Kilo Dalton |
| LCST | Lower critical solution temperature |
| LC/MS | Liquid chromatography mass spectrometry |
| LSV | Linear sweep voltammetry |
| MHC | Major histocompatibility complex |
| MIC | Minimum Inhibitory Concentration |
| MPa | Megapascals |
| mRNA | Messenger RNA |
| *M.R.S.A.* | *Methicillin-resistant Staphylococcus aureus* |
| MSCRAMM | Microbial surface components recognizing adhesive matrix molecule |
| Msr | Methionine sulfoxide reductase |
| N | Newton |
| NADPH | β-Nicotinamide adenine dinucleotide phosphate |
| NaOH | Sodium hydroxide |
| NF-κB | Nuclear transcription factor kappa |
| NMR | Nuclear magnetic resonance |
| NO | Nitric oxide |
| OD | Optical density |
| ON | Ophthalmia neonatorum |
| PAMP | Pathogen-associated molecular pattern |
| PBS | Phosphate buffered saline |
| PCR | Polymerase Chain Reaction |
| PEG | Poly(ethylene glycol) |
| pI | Isoelectric point |
| PIPES | 1,4-piperazinediethanesulfonic acid |
| PNIPAAm | Poly(*N*-isopropylacrylamide) |

| | |
|---|---|
| PRR | Pattern recognition receptors |
| PVA | Poly(vinyl alcohol) |
| PVL | Panton-Valentine leukocidin |
| QAC | Quaternary ammonium compound |
| RNA | Ribonucleic acid |
| ROS | Reactive oxygen species |
| RT | Room temperature |
| SCC*mec* | Staphylococcal cassette chromosome |
| SDS | Sodium dodecyl sulphate |
| SDS-PAGE | Sodium dodecyl sulfate polyacrylamide gel electrophoresis |
| SE | *Staphylococcus* enterotoxin |
| SEM | Scanning Electron Microscopy |
| SFP | Staphylococcal food poisoning |
| SOD | Superoxide dismutase |
| SSD | Silver sulphadiazine |
| SSI | Surgical site infections |
| SSS | Scalded skin syndrome |
| $T_c$ | Crystallisation temperature |
| tdda$H_2$ | Trioxaundecandioic Acid |
| TEMED | N,N,N´,N´-Tetramethylethylene diamine |
| TLCK | N-α-p-tosyl-L-lysine chloromethylketone hydrochloride |
| TLR | Toll-like receptor |
| $T_m$ | Melting temperature |
| TMS | Tetramethylsilane |
| TNF-α | Tumour necrosis factor alpha |
| TRAP | Target of RNAIII-activating protein |

| | |
|---|---|
| tRNA | Transfer RNA |
| TSS | Toxic shock syndrome |
| UCST | Upper critical solution temperature |
| YEPD | Yeast Extract Peptone Dextrose |
| ZOI | Zone of inhibition |

# Chapter 1

Introduction

# 1.0 Aims of the Project

The aims of this study were (i) to synthesise a surgical Bioglue incorporating antimicrobially active Ag(I) ions in order to prevent the occurrence of nosocomial infections during surgery, and (ii) to determine the possible mode(s) of action of Ag(I) ions against the bacterium, *Staphylococcus aureus*.

# 1.1 Introduction to Silver

## 1.1.1 Silver

The chemical symbol for silver, Ag, is derived from the Latin argentum, meaning shiny or glistening. Silver is found in the earth's crust with an abundance of 0.07 ppm.[1,2] It has 2 main isotopes,[1] $^{107}$Ag and $^{109}$Ag with a natural abundance of 51.82% and 48.18%, respectively.[2] Silver occurs as either an element in nature or in a combined state such as sulfidic ores, $Ag_2S$ (argentite),[3] as horn silver (chlorargyrite) AgCl, and AgBr (bromargyrite).[4] Silver is also produced as a by-product in the processing of ores, such as PbS (galena) and $CuFeS_2$ (copper pyrite). When lead and copper are extracted from these ores the silver collects in the crude lead or copper where it can then be isolated and purified using electrolysis.[4] Pure silver exists as a ductile and malleable metal (Fig. 1.1).

**Fig. 1.1:** Metallic silver.[5]

### 1.1.2 Coordination chemistry of silver

Silver has the electronic configuration, [Kr]4$d^{10}$5$s^1$. The energy difference between the filled *d* orbitals and the unfilled valence shell *s* orbital is relatively small and this allows for extensive hybridisation of the $d_z^2$ and *s* orbitals (Fig 1.2). Initially, the electron pair in the $d_z^2$ orbital occupies $\psi_1$, which gives a circular region of relatively high electron density from which the ligands are repelled.[6] The regions above and below this ring in which the electron density is relatively low, attracts ligands. By further mixing $\psi_2$ with the $p_z$ orbital, two hybrid orbitals suitable for forming a pair of linear covalent bonds can be formed.[6]

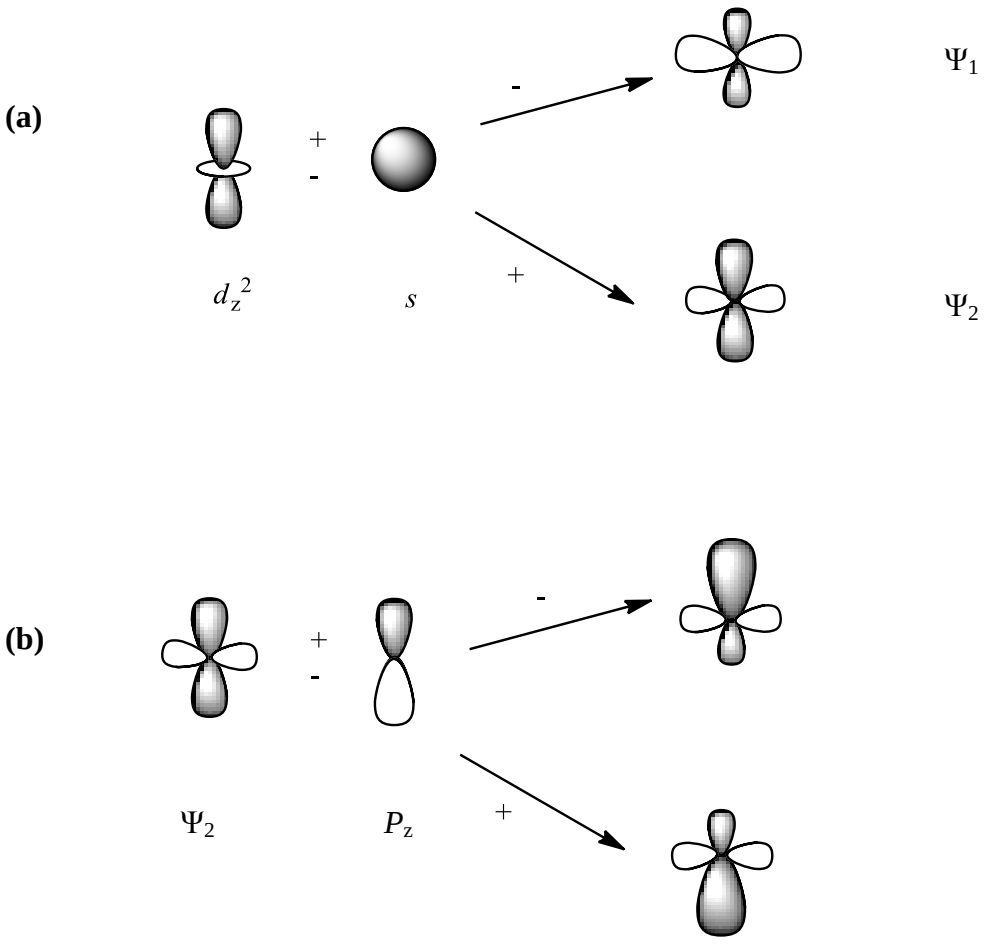


**Fig. 1.2:** The hybrid orbitals formed from (a) a $d_z^2$ and an *s* orbital ($\Psi_1$ and $\Psi_2$), and (b) the hybrids from a $\Psi_2$ and $p_z$ orbital.

Silver ions can exist in four oxidation states: Ag(I), Ag(II), Ag(III) and Ag(IV), with Ag(I) being the most dominant.[2] The most common coordination number for Ag(I) is two where the ligands are in a linear arrangement, e.g. $[Ag(NH_3)_2]^+$.[4]

An example of some of the other coordination geometries can be seen in the following complexes: $[(Me_2NC_6H_4PEt_2)_2AgI]$, where the metal has the coordination number three and is trigonal; $[Ag(SCN)_4]^{3-}$ is an example of a tetrahedral arrangement with a coordination number of four; $[Ag(L)]^{+2}$, where L is an $N_5$ macrocyclic ligand, is a five-coordinate complex in a pentagonal pyramidal arrangement; AgCl which is an example of an octahedral, six-coordinate complex.[6]

The Ag(II) ion is produced as an orange transient species, $[Ag(H_2O)_6]^{2+}$, through oxidation of silver(I) salts with ozone in strongly acidic solutions.[2] Silver(II) fluoride, $AgF_2$, is obtained as a dark-brown solid by fluorination of AgF or other silver compounds at elevated temperatures.[6] $AgF_2$ is antiferromagnetic, with a magnetic moment well below that expected for a species with one unpaired electron.[2] Silver(II) forms stable complexes with a variety of nitrogen donor ligands, such as pyridine, 2,2′-bipyridyl, and 1,10-phenanthroline (Fig. 1.3). These are some examples of complexing agents which all from planar arrangements with the four N atoms around the Ag(II) ion.[6]

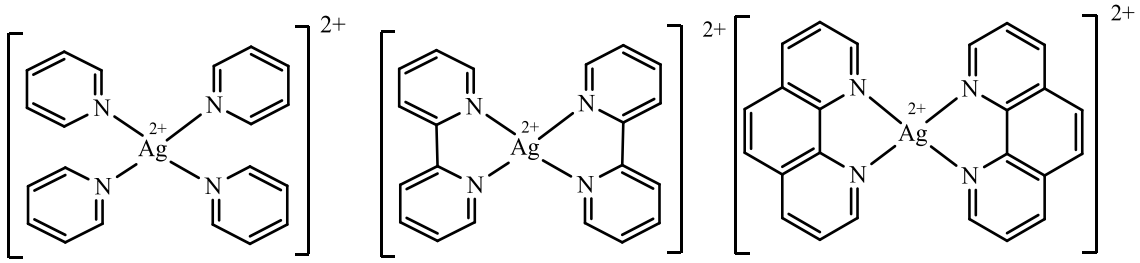


(a) (b) (c)

**Fig. 1.3:** Structures of silver(II) complexes containing (a) pyridine, (b) 2,2′-bipyridyl, and (c) 1,10-phenanthroline.

Silver(III) is produced by the anodic oxidation of neutral aqueous solutions of $AgClO_4$ or $AgBF_4$, producing black, metallic lustrous crystals of $Ag_2O_3$ which contains square-planar Ag(III) centres.[2] Silver monoxide, AgO, has been shown to contain both monovalent Ag(I) and trivalent Ag(III) in a linear and square-planar arrangement, respectively.[6] AgO can be obtained by the oxidation of $Ag_2O$ with $S_2O_8^{2-}$ in alkaline solution.[2] Fluorination of a mixture of CsCl and AgCl under pressure yields the complex salt, $Cs_2[Ag^{IV}F_6]$, containing tetravalent silver(IV).[2]

Due to its $d^{10}$ outer electronic configuration, silver metal is borderline between the main group metals and the transition metals. Silver metal, Ag(0), is relatively unreactive, but can be oxidised to the biologically active Ag(I) ion under certain conditions. The reduction potential for the $Ag^+/Ag^0$ complex is given below:

$$Ag^+ + e^- \longrightarrow Ag^0 \qquad E^0 = +0.7996\ V$$

The reduction potential can vary when the Ag(I) ions are complexed. Generally, complexation lowers the redox potential and therefore the reducibility of silver ions.[7] For example, when the Ag(I) ion is complexed to two ammonia ligands, reduction to Ag(0) becomes more difficult, and when it is ligated with cyano ligands, reduction becomes even less viable.

$$[Ag(NH_3)_2]^+ + e^- \longrightarrow Ag^0 + 2NH_3 \qquad E^0 = +0.37\ V$$

$$[Ag(CN)_2]^- + e^- \longrightarrow Ag^0 + 2CN^- \qquad E^0 = -0.31\ V$$

Ag(I) has four well characterised halides (Cl, Br, I) and all, except AgI, have a rock-salt structure.[3] The colour darkens from white to yellow and insolubility increases in the series Cl < Br < I.[6] The fluoride is unique in forming hydrates such as $AgF{\cdot}4H_2O$, and these can be prepared by dissolving AgO in hydrofluoric acid and evaporating the solution until the solid crystallises. The rest of the halides can be prepared directly by addition of $X^-$ to $Ag^+$ solutions, such as aqueous $AgNO_3$.[3] The most important property of the halides, in particular AgBr, is their sensitivity to light, which is the basis for their use in photography.

A photograph is a permanent record of an image formed on a light-sensitive surface which is coated with a silver halide dispersed in a gelatine support. The halide is

carefully precipitated to produce small uniform crystals or "grains".[3] When the light-sensitive layer is exposed to light, the silver bromide is photochemically decomposed, producing traces of colloidal Ag(0) metal.

The main principle behind this process is that when a suitably energetic photon strikes a halide ion in a grain of silver halide, an outer electron from the halide is excited into the conduction band, through which it passes and is then able to reduce a Ag(I) ion:[4]

$$X^- + h\nu \longrightarrow X + e^-$$

$$Ag^+ + e^- \longrightarrow Ag^0$$

The resulting Ag(0) atoms are distributed in the silver bromide layer and the free bromine is bound to the gelatin. The more intense the light exposure the greater the number of Ag(0) grains are formed.[4] The image is usually still invisible at this stage due to the relatively small amount of Ag(0) precipitated. This is called the latent image and it is then further developed using a reducing agent, such as hydroquinone, in the dark. The developer reduces the silver bromide to Ag(0).[4]

$$AgX \xrightarrow{H^+} Ag + HX$$

After this stage the image on the negative is fixed by dissolving away all the remaining AgBr to prevent its further reduction. This dissolution process requires the use of a complexing agent (ammonium or sodium thiosulphate being the most common) since the reaction goes to completion and both products are water-soluble.[3]

$$AgX_{(s)} + 2Na_2S_2O_3 \longrightarrow Na_3[Ag(S_2O_3)_2] + NaX$$

### 1.1.3 Silver nanotechnology

Nanotechnology is one of the most rapidly growing areas in science.[8] 'Nano' originates from the Greek meaning 'dwarf' and refers to the microscopic size that nanotechnology deals with.[9] Nanoparticulate structures usually range from 1-100 nm in size.[10] More than 800 products available on the market claim nanomaterial content and 30% of those are said to contain Ag(0) nanoparticles.[11] Such silver-containing

products range from clothing, cosmetics, electronics, water disinfectants and washing detergent (Fig. 1.4).


**(a)** **(b)** **(c)**

**Fig. 1.4:** Nano Ag(0)-based products: (a) antibacterial leggings, (b) hair shampoo and (c) washing detergent.

A broad range of synthetic methods for obtaining nanosilver(0) are available, with the most popular being the reduction of Ag(I) nitrate using sodium borohydride, citrate, glucose or ascorbate.[12] Other methods include photochemical reduction, laser ablation, vacuum ion sputtering and microwave radiation.[9] Metal(0) nanoparticles display unique optical properties, such as the presence of an absorption band in the visible region of the electromagnetic spectrum. The UV-Visible spectrum of Ag(0) nanoparticle suspension contained a band with $\lambda_{max}$ values in the range 400-500 nm.[13]

It has been suggested that the antimicrobial properties of Ag(0) nanoparticles are due to their ability to release Ag (I) ions as a result of particle oxidation.[8] Oxidation may occur upon contact with moisture in the skin or wound exudate, and as a result the nanoparticles become ionised.[14] Smaller Ag(0) particles have an overall greater surface area, and thus have a greater ability to release Ag(I) ions and cause a larger antimicrobial effect.[8] As in the case of the Ag(I) ion, the exact mechanism of how Ag(0) nanoparticles interact with microorganisms is not yet fully understood. Proposed mechanisms suggest that Ag(0) nanoparticles i) release Ag(I) ions which in turn generate reactive oxygen species (ROS), ii) cause direct damage to cell

membranes and affect their permeability, iii) uptake of free Ag(I) ions is followed by disruption of ATP production and DNA replication (Fig. 1.5).[12]

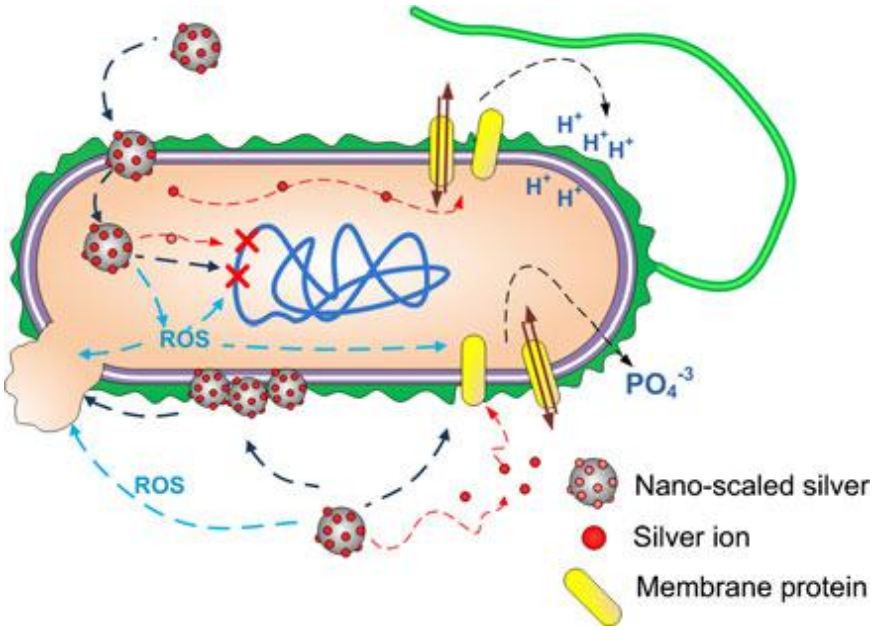


**Fig. 1.5:** Image depicting the proposed interaction of Ag(0) nanoparticles with bacteria.[12]

Due to the increased use of Ag(0) materials, concerns have been raised about the effect of increased exposure to humans and also aquatic environments.[12] Ag(0) nanoparticles may be released into the environment due to leaching from household products, washing of fabrics containing silver and washing detergents containing silver.[12] This, in turn, can possibly endanger surrounding lakes and streams by disrupting aquatic organisms.[11] Also, it has been suggested that frequent use of silver-based products may lead to increased cases of microbial resistance to the metal, equivalent to the emergence of antibiotic-resistant bacteria.[15] It remains unclear whether the toxic effects are due to the Ag(0) nanoparticles, Ag(I) ions or a combination of both. The use of Ag(0) nanoparticles in biomedical and household applications have allowed for the development of new antimicrobial agents.[14] However, further research is needed to understand its mode of action and also any toxic side-effects.

### 1.1.4 Biological activity of silver

Silver is not an essential trace element in the body and it fulfils no physiological or biochemical role in any tissue, even though it interacts with key elements, such as zinc and calcium.[16] The metal does not appear to be a cumulative poison.[16] Low concentrations (2.3 μg/L) of silver have been found in the bloodstream and also in tissues of the liver and kidneys, which are the main routes for silver excretion.[17] Ag(I) is readily absorbed into the body with food, drink and by inhalation.[16] Silver granules accumulate in the cytoplasm of phagocytic cells, hepatocytes and renal tubular epithelium bound in lysosomal vesicles, and are then released into bile ducts and urinary ducts for excretion.[18]

Metallic Ag(0) readily ionises in the presence of body fluids and wound exudates to produce the biologically active Ag(I) ion, which binds strongly to electron donor atoms of biological molecules containing sulphydryl groups and other anionic ligands derived from deprotonated amino acid residues in proteins, cell membranes and tissue debris.[19] The Ag(I) ion is highly active against a range of microorganisms through interactions with the cell wall, which result in conformational changes.[20] This allows the Ag(I) ion to penetrate cells causing cell leakage, denaturation and inactivation of proteins and essential enzymes, such as RNA- and DNA-ases, and ultimately leads to cell death.[21]

The action of Ag(I) ion on the cell wall has been studied using the fungus, *Candida albicans*, and it has been shown to bind to cysteine residues of the enzyme, phosphomannose isomerise (PIM), and causing its inhibition.[22] This enzyme plays an important role in cell wall biosynthesis[23] and inhibition can lead to leakage of important nutrients from the cytoplasm, such as phosphates and succinates.[18] The inhibitory action of the Ag(I) ion can be attributed to its strong binding affinity for thiol groups present in cell respiratory enzymes, its interaction with structural proteins and its binding with DNA bases which inhibits replication.[24]

### 1.1.5 Silver in healthcare

The antimicrobial properties of silver have been known for many centuries. Silver containers were used to transport water to prevent contamination as far back as Babylonian times,[1] and, more recently, Ag(I) ion was used aboard both the Russian MIR space station and on the NASA space shuttle to sterilise recycled drinking water.[15] Ag(I) compounds were also exploited for their antimicrobial properties to treat tetanus and rheumatism in the 19$^{th}$ century.[24] One of the first publications on the use of silver in medicine was in the 1880s by Carl S.F. Credé, who introduced a simple technique of cleaning the eyes of newborn infants with a 2% w/v aqueous solution of silver nitrate for the treatment of ophthalmia neonatorum (ON) (neonatal conjunctivitis).[25] This infection was mostly caused by the bacterium, *Neisseria gonorrhoeae,* which was transmitted from mother to infant during delivery. The $AgNO_3$ treatment reduced the number of cases of ON from 30-35 cases per year to only one by the end of 1880 in Credé's maternity hospital in Leipzig.[25] Credé's prophylaxis is still the "gold standard" in most parts of the world today, however, the concentration has been reduced to 1% w/v aqueous silver nitrate solution to lessen irritation.[25]

With the advent of the penicillin antibiotics, interest in the use of silver salts or silver salt solutions disappeared around the time of the Second World War.[26] A resurgence in the use of silver in the 1960s has been accredited to C.A Moyer, who popularised the use of silver with publications suggesting that 0.5% w/v silver nitrate solution should be used as an antiseptic agent to prevent invasive infection.[26,27] This was the lowest concentration which was effective against bacteria *in vitro* and *in vivo* on burns, without being toxic to growing epidermal cells,[26] and it was found to reduce mortality from 81% to 33%.[22]

Silver sulphadiazine (SSD) (Fig. 1.6) was introduced onto the market in 1968 by Charles Fox to treat burn wounds infected with the bacterium, *Pseudomonas aeruginosa*. It has also shown to be effective against other bacteria such as *Escherichia coli*, *Enterobacter cloacae*, *Proteus morganii*, *Staphylococcus aureus* and also *Staphylococcus epidermis*.[28] Silver sulphadiazine is formulated from silver nitrate and sodium sulphadiazine by substituting an Ag(I) ion for a $H^+$ ion in the

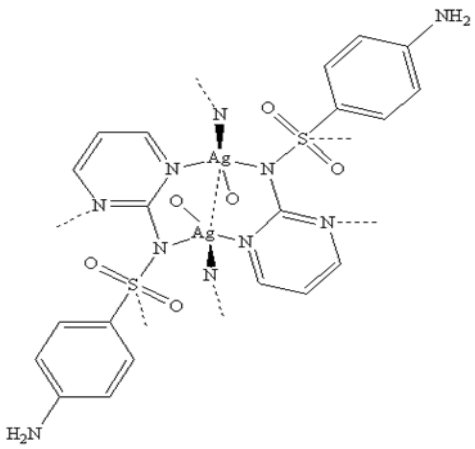

**Fig. 1.6:** Structure of silver sulphadiazine.

sulphadiazine molecule.[24] The resulting complex (SSD) is a white, fluffy solid that is essentially insoluble in water.[28] In formulating SSD, Fox combined the antimicrobial properties of the Ag(I) ion with the antibacterial properties of the sulphonamide moiety. SSD has become one of the most popular antibiotics for topical treatments (Fig 1.7) in burn clinics due to its efficacy in treating *P. aeruginosa* infections. SSD acts as a reservoir of available Ag(I) ions in the wound[29] and it is thought that its success is due to the slow, continuous release of Ag(I) ions in the presence of body secretions and burn wound exudates. A lot of the released Ag(I) ions bind to albumins and macroglobulins, leaving the remainder to provide the antimicrobial function.[28] It has been suggested that the primary biocidal action of SSD is provided by the Ag(I) ion, while the sulfadiazine serves to prevent the formation of light-sensitive colloidal Ag(0) which can cause discolouration of the skin.[30] SSD is marketed under the names Silvadene® and Flammazine®. Some of the advantages of silver sulphadiazine include, no discolouration of the skin (unlike silver nitrate), and a slower release of the Ag(I) ion to give a longer lasting therapeutic effect. A wider range of antimicrobial efficacy has been reported when the Ag(I) ion or sulphadiazine are used in combination, rather than by the additive effects of just Ag(I) or sulphadiazine alone.[28]

**Fig. 1.7:** Image depicting the application of a cream containing silver sulphadiazine (SSD).

Wound healing is a complex process, involving inflammation around the site of injury, angiogenesis, development of granulation tissue, repair of the connective tissue and epithelium and ultimately leading to a healed wound.[24] Once a wound becomes infected this healing process is delayed. If a wound becomes infected with an antibiotic-resistant microorganism, this can further increase mortality in the patient and also increase the cost of the treatment.[31] To overcome this, there are a wide variety of silver-based products, such as plasters and dressings, on the market (Fig. 1.8) for wound care and the treatment of burns. These dressings are designed to allow for the controlled release of Ag(I) ions into the wound, allowing the dressing to be changed less frequently, a procedure which can sometimes be painful to the patient.[27] The dressings vary in their total Ag(I) ion content, technology and application, but they all work on the basis that the wound fluids and exudates trigger the release of the biologically active Ag(I) ion for bactericidal or fungicidal action, and with the ideal that metal ion release will continue for the life-span of the dressing.[18]

In recent years, there has been a large increase in the number of silver-based products on the market, ranging from medical devices to household items. Examples include in-dwelling catheters, cardiac valves and prostheses, orthopaedic pins, dental devices, socks, toothbrushes, pyjamas, paints and washing machines (Fig. 1.9). Whether they are for hospital or domestic use, all of these products have the overall objective of preventing infection.


**(a)** **(b)** **(c)**

**Fig. 1.8:** (a) Contreet Biatain silver adhesive foam dressing (b) Elastoplast plaster containing silver and (c) a range of silver-based products from Silverlon.


**(a)** **(b)** **(c)**

**Fig. 1.9:** (a) Toothbrush incorporating silver (b) Marks and Spencer range of pyjamas incorporating a fine thread of silver metal into the fabric and (c) Johnstone's antibacterial paint formulated using silver ion technology.

### 1.1.6 Argyria

Argyria is one of the most widely publicised conditions associated with chronic silver exposure. The condition is usually associated with prolonged exposure to silver (especially colloidal silver, which usually contains metallic silver particles suspended in a solution with <10% ionised silver)[32] either occupationally or therapeutically, which leads to an accumulation of silver in the blood and soft tissues.[16] Light acts as a catalyst for the photo-reduction of Ag(I) to metallic Ag(0) which is then oxidised in the body to form silver selenide and silver sulphide, which are in turn, deposited in the connective tissues of the dermis and resulting in a permanent blue-grey colouration of the skin, buccal membranes, hair and nail bed (Fig. 1.10). In addition to these silver deposits, pigmentation can also result from silver stimulation of melanocytes, which increases melanin production.[33] Discolouration is more prominent in sun exposed areas due to the photo-reduction of the Ag(I) ion. Although cosmetically undesirable, argyria is not known to be life-threatening.[19,34,35] Fatalities in patients with argyria have been attributed to pre-existing medical conditions.[19]

**Fig. 1.10:** Rosemary Jacobs developed argyria due to the prolonged intake of colloidal silver.[36]

### 1.1.7 Silver resistance

Resistance has been defined as the ability of an organism to survive and/or multiply under conditions that would destroy or inhibit the growth of other members of the strain, either on a temporary or a permanent basis.[37] The widespread use of antibiotics has led to the emergence of antibiotic-resistant and even multi-drug resistant strains of microorganisms.[38] Bacterial silver resistance is frequently encoded by genes located on plasmids, the most studied of which was isolated from a *Salmonella* species.[30]

The first case of a silver-resistant bacterium was reported in the Massachusetts General Hospital in Boston, and it was isolated from burns patients who were treated with a 0.5% w/v silver nitrate solution.[39] Persistent strains of *S. typhimurium* were identified and plasmid pMG101 was established as the molecular basis of silver resistance.[40,41] The plasmid was 180 kb in size and belonged to the IncH1 incompatibility group plasmids[42] which are large, multiple antibiotic-resistant plasmids.[30,43] The region of the plasmid which induced silver resistance also conferred resistance to mercury, tellurite, ampicillin, chloroamphenicol, tetracycline, sulphonamide and streptomycin.[40,43] This region of pMG101 which was responsible for resistance was subsequently cloned and sequenced. The gene cluster for silver resistance contains 9 genes, 7 of which are named (*silP*, *silA*, *silB*, *silC*, *silS*, *silR*, *silE*) and 2 are referred to as open reading frames (*orf105*, *orf96*) (Fig. 1.11a).[15] Functions for the named genes were determined on the basis of homologies to known genes for other metal resistances, and the two unnamed ORFs lack any homology (Fig. 1.11b).[43]

With respect to Fig. 1.11a, beginning from the right is *silE* (Fig. 1.11 a), which encodes for a small periplasmic Ag(I)-binding protein and is 47% homologous to PcoE, which is involved in the *E. coli* copper-resistance system.[44] SilE (Fig. 1.11 b) binds Ag(I) ions at the cell surface, thus protecting the cell from toxicity.[45] SilE lacks cysteine residues, which are the primary metal cation ligands used in metal-binding proteins but it does have ten histidine residues which are used for metal-binding.[46] Upstream of *silE* is a presumed two component signal transduction pair, which is made up of *silS*, a membrane kinase sensor and s*ilR*, a transcriptional regulator[15] and are thought to be involved in controlling mRNA transcription in silver resistance.[45]

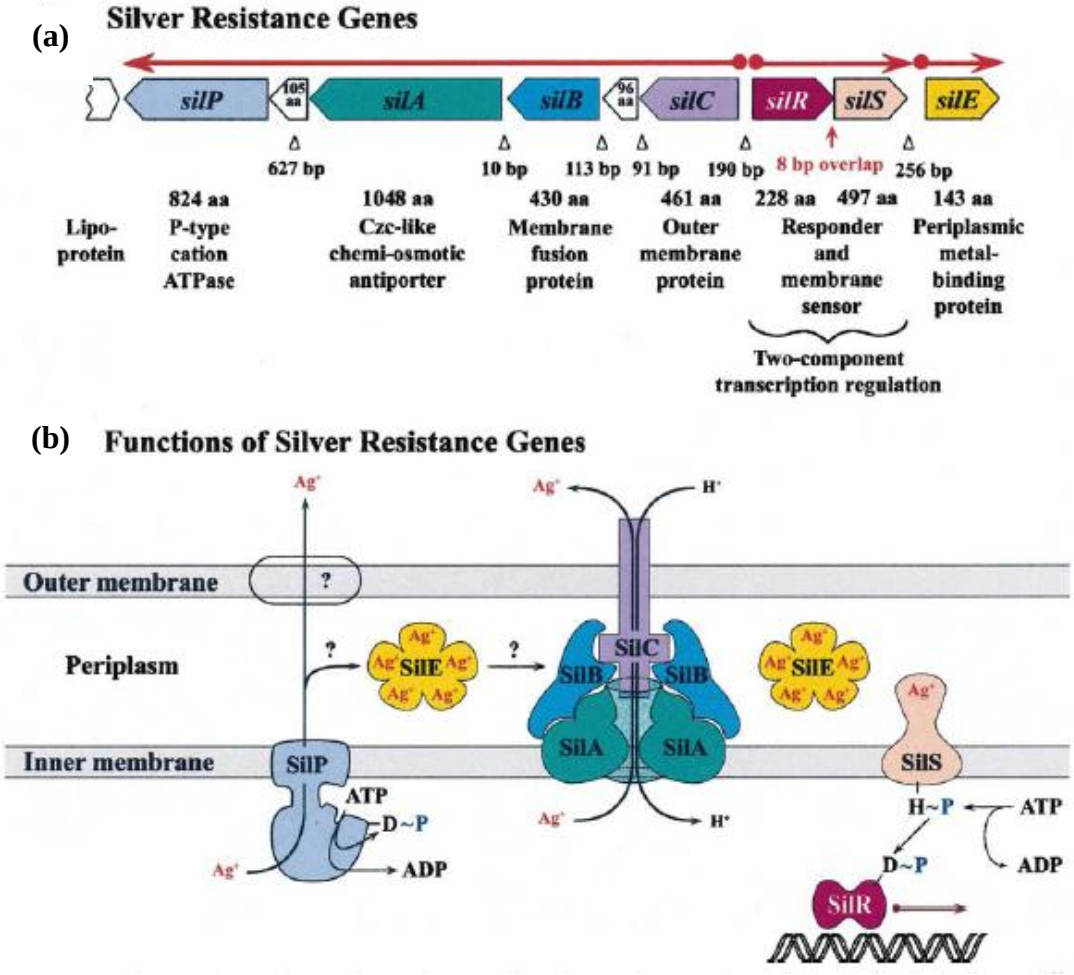


**Fig. 1.11:** (a) Silver resistant genes and (b) their proposed function.[15]

The copper resistance Pco system also includes genes for a two-component regulator, *pcoRS*, which is also upstream from *pcoE*.[15] The next four genes, *silCBAP*, are transcribed in the opposite direction. The *silCBA* genes determine a SilCBA complex which functions as a cation/proton antitransporter. The components of this proposed efflux system are silA, a large 1048-amino acid inner membrane proton/cation antiporter which exports Ag(I) ions from the cytoplasm, the cytoplasmic membrane or the periplasm across the outer membrane directly to the outside,[47] in this case the membrane protein, SilC. [15] The third protein, SilB, is a membrane fusion protein which attaches into the inner membrane and connects the outer membrane protein, SilC.[46] Finally, the *silP* gene is a 824 amino acid P-type ATPase which is thought to pump Ag(I) ions from the cell cytoplasm to the

periplasmic space.[15,48] The exact mechanism of how this occurs is not fully understood but it has been suggested[15] that the Ag(I) ion is sequestered by SilE, possibly followed by movement across the outer membrane by the SilABC complex.

The widespread use of silver-containing products could lead to an increase in the emergence of resistant organisms, which would be unfavourable considering its prominent use for clinical and hygiene purposes. With the identification of the silver-resistant determinant from *S. typhimurium*, this should make the identification of new resistant strains from other pathogens a much quicker process.

## 1.2 Hydrogels

### 1.2.1 General properties of hydrogels

Hydrogels are three-dimensional, hydrophilic, polymeric networks which are capable of absorbing large amounts of water or biological fluids,[49] making them an ideal candidate for biomedical applications.[50] Hydrogels can be used as contact lenses, membranes, biosensors, material for artificial skin[49] and also as barrier materials to regulate biological adhesions.[50]

'Reversible' or 'physical' hydrogels refer to polymer networks which are held together by molecular entanglements and secondary forces such as ionic, hydrogen-bonding or hydrophobic interactions. Due to the occurrence of either molecular entanglement clusters, or hydrophobically- or ionically-associated domains, physical hydrogels are not homogeneous.[51] Covalently-crosslinked networks give rise to 'permanent' or 'chemical' hydrogels.[51] As in the case of physical hydrogels, chemical hydrogels are also not homogeneous as they contain areas of low water swelling and high crosslink density.[51]

Hydrogels can be either natural or synthetic polymers.[50] Natural polymers have many advantages such as bioactivity, ability to present receptor-binding ligands to cells and some of these are susceptible to cell-triggered proteolytic degradation.[52] Examples of natural polymers include alginic acid (Fig. 1.12) and chitosan (Fig. 1.13). Alginic acid is found in the cell walls and intracellular spaces of brown algae

and is a copolymer of (1-4) glycosidically-linked monomers of D-mannuronic acid and L-guluronic acid.[53] Alginate polymers have been utilised in cartilage tissue engineering, surgical dressings[53] and cell encapsulation matrix.[54] Chitosan is derived from chitin, which is found in the exoskeleton of arthropods and is a linear polysaccharide made up of *N*-acetyl-D-glucosamine (acetylated subunit) and β-1,4-linked D-glusosamine (deacetylated unit).[53] Chitosan has found medical applications as a scaffold in tissue engineering,[54] as a topical ocular application, and in implantation and injection.[55]

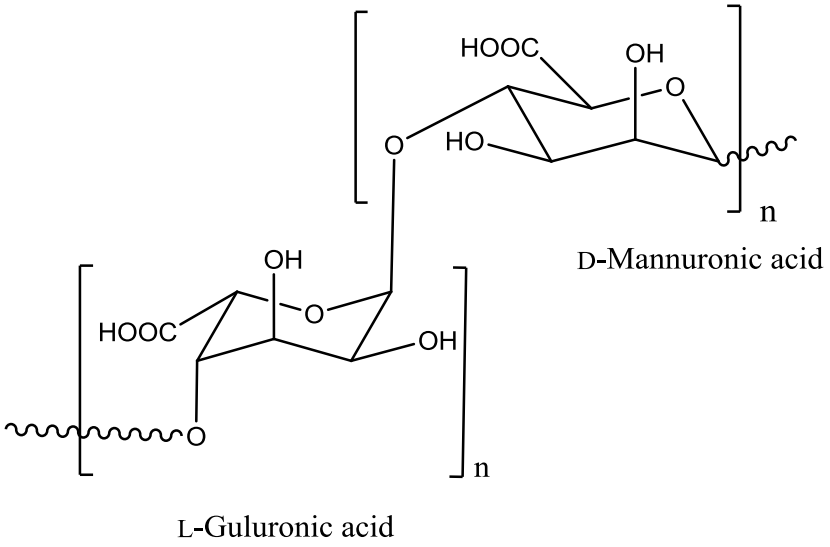


**Fig. 1.12:** Structure of alginic acid.

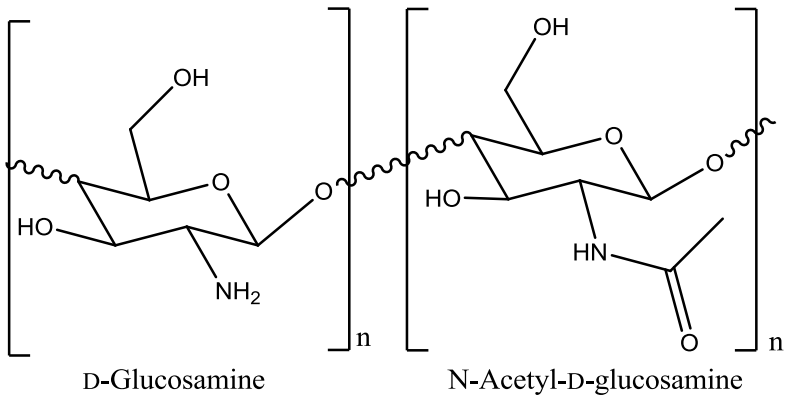


**Fig. 1.13:** Structure of chitosan.

Synthetic hydrogel polymers, in general, have more predictable properties and batch-to-batch uniformity. Some examples of synthetic polymers include poly(vinyl alcohol) (PVA) and poly(ethylene glycol) (PEG) (Fig. 1.14). Both of these synthetic polymers have found applications in tissue engineering, with PVA being used for avascular tissue, and PEG has been used as a surface coating for biomaterials.[53]

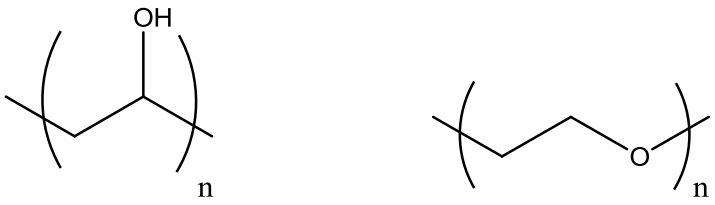


**(a)** (b)

**Fig. 1.14:** Structures of (a) poly(vinyl alcohol) and (b) poly(ethylene glycol).

### 1.2.2 Swelling in hydrogels

The hydrophilicity of hydrogels is due to the presence of hydroxyl, carboxyl and amine groups along the polymer backbone and side chains.[50] The maximum amount of water a hydrogel can absorb is known as the equilibrium swelling capacity and depends on factors such as hydrogel structure, cross-link density, ionic content and hydrophilic content.[56] Highly crosslinked hydrogels have a more tightly bound structure and therefore will swell less compared to the same hydrogel with a lower crosslinking density.[49] Also, hydrogels which have hydrophilic groups will swell more than those containing hydrophobic groups. Hydrophobic groups collapse in the presence of water and so reduce their exposure to the water molecules.[49]

Based on the nature of their side groups, hydrogels can be classified as either ionic or non-ionic.[50] The driving force for swelling in non-ionic hydrogels can be analysed using the Flory-Rehner theory. The combination of thermodynamic and elasticity theories states that a crosslinked hydrogel placed in a fluid and allowed to equilibrate with its surroundings is subject to two opposing forces: the thermodynamic force of mixing and the retractive force of the polymer chains.[50] At equilibrium, these two

forces are equal and the physical situation can be described in terms of the Gibbs free energy:

$$\Delta G_{total} = \Delta G_{elastic} + \Delta G_{mixing}$$

where $\Delta G_{elastic}$ is the contribution due to the elastic retractive forces developed inside the gel, and $\Delta G_{mixing}$ is due to the spontaneous mixing of the fluid molecules with the polymer chains and is a measure of the compatibility of the gel with the surrounding fluid.[49] The presence of ionic moieties can make the theoretical treatment of swelling much more complex. Along with $\Delta G_{elastic}$ and $\Delta G_{mixing}$, the ionic nature of the network also contributes to the total change in the Gibbs free energy:[57]

$$\Delta G_{total} = \Delta G_{elastic} + \Delta G_{mixing} + \Delta G_{ionic}$$

### 1.2.3 Stimuli-sensitive hydrogels

#### 1.2.3.1 pH-sensitive hydrogels

The mechanism of pH-sensitive swelling involves the protonation of amine groups as a result of decreasing the pH, which can lead to chain repulsion[55] and, as a result, the uptake of solvent is increased.[49] In neutral hydrogels, the degree of swelling only depends on the chemical composition of the hydrogel.[50] However, with ionic hydrogels swelling not only depends on the chemical composition but also on the pH of the surrounding fluid.[50] If the hydrogel is classified as being anionic, it will deprotonate and swell to a greater extent when the external pH is higher than the $pK_a$ of the ionisable groups bonded onto the polymer chains. Cationic hydrogels, on the other hand, protonate and swell when the external pH is lower than the $pK_b$ value of the ionisable groups.

#### 1.2.3.2 Temperature-sensitive hydrogels

Temperature-sensitive hydrogels have received much attention due to their ability to swell or de-swell as a result of a change in temperature of the surrounding fluid. Such hydrogels can be classified as either positive or negative temperature systems.[49] Negatively-thermosensitive hydrogels exhibit lower critical solution temperature

(LCST) behavior.[50] They tend to shrink or collapse when the temperature is increased above the LCST and swell when the temperature drops below the LCST.[50] Positively-thermosensitive hydrogels on the other hand have an upper critical solution temperature (UCST), and they swell at high temperature and shrink at lower temperatures.[50] These systems are mostly based on poly(*N*-isopropylacrylamide) (PNIPAAm) which has a LCST of 32 °C.[50] This hydrogel can exhibit a hydrophilic nature below the LCST and a hydrophobic nature above the LCST, and it has gained attention as a surface for cell culture systems,[49] drug delivery and also tissue engineering.[57]

## 1.3. Bioglue Formulation

### 1.3.1 General properties of adhesives

Skin is the first line of defence against microorganism invasion as it provides a protective barrier and has the ability to repair minor wounds with great efficacy. However, in circumstances when immediate cover of the wound is required to protect and accelerate wound healing,[54] the application of surgical adhesives provides a convenient method for wound closure.[58] Adhesives can be defined as glues which are able to bond tissues together, including a range of surfaces such as skin, muscle and blood vessels.[59] Surgical adhesives provide many advantages over sutures and staples as they do not require a local anaesthetic and are therefore less time consuming.[60] Adhesives are also less traumatic to the surrounding tissues, provide easy application, quality and strength of seal.[58] Adhesives must provide sufficient mechanical resistance,[61] allow satisfactory healing by holding joined tissues in close proximity and prevent the leakage of bodily fluids.[58] There is currently a wide variety of medical adhesives available commercially and these can be separated into three categories: fibrin, cyanoacrylate and albumin/gluteraldehyde sealants.[59] Each category of adhesive has advantages and disadvantages, and as a result will determine the procedure in which they will be used.

Fibrin glues are biological glues which are composed of concentrated fibrinogen and thrombin which mimic the final stages of the blood clotting cascade.[62] They can produce a fibrin clot which is biodegradable and can be resorbed within days to

weeks as part of the normal healing process.[63] An example of commercial fibrin glue is Tisseel (Fig. 1.15). However, these fibrin glues are known to have weak tensile and adhesive strengths[58] and so cannot be considered as a vascular adhesive.[64] If commercial human plasma is used instead of the patient's own plasma, this results in a multi-donor exposure for the patient[64] and, if not screened properly, may lead to exposure to hepatitis or HIV.[58]


**Fig. 1.15:** The commercial fibrin glue product, Tisseel.

Cyanoacrylates are synthetic adhesives which polymerise upon contact with water or blood.[63] Based on their chemical structure these glues can be further sub-divided into butyl or octyl cyanoacrylate.[59] 2-Octyl-cyanoacrylate is commercially available as Dermabond and is used for superficial wound closure (Fig. 1.16).[63] Cyanoacrylate glues have been shown to have good tensile strength,[64] however, one major issue with them is that their polymerisation is an exothermic reaction and this could lead to thermal injury in vascular applications.[64]

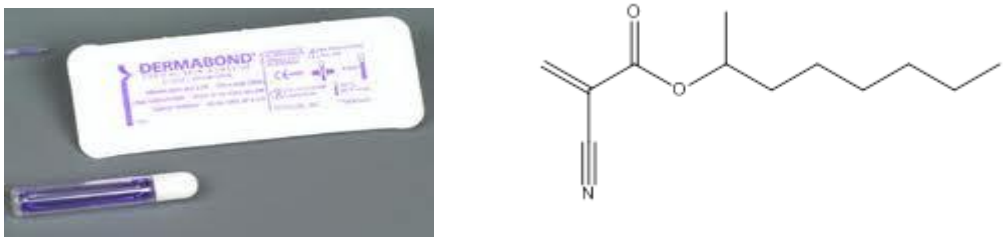


**(a)** **(b)**

**Fig. 1.16:** (a) Dermabond commercial product and (b) structure of the monomer used in making Dermabond.

Adhesives provide many advantages over sutures in that only a topical anaesthetic may be required, they are much faster to apply and they provide a water-resistant covering. Overall, adhesives provide a less traumatic experience for the patient. However, good wound management should not be overlooked for a quick repair as this may cause an increase in infection.[65] The use of adhesives should be continued to expand the knowledge of their biodegradation, safety and delivery and should be used in conjunction with techniques which are already well established.[66]

### 1.3.2 Properties of Bioglue

Bioglue is a surgical adhesive, constituted from the protein bovine serum albumin (BSA) (45% w/v) and glutaraldehyde (GLA) (10% w/v) mixed in a 4:1 ratio.[67] The glue provides a flexible, mechanical seal which is independent of the body's own clotting mechanism.[68] Bioglue has been found to provide good homeostasis, a decrease in blood loss and thus the number of transfusions,[67] and is an effective tissue strengthener and adherent.[69] Bioglue is applied using a sterile, reusable double-barrelled syringe delivery system (Fig. 1.17) in which the two components are kept separate prior to mixing. Mixing occurs in the attached single nozzle which can be replaced for subsequent applications.[69] Once the two components are mixed, polymerisation occurs within 20-30 secs, with the Bioglue reaching full bonding strength in 2 min.[70]

**Fig. 1.17:** Bioglue double-barrelled delivery system.[67]

### 1.3.3 General properties of a protein

Proteins account for 50% of the dry weight of cells and are involved in many processes such as structural support, storage, transport, signalling from one part of the organism to another, movement and defence.[71] Proteins are polymers of amino acids and are known as polypeptides. Amino acids contain a carboxylic acid and an amino functionality, the general structure of which is shown in Fig. 1.18 (R is the variable group). The sequence of amino acids determines the 3-D conformation, and this, in turn, establishes what function the protein will have. As a polypeptide chain is synthesised, the chain folds spontaneously to give the functional conformation of the protein. Proteins have four levels of structure, known as primary, secondary, tertiary and quaternary.

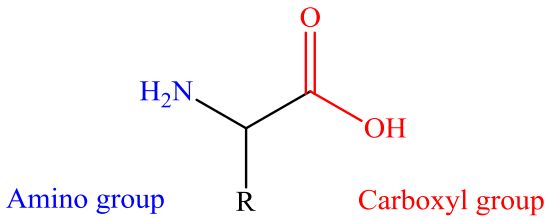


**Fig. 1.18:** General structure of amino acids.

#### 1.3.3.1 Primary structure

The primary structure is the unique sequence of amino acids which make up the protein and these amino acids are linked together by a peptide bond.

#### 1.3.3.2 Secondary structure

Most proteins have regions of coiled or folded patterns along the polypeptide chain which contributes to the overall conformation. These folds or coils are mainly due to hydrogen-bonding interactions at regular intervals along the polypeptide chain. Examples of this would include the alpha (α) helix (Fig. 1.19) and the beta (β) pleated sheet (Fig. 1.20). The α-helix is a delicate coil which occurs in such a way that the peptide bonds are able to form hydrogen bonds between each other.[72] The remaining components of the amino acids protrude from the helix at right angles,

which minimises steric interactions and has the overall effect of stabilising the structure.[72]

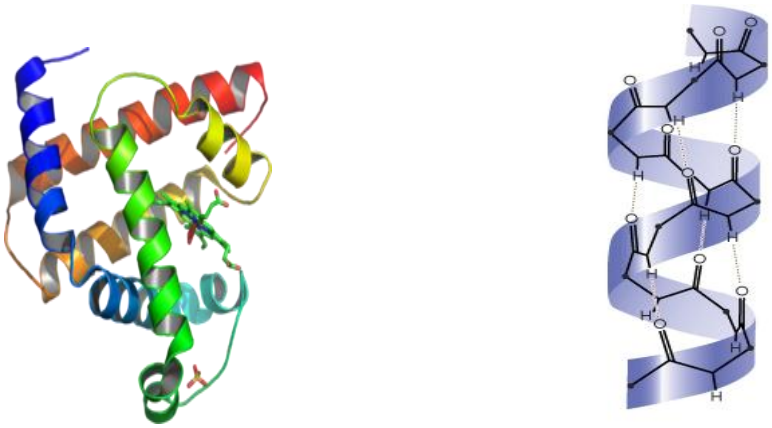

**(a)** **(b)**

**Fig. 1.19:** (a) Ribbon structure of an α-helix and (b) an α-helix illustrating hydrogen-bonding in a protein.[73]

The β-pleated sheet is due to a layering of protein chains above and below the plane, giving the appearance of pleats.[74] Hydrogen-bonding occurs between parts of the backbone in either a parallel or anti-parallel form, holding the structure together.[71]

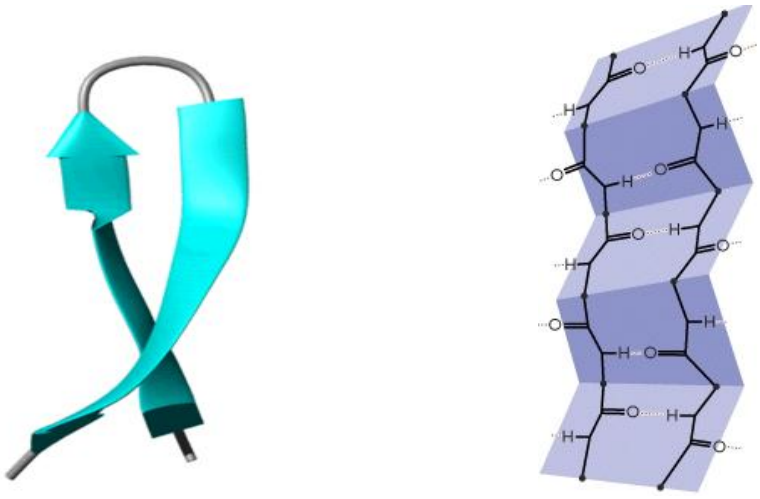

**(a)** **(b)**

**Fig. 1.20:** (a) Ribbon structure of a β-pleated sheet and (b) a β-pleated sheet illustrating hydrogen-bonding in a protein.[73]

### 1.3.3.3 Tertiary structure

The tertiary structure of a protein is due to contortions formed from bonding between side chains of the various amino acids and gives the overall 3-D structure of the protein (Fig. 1.21). As the residues interact, some will attract and others repel each other, which causes the protein to twist and turn until the most favourable conformation has been achieved. Many types of bonding contribute to the tertiary structure such as hydrophobic interactions, van der Waals forces, hydrogen-bonding and also disulfide bridges.

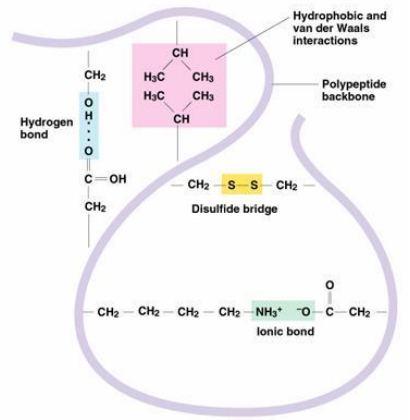


**Fig. 1.21:** Types of bonding which contribute to the tertiary structure.[71]

### 1.3.3.4 Quaternary structure

Quaternary structure arises when two or more polypeptide chains aggregate to form one functional macromolecule (Fig. 1.22). Ionic bonding plays an important role in quaternary structure as it involves interactions between the exterior surfaces of the protein.[72]

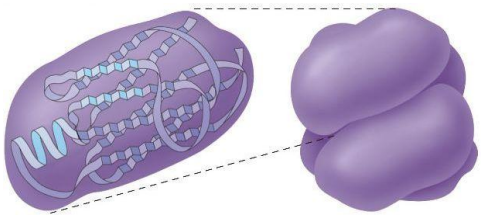

**(a)** **(b)**

**Fig. 1.22:** (a) Tertiary structure and (b) quaternary structure of proteins.

### 1.3.4 Bovine serum albumin

Bovine serum albumin (BSA), which is homologous to human serum albumin (HSA), is a single polypeptide chain consisting of 585 amino acids in length.[75] Serum albumin (66.5 kDa) is one of the most abundant proteins in plasma (Fig. 1.23).[76] It is a versatile carrier protein involved in the transport of hormones, vitamins, fatty acids, xenobiotics, drugs and metabolites.[77] Serum albumin accounts for 60% of the total protein in blood serum[78] and has a typical concentration of 0.63 mM.[79] There are three domains in the protein (I, II and III), and each of these is divided into two subdomains, A and B.[80] $^{1}$H NMR data have suggested that serum albumin is a heart-shaped molecule (Fig. 1.23), made up of mainly helical domains (67%)[76] and contains 17 disulphide bonds.[81] The disulphide bridges ensure some rigidity within each subdomain, but they allow modifications in the shape and size of the serum albumin in response to changes in pH and other influences.[82] Albumin contains one reduced cysteine residue (Cys$^{34}$) which, due to the large amount of albumin in plasma, accounts for the largest fraction of free thiols in circulation.[83] Serum albumin is responsible for maintaining blood pH and contributes 80% to the colloidal osmotic pressure.[84]

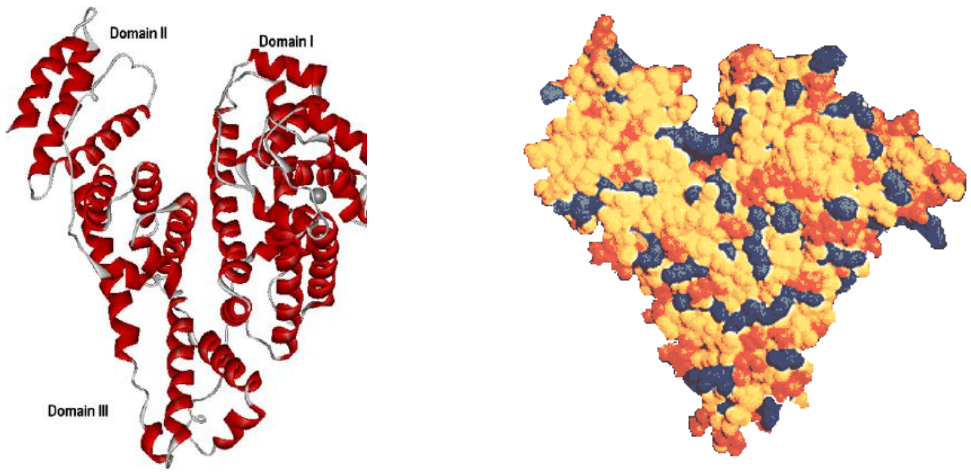


**(a)** **(b)**

**Fig. 1.23:** (a) Ribbon structure of albumin[75] and (b) space filled model of albumin.[84]

Many factors have been shown to affect the conformation of serum albumin such as heat, pH, organic solvents, detergents and pressure.[85] Heat denaturation has been found to cause a partial loss of alpha-helical structure and an increase in beta sheet formation when the protein is heated above 65-70 °C.[86] Serum albumin, when heated, goes through two structural stages. The first is reversible, whereas the second is irreversible.[86] In the reversible stage, some of the alpha-helices are transformed into random coils. The conformational change can be reversed by simply restoring the original conditions.[87] If the temperature is increased past the reversible stage, unfolding of the pocket around $Cys^{34}$ occurs, causing it to be exposed.[86] Intramolecular disulphide bonds, which play an important role in maintaining the native structure, are broken and this allows for the formation of intermolecular disulphide bonds.[88] As disulphide bonds are covalent bonds, this stage is irreversible.

Serum albumin can undergo reversible conformational isomerisation as a result of changes in pH. There have been five isomeric forms identified with increasing pH, from expanded (E), to fast (F), normal (N), basic (B) and aged (A) forms.[89] The N form is predominant in the pH range 3.5-7, the N-F transition occurs between pH 4.5 and 4.0, the F form is produced when the pH is lowered abruptly below pH 4.0 and the E form occurs when the pH is below 3.0.[90] During the N to F structural transition, a decrease is observed in the alpha-helical content from approximately 51% to 44%.[91] There are very little changes to the helical content during the F to E transition but an increase in intrinsic viscosity is observed.[74,91] At pH 9.0, serum albumin changes conformation to the B form. If this pH is maintained for three days at a low ionic strength at 3 °C, the A isomerisation occurs.[74]

One of the most outstanding properties of albumin is its ability to bind reversibly to a wide range of molecules such as bilirubin, hormones, drugs and ions.[85] Albumin represents the main antioxidant in plasma and functions either by binding and carrying radical scavengers, or by sequestering transition metal ions with pro-oxidant activity.[92] 25% of $Cys^{34}$ forms a disulphide bond with small sulphydryl compounds such as cysteine, homocysteine and glutathione.[83,93] Albumin is able to scavenge hydroxyl radicals through the reduced $Cys^{34}$ entity.[83] Oxidation of $Cys^{34}$ can lead to the formation of either the sulphinic ($RSO_2H$) or sulphonic ($RSO_3H$) acid form.[83,93] Sulphenic acid (RSOH) has been described as a central intermediate. Albumin is a

major nitric oxide carrier and this binding of NO can lead to covalent modifications.[92]

As serum albumin has a high content of charged residues such as glutamine and lysine, this allows for strong interactions with anionic and cationic species (e.g. metal ions).[75] Albumin has binding sites for a number of metal cations such as copper, nickel, calcium, manganese, zinc, cadmium, mercury, aluminium and cobalt.[93] Four metal-binding sites have been identified for albumin. $Cys^{34}$ is located in a hydrophobic pocket, which selectively binds hydrophobic complexes of heavy metals such as $Pt^{2+}$ and $Au^{+}$.[77] Another binding site is found at the N-terminal, which is made up of the first three amino acid residues of the albumin sequence, Asp-Ala-His.[94] This site is also called the ATCUN (amino terminal Cu and Ni binding) which is suitable for binding metal ions that have a preference for square-planar coordination, and provides four N-donor atoms which include an imidazole nitrogen of His, the N-terminal amino group and two deprotonated backbone amide nitrogens.[95] This is the primary binding site for the coordination of $Cu^{2+}$ and $Ni^{2+}$.[77] The third binding site has been located at the interface of domain I and domain II, with each domain providing two ligands: $His^{67}$ and $Asn^{99}$ from domain I, and $His^{247}$ and $Asp^{249}$ from domain II. This site has been referred to as site $A^{95}$ and also as MBS, a multi-binding site,[77] and is the primary binding site for $Zn^{2+}$ and other metal dications such as $Cu^{2+}$, $Ni^{2+}$, $Cd^{2+}$ and $Co^{2+}$ (Fig. 1.24).[77] The last binding site has been referred to as site B, which is the primary binding site for $Cd^{2+}$, but its location remains unknown.[77,95]

Shahabadi *et al*[96] recently reported the interaction of the Ag(I) complex, [Ag(2,9-dmp)$_2$](NO$_3$) (dmp = 2,9-dimethyl-1,10-phenanthroline), with bovine serum albumin (BSA). It was postulated that interactions between the cationic Ag(I) complex and the biological macromolecule are attributable to hydrogen-bonding, electrostatic attractions and van der Waals forces.[96]

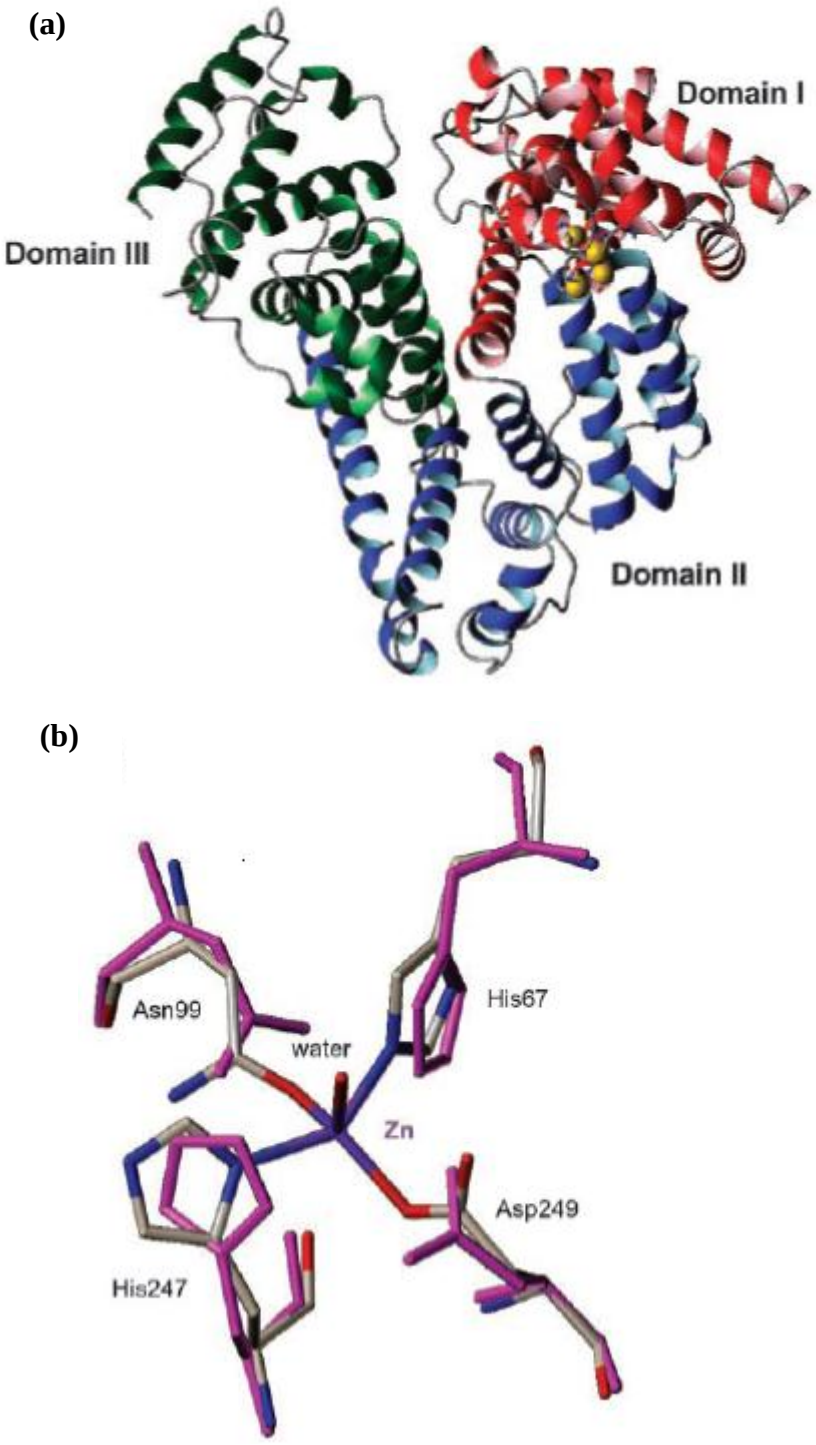


**Fig. 1.24:** (a) Proposed $Zn^{2+}$ binding site in HSA. Ligand atoms (Nε of $His^{67}$, Nδ of $His^{247}$, amide oxygen of $Asn^{99}$ and carbonyl oxygen of $Asp^{249}$) for zinc binding are highlighted in yellow, domain I in red, domain II in blue and domain III in green. (b) overlay of the zinc binding site in the X-ray structure.[94]

### 1.3.5 Mechanism of protein crosslinking by glutaraldehyde

Glutaraldehyde (GLA) (Fig. 1.25) is a linear, pale straw-coloured liquid, 5-carbon dialdehyde which is soluble in water, alcohol and general organic solvents.[97] In its simplest form, GLA exists as a monomeric dialdehyde with molecular formula, $CHO(CH_2)_3CHO$ (Fig 1.25a). GLA can also exist as a dimer, trimer and polymer (Fig. 1.25b).[98]

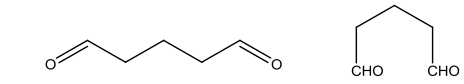


**(a)**

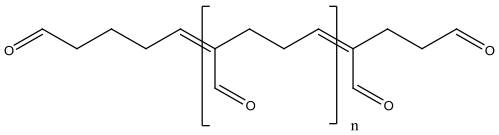


**(b)**

**Fig. 1.25:** Structure of (a) monomeric forms of glutaraldehyde and (b) poly(glutaraldehyde).

The reactivity of GLA towards proteins at neutral pH is due the presence of numerous functional groups in the proteins[97] such as thiol, amine, phenol and imidazole. Crosslinking mainly occurs through reactions with the ε-amino groups of lysine residues.[99] Many mechanisms have been proposed for the crosslinking effect of glutaraldehyde with these ε-amino groups due to the numerous molecular forms that GLA can adopt in aqueous solution, and this can lead to many possible reactions taking place.[97] One possible reaction is that the aldehydes can form Schiff bases upon nucleophilic attack by the ε-amino groups of the lysine residues in the protein, resulting in the formation of an imine bond which is stabilised by conjugation (Scheme 1).[97] Another possibility is that the crosslinking reaction proceeds by a Michael-type addition, involving the conjugate addition of protein amino groups to ethylenic double bonds of the α,β-unsaturated GLA oligomers (Scheme 2).[97] The electrophile, which is the α,β-unsaturated carbonyl compound, accepts a pair of

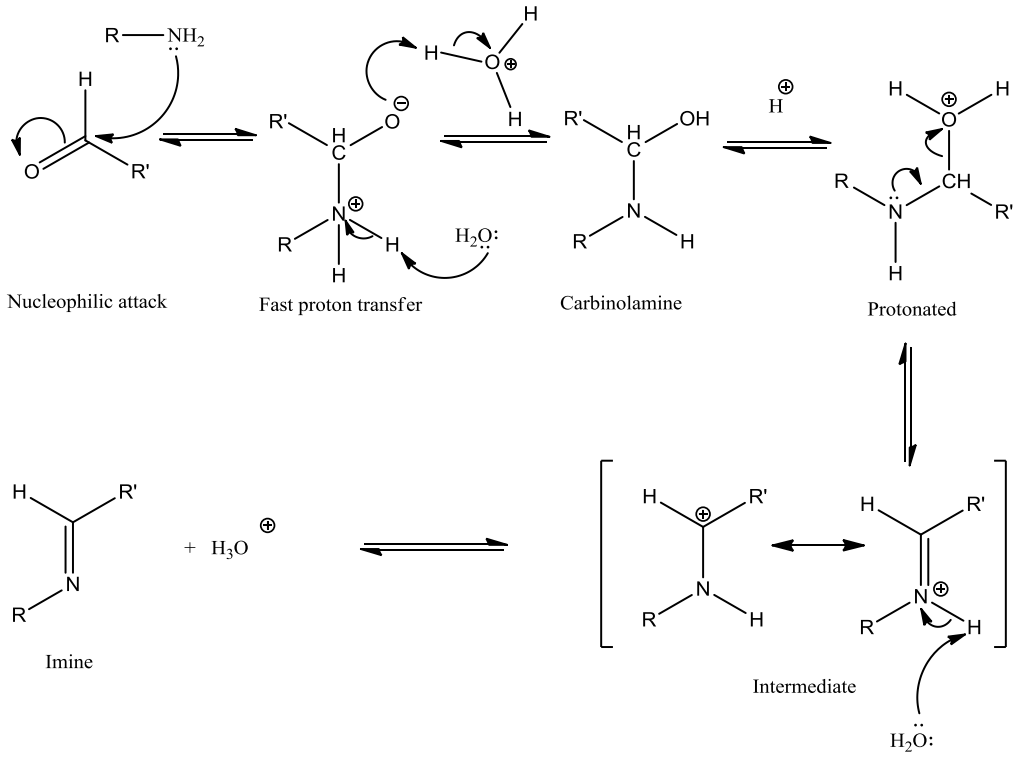


**Scheme 1:** General mechanism for a Schiff base reaction.[100]

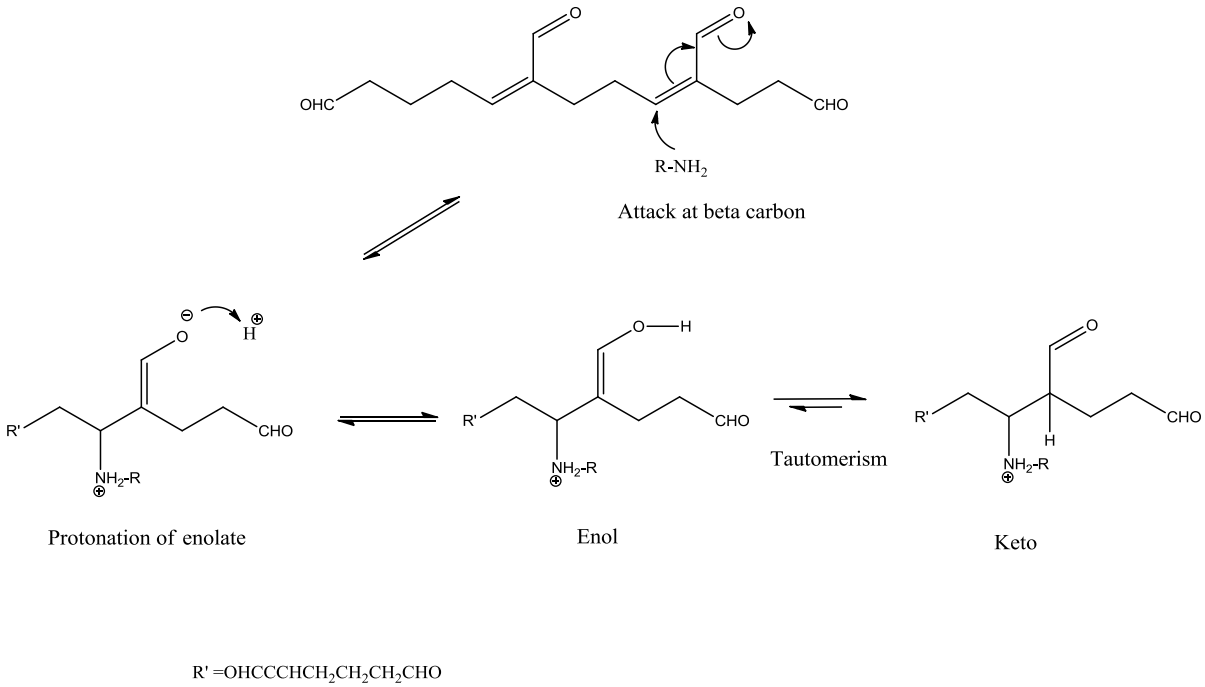


**Scheme 2:** General mechanism for a Michael addition reaction using poly(GLA).[100]

electrons and is known as the Michael acceptor. The attacking nucleophile, which is the amine of the protein, donates a pair of electrons and is therefore the Michael donor.[100]

It has been suggested that the products formed from the reaction between GLA and proteins can vary depending on the pH conditions. Under acidic or neutral conditions, glutaraldehyde can exist either as a mixture of monomers or as a polymer (Fig.1.26) which can form Schiff bases upon nucleophilic attack. However, Schiff bases formed under acidic conditions are inherently unstable.[97] Under basic conditions, the α,β-unsaturated GLA oligomers can react with an amine to give two products, a Schiff base and a Michael addition product (Fig. 1.26), as already discussed. The mechanism by which protein crosslinking occurs is still not fully understood and depending on the form of GLA present, several reaction mechanisms could be operative at the same time.[97]

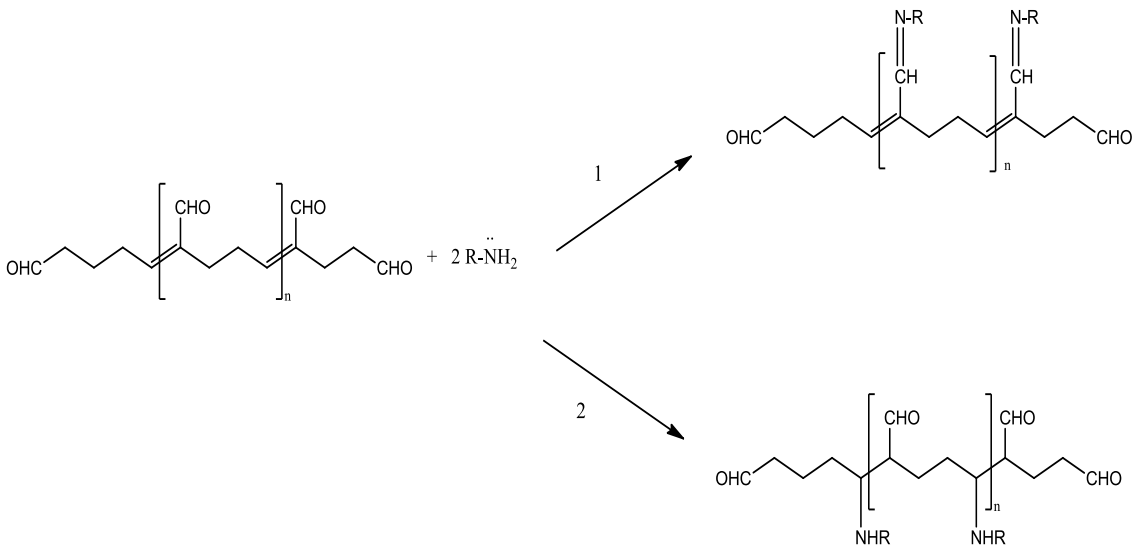


**Fig. 1.26:** Products of 1) Schiff base and 2) Michael-type addition reactions of glutaraldehyde with proteins.[97]

### 1.3.6 Applications of Bioglue

Bioglue is a relatively new adhesive which was approved by the US Food and Drug Administration (FDA) in 2001 for use as an adjunct in adult patients undergoing repair of the aorta, femoral and carotid arteries.[101,102] Bioglue is used as an adjunct to reinforce, bond or seal tissue in vascular, thoracic and neurological procedures.[68] As previously mentioned, Bioglue offers many advantages such as good homeostasis and the ability to reduce blood loss and consequently the number of transfusions. It has been found that Bioglue used in cardiac procedures actually strengthened aortic tissue at the site of anastomoses.[69] The strengthening and hemostatic properties were able to control bleeding from very fragile tissues and it was also a versatile and reliable alternative to gelatin-resorcinol-formaldehyde (GRF) glue. Toxicity issues with GRF were raised due to the formaldehyde component of the glue[69] which can be present at high concentrations (37%).[103] There have also been many advantages to the use of Bioglue in nephron-sparing surgery carried out after tumour resection (Fig. 1.27), such as reducing the formation of urinary fistula, shorter operative times and also the warm ischemic time, which is the time between interruption and re-establishment of the blood supply. The latter property has been one of the major disadvantages to the old technique of suturing.[67]

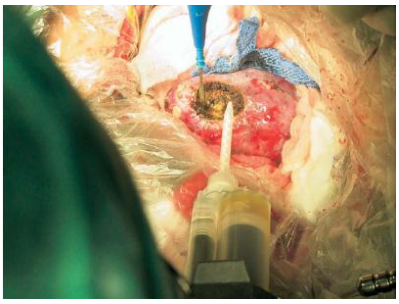

**Fig. 1.27:** Bioglue applied to a dry tumour bed and protecting the surrounding tissue in the process.[67]

Despite the many advantages Bioglue offers as an adjunct to suturing, there have been reports to the contrary. LeMaire *et al*[101] found that direct contact between Bioglue and the phrenic nerve consistently caused nerve damage and paralysis of the diaphragm in their pig model. The use of an adhesive in cardiovascular operations in

neonates has the added requirement of allowing the vascular anastomoses to enlarge as the patient grows.[104] Further studies carried out by LeMaire *et al*[104] showed that Bioglue causes severe fibrosis surrounding the aorta, which is an excess of fibrous tissue resulting from inflammation, irritation or healing. This observation was then translated to suggest that Bioglue impairs vascular growth and also causes stricture (abnormal narrowing) when applied to cardiovascular anastomoses in four week old piglets, which are designed to mimic a paediatric patient.[104] The cytotoxic effects of Bioglue on tissue of the lung, liver and aorta in rabbits was assessed by Fürst *et al*.[105] It was found that the glutaraldehyde component caused sensitivity to tissues of the lung and liver but no difference was observed in the tissue of the aorta. This corresponds with the fact that Bioglue was originally approved as an adjunct in adult patients undergoing repair of the aorta, femoral and carotid arteries.[101]

Other conflicting reports regarding the use of Bioglue have been documented. For example, Ngaage *et al*[106] suggested that the use of Bioglue results in an inflammatory process which lasts two years after initial application and may retard normal healing. Pasic *et al*[107] suggest that Bioglue may produce a foreign body reaction as long as the glue is present. As the major component of Bioglue is albumin, it degrades by proteolysis and is resorbed slowly[108] which may cause a prolonged inflammatory response.[107] In contradiction to this, Yuen *et al*[109] found that after two years the Bioglue was present unaltered, and not associated with any inflammatory, foreign body or allergic reactions or any local tissue toxicity. Using a sheep model, Hewitt *et al*[110] observed only minimal and inconsistent inflammatory responses, and preliminary results also suggested minimal reactions in humans, two and nine months after an aortic repair. This is in contrast to the findings mentioned earlier by LeMaire *et al*.[104] Gaberel *et al*[111] observed that, over an eighteen month period, a substantial increase of 5.4% in surgical site infections (SSI) occurred when Bioglue was used, and that this returned to the normal rate of 1% when its use was discontinued. A wide variety of microorganisms were found to be responsible for infection and included: 17 *Staphylococcus* species, 9 Gram-negative species and 2 *Streptococcus* species. It was suggested that Bioglue can be the cause of bacterial infection through two methods. Firstly, that bacteria can become trapped in the wound during surgery which is the main route of exposure in SSI. Secondly, it was

proposed that the inflammation response can prevent wound healing and may weaken the wound incision, causing it to separate. Once separation occurs, the skin microbial flora can enter the wound and migrate deeper into the tissue.[111] Within this report, many other factors were considered to increase the rate of SSI such as the use of Neuropatch® (a synthetic graft) in combination with Bioglue, and also surgery duration time. The report set out to determine all risk factors causing SSI, and not just to prove if Bioglue was the main source. The authors even suggested caution in the interpretation of the results as the controls were not paired with known risk factors of SSI.[111]

In the present study, microbial growth was observed on normal Bioglue samples prepared in the laboratory (Fig. 1.28). In this respect, one of the objectives of the present study was to incorporate a biocidal agent (namely Ag(I) ions) into the Bioglue formulation in an attempt to inhibit microbial growth.

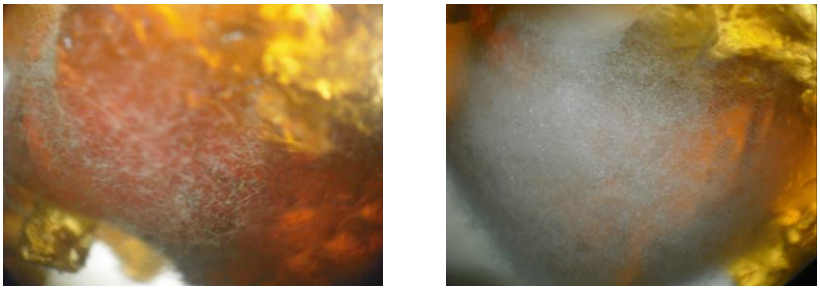

**Fig. 1.28:** Microbial growth (white) on Bioglue (golden coloured).

Many of the negative findings associated with the use of Bioglue are advertised by the manufacturer's, CryoLife®, as precautions to be taken into account before using Bioglue.[112] Tissue adhesives have provided immense adjunct support in surgery and the issue regarding inflammation could be regarded as a typical foreign body response.[110] However, these issues have highlighted the need for further long-term studies with respect to the use of Bioglue and to evaluate these effects.

## 1.4 *Staphylococcus aureus*

*Staphylococcus aureus* is a Gram-positive, versatile bacterial pathogen (Fig. 1.29a) which has the ability to survive in nutrient-limiting and stressful conditions. These factors contribute to its infectious nature in a hospital environment, which can take place by direct contact with wounds, airborne carriage and contact with indwelling devices such as catheters.[113] Approximately 30-50% of healthy individuals carry *S. aureus*, most commonly in the anterior nares (i.e. nose), with up to 10-20% of these individuals remaining persistently colonised.[114] *S. aureus* has been identified as one of the main pathogens associated with infections of the skin and soft tissue (40%)[115] (Fig. 1.29b), and it can lead to more serious diseases such as toxic shock syndrome (TSS), scalded skin syndrome (SSS) and also sepsis.[116]

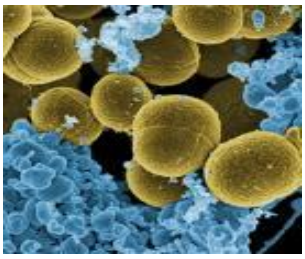

**(a)**

**(b)**

**Fig. 1.29:** (a) *S. aureus* cells (golden colour)[117] and (b) a leg ulcer infected with *S. aureus*.[118]

*S. aureus* was first identified in the 1880s by Sir Alexander Ogston, and before the discovery of antibiotics for the treatment of such an infection, the mortality rate from an *S. aureus* infection was approximately 80%.[119] Penicillin-resistant strains of *S. aureus* were first observed two years after the introduction of penicillin as a successful treatment. A new treatment of methicillin was introduced, but again, resistance was observed.[120] In the UK alone, over 20,000 cases of *S. aureus* infection are reported each year, with half of these cases being antibiotic-resistant.[121] Data collected as part of the European Antimicrobial Resistance Surveillance Network (EARS-Net), found that in Ireland there were 1,412 reported *S. aureus* infections identified by analysts working in 42 different microbiology laboratories in 2006.[122] Of these, 41.9% were found to be methicillin-resistant. This figure decreased by

2010 to 1,251 cases of *S. aureus* infections and of these, 24.4% showed emergence of resistance.[122] Even though the overall trend shows that the incidence of resistance is decreasing, Ireland was ranked 9th highest out of 28 countries in 2009 regarding the number of *M.R.S.A.* cases reported.[122] The cost of treating *M.R.S.A.* infections in hospitals has been estimated to be €23 million annually and the need for more frequent after-care can add to this.[123] This financial problem has contributed to the need for continuing research into the pathogenesis and mode of action of *S. aureus* in order to develop a diverse portfolio of complementary approaches to prevent the spectre of untreatable infections.[121]

### 1.4.1 Pathogenesis of *S. aureus*

Many factors contribute to the pathogenesis of *S. aureus* such as the presence of a capsule, the expression of adhesins, the secretion of various toxins and also immunomodulators (Fig. 1.30).[124] The capsule is composed of capsular polysaccharides which aid *S. aureus* in the evasion of opsonophagocytosis.[121] Opsonophagocytosis is a process where white blood cells can efficiently consume bacteria that contain opsonin, which is an antibody or product of the complement activation in blood serum that causes bacteria or other foreign cells to become more susceptible to the action of phagocytes. This was suggested on the basis of findings that a reduced uptake by human neutrophils of bacterial cells containing a capsule occured *in vitro*.[125] The capsule is composed of serotype 5, serotype 8 or serotype 336. Serotypes 5 and 8 have been associated with increased virulence in animal infection models,[125] and recent studies from the United States and the Netherlands have found that 92% and 82% of *S. aureus* isolates were either serotype 5 or serotype 8, respectively.[126] It can be seen that the presence of a capsule can effectively protect *S. aureus* by providing a barrier to help evade an immune response. The presence of teichoic acids, which is a shared feature of the cell wall and the membrane, also assists in the protection of *S. aureus* from a host immune response. Teichoic acids are composed of polyglycerol phosphate or polyribitol phosphate polymers coated with sugar substituents or esterified with D-alanyl groups, and it is the positively charged free amino moiety of the D-alanyl groups that neutralise the anionic properties imposed by the phosphate groups. This, in turn, protects *S. aureus* from

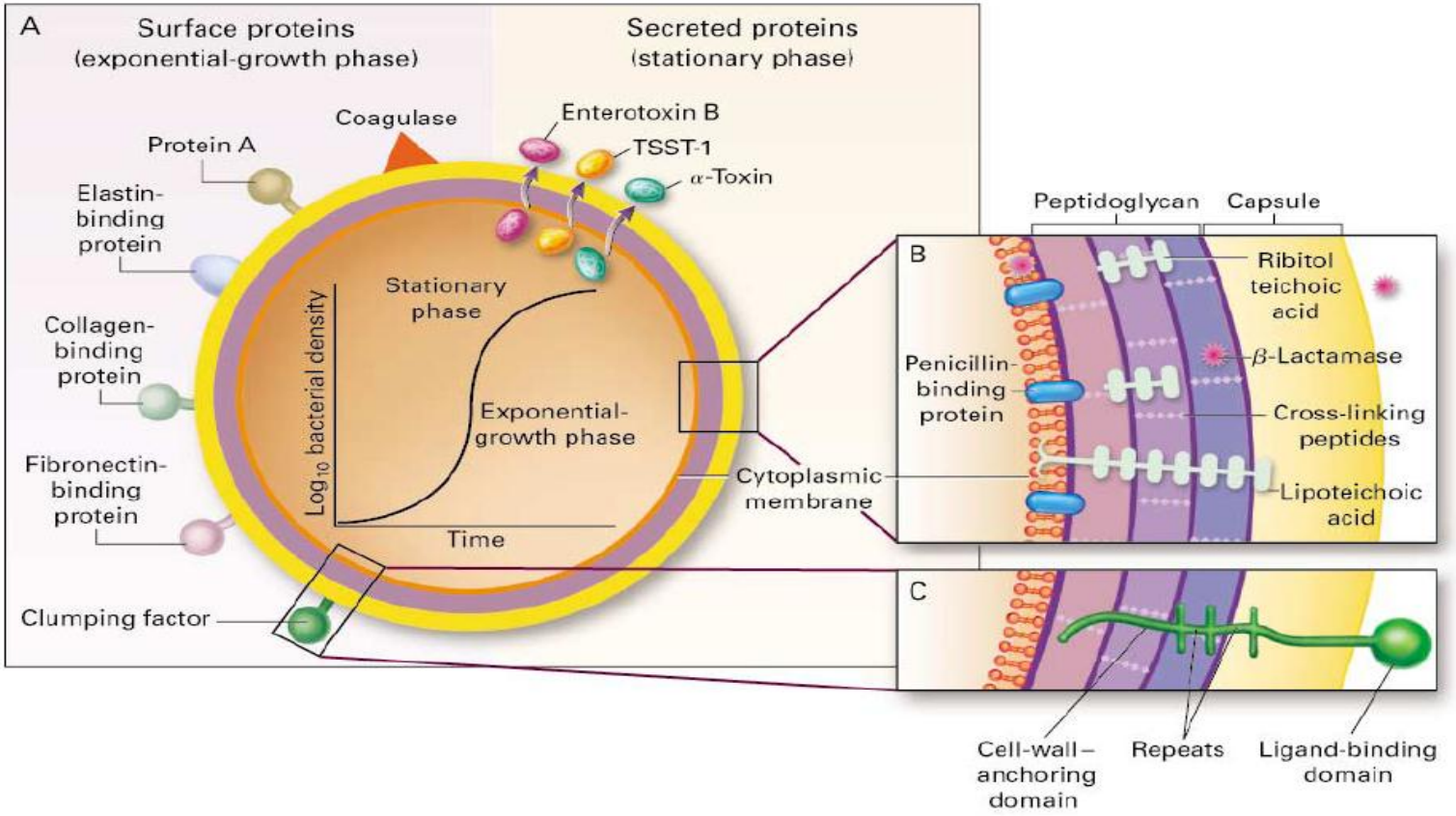


**Fig. 1.30:** (a) Surface and secreted proteins of *S. aureus*, (b) and (c) are cross sections of cell envelope.[127]

attack by the cationic antimicrobial peptides (CAMPs) which are part of the host immune response.[121]

Adherence is a critical first step in bacterial pathogenesis and is needed for colonizing a host. The process of adherence is usually carried out by adherence factors called adhesins, which are produced by bacteria and which recognise and bind to the host extracellular matrix.[128] Adhesion is effected by several cell wall-associated proteins, known as microbial surface components, which recognise adhesive matrix molecules (MSCRAMMS).[121] The best characterised of these are the fibronectin-binding proteins (FnBpA and FnBpB), the collagen-binding protein (Cna) and the fibrinogen-binding proteins clumping factor (ClfA and ClfB).[121] The N-terminus of these binding proteins contains a signal sequence made up of about 40 residues, followed by an A domain which is exposed to the bacterial surface and which contains a ligand binding region.[129] The C-terminus contains the LeuProXThrGly (LPXTG) motif, which is cleaved by sortase and covalently link the adhesins to the bacterial cell peptidoglycan.[130] Fibrinogen, and especially fibronectin, can be present as secreted or plasma membrane-associated molecules.[131] FnBpA has been found to bind to extracellular matrix-associated fibronectin which, in turn, induces the clustering of fibronectin-bound integrin receptors ($\alpha_5\beta_1$) which activates intracellular signalling.[128,132] This clustering leads to focal adhesion kinase (FAK) activation, a protein tyrosine kinase which is engaged at an early stage to focal adhesions and which ultimately leads to actin-binding protein recruitment to the attachment site and promotes the internalisation of *S. aureus*.[133] The collagen-binding protein, Cna, mediates bacterial adherence to collagenous substrates and tissues. It has been found that the presence of Cna is sufficient and necessary for *S. aureus* cells to adhere to cartilage *in vitro* due to the fact that antibodies against Cna inhibit binding to collagen and also block adherence to cartilage.[134] The N-terminal A domain of ClfA binds to the γ-chain of fibrinogen. If cells are densely packed in suspension, the γ-chain C-termini located at either end of the fibrinogen molecule can bind simultaneously to two ClfA molecules on two different bacterial cells, leading to clumping of cells.[125] ClfA mediates bacterial attachment to plasma clots formed *in vitro* and also to plastic biomaterials which were exposed to canine and human blood for short-term conditioning, suggesting that it is an important factor in

wound and foreign body infection.[134] Although attachment of the bacterial adhesins to the host cell is beneficial for bacterial colonization it can also stimulate an immune response.[135]

Staphylococci are the main coloniser of in-dwelling devices such as catheters (Fig. 1.31).[136] After the device has been implanted in the patient, the surface is rapidly coated by host proteins such as fibronectin and fibrin, which are the main ligands that facilitate the binding of *S. aureus.*[137] The bacteria then encase themselves in a hydrated matrix of polysaccharide and protein, which forms a slimy layer, known as a biofilm.[138] Adhesion to the surface is a critical transition from free-floating planktonic cells to biofilm formation. Once attachment has taken place, the bacteria start to accumulate in mass and this results in a multi-layered cell structure.[139] Once the biofilm aggregates and matures, clusters of cells break away from the film and distribute to distant sites which facilitates the spread of a biofilm-associated infection.[139] Quorum sensing is a cell to cell signalling mechanism that allows the bacteria to control gene expression. The signals of quorum sensing systems are molecules called autoinducers (AIs) which are at a low concentration when the cell density is also low. Once a certain cell density is reached, AIs reach a threshold concentration and activate a transcription factor.[140] This, in turn, regulates the expression of various genes, including virulence factors,[139] and allows optimal expression which conserves energy and maximises their survival, to the disadvantage of the host.

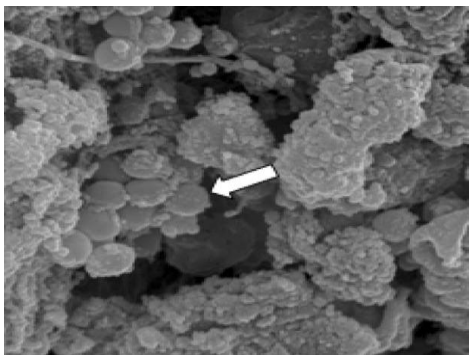

**Fig. 1.31:** SEM of *S. aureus* adhering to catheter pieces placed in tissue cages. Microcolonies (arrow) of *S. aureus* were found attached to the catheter.[141]

*S. aureus* produces a wide variety of cytotoxins which have potent effects on the cells of the host immune system.[142] Some examples of these include hemolysin (α, β, γ, δ), leukocidin, toxic shock syndrome toxin-1 and also enterotoxins. The ability of a bacterial protein toxin to cross a cellular membrane is an important function in order to allow access to the host's cytosolic molecular targets. Alpha-hemolysin is one of the main pore-forming toxins of *S. aureus*. Monomers are secreted which attach to the membrane of a host cell, where a cylindrical heptamer is formed with β-strands from each monomer contributing to the formation of a β-barrel which spans across the membrane (Fig. 1.32).[125] Once this occurs, a 1-2 nm pore forms which allows for the rapid efflux of $K^+$ and influx of $Na^+$, $Ca^+$ and other small molecular weight molecules into the target cell.[142] Osmotic swelling ultimately results in rupture due to a breakdown in cell integrity and thus allowing greater vascular permeability.[142] The overall structure of the pore was found to be in the shape of a mushroom, which is divided into three domains: the cap, rim and stem (Fig. 1.32).[143] The cap domain is mainly hydrophilic and, with the rim domain, projects from the extracellular surface of the membrane and forms the core of the protein.[143] A prominent feature of the core is the amino latch[144] which is formed when the N-terminal extremity detaches from each monomer and interacts with the next two protein subunits at the entrance of the pore.[143] The stem domain is formed by the 14-strand, anti-parallel β-barrel, which defines the transmembrane portion of the pore (channel).[144]

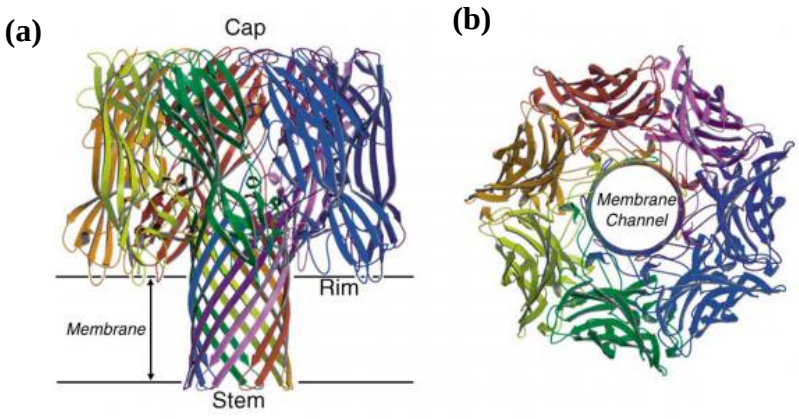


**Fig. 1.32:** Ribbon representation of the α-hemolysin heptamer (a) with cap, rim and stem domains labelled and (b) depiction of the membrane pore (channel).[144]

Leukotoxins target leukocytes and are made up of two subunits, S and F components, named as such because of their relative elution positions on an ion exchange column.[142,145] Leukotoxins are secreted separately and assemble into hexameric or heptameric oligomers in the membrane of leukocytes.[125] Leukotoxins include γ-hemolysin and Panton-Valentine leukocidin (PVL). γ-Hemolysin is made by virtually every strain of *S. aureus*, while PVL is made by only 2-3% of strains.[138] The two components of PVL are LukS-PV and LukF-PV, with LukS-PV initiating binding on the leukocyte membrane, where it dimerises with LukF-PV. This is followed by the alternate binding of LukF-PV and LukS-PV components until the heptamer is formed.[146] Binding of PVL results in the activation of the target cell by the opening of calcium ion channels, and this can lead to the production of interleukins and other inflammatory mediators.[147] PVL has been associated with skin infections such as furunculosis[148] and also necrotising pneumonia.[149] Necrotising pneumonia is characterised by high fever, hypotension, leucopenia and multilobular alveolar infiltrates which usually progress into abscesses.[147] Histopathological studies have shown the presence of necrotic lesions of the tracheal mucosa and alveolar septa and numerous clusters of Gram-positive cocci have been observed. The production of interleukins and inflammatory mediators is most likely the cause of local vasodilation and also the progression to acute respiratory distress syndrome.[147] *S. aureus* secretes toxins which can act as superantigens and also induce vomiting (an emetic response) when ingested.[148] Examples of these include Toxic Shock Syndrome Toxin-1 (TSST-1) and Staphylococcal enterotoxins.[142] TSST-1 is associated with Toxic Shock Syndrome (TSS), an acute and potentially fatal illness, which is characterised by a high fever, rash, desquamation of the skin one to two weeks after onset, hypotension and involvement of three or more organ systems.[138,142] Superantigens have the ability to bind to the exterior surface of the major histocompatibility complex II (MHC) molecules on the surface of antigen-presenting cells and link them to the T-cell receptors which are on the surface of the T-cell.[148] In normal antigen processing, proteins which have been endocytosed are degraded within the cell by enzymes and are presented via the inner groove of the MHC class II molecule on the outside surface so they can be recognised by the T-cell, activating an immune response (Fig. 1.33).[150] In this case, binding occurs

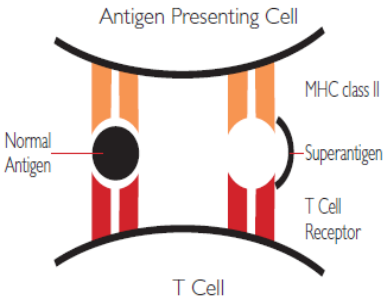


**Fig. 1.33:** An illustration of the interaction of a normal antigen (left) and a superantigen (right) with a T-cell and MHC class II on an antigen presenting cell.[150]

without MHC class II having to present to the T-cell receptor.[148] The expression of superantigens during an infection prevents a normal immune response. Antigen-specific T cells fail to proliferate antigens which are presented normally by MHC class II.[125] This results in immunosuppression due to the failure to induce an appropriate immune response and a lack of immunological memory[125] which, in turn, prevents the production of antibodies to the superantigen toxin which is characteristic to TSS patients.[125] TSS is usually classified into two categories: menstrual TSS (MTSS) and non-menstrual TSS (NMTSS).[138] MTSS has been associated with the use of tampons which are thought to introduce oxygen into the normally anaerobic vagina, an environment which is required for TSST-1 production.[138] NMTSS can occur in men, women and children and is associated with localised infections of surgical wounds, abscesses, lacerations, furuncles (a hair follicle infection) and burns.[150]

*Staphylococcus* enterotoxins (SEs) have been implicated in outbreaks of food poisoning, which is known as staphylococcal food poisoning (SFP). This usually results from the ingestion of SEs on food contaminated by *S. aureus*.[142] SFP is characterised by nausea, vomiting, abdominal pain and diarrhea[151] and usually resolves within 24-48 h.[142] There are a variety of SEs, ranging from SEA-SEE and SEG-SEJ, with SEA and SED being the most common enterotoxins responsible for food poisoning in the US (77.8% and 37.5% of all outbreaks, respectively).[151]

Antibodies to one SE will not necessarily provide immunity to SFP due to the multiple SEs capable of causing disease.[142]

In conclusion, it can be seen that the pathogenesis of *S. aureus* is attributed to the numerous secreted and cell-surface-associated virulence factors which promote the success of an infection. However, once *S. aureus* breaches the skin and mucous surfaces, the organism has to deal with the hosts' immune system.

### 1.4.2 Host immune response

The immune system is made up of two defense mechanisms: the innate immune response and the adaptive or specific immune response. The innate immune response is the host's first line of defense against invading pathogens and consists of macrophages, neutrophils, natural killer cells and dendritic cells. The main functions of the innate immune system are: to recruit cytokines to the site of infection and inflammation; to activate the complement cascade to identify bacteria; to remove foreign organisms from the body and to activate the adaptive immune response by antigen presentation. The adaptive immune system has the ability to remember certain pathogens and recognise them in the event of a repeated exposure to that pathogen. This leads to immunological memory, which results in a more effective and faster process to eliminate pathogens.

The skin forms the first line of defence against the invasion of microbial pathogens. The uppermost layer, the corneal layer, is composed of dead keratinocytes which provide the physical barrier of the skin. These cells contain antimicrobial peptides such as defensins, which can be induced in response to infection.[152] Beneath this layer are the granular, spinous and basal layers which are made up of keratinocytes which express pattern recognition receptors (PRRs) that, in turn, recognise the pathogen-associated molecular patterns (PAMPs) of invading microorganisms.[152] Each PAMP is recognised by a specific, toll-like receptor (TLR) which can be found extra- and intra-cellularly and are produced in response to pathogens. TLRs allows for the activation of phagocytes and tissue dendritic cells to respond to pathogens by releasing chemokines and cytokines.[153] The interaction of TLRs with their specific

PAMP results in the activation of the nuclear transcription factor, kappa (NF-κB),[154] which causes translocation to the nucleus and, in turn, activates inflammatory target genes, including those which encode for cytokines, cytokine receptors, adhesion molecules, stress-associated proteins and also defensins.[155]

A characteristic of an *S. aureus* infection is the formation of a neutrophil abscess, which is necessary for bacterial clearance.[152] Neutrophils are key innate immune cells which express many PRRs, and it is through these receptors that neutrophils first detect *S. aureus*. TLR2 is considered to be the main PRR for Gram-positive bacteria, as lipoteichoic acids signal through this receptor.[156] The recruitment of neutrophils is governed by pro-inflammatory mediators such as cytokines (Interleukin-1, IL-1 and tumour necrosis factor alpha, TNF-α) and chemokines (CXCL-1 and CXCL2).[156] Cytokines are proteins which can be induced, and are produced on stimulation of white blood cells and are therefore necessary for a host immune response.[157] Once neutrophils encounter *S. aureus*, phagocytosis occurs which is followed by an oxidative burst to facilitate bacterial killing. This process involves the generation of reactive oxygen species (ROS) such as superoxide, hydrogen peroxide and also hypochlorous acid, which mediate bacterial killing. Despite this, the numerous virulence factors associated with *S. aureus* provide a means of avoiding recognition and phagocytosis by neutrophils, which is advantageous to the organism.[156]

### 1.4.3 *S. aureus* antibiotic resistance

The phenomenon of antibiotic resistance stimulated research into trying to firstly understand the mechanisms behind it and, secondly, in doing this, to produce novel therapeutic agents to keep one step ahead of the organism by providing a wide range of treatments.

Antibiotic resistance was first reported in 1942, two years after the introduction of penicillin for the treatment of *S. aureus* infections.[120] One mechanism of resistance is the production of enzymes which inactivate the antibiotic either by hydrolysis or the formation of inactive derivatives.[158] Penicillin is inactivated by the enzyme β-

lactamase, a serine protease that hydrolyses the β-lactam ring.[127] With the introduction of methicillin, a penicillinase-resistant penicillin, resistance was once again observed due to the acquisition by the bacterium of the staphylococcal cassette chromosome (SCC*mec*).[159] SCC*mec* is a 21-67 kilo base (kb) fragment of DNA which carries the *mec* gene complex which encodes for β-lactam resistance.[159] The *mecA* gene codes for the 78 kDa penicillin-binding protein, 2a (PBP2a), a transpeptidase which catalyses the formation of cross-bridges in bacterial cell peptidoglycan.[159] In susceptible cells, β-lactam antibiotics bind to PBPs present in the *S. aureus* cell wall, causing disruption of the synthesis of the peptidoglycan layer and resulting in cell death.[120] In *M.R.S.A.*, however, PBP2a is present, preventing the binding of β-lactam antibiotics. The growth of *M.R.S.A.* is observed as the peptidoglycan layer synthesis is not disrupted.[120] Another mechanism adopted by organisms is target alteration. This process involves the alteration of cellular targets by either mutation or enzymatic modification, which reduces the affinity of the target for the antibiotic.[158] Lastly, another proposed mechanism is the removal of antibiotics from the organisms by efflux systems.[160] Bacterial efflux pumps are responsible for the removal of toxins produced by the cell itself and also the efflux of toxic compounds that the cell encounters, such as antibiotics.[160] Some examples of efflux pumps for *S. aureus* are the quaternary ammonium compounds (QAC) efflux system which encodes the genes *qacA-D*, with *qacC* and *qacD* being identical to the *ebr* gene which encodes resistance to ethidium bromide and which explains why resistance to QAC is often observed with ethidium bromide resistance.[37] Another efflux pump associated with *S. aureus* is NorA, which is responsible for resistance to fluoroquinolones.[161] The ability of *S. aureus* to adapt to and evolve resistance against a range of antibiotics makes the treatment of infections limited and causes added expense to the healthcare system.

### 1.4.4 Treatment of *S. aureus*

The appearance of resistance in *S. aureus* to various treatments only reinforces the importance of research into novel therapies. One suggestion has been to target the auto-inducing peptides used in quorum sensing by synthesizing analogues to

compete with these autoinducing peptides. This will, in turn, prevent any cell-cell signalling from occurring.[162]

Although the structure of the *S. aureus* cell is quite complex it provides many cellular targets for drug intervention.[121] One suggested avenue would be to inactivate the genes that esterify teichoic acids with D-alanine as this would result in the mutants becoming sensitive to cationic, antimicrobial peptides (CAMPs) which are part of the innate immune response causing the production of defensins that protect the skin from invading organisms.[163] Another area that could act as a potential target is the peptidoglycan of the cell wall.[121] Peptidoglycan is made up of a pentaglycine bridge which is required for structural integrity. Lysostaphin has been used due to its ability to cleave the pentaglycine cross-bridges in the cell wall. This has been very successful in the prevention and eradication of *S. aureus* colonization of both inert materials such as catheters and also living tissue.[164] As mentioned earlier, Cna which is a collagen-binding protein, ClfA which is a fibrinogen-binding protein clumping factor and FnbpB, a fibronectin-binding protein, provided promising results when used as vaccines in rodent models. The binding proteins had the ability to reduce the severity of symptoms caused by the bacteria and reduced the mortality rates by 2-6 fold.[165-167]

Many silver-based dressings have been used in the treatment of *S. aureus*. Edwards-Jones[168] found that nano Ag(0) dressings (Acticoat and Acticoat Absorbent) provided an effective barrier, by preventing the penetration of *M.R.S.A.* through the dressing. This, in turn, prevents the spread of *M.R.S.A.* from the wound surface to the surrounding area.[168] Rattanaruengsrikul *et al*[169] found that a Ag(0)-nanoparticle loaded gelatin hydrogel pad was more effective against *S. aureus*, *E. coli* and *P. aeruginosa* than the neat gelatin hydrogel.

*S. aureus* has been shown to be a very versatile, colonizing pathogen and has been isolated from both hospital and community acquired infections. The consequences of an *S. aureus* infection can be detrimental to the host, with 4% of cases each year being fatal.[121] This is especially the case when resistance emerges, as has been found in the case of *M.R.S.A.* and other resistant strains of *S. aureus*. As the main coloniser

of wounds and a major problem for burn patients, patients with open wounds and in-dwelling catheters, it is essential to gain an understanding to the mode of action of *S. aureus* in order to have new therapeutic options available when resistance eventually emerges. As this has occurred with the introduction of the first method of treatment using penicillin, and has continued with the introduction of each new antibiotic, such as methicillin and vancomycin, it is vital to continue in the search for novel treatments, whether it is in the form of prophylactic or therapeutic agents.

## 1.5 Other Microorganisms Used in this Study

### 1.5.1 *Escherichia coli*

*E. coli* is a Gram-negative, rod-shaped bacterium (Fig. 1.34) which is found mainly in the lower intestinal tract. Harmless strains are part of the normal flora of the gut and can even benefit the host with the production of vitamin K and also by preventing pathogenic bacteria from establishing in the host's intestine. Despite this, there are some strains of *E. coli*, namely O157, which are pathogenic and are known to cause disease.[170] *E. coli* O157 has the potential to be life-threatening, with the US Centre for Disease Control estimating that it accounts for at least 20,000 cases of infection and 250 deaths per year in the USA alone.[170]

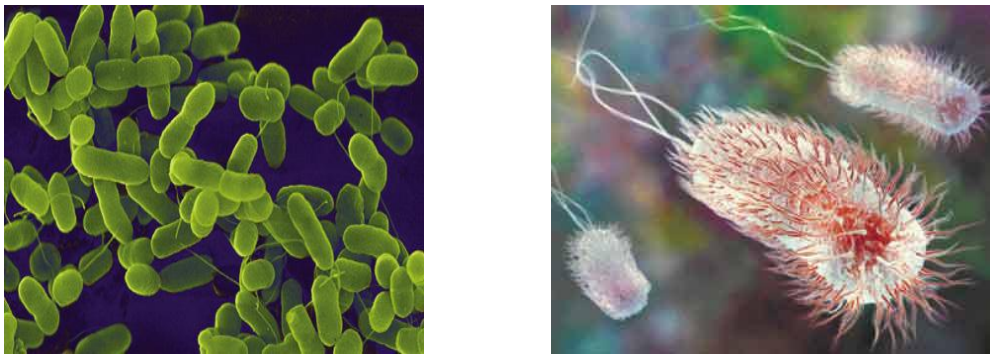

**Fig. 1.34:** *E. coli* cells.

### 1.5.2 *Pseudomonas aeruginosa*

*P. aeruginosa* is also a Gram-negative bacterium (Fig. 1.35a) which has the ability to cause a range of infections in both a community and hospital environment. In the community, the bacterium has been known to cause folliculitis (Fig. 1.35b) and also green nail or hot foot syndromes, usually caused by exposure to contaminated hot tubs or swimming pools.[171] This opportunistic pathogen is a leading cause of nosocomial infections and also contributes to chronic lung infections of cystic fibrosis patients.[172] A US National Healthcare Safety Network listed *P. aeruginosa* as the sixth most frequently occurring bacterial pathogen, the second most important pathogen in ventilator-associated pneumonia and also the sixth leading cause of catheter-related, bloodstream infections.[171]

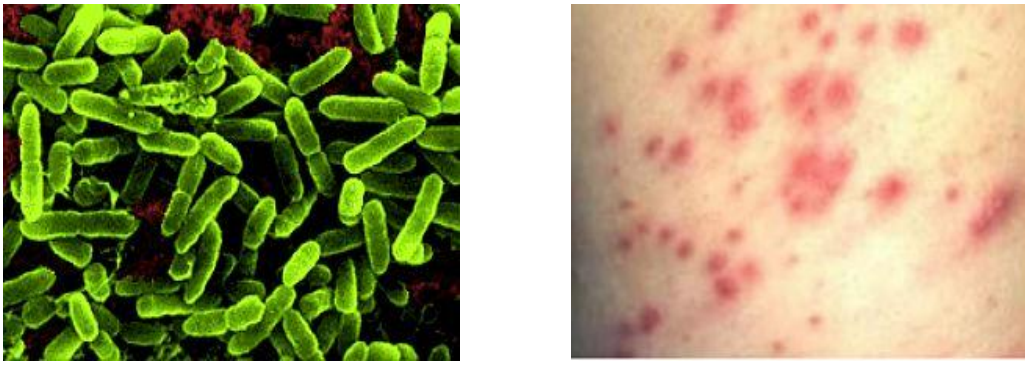

**(a)** **(b)**

**Fig. 1.35:** (a) *P. aeruginosa* cells and (b) *P. aeruginosa* folliculitis infection.

### 1.5.3 *Candida albicans*

The *Candida* genus of yeast consists of many species of which *C. albicans* is a member. *C. albicans* is a dimorphic yeast (Fig. 1.36a) and is carried unknowingly by humans on the epithelial surfaces of the mouth, gastro-intestinal tract (GI tract), vagina and skin. In healthy individuals they are harmless, but in individuals with an impaired immune system the organism can overgrow and cause harm. For this reason it is known as an opportunistic pathogen.[173] When *C. albicans* has overcome the host's immune system it can lead to a number of infections, which are either superficial or systemic.[174] Superficial infections affect the skin, mucous membranes

of the oral cavity (Oropharyngeal Candidosis, oral thrush) (Fig. 1.36b) and the vagina (Vulvovaginal Candidosis, thrush), while systemic infections occur when the *C. albicans* cells penetrate through the outer layers of the skin and mucosal surfaces and enter the bloodstream causing Candidaemia.[175]

**(a)** **(b)**

**Fig. 1.36:** (a) *C. albicans* cells and (b) an oral *C. albicans* infection

## 1.6 Previous Research from laboratory

Previous work within our group at N.U.I. Maynooth has focused on the antimicrobial effects of Ag(I) complexes incorporating ligands such as 1,10-phenanthroline (phen), 1,10-phenanthroline-5,6-dione, imidazoles and salicylates (Fig. 1.37).[176-179] It was found that Ag(I) complexes incorporating 1-10-phenanthroline e.g. ($[Ag_2(phen)_3(mal)].2H_2O$) ($malH_2$ = malonic acid) damage mitochondrial function and also inhibit cytochrome biosynthesis, which leads to a decrease in cellular ergosterol content. The imidazole/salicylates complex ($[Ag_2(imH)_4](salH)_2$ ($(imH)_4$ = imadazole, $(salH)_2$ = salicylic acid) was found to be 47 times more potent than the marketed drug, ketoconazole, against the fungal pathogen *C. albicans*.[179] A range of Ag(I)-coumarin complexes were also synthesised and it was found that they had the ability to disrupt fungal respiration, leading to an increase in cell membrane permeability, loss of cytochrome c, which triggers an apoptotic response within the cell and can lead to DNA cleavage.[180] The effect of $AgClO_4$ on *C. albicans* was also

assessed. The activation of two stress response pathways (Cap1p and Hog1p) was observed, indicating that the cells were experiencing oxidative stress as a result of exposure to the Ag(I) ion.[174]

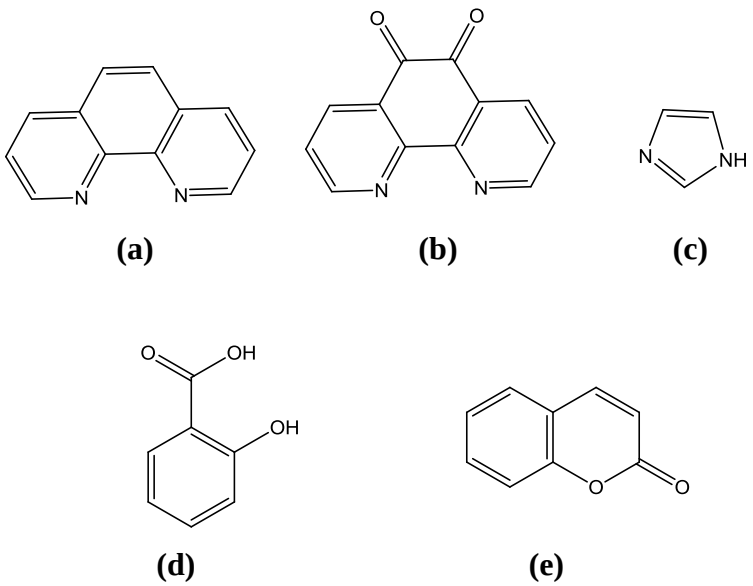


**(a)** **(b)** **(c)**

**(d)** **(e)**

**Fig. 1.37:** Structures of (a) 1,10-phenanthroline, (b) 1,10-phenanthroline-5,6-dione, (c) imidazole, (d) salicylic acid and (e) coumarin.

# Chapter 2

Experimental

## 2.1 Instrumentation

Bioglue samples for subjection to atomic absorption, infrared spectroscopy, differential scanning calorimetry and scanning electron microscopy analysis were pre-dried at room temperature under high vacuum (approx. 8 h) until a constant mass was obtained.

Infrared (IR) spectra were obtained on a Perkin Elmer System 2000 FT IR spectrometer and were recorded in the range of 4,000-370 $cm^{-1}$. Solid samples were ground with an excess of anhydrous KBr and liquid samples were placed between two NaCl plates.

$^{1}H$ NMR spectra were recorded on a Bruker Avance 300 MHz spectrometer at a probe temperature of 25 ˚C using $D_2O$ and with tetramethylsilane (TMS) as an internal standard.

Differential Scanning Calorimetry (DSC) measurements were carried out using a Perkin Elmer Pyris 6 DSC. The parameters for the first experiment were; hold for 1 min at 25 °C, heat from 25-50 °C at 3 °C/min, cool from 50-30 °C at 3 °C/min, hold for 1 min at 30 °C, and this was repeated three times. The parameters for the second experiment were; hold for 1 min at 25 °C, heat from 25-50 °C at 3°/min, cool from 50-37 °C at 3 °/min, hold at 37 °C for 3 h, cool from 37-30 °C and hold for 1 min at 30 °C.

Atomic Absorption Spectrometry (AAS) was performed using a Perkin Elmer AAnalyst 200 and calibration plots were obtained using $AgNO_3$ (99.99% purity).

Tensile testing was performed on a LLOYD Instruments LRX instrument and the data were analysed using the NEXYGEN software package. The parameters used for tensile testing of the pre-measured pieces of wood were; general purpose, pull to break, preload; 1 N, speed; 20 mm/min, gauge length; 20 mm, area; 5 mm x 3 mm, break; load drops to 5%. The parameters used for tensile testing of the pre-measured pieces of pig skin were; general purpose, pull to break, preload; 1 N, speed; 20 mm/min, gauge length; 40 mm, area; 25 mm x 5 mm, break; load drops to 5%.

Microanalytical data were obtained using a Flash EA 1112 series CHN Analyser.

Mass spectrometry for the determination of molecular weight of the [$Ag_2$(3,6,9-tdda)] (tddaH$_2$ = trioxaundecanedioic acid) samples was carried out on an Agilent Technologies 6210 Time of Flight LC/MS mass spectrometer. An Agilent Technologies 6340 Ion Trap LC/MS spectrometer was used for proteomic analysis.

Scanning Electron Microscopy was carried out on a Hitachi S-3200 N Scanning Electron Microscope, using Au sputtering.

All electrochemical work was completed using the CH Instruments Electrochemical Workstation. Analysis of data was carried out using chi760c program.

All worktops and benches were washed down with 70% (v/v) ethanol prior to use. Sterilisation of all growth media and materials required for aseptic techniques was achieved by autoclaving in either a TOMY SX-500 E autoclave at 121 °C and 15 lb/sq.in or in a Dixons ST2228 autoclave at 121 ˚C and 18 lb/sq.in for 20 min. Any solutions that were not suitable for autoclaving were filter-sterilised using 0.22 μM Millipore membrane filters (Sarstedt, Nümbrecht, Germany). All cultures were autoclaved prior to final disposal.

A Bio-Tek Synergy HT spectrophotometer was used at λ=540 nm for the anti-fungal and anti-bacterial susceptibility testing, and at λ=450 nm for the superoxide dismutase assay. A Cary IE UV-Visible spectrophotometer was used at λ=340 nm for the glutathione reductase assay. A Unicam UV500 UV-Visible spectrophotometer was used for UV-Visible analysis of Ag(0)-Bioglue supernatants in the range 190-900 nm. The $OD_{600nm}$ of an overnight bacterial culture was determined using a Biophotometer, Eppendorf spectrophometer.

Centrifugation was carried out on either a Beckmann GS-6 Centrifuge or on an Eppendorf 5417R centrifuge when a controlled temperature was required. A Heto DNA Mini vacuum centrifuge was used during mass spectrometry preparation.

Sonication was performed using either a Bandelin Sonopuls HD 2200 sonicator probe to disrupt external proteins for SDS-PAGE electrophoresis or in a Fisher Scientific FB 15050 sonicator bath as part of protein preparation for mass spectrometry analysis.

Iso-electric focusing was performed on an Ettan IPGphor II, supplied by Amersham Biosciences, NJ, USA.

SDS-PAGE gels were cast on the Bio-Rad PROTEAN II casting unit and were electrophoresed on the Bio-Rad PROTEAN PLUS Dodeca cell system.

RNA quality was measured using a Mason Technology nanodrop 1000 spectrophotometer.

Polymerase chain reactions (PCR) were carried out on an Eppendorf Mastercycler PCR instrument.

## 2.2 Theoretical Background and Specific Instrumental Techniques

### 2.2.1 Tensile Testing

The mechanical behaviour of an adhesive is one of its most fundamental properties. Such behaviour can be assessed by having the test sample clamped at each end with one end being fixed, whilst a hydraulic piston applies a gradual upward load until the sample breaks apart (Fig. 2.1).[181]

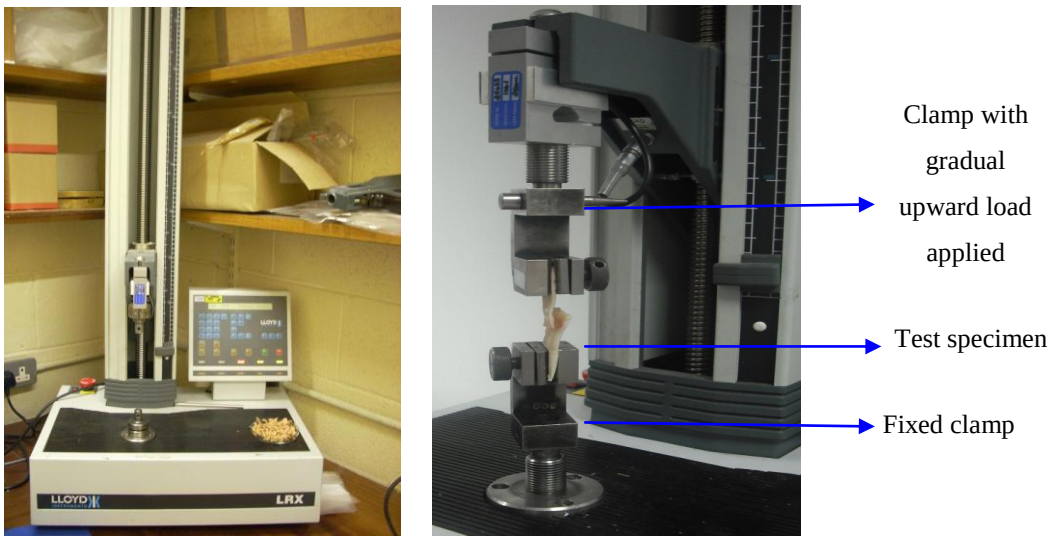


**(a)** **(b)**

**Fig. 2.1:** (a) LLOYD Instruments LRX tensile testing machine and (b) set-up of clamping system.

There are a number of mechanical testing protocols such as tensile, compression and shear. Tensile stress measurements provide information on the resistance of a material to stretching forces, whereas compression stress measurements indicate the resistance of a material to 'squashing' forces. Shear stress measures the resistance to 'push and pull' forces.[182]

Tensile testing gives an insight into the tensile strength, stress-strain behaviour and Young's modulus of the material being tested. The tensile strength is the force that a material can be subjected to before failure. The degree by which a material will

strain depends on the stress being imposed, and this stress (σ) is defined as the load (F) per unit area (A): [182,183]

$$\sigma = F / A \quad \text{(Pascal, Pa)}$$

The strain (ε) is the amount of deformation per unit length of the material as a function of the load being applied:

$$\varepsilon = \Delta L / L_o$$

where ΔL is the amount of elongation ($mm^2$) and $L_o$ is the original length ($mm^2$). The Young's modulus, or the modulus of elasticity (E), is calculated as the slope of a linear stress vs strain graph. In the linear region, the line obeys Hooke's law, where the ratio of stress to strain is a constant:

$$E = \sigma / \varepsilon \quad \text{(Pascal, Pa)}$$

The modulus of elasticity refers to the stiffness of a material but only in the linear region. If the load is removed within this region the specimen will return to its original condition. However, if the load remains, the curve is no longer linear and so Hooke's law does not apply.[183]

### 2.2.2 Differential Scanning Calorimetry

Differential scanning calorimetry (DSC) is a thermoanalytical technique which measures a physical property of a material as a function of temperature.[182] The process involves measuring the energy needed to maintain an almost zero temperature difference between a sample and an inert reference material in an assembly where the two materials are subjected to the same heating conditions (Fig.2.2).[184] The sample holder is commonly an aluminium pan, and the reference material is either an empty pan or a pan containing an inert material such as anhydrous alumina.[181] A constant flow of nitrogen gas is maintained over the samples to create a reproducible and dry atmosphere, and it also eliminates air oxidation of the samples from occurring at high temperatures. [185]

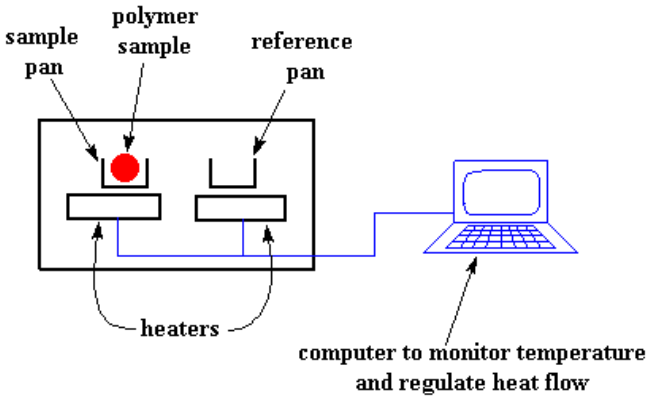


**Fig. 2.2:** Schematic representation of a DSC assembly.[186]

The DSC profile for a typical polymer is shown in Fig. 2.3. The shift in baseline at the starting transient can be calculated as the heat capacity, $C_p$.[185] After further heating the sample goes through a small endothermic event which is the glass transition, $T_g$. Above the glass transition phase, the polymer is more mobile and has gained enough energy to move into an ordered arrangement.[186] This is the crystallisation phase and is observed as an exothermic event in the DSC profile. The crystallisation temperature, $T_c$, is the lowest point of this peak and the area of the peak is the latent energy of crystallisation of the material.[186] Further heating results in another phase transition, melting. Upon melting, the crystals begin to move more freely and lose their ordered arrangement. This is observed as an endothermic event. The melting temperature, $T_m$, is the highest point of the peak and the area of the peak is the latent heat of melting.[186]

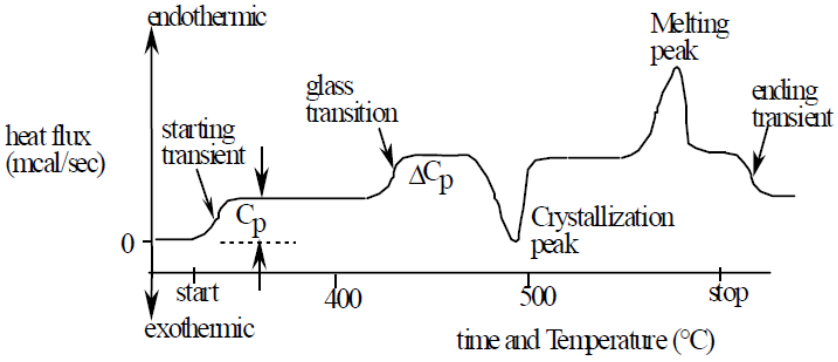


**Fig. 2.3:** DSC profile for a typical polymer sample.[185]

### 2.2.3 Proteomics

Proteomics is the study of the proteome which is described as the set of proteins encoded by the genome.[187] As 1-dimensional electrophoresis separates proteins on the basis of molecular weight, 2-dimensional electrophoresis is used in proteomic analysis as it provides comprehensive resolution of complex protein mixtures.

Proteins carry positive, negative or zero net charges depending on the pH of the solution.[188] Each protein has a specific isoelectric point (pI) where the net charge is zero, and it is this property which is exploited for first dimension isoelectric focusing (IEF) which separates proteins based on their pI.[189] This is achieved by introducing the immobilised pH gradient (IPG) strip containing the protein to a pH gradient using carrier ampholytes and then applying an electric potential difference across the strip (Fig. 2.4). During electrophoresis, the net charge on the protein will determine which direction the protein will migrate; at a pH value below the pI the protein will migrate towards the cathode and at a pH value above its pI, it will travel towards the anode.[188] Following IEF, strips must be equilibrated to ensure that the proteins are denatured, and this allows for efficient separation based on molecular weight.[190] Dithiothreitol (DTT) is used to reduce inter- and intra-disulphide bonds in proteins, whereas iodoacetamide (IAA) is used as an alkylating agent to prevent the reformation of these bonds by alkylating the sulphur atoms.[190] Once the strips are equilibrated, they are ready for separation in the second dimension.

**Fig. 2.4:** Isoelectric focusing experimental assembly.

Sodium dodecyl sulphate-polyacrylamide gel electrophoresis (SDS-PAGE) separates proteins based on their molecular weight and makes up the second dimension. Polyacrylamide gel is the main medium for protein electrophoresis and it can be cast in a multi-chamber gel casting unit (Fig. 2.5 (a)). The polyacrylamide gel is prepared using acrylamide, bisacrylamide and SDS with the polymerization reaction being aided by ammonium persulfate (APS) and N,N,N',N'-tetramethylethylenediamine (TEMED). APS acts as a catalyst, TEMED is used to form the free radicals needed for polymerisation[191] and bisacrylamide functions as a cross-linker in the gel.[190] TEMED accelerates the decomposition of persulphate molecules into sulphate free radicals, which in turn initiates the polymerisation.[191] The IPG strip containing the isoelectrically focused proteins is then placed in contact with the SDS-PAGE gel, which is then covered with agarose sealing solution containing added bromophenol blue to act as a tracking dye. The electric current in the electrophoresis cell (Fig. 2.5 (b)) is carried by the ions in the running buffer. Smaller molecular weight proteins migrate through the gel faster, with the larger molecular weight proteins remaining near the top of the gel. Gels are subsequently stained to visualise protein spots, excised and digested for mass spectrometry analysis.

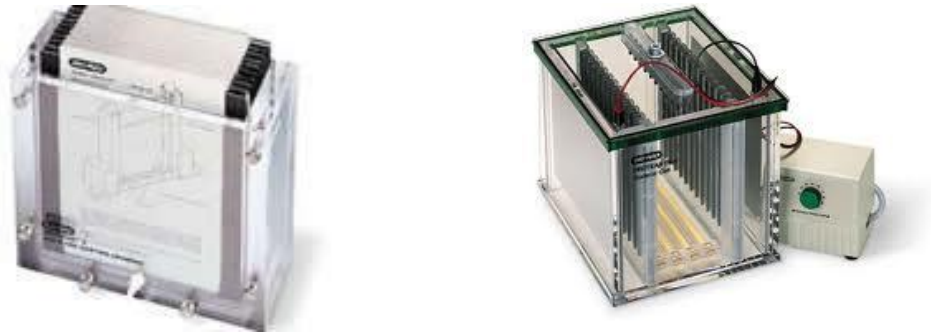

**(a)** **(b)**

**Fig. 2.5:** SDS-PAGE (a) multi-chamber gel casting unit and (b) electrophoresis apparatus.

### 2.2.4 Electrochemistry

A three-electrode electrochemical assembly was used (Fig. 2.6). The working electrode was a glassy carbon (GC) with a diameter of 2 mm, the auxiliary or counter

electrode was a platinum wire and the reference electrode was a saturated calomel electrode (SCE). The working electrode is the electrode at which the analyte is oxidised or reduced.[192] The counter electrode provides a pathway for current to flow in the electrochemical cell without passing significant current through the reference electrode.[193] Platinum is the most commonly used counter electrode due to its inertness and the speed at which most electrode reactions occur at its surface.[193] The SCE works using the calomel redox couple and therefore contains chloride ions. To prevent the precipitation of AgCl, the SCE electrode was separated from the test solution and placed in a separate cell with filter paper as a salt-bridge circuit connection. The SCE is a half cell composed of mercurous chloride ($Hg_2Cl_2$, calomel) in contact with mercury metal. The half reaction is described by;[194]

$$Hg_2Cl_{2(s)} + 2e^- \rightleftharpoons 2Hg_{(l)} + 2Cl^-$$

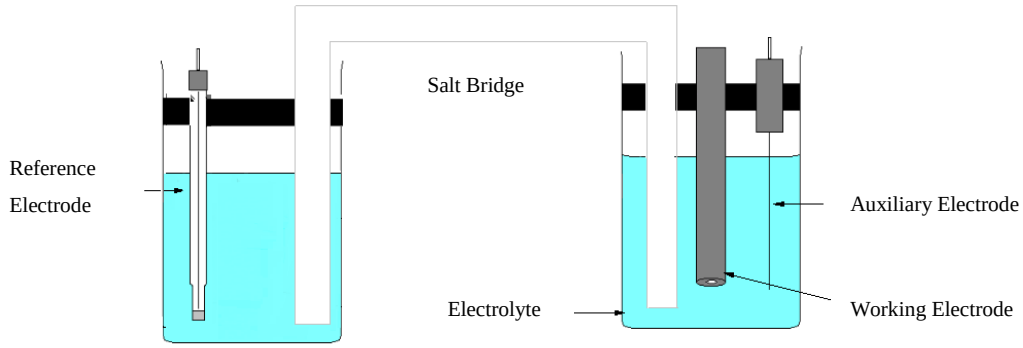


**Fig. 2.6:** Electrochemical cell assembly.

All electrode reactions are conducted using a non-reactive supporting electrolyte.[192] The electrolyte, $NaNO_3$, is a salt added in excess to the analyte solution and is the principal source of electrically conducting ionic species and has a concentration of at least 100 times that of the electroactive species.[195]

Metal deposition involves a constant potential being applied to the GC working electrode causing the reduction of the Ag(I) ions in the sample and their deposition as Ag(0) on the GC electrode surface.[192] The electrode is maintained at this potential for 60 s, followed by an anodic stripping. In anodic stripping, the working electrode

behaves as a cathode during the deposition step and as an anode during the stripping step, where the analyte is being oxidised back to its original form (Ag(0) → Ag(I)).[192] Following deposition, the potential of the electrode is increased linearly to more positive values (to oxidise deposited Ag(0) back to Ag(I) ions), while the current in the cell is recorded as a function of time or potential.[192] Linear sweep voltammetry (LSV) involves the sweeping of the electrode potential between the limits $E_i$ and $E_t$ at a known sweep rate, *v*, before stopping the potential sweep.[196] A typical LSV response curve can be seen in Fig. 2.7. The scan begins at a potential more positive of $E^{0'}$ for the reduction, when only non-faradaic current flows.[197] Once the electrode potential reaches $E^{0'}$ the reduction begins and current starts to flow.[197] As the potential becomes more negative, analyte flux to the surface increases, resulting in a current increase.[197] As the potential proceeds past $E^{0'}$, the surface concentration drops almost to zero, mass transfer to the surface reaches a maximum and then declines once depletion sets in. This results in a peaked current-potential curve (Fig. 2.7).[197]

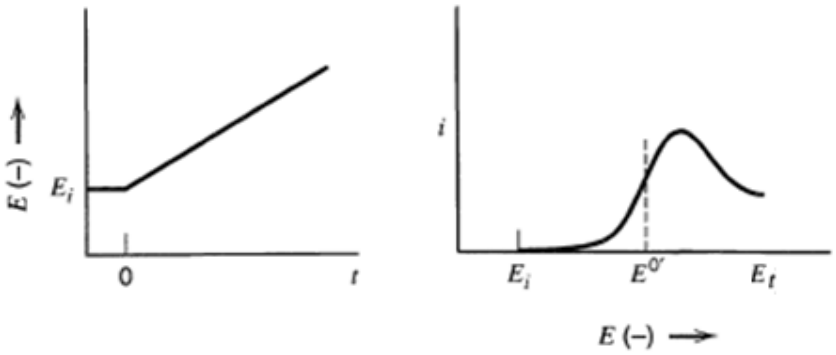


**(a)** **(b)**

**Fig. 2.7: (**a) Linear potential sweep or ramp starting at $E_i$ and (b) resulting *i-E* curve.[197]

The oxidation/reduction of silver is a reversible $1e^-$ process,

$$Ag^+ + 1e^- \rightleftharpoons Ag^0$$

and so the Nernst equation can be used to derive the expression:[198]

$$E_{1/2} = E^{0'} + RT/nF \ln C^*_{Ag+}$$

Where $C^*_{Ag+}$ is the Ag(I) ion concentration, $E_{1/2}$ is the half-wave potential, R is the gas constant (8.314 $J K^{-1} mol^{-1}$), T is temperature in K, n is the stoichiometric number of electrons involved in the process, F is the Faraday constant (96,485 C $mol^{-1}$).

Therefore, the half-wave reaction is expected to shift 60 mV with every ten-fold dilution of the Ag(I) ion.[198] In the present experiments, at relatively high concentrations of Ag(I) ions the behaviour followed this prediction. However, at lower Ag(I) ion concentrations, multiple-peaked curves were observed (Fig. 2.8).

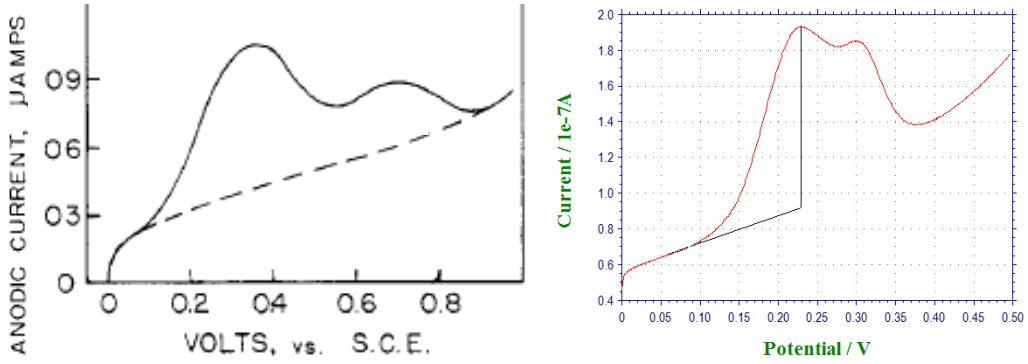


**(a)** **(b)**

**Fig. 2.8:** An example of multiple-peaked curves in Ag(I) ion analysis as found by (a) Perone *et al*[198] and (b) in the present study.

### 2.2.4.1 Experimental set-up

Cyclic voltammetry was performed on a standard silver nitrate solution (4.5 x $10^{-4}$ M) with the potential swept between 0.06 and -0.10 V, at a scan rate of 0.02 V/s. A reduction potential of 0.04 V was chosen for all silver deposition experiments. Silver was stripped from the electrode surface using linear sweep voltammetry (LSV), swept over the potential range of 0.2 to 1.0 V. A constant potential of 0.9 V was applied to ensure that all the silver was removed from the electrode and returned to

the solution. The electrode was removed, washed with deionised water and then polished with 0.05 µm alumina paste before the next measurement was recorded.

**Calculation of Ag(I) concentration**

1) Using peak height

   $I_p$: $1.5190 \times 10^{-7}$

   Divide by deposition time (60 s): $2.5317 \times 10^{-9}$

   Divide by slope (2.6899e-3): $9.4116 \times 10^{-7}$ $[Ag^+/M]$

2) Using charge

   Have to calculate charge first: Integrate the area under the curve using chi760c program (dataproc, integration), use cursor to find values on the right and left of curve and subtract these values from each other (left from right).

   Left: $9.440 \times 10^{-8}$, Right: $1.1940 \times 10^{-6}$, Charge: $1.0966 \times 10^{-6}$

   Divide by deposition time (60 s): $1.827 \times 10^{-8}$

   Divide by slope ($5.6780 \times 10^{-3}$): $3.2187 \times 10^{-6}$ $[Ag^+/M]$

### 2.2.5 Atomic absorption

Pre-weighed Ag(I)-Bioglue samples were ashed in a ceramic crucible over a Bunsen burner and the residue dissolved in aqueous nitric acid (20 mls, 50% (v/v)). The acid solutions of the samples were gravity filtered once the solution had cooled. The filtrates were placed in a 250 $cm^3$ volumetric flask and made up to the mark using distilled water. From this stock solution, a 1 in 25 dilution was carried out and the $Ag^{+1}$ content measured against a standard curve using known concentrations of $AgNO_3$.

**Calculation of Ag(I) content**

Weight of sample: 50 mg Absorbance: 0.088 mg/L

50mg in 250 ml of water: 50 / 0.25 = 200 mg/L

Divide by second dilution factor: 200 / 25 = 8 mg/L (theoretical conc. of sample)

% Ag(I): actual/theoretical * 100

Therefore: 0.088/8.00 * 100 = 1.1%

## 2.3 Chemicals, Yeast and Bacterial Strains

Starting material chemicals and assay kits were obtained from the commercial suppliers listed below. These chemicals were used without further purification.

**Table 2.1:** Commercial suppliers

| Chemical | Supplier |
|---|---|
| Agarose | Melford labs, Ltd. Ipswich, England |
| Alumina paste | Logitech Ltd., Erskine Ferry Rd., Old Kilpatrick, Glasgow, G60 5EU, Scotland. |
| Bacteriological peptone | Difco Labs. Le Pont de Claix, France |
| Bovine serum albumin | Sigma-Aldrich Chemical Company, St. Louis, USA |
| Bradford reagent | Bio-Rad, Munich, Germany |
| CHAPS | Sigma-Aldrich Chemical Company, St. Louis, USA |
| Deoxyribonuclease I (AMP-D1) kit | Invitrogen, CA, USA |
| Dithiothreitol (DTT) | Sigma-Aldrich Chemical Company, St. Louis, USA |
| D-Glucose | Sigma-Aldrich Chemical Company, St. Louis, USA |
| Glass vials | Agilent Technologies UK Limited, Lakeside, Cheadle Royal Business Park, Stockport, Cheshire SK8 3GR |

| | |
|---|---|
| Glutaraldehyde | Sigma-Aldrich Chemical Company, St. Louis, USA |
| Immobiline™ DryStrip | GE Healthcare Bio-Sciences AB, Uppsala, Sweden |
| IPG buffer pH 3-10 | GE Healthcare Bio-Sciences AB, Uppsala, Sweden |
| Nutrient agar | Oxoid Ltd., Basingstoke, Hampshire, England |
| Nutrient broth | Oxoid Ltd., Basingstoke, Hampshire, England |
| RNA protect bacteria reagent | Qiagen, Fleming way, Crawley, West Sussex, RH10 9NQ |
| RNeasy Minikit | Qiagen, Fleming way, Crawley, West Sussex, RH10 9NQ |
| Silver nitrate (99.0%) | Sigma-Aldrich Chemical Company, St. Louis, USA |
| Silver nitrate (99.9999%) | Sigma-Aldrich Chemical Company, St. Louis, USA |
| Spin filters | Corning Incorporated, Corning, NY, 14831 |
| Superoxide Dismutase Assay kit | Sigma-Aldrich Chemical Company, St. Louis, USA |
| Superscript III First-Strand Synthesis System | Invitrogen, CA, USA |
| 3,6,9-Trioxaundecanedioic acid | Sigma-Aldrich Chemical Company, St. Louis, USA |
| Thiourea | Sigma-Aldrich Chemical Company, St. Louis, USA |
| Triton-X 100 | Sigma-Aldrich Chemical Company, St. Louis, USA |
| Trypsin | Promega, Madison, WI, USA |
| Urea | Sigma-Aldrich Chemical Company, St. Louis, USA |
| Yeast extract | Oxoid Ltd., Basingstoke, Hampshire, England |

The yeast and bacterial strains used in this study are shown in Table 2.2.

**Table 2.2:** Microbial strains used in this study.

| Microbial Strain | Origin | Reference |
|---|---|---|
| *Candida albicans* 10231 | American Type Culture Collection (ATCC), Marassas, VA, USA | ATCC |
| *Pseudomonas aeruginosa* 10145 | American Type Culture Collection (ATCC), Marassas, VA, USA | ATCC |
| *Pseudomonas aeruginosa* 27853 | American Type Culture Collection (ATCC), Marassas, VA, USA | ATCC |
| *Escherichia coli* | Gastro-intestinal tract infection, St. James's Hospital, Dublin | Clinical Isolate |
| *Staphylococcus aureus* | Urinary tract infection, St. James's Hospital, Dublin | Clinical Isolate |
| *Methicillin-resistant Staphylococcus aureus (M.R.S.A.)* | American Type Culture Collection (ATCC), Marassas, VA, USA | ATCC |

## 2.4 Buffers

Lambert's breaks buffer

- KCl 10.0 mM
- NaCl 3.0 mM
- $MgCl_2$ 4.0 mM
- PIPES 10.0 mM

Glutathione Assay Buffer

- EDTA 1.0 mM
- $K_2HPO_4$ 100.0 mM
- pH 7.5

Ninhydrin Solution

- Ninhydrin 0.37 g
- Ethanol 100 mls

Iso-Electric Focusing (IEF) Buffer

- Urea 8.0 M
- Triton-X 100 1% (v/v)
- CHAPS 4% (w/v)
- Tris-HCl 10.0 mM
- Thiourea 2.0 M
- Dithiothreitol (DTT) 65.0 mM
- IPG buffer pH 3-10 0.8% (v/v)

Reducing Buffer for Equilibration

- Glycerol 30% (v/v)
- SDS 2% (w/v)

- Urea 6.0 M (w/v)
- Tris HCl 50.0 mM (w/v)
- Dithiothreitol (DTT) 2%
- pH 6.8

Alkylation buffer for Equilibration

- Glycerol 30% (v/v)
- SDS 2% (w/v)
- Urea 6.0 M (w/v)
- Tris HCl 50.0 mM (w/v)
- Iodoacetamide (IAA) 2.5%
- pH 6.8

Solutions and buffers used in 1- and 2- dimensional electrophoresis are listed below.

Stacking Gel Buffer

- Tris-HCl 0.5 M
- pH 6.8

Separating Gel Buffer

- Tris-HCl 1.5 M
- pH 8.8

10X Running Buffer

- Tris-HCl 20 mM
- Glycine 200 mM
- SDS 0.1% (w/v)

Running buffer was diluted to 1X prior to running gels. pH 8.9

Ammonium Persulphate (APS)

- APS 10% (w/v) in distilled water

Sodium Dodecyl Sulphate (SDS)

- SDS 10% (w/v) in distilled water

Sample Buffer (10X)

- 0.5M Tris-HCl 1 ml, pH 6.8
- Glycerol 1.6 ml
- 10% SDS 1.6 ml
- β-Mercaptoethanol 0.4 ml
- 0.5% (w/v) Bromophenol Blue 0.4 ml
- Distilled $H_2O$ 3 ml

Coomassie Staining Solution

- Brilliant Blue 0.2% (w/v)
- Methanol 45% (v/v)
- Acetic Acid 10% (v/v)
- Distilled $H_2O$ 44.8 % (v/v)

Destain Solution

- Acetic Acid 10% (v/v)
- Methanol 20% (v/v)
- Distilled $H_2O$ 70% (v/v)

Colloidal Fixing Solution

- Ethanol 50% (v/v)

- Phosphoric Acid 3% (v/v)
- Distilled $H_2O$ 47% (v/v)

Colloidal Coomassie Staining Solution

- Methanol 34% (v/v)
- Phosphoric Acid 3% (v/v)
- Ammonium Sulphate 17% (w/v)
- Serva Blue ≈ 0.4 g
- Distilled $H_2O$ 46% (v/v)

2.5% Polyacrylamide Stacking Gel

- Distilled $H_2O$ 3.4 ml
- Acrylamide 0.83 ml
- 0.5M Tris-HCl 0.63 ml
- 10% (w/v) SDS 0.05 ml
- 10% (w/v) APS 0.05 ml
- TEMED 0.005 ml

12.5% Polyacrylamide Separating Gel

- 1.5M Tris-HCl 3 ml
- Distilled $H_2O$ 3.8 ml
- Acrylamide 5 ml
- 10% (w/v) SDS 0.12 ml
- 10% (w/v) APS 0.075 ml
- TEMED 0.003 ml

Agarose Sealing Solution

- Agarose 1% (w/v)

- Bromophenol Blue 0.5 % (w/v)
- 1X Running Buffer 100 ml

Y1 buffer

- Sorbitol 1 M
- EDTA 0.1 M (pH 7.4)
- β-mercaptoethanol 0.1% (v/v)
- Zymolase 0.125 g/sample

10X FA gel buffer

- MOPS 200 mM
- Sodium acetate 50 mM
- EDTA 10 mM, pH 7

A 1/10 dilution of this was made for 1X running buffer

cNDA synthesis master mix

- 10X RT buffer 2 µl (supplied)
- 25 mM $MgCl_2$ 4 µl
- 0.1 M DTT 2µl
- RNaseOUT 1 µl (supplied)

# 2.5 IR spectra of starting materials

## 2.5.1 IR spectrum of bovine serum albumin (BSA) (KBr)

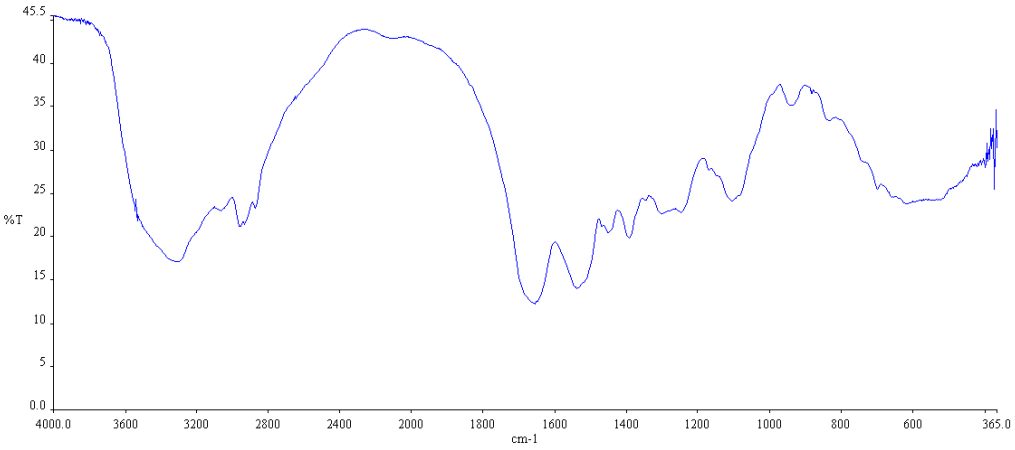


## 2.5.2 IR spectrum of gluteraldehyde (GLA) (thin film between NaCl plates)

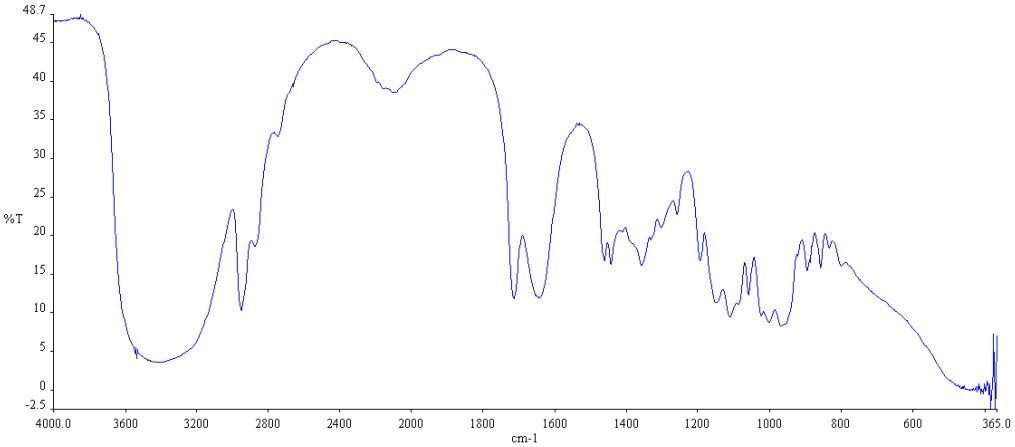

### 2.5.3 IR spectrum of 3,6,9-trioxaundecandioic acid (3,6,9-tddaH$_2$) (thin film between NaCl plates)

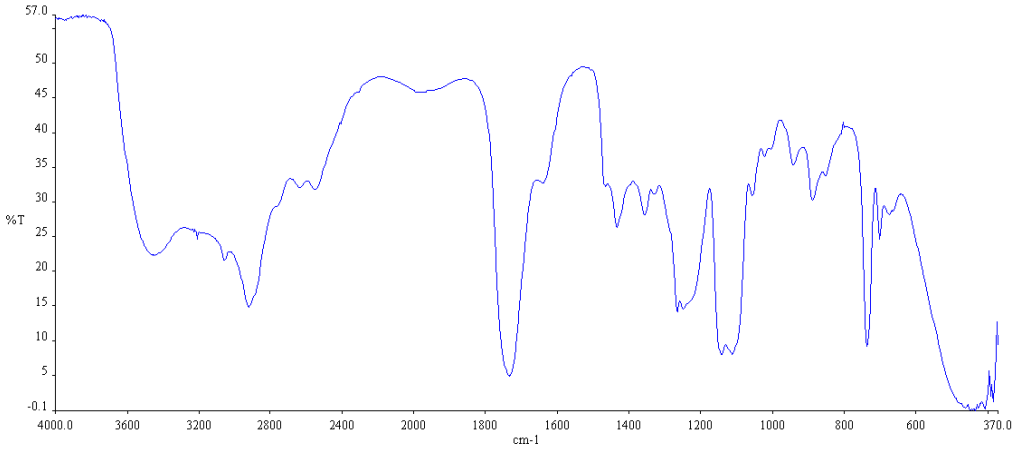


### 2.5.4 IR spectrum of $AgNO_3$ (KBr)

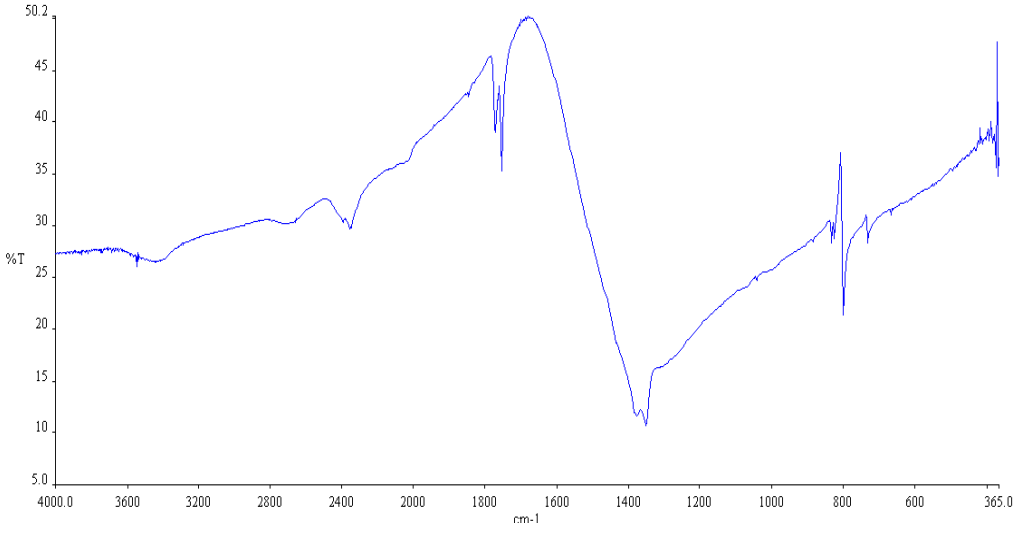

# 2.6 UV-Vis Spectra of Starting Materials

## 2.6.1 UV-Vis spectrum of bovine serum albumin (BSA) solution (1.5 x $10^{-3}$ M)

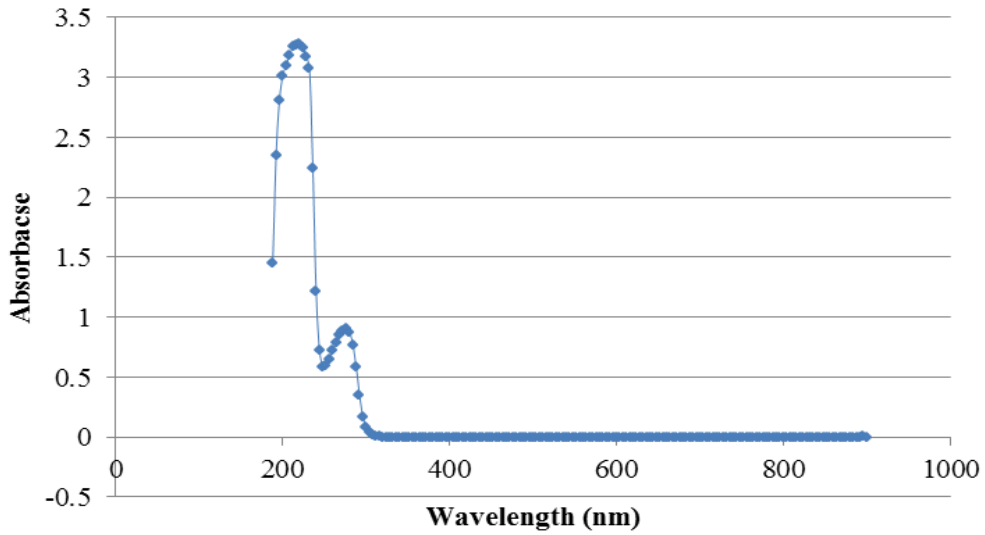


## 2.6.2 UV-Vis spectrum of glutaraldehyde (GLA) solution (1.1 M)

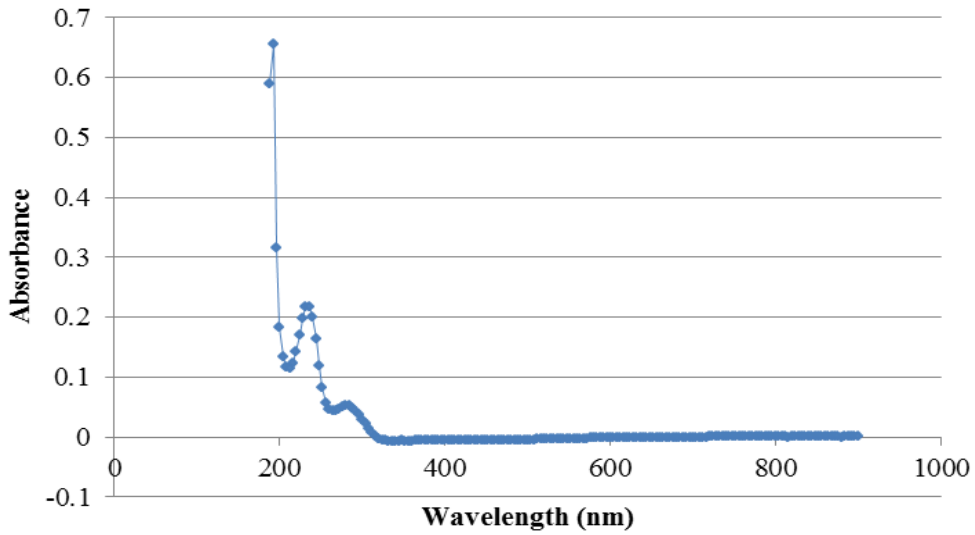

### 2.6.3 UV-Vis spectrum of $AgNO_3$ (0.05 M)

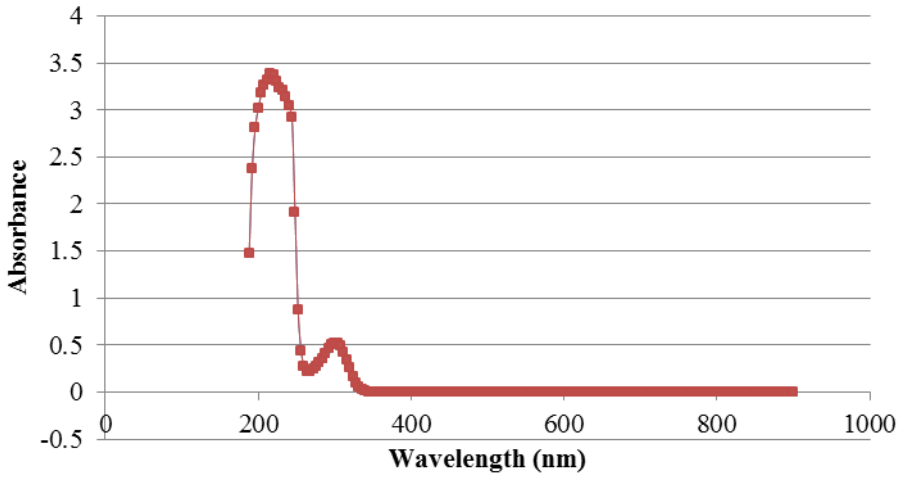


### 2.6.4 UV-Vis spectrum of sodium borohydride ($NaBH_4$) (0.01 M)

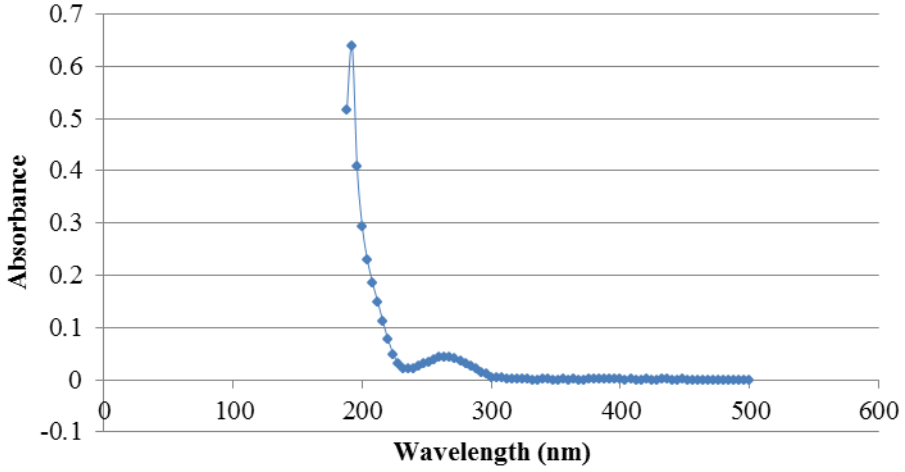

### 2.6.5 UV-Vis spectrum of sodium citrate (0.04 M)

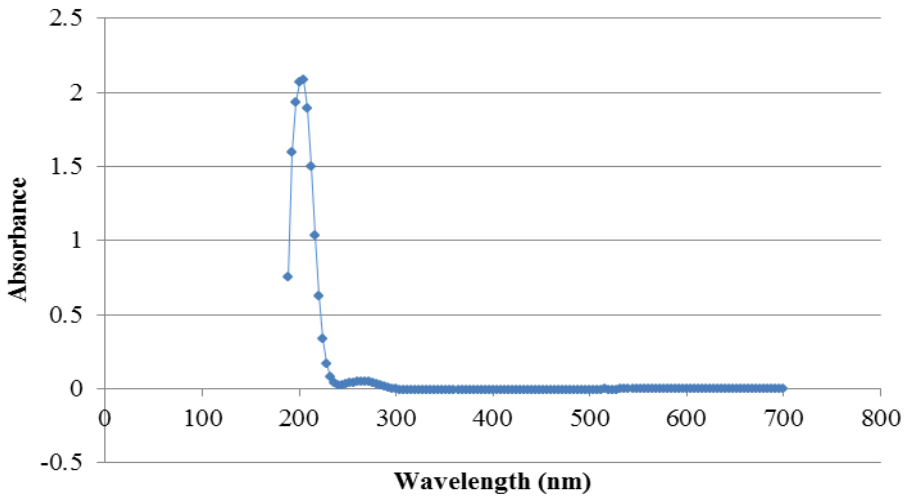


All reactions involving Ag(I) ions were conducted in the dark. All Ag(I)-containing samples were stored in the absence of light.

## 2.7 Synthesis of Silver(I) Complex of 3,6,9-Trioxaundecanedioic Acid (3,6,9-tddaH$_2$)

### 2.7.1 Determination of the concentration of the supplied solution of 3,6,9-trioxaundecanedioic acid (3,6,9-tddaH$_2$) using standardised NaOH

Sodium hydroxide (2.00 g, 50.00 mmoles) was weighed out accurately and dissolved in distilled water (100.0 mls). This solution was transferred to a 500 ml volumetric flask and made up to the mark. Oxalic acid $(COOH)_2$ (2.25 g, 25.00 mmoles) was weighed out accurately and dissolved in distilled water (100.0 mls). This solution was transferred to a 250 ml volumetric flask and made up to the mark to give a standard solution of oxalic acid. This standard $(COOH)_2$ solution was titrated against the NaOH solution using phenolphthalein indicator. The titration was carried out three times in order to obtain reproducible results and establish the concentration of the NaOH solution (0.098 M). The NaOH solution was then titrated against the supplied 3,6,9-trioxaundecanedioic acid solution (2.00 g, 9.00 mmoles) using

phenolphthalein as the indicator. Again, three titrations were carried out to obtain reproducible results and to establish the concentration of the 3,6,9-tddaH$_2$ solution (0.08 M).

### 2.7.2 Synthesis of [Ag$_2$(3,6,9-tdda)].2H$_2$O using a known concentration of 3,6,9-tddaH$_2$, NaOH and AgNO$_3$

Using the values calculated from the titrations in Section 2.4.1, 3,6,9-tddaH$_2$ (1.48 g, 6.66 mmoles) was added to ice-cold H$_2$O (10.0 mls). NaOH (0.098 M) and AgNO$_3$ (2.00 g, 11.77 mmoles) along with 3,6,9-tddaH$_2$, were added to a conical flask on ice and left stirring in the dark for 4 h. This suspension was filtered using a glass frit and the brown solid was washed with ice-cold water, ethanol and ether. The solid was dried under high vacuum and stored in the absence of light.

Yield: 1.04 g (36.4%)

### 2.7.3 Synthesis of silver(I) complex [Ag$_2$(3,6,9-tdda)].2H$_2$O from the potassium salt K$_2$(3,6,9-tdda) and AgNO$_3$

Potassium hydroxide (0.90 g, 16.04 mmoles) was weighed out accurately and dissolved in distilled water (10.0 mls) and the solution was then cooled on ice. 3,6,9-TddaH$_2$ (1.20 g, 5.41 mmoles) was made up to 10.0 mls and stirred on ice. To this stirred solution, the aqueous KOH solution was added until pH=7 (monitored using a pH meter). The solution was transferred to a 25 ml volumetric flask and made up to the mark using distilled water to give a stock solution of K$_2$(3,6,9-tdda) (1.6 M). The stock solution of K$_2$(3,6,9-tdda) (3.0 mls, 0.2 M) was transferred to a conical flask containing distilled water (20.0 mls). To this stirred solution, a solution of AgNO$_3$ (0.15 g, 0.88 mmoles) in distilled water (2.0 mls) was added drop-wise. The solution was allowed to stir in the dark for 4 h. Acetone (50.0 mls) was added and the mixture allowed to stir for a further 1 h. The resulting suspension was filtered using a glass frit and the pinkish-white solid was washed with ice-cold water, acetone and ether. The solid was dried under high vacuum and stored in the absence of light.

Yield: 0.139 g (72.8%)

[$Ag_2$(3,6,9-tdda)].2$H_2O$ Calc. Molecular Weight: 471.95 g $mol^{-1}$

Mass Spectrometry Found: (245.06, 3,6,9-tdda$H_2$ + $Na^+$), (434.87, 436.87, 438.87 [$Ag_2$(3,6,9-tdda)]$^+$) g $mol^{-1}$ (see Appendix I)

Anal. Calc.: H, 2.56; C, 20.36; Ag, 45.71% ($C_8H_{16}O_{10}Ag_2$)

Anal. Found: H, 2.50; C, 20.34; Ag, 45.48%

Solubility: soluble in hot $H_2O$ and hot DMSO

IR (KBr): 3425 (O-H), 2896 (C-H), 1614 $_{asym}$ (O-C-O), 1406 $_{sym}$ (O-C-O), 1116 (C-O-C) $cm^{-1}$

$^1$H NMR ($D_2O$, ppm): 3.81 (s, 4H), 3.56 (s, 8H)

IR (KBr): [$Ag_2$(3,6,9-tdda)].2$H_2O$

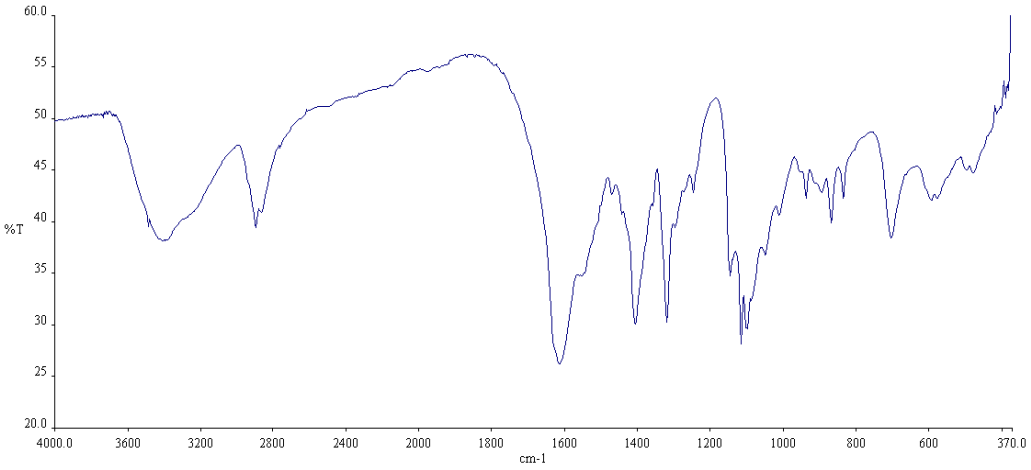

$^{1}$H NMR ($D_2O$, ppm): 3,6,9-tddaH$_2$

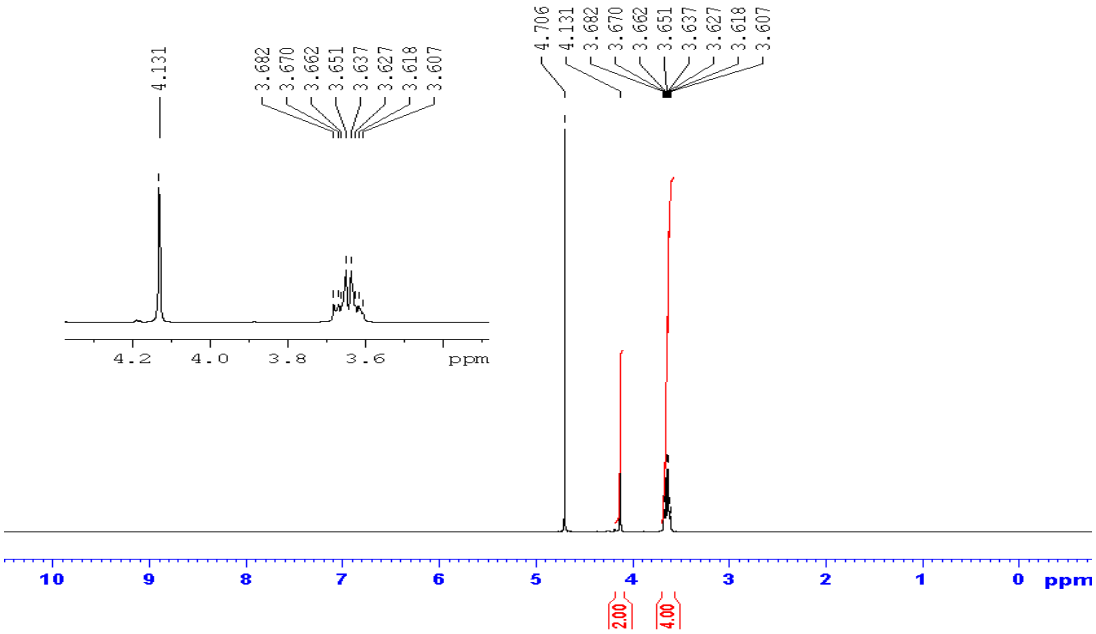


$^{1}$H NMR ($D_2O$, ppm): [Ag$_2$(3,6,9-tdda)].2H$_2$O

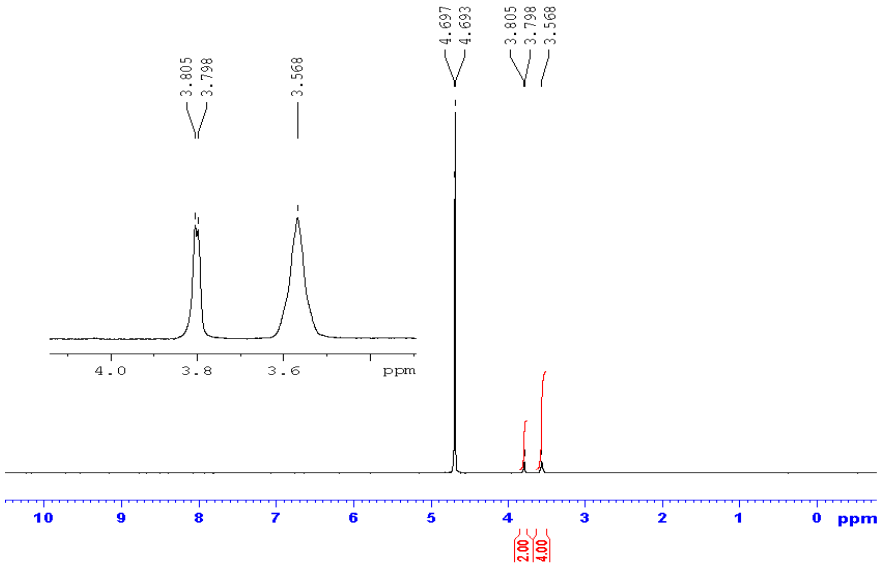

# 2.8 Synthesis of Bioglue

### 2.8.1 Preparation of bovine serum albumin/glutaraldehyde Bioglue

Bovine serum albumin (BSA) (0.50 g, 7.46 x $10^{-3}$ mmoles) was added to distilled water (2.0 mls) and the mixture vortexed until all the solid had dissolved. A stock solution of glutaraldehyde (GLA) (0.11 g, 1.09 mmoles) was prepared in distilled water (1 ml). The GLA solution (0.25 mls) was slowly added by a 1 ml pipette to the BSA solution. The mixture was vortexed briefly and after approximately 2 min the golden-coloured, gel-like Bioglue formed. The sample was dried under high vacuum to a constant weight.

Yield: 0.49 g

IR (KBr): 3435 (N-H, O-H), 2862 (C-H), 1647 (C=O), 1534 (N-H), 1446 (C-H) $cm^{-1}$

IR (KBr): Bovine Serum Albumin/Glutaraldehyde Bioglue

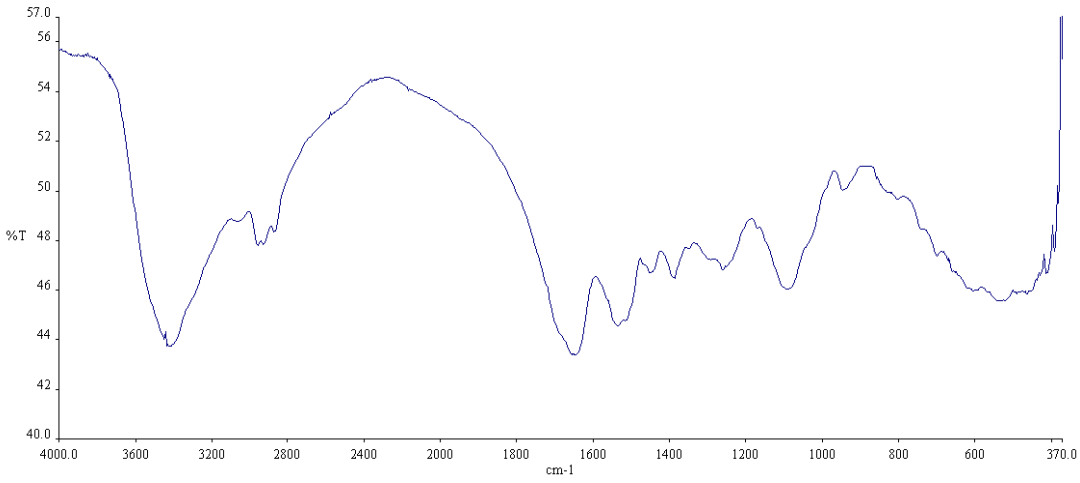


# 2.9 Synthesis of Ag(I)-Containing Bioglues

### 2.9.1 Preparation of bovine serum albumin/glutaraldehyde Bioglue encapsulating various amounts of added $AgNO_3$

The general procedure for the preparation of a Bioglue encapsulating $AgNO_3$ (0.10 g) is outlined below.

BSA (0.50 g, 7.46 x $10^{-3}$ mmoles) was added to distilled water (1.0 ml) and vortexed until the solid had dissolved. A stock solution of GLA (0.11 g, 1.09 mmoles) was prepared in distilled water (1.0 ml). Silver nitrate (1.00 g, 5.89 mmoles) was dissolved in water (10.0 mls). Solutions of GLA (0.25 mls) and $AgNO_3$ (1.0 ml) were mixed in a test-tube and then added slowly to the BSA solution. The mixture was vortexed briefly. The gel-like Bioglue did not form. The mixture was originally white in colour turning orange as the reaction progressed. The sample was dried under high vacuum to a constant weight and stored in the absence of light.

Yield: 0.57 g

Ag(I)-Bioglues containing varying weights of added $AgNO_3$ (0.01-0.0001 g) were prepared using the same method. These preparations resulted in the formation of an orange to golden-coloured gel with a sticky consistency.

IR (KBr): 3408 (N-H, O-H), 2875 (C-H), 1656 (C=O), 1536 (N-H), 1439 (C-H), $cm^{-1}$

IR (KBr): Bovine Serum Albumin/Glutaraldehyde Bioglue Encapsulating $AgNO_3$ (0.10 g)

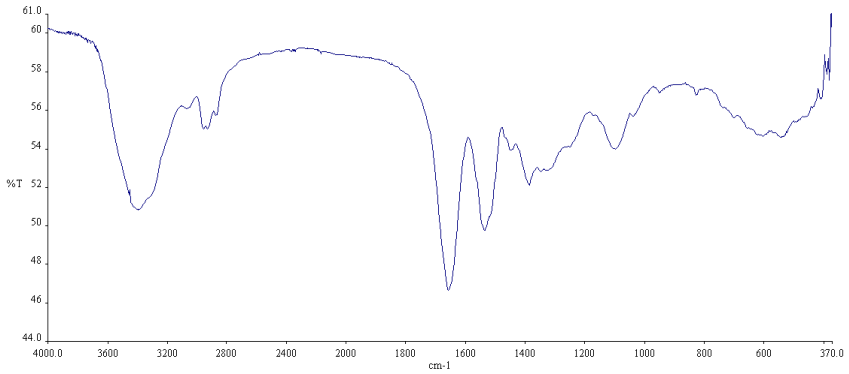

### 2.9.2 Preparation of bovine serum albumin/glutaraldehyde Bioglue encapsulating various amounts of the disilver(I) salt of 3,6,9-trioxaundecanedioic acid [$Ag_2$(3,6,9-tdda)].2$H_2O$

The general procedure for the preparation of a Bioglue encapsulating [$Ag_2$(3,6,9-tdda)].2$H_2O$ (0.010 g) is outlined below.

BSA (0.50 g, 7.46 x $10^{-3}$ mmoles) was added to distilled water (1.0 ml) and vortexed until the solid was dissolved. A stock solution of GLA (0.11 g, 1.09 mmoles) was prepared in distilled water (1.0 ml). A stock solution [$Ag_2$(3,6,9-tdda)].2$H_2O$ (0.10 g, 0.21 mmoles) was dissolved in water (10.0 mls) with heat. Solutions of GLA (0.25 mls) and [$Ag_2$(3,6,9-tdda)].2$H_2O$ (1.0 ml) were mixed in a test-tube and were slowly added to the BSA solution. The mixture was vortexed briefly and after approximately 2 min the gel-like Bioglue formed. The sample was dried under high vacuum to a constant weight and was stored in the absence of light.

Yield: 0.51 g

Ag(I)-Bioglues containing varying weights of added [$Ag_2$(3,6,9-tdda)].2$H_2O$ (0.001-0.00001 g) were prepared using the same method. These preparations resulted in the formation of an orange to golden-coloured gel with a sticky consistency.

IR (KBr): 3415 (N-H, O-H), 2867 (C-H), 1652 (C=O), 1539 (N-H), 1443 (C-H) $cm^{-1}$

IR (KBr): Bovine Serum Albumin/Glutaraldehyde Bioglue Encapsulating [$Ag_2$(3,6,9-tdda)].2$H_2O$ (0.01 g).

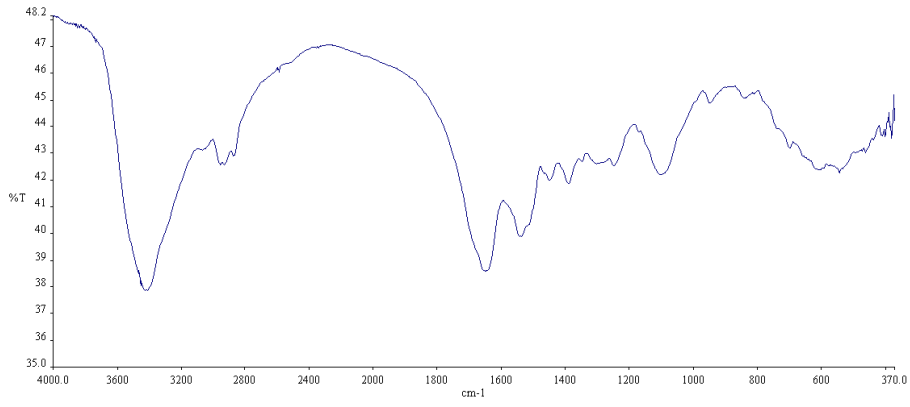

## 2.10 Bioglue Swelling Studies

A similar procedure to that used by Butler *et al*,[199] who prepared a gel (already hydrated to some extent), and after allowing to stand for 16 h, then proceeded to conduct swelling measurements by placing pre-hydrated gels in either aqueous acid or aqueous base (pH range 1-12) and measuring the swelling ratio (r). It should be noted that their swelling measurements were not conducted starting from a pre-hydrated polymer sample.[199] In the current experiments, a freshly made, partially hydrated Bioglue was used as a starting point for the swelling studies. Each Bioglue sample was made in triplicate (Section 2.8.1, 2.9.1 and 2.9.2) and allowed to stand overnight. Before proceeding with the swelling measurements, the initial weight of the sample was recorded. Each sample was placed in a beaker containing water (25 mls) and the beaker was then placed into a water bath to maintain a constant temperature (25 °C). At each time point, the Bioglue sample was removed from the beaker, pat dried using filter paper and weighed before being returned to the beaker. Every 3 h the water volume was restored to 25 mls. This process was repeated until an equilibrium mass was achieved. The swelling ratio (r), was determined using the following equation:[199]

$$r = (m_f\text{-}m_i/m_i) \times 100\%$$

where $m_f$ is the final mass and $m_i$ is the initial mass.

## 2.11 Synthesis of Ag(0) Nanoparticles

### 2.11.1 Reduction of Bioglue samples with and without added $AgNO_3$ using sodium borohydride

$NaBH_4$ (0.95 g, 25.01 mmoles) was weighed out and made up to 250 mls with deionised water in a clean, dry volumetric flask to give a 0.1 M solution. The flask was inverted with caution due to the production of $H_2$. A 1:10 dilution of this solution was made to give a 0.01 M solution. A further 1 in 10 dilution was made to yield a 0.001 M solution of $NaBH_4$. The three separate $NaBH_4$ solutions (45 mls) were each poured into a falcon tube. The Bioglue samples, without Ag(I) ions

(Section 2.8.1) and with added $AgNO_3$ (0.01 g) (Section 2.9.1), were prepared in triplicate and left for 1 h in the relevant $NaBH_4$ reducing solution. The liquid was decanted off and the Bioglue samples were washed three times with deionised water.

### 2.11.2 Reduction of Bioglue samples, with and without added $AgNO_3$, using sodium citrate

Bioglue samples, without Ag(I) ions (Section 2.8.1) and with added $AgNO_3$ (0.01 g) (Section 2.9.1), were prepared in triplicate. The Bioglues were placed in beakers containing the relevant solvent (25 mls) and then treated under the following three different experimental conditions: i) water and exposed to light, ii) sodium citrate solution (1%, w/v) and light, and iii) sodium citrate solution (1%, w/v) only (stored in the dark). The samples were kept at 25 °C and left for 1 week.

### 2.11.3 Reduction of Ag(I) to Ag(0) using sodium citrate

A procedure similar to that used by Liu *et al*[200] was employed for the production of Ag(0) nanoparticles. $AgNO_3$ (0.031 g, 0.185 mmoles) was added to deionised water (175 ml) and the resulting solution was heated to 100 °C. To this hot, stirred solution was added, drop-wise, an aqueous solution of sodium citrate (4 mls, 1% w/v) and the mixture allowed to stir for 35 min. After cooling to room temperature, deionised water (200 mls) was added to yield a suspension of $10^{-4}$ g/ml Ag(0) nanoparticles. The yellow/green suspension was preserved in the dark at 4 °C.

UV-Vis of suspension ( $\lambda_{max}$): 424 nm

### 2.11.4 Interaction of Bioglue (without Ag(I) ions) with an Ag(0) nanoparticle suspension

The Bioglue samples, without Ag(I) ions (Section 2.8.1), were prepared in triplicate and were placed in beakers containing a diluted Ag(0) nanoparticle suspension (Section 2.11.3) (66 mls made up to 100 mls with deionised water) and left to stand for 120 h in the dark. A control experiment was conducted by placing the Bioglue

samples in deionised water only (100 mls) and leaving to stand for 120 h. The UV-Visible spectra of the Ag(0) nanoparticle suspension and deionised water were recorded initially, every hour up to 12 h and then every 24 h until the end of the experiment.

## 2.12 UV-Vis Studies of Bioglue Supernatant

Each Bioglue sample (with and without Ag(I) ions) was placed in a falcon tube containing deionised water (45 mls) and left to stand for 1 week. The supernatant was centrifuged at 78 x g for 30 min and the UV-Visible absorption was recorded to determine if Ag(0) nanoparticles were present. Deionised water was used as a blank.

## 2.13 Fungal and Bacterial Growth Media

### 2.13.1 Media for culturing yeast

**Yeast Extract Peptone Dextrose (YEPD)**

YEPD media was prepared using yeast extract (2% (w/v)), bacteriological peptone (2% (w/v)) and D-glucose (1% (w/v)) in distilled water, and the mixture was autoclaved and stored at 4 ˚C until further use.

To make YEPD agar plates, agar (2% (w/v)) was added to the medium, autoclaved and poured into sterile petri dishes and stored at 4 ˚C until further use.

### 2.13.2 Media for culturing bacteria

**Nutrient Broth**

Nutrient broth (13 g/L) was prepared in distilled water and autoclaved prior to use.

**Nutrient Agar**

Nutrient agar (28 g/L) was prepared in distilled water, autoclaved, poured into sterile petri dishes and stored at 4 ˚C for further use.

## 2.14 Fungal and Bacterial Culture Conditions

### 2.14.1 Fungal culture conditions

All parent yeast stocks were kept in a sterile mixture of 50% (v/v) glycerol and 50% YEPD media (v/v) at -70 ˚C for long-term storage. Yeast strains were grown on YEPD agar plates at 37 ˚C for 24 h and kept at 4 ˚C for short-term storage. Working stocks of the yeast were routinely sub-cultured onto fresh agar plates every 4-6 weeks. For liquid culturing, yeast strains were cultured overnight in a fully aerated conical flask in an orbital shaker at 37 ˚C and 200 rpm using YEPD as the medium.

### 2.14.2 Bacterial culture conditions

All parent bacterial stocks were kept in a sterile mixture of 50% (v/v) glycerol and 50% nutrient broth media (v/v) at -70 ˚C for long-term storage. Bacterial strains were grown on nutrient agar plates at 37 ˚C for 24 h and kept at 4 ˚C for short-term storage. Working stocks of the bacteria were routinely sub-cultured onto fresh agar plates every 4-6 weeks. For liquid culturing, bacterial strains were cultured overnight in a fully aerated conical flask in an orbital shaker at 37 ˚C and 200 rpm using nutrient broth as the medium.

## 2.15 Determination of Fungal and Bacterial Cell Density

### 2.15.1 Determination of fungal cell density

Dilutions (1:20) of overnight yeast liquid cultures in YEPD medium were added to a haemocytometer (Neubauer) and cells were counted using a light microscope at a magnification of x 100.

### 2.15.2 Determination of bacterial cell density

The $OD_{600nm}$ of an overnight bacterial culture was determined using a spectrophometer.

## 2.16 Disk Diffusion Assay

### 2.16.1 Anti-fungal disk diffusion assay

Liquid cultures were grown in YEPD medium to the stationary phase (approximately $1x10^8$ cells $cm^{-3}$) overnight at 37 $^oC$ and in a shaking incubator at 200 rpm in YEPD medium. Cells were counted as described in Section 2.15.1. The culture was diluted in YEPD medium to yield a cell suspension that contained $1x10^6$ cells $cm^{-3}$. The culture (100 µl) was spread over a YEPD agar plate and placed in an incubator at 37 ˚C for 1 h. The solid test sample was placed on the plate, and the plates were then incubated for 24 h at 37 $^oC$. The zones of inhibition were measured and photographically recorded. This was obtained by measuring the area of the sample and the area of the sample plus the zone of inhibition. The area of the sample was then subtracted from the area of the sample plus the zone of inhibition to give the area of the zone of inhibition ($mm^2$). This procedure was repeated on three separate occasions.

### 2.16.2 Anti-bacterial disk diffusion assay

All bacterial strains were taken from nutrient agar plates and were cultured to the stationary phase ($OD_{600nm}$ of 2) overnight at 37 ˚C with shaking at 200 rpm in nutrient broth. The $OD_{600nm}$ of the overnight cultures was determined as described in Section 2.15.2. The culture was diluted with nutrient broth to yield a cell suspension with an $OD_{600nm}$ of 0.1. The culture (100 µl) was spread over a nutrient agar plate and placed in an incubator at 37 ˚C for 1 h. The solid test sample was placed onto the plate, which was then incubated for 24 h at 37 $^oC$. The zones of inhibition were measured and photographically recorded as described in Section 2.16.1. This procedure was repeated on three separate occasions.

## 2.17 Anti-Fungal and Anti-Bacterial Susceptibility Testing

### 2.17.1 Anti-fungal susceptibility testing

Cultures were grown to the stationary phase (approximately $1x10^8$ cells $cm^{-3}$) overnight at 37 $^oC$ and shaking at 200 rpm in YEPD medium. Cells were counted as described in Section 2.15.1. The culture was diluted in YEPD medium to yield a cell suspension that contained $5x10^6$ cells $cm^{-3}$. To each well of a 96–well round-bottomed plate, fresh YEPD medium (100 µl) was added. A stock suspension of compound (100 µl, 200 µg/ml) to be tested was prepared, added to each well (starting at the last column), and a serial dilution was carried out across the plate to the third column to give a concentration range of 0.195-100 µg/ml. Finally, yeast culture (100 µl, $5x10^6$ cells $cm^{-3}$) was added to each well apart from the first two columns. The plates were incubated at 30 ˚C overnight and the $OD_{540nm}$ of the plates was determined spectrophotometrically using a microplate reader. All micro-dilutions were performed on three separate occasions and the results analysed using Excel ©.

### 2.17.2 Anti-bacterial susceptibility testing

Bacterial strains were taken from nutrient agar plates and were cultured to the stationary phase ($OD_{600nm}$ of 2) overnight at 37 ˚C with shaking at 200 rpm in nutrient broth. The $OD_{600nm}$ of the overnight cultures was determined as described in Section 2.15.2. The culture was diluted to yield a cell suspension with an $OD_{600nm}$ of 0.1 in nutrient broth. To each well of a 96–well round-bottomed plate, fresh nutrient broth medium (100 µl) was added. A stock suspension of compound (100 µl, 200 µg/ml) to be tested was prepared, added to each well (starting at the last column), and a serial dilution was carried out across the plate to the third column to give a concentration range of 0.195-100 µg/ml. Finally, bacterial culture (100 µl, $OD_{600nm}$ 0.1) was added to each well apart from the first two columns. The plates were incubated at 37 ˚C overnight and the $OD_{540nm}$ of the plates was determined spectrophotometrically using a microplate reader. All micro-dilutions were performed on three separate occasions and the results analysed using Excel ©.

The $MIC_{80}$ (Minimum Inhibitory Concentration) of any given compound was taken to signify the concentration of compound that would inhibit the growth of that microorganism by 80%.

## 2.18 Whole Cell Protein Extraction

Liquid nutrient broth medium (100 ml) was inoculated with a loopful of bacterial culture, previously aseptically taken from a fresh culture plate, and grown to stationary phase ($OD_{600nm} \approx 2$). Silver nitrate ($MIC_{80}$ 3.0 μg/ml) was added and the cultures were grown for 1, 2 or 4 h. Cells were harvested by centrifugation for 10 min at 1814 x g and the cell pellet was washed twice with sterile phosphate buffered saline (PBS). Cells were re-suspended in Lambert's breaks buffer (2.0 mls). In addition, protease inhibitors, at a concentration of 10 μg/ml, were used (Leupeptin, Pepstatin A, Aprotinin and N-α-p-tosyl-L-lysine chloromethylketone hydrochloride (TLCK)). Two methods were employed to extract protein from *S. aureus* cells.

**1)** Cell suspensions were sonicated with two 10 sec blasts using a soniprobe sonicator to dislodge cell wall proteins. The suspension was then centrifuged at 239 x g for 4 min at 4 ˚C and the supernatant retained. Protein concentration was determined using the Bradford reagent.

**2)** Acid-washed glass beads (w/v) were added to the mixture and vortexed on ice for 5 min. The suspension was then centrifuged for 5 min at 454 x g and the resulting supernatant was centrifuged at 239 x g for 4 min at 4 ˚C. Protein concentration in the supernatant was determined using the Bradford reagent.

## 2.19 Enzymatic Assays

### 2.19.1 Glutathione reductase (GLR) assay

This assay is conducted as described by Foster and Hess[201] and is based upon the reduction of glutathione (GSSG) by NADPH in the presence of glutathione reductase (GLR).

$$NADPH + H^+ + GSSG \rightarrow NADP^+ + 2GSH$$

The reaction is monitored by a reduction in the absorption band for NADPH at λ=340 nm with the extinction co-efficient (ε) of 6.22 $mM^{-1}cm^{-1}$. After exposure of *S. aureus* cells to $AgNO_3$ over given time periods the cells were then lysed (Section 2.18) and centrifuged at 17,949 x g for 30 min at 4 ˚C. The supernatant was then used immediately after extraction. Into a 1 ml quartz cuvette was added oxidised glutathione (GSSG) (500 µl, 2.0 mM), glutathione assay buffer (400 µl), protein (50 µl, 1 µg/µl) and NADPH (50 µl, 2.0 mM). The reference assay blank contained oxidised glutathione (GSSG) (500 µl, 2.0 mM), assay buffer (450 µl) and NADPH (50 µl, 2.0 mM). The contents of the cuvette was mixed by gentle inversion and the absorbance monitored at λ=340 nm. After each reading, the cuvette containing the protein was emptied and washed with molecular biology grade absolute ethanol and then with the assay buffer before a new protein sample was added. The GLR activity was calculated as follows:

$$\text{GLR Activity (units/ml)} = \frac{\text{(Rate of change of sample-Rate of change of blank)}}{(6.22\ mM^{-1}cm^{-1} \times \text{Concentration of protein})}$$

**2.19.2 Superoxide dismutase (SOD) assay**

SOD activity of *S. aureus* cells treated with $AgNO_3$ was determined using the SOD Assay kit. The SOD activity was measured using the WST-1 tetrazolium salt, 2-(4-iodophenyl)-3-(4-nitrophenyl)-5-(2,4-disulphphenyl)-2*H*-tetrazolium monosodium salt, which produces a formazan dye upon reaction with a superoxide anion ($O_2^{-\bullet}$) (Scheme 1).

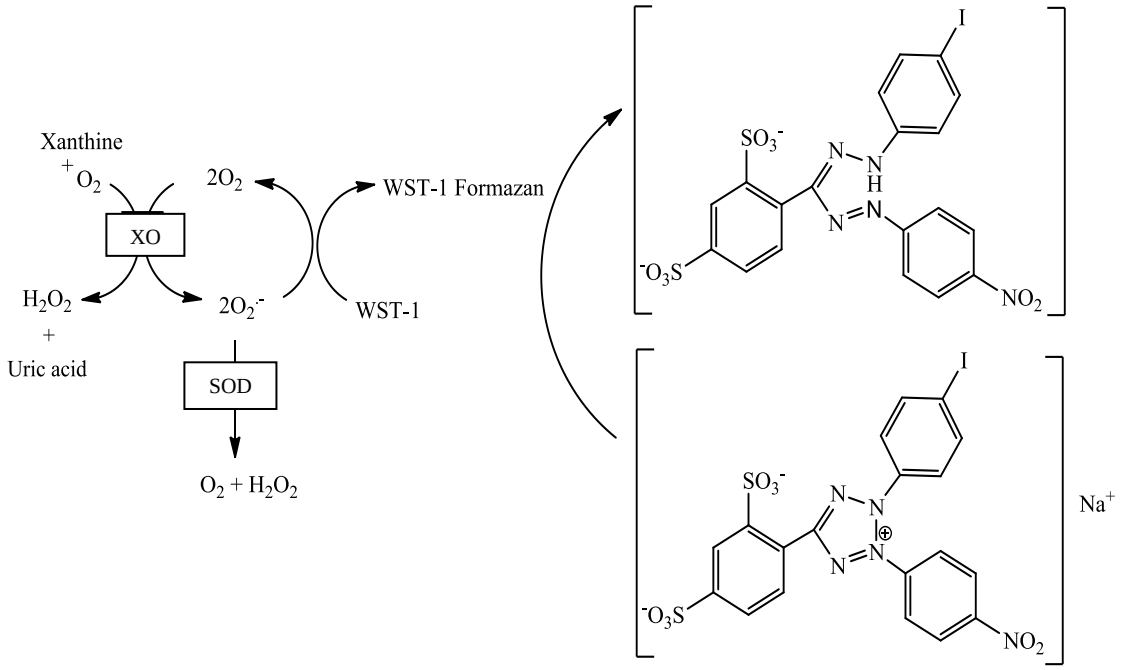


**Scheme 1:** Reaction scheme for the detection of SOD activity.

Freshly extracted *S. aureus* protein (20 µl) was used for the determination of SOD activity which was carried out using the supplied buffers according to the manufacturer's instructions (Table 2.3). The SOD activity was determined at λ=450 nm using a microplate reader and the activity was calculated using the following equation:

$$\text{SOD Activity (inhibition rate \%)} = \frac{[(A_{blank1} - A_{blank3}) - (A_{sample} - A_{blank2})] \text{ X } 100}{(A_{blank1} - A_{blank3})}$$

**Table 2.3:** Composition of sample, blank 1, blank 2 and blank 3 solutions.

| | **Sample (µl)** | **blank 1 (µl)** | **blank2 (µl)** | **blank 3 (µl)** |
|---|---|---|---|---|
| Sample Solution | 20 | | 20 | |
| $H_2O$ | | 20 | | 20 |
| WST Working Solution (supplied) | 200 | 200 | 200 | 200 |
| Dilution Buffer (supplied) | | | 20 | 20 |
| Enzyme Working Solution (supplied) | 20 | 20 | | |

### 2.19.3 Catalase (CAT) assay

Fresh protein extracts were prepared as described in Section 2.18. Protein extract (100 µl, 250 µg/ml) was added to $H_2O_2$ (1.8 ml, 17 mM) in a sterile tube. The mixture was mixed well by pipetting and left at room temperature for 15 min. After this time, the suspension was centrifuged at 10,000 x g for 1 min to stop the reaction. The supernatant was removed and placed in a clean quartz cuvette. The absorbance at $\lambda$=240 nm was obtained. A blank consisted of 17 mM $H_2O_2$.

### 2.19.4 Amino acid leakage assay

Amino acid leakage of $AgNO_3$-treated *S. aureus* cells was determined using the ninhydrin calorimetric assay.[202] Proteins contain free amino groups on the alpha-carbon which can react with ninhydrin to produce a blue-purple product known as Ruhemann's purple (Scheme 2).[203] Amino acids that contain a secondary amino group can also react with ninhydrin but in this case, the product is yellow.

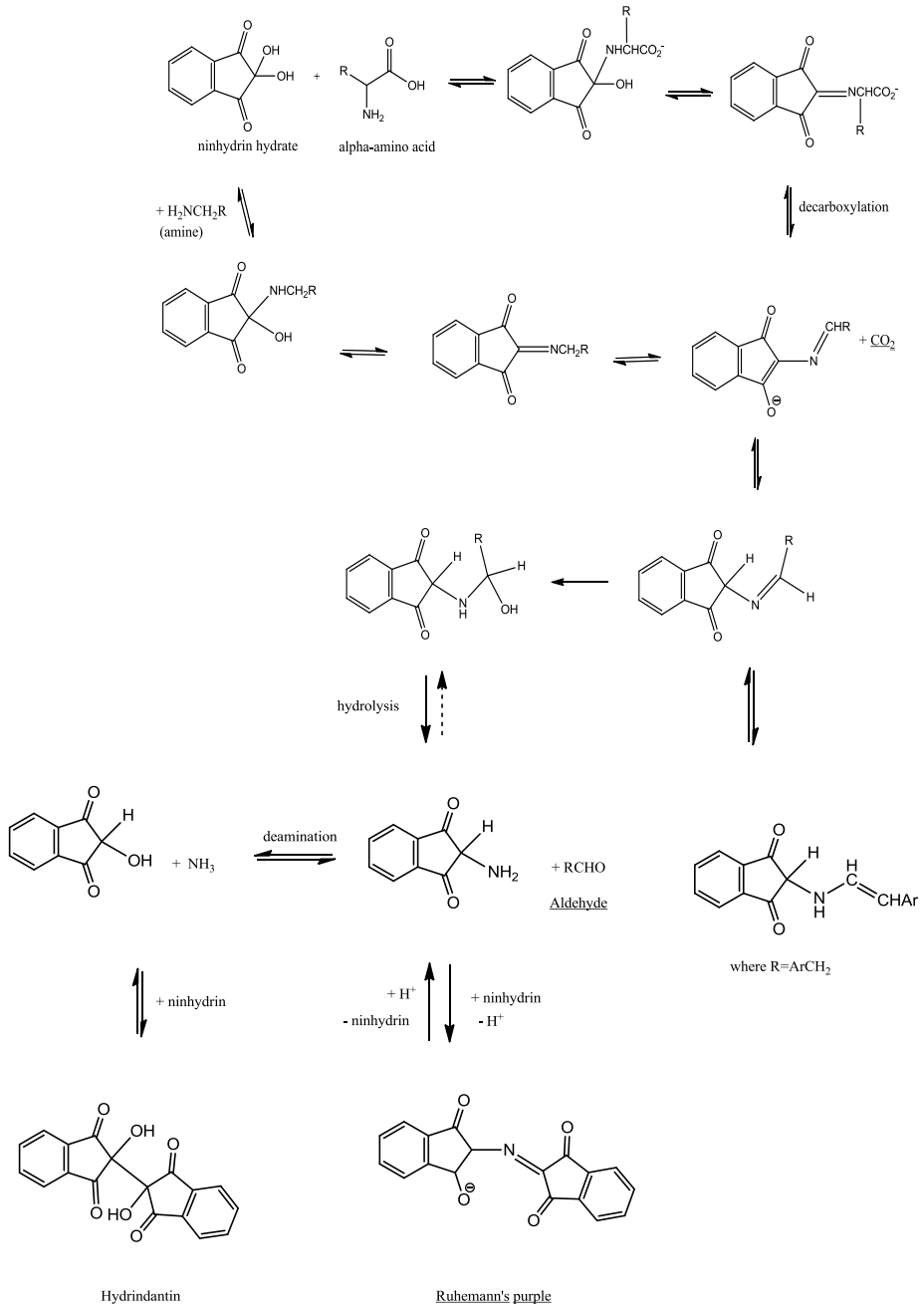


**Scheme 2:** Reaction scheme to depict the detection of free amino groups using the ninhydrin calorimetric assay.[203]

Overnight cultures of *S. aureus* (5 ml) were sub-cultured into fresh nutrient broth media and then grown to exponential phase (6 h). Cells were harvested by centrifugation (1814 x g, 5 min), washed twice in PBS and the pellet then resuspended in deionised $H_2O$ and either DMSO (10% (v/v), positive control) or $AgNO_3$ (3 µg/ml, test compound) and incubated at 37 ˚C and 200 rpm for a further 1, 2 or 4 h.

The amino acid concentration was determined by the ninhydrin calorimetric assay in which aspartic acid and glutamic acid were used as standards (Fig. 2.8). A ninhydrin solution (250 µl) was added to each sample (1.0 ml) and heated at 95 ˚C for 8 min. After the samples were allowed to cool, the absorbance at λ=570 nm was recorded. A standard curve was plotted of absorbance Vs concentration (µg/ml) of aspartic acid and glutamic acid. The concentration of the test sample was found using the equation of the line; y = mx + c.

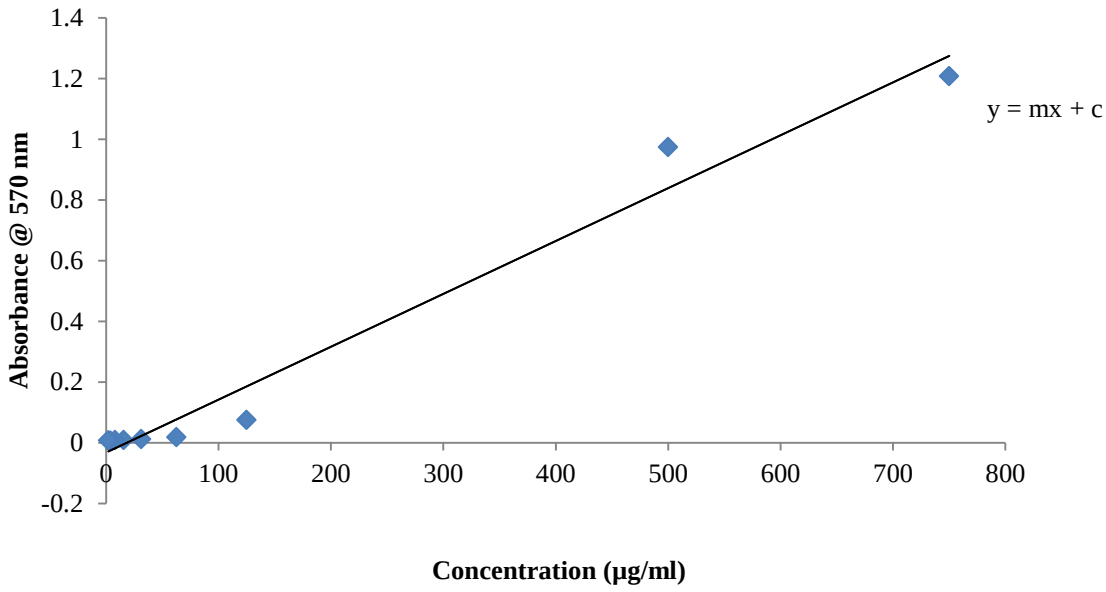


**Fig. 2.8:** Standard curve of amino acid concentration using aspartic acid and glutamic acid as references.

## 2.20 RNA Extraction

### 2.20.1 Preparation of RNase-free buffers and equipment

All glassware was autoclaved twice prior to use so as to reduce RNase contamination. Diethyl pyrocarbonate (DEPC), at a concentration of 1% (v/v), was used to treat the water. The mixture was left to stir overnight and it was then incubated for a minimum of 4 h at 37 °C prior to sterilisation. This DEPC-treated

water was then used for the preparation of all buffers needed for the RNA extraction. All bottle lids, O-rings and magnetic stirrers were soaked in DEPC water overnight and autoclaved before use. All chemicals were weighed out without the use of a spatula. Gloves were worn at all times and changed frequently. Pipette tips were taken from freshly-opened bags and autoclaved twice before use.

### 2.20.2 RNA extraction using the Qiagen RNeasy® minikit

Cultures of *S. aureus* cells were grown overnight, sub-cultured (10 mls) in fresh nutrient broth media (50 mls) and grown to exponential phase at 37 °C for 3-4 h. $AgNO_3$ (3.0 µg/ml) was added and incubated further for relevant timepoints. At each timepoint, cells were harvested by centrifugation at 1814 x g for 5 min. The supernatant was removed and cells were then resuspended in fresh Y1 buffer (1.5 mls) and placed in an incubator (37 °C, 200 rpm) for 20 min to generate spheroplasts. The cell suspension was centrifuged at 300 x g for 5 min and the supernatant then carefully removed. Buffer RLT (350 µl, supplied) was added and the mixture then vortexed to lyse the spheroplasts. Ethanol (350 µl, 70% (v/v)) was added and the mixture inverted gently. The lysate was transferred to an RNeasy Mini spin column placed in a 2 ml collection tube (supplied) and centrifuged for 15 sec at 8000 x g. The flow-through was discarded. Buffer RW1 (700µl, supplied) was added to the RNeasy spin column and the mixture centrifuged for 15 sec at 8000 x g to wash the spin column membrane. The RNeasy spin column was placed into a new 2 ml collection tube and Buffer RPE (500 µl, supplied) was added. This was then centrifuged for 15 sec at 8000 x g to wash the spin column membrane. The flow-through was discarded. Buffer RPE (500 µl, supplied) was added to the spin column, and centrifuged for 2 min at 8000 x g to wash the spin column membrane. The RNeasy spin column was placed in a new collection tube (1.5 ml, supplied) and RNase-free water (40 µl) was added and centrifuged for 1 min at 8000 x g to elute the RNA. This step was repeated with a further 20 µl of RNase-free water and the final solution was aliquoted and stored at -70 °C. Extracted RNA was quantified spectrophotometrically at 260/280 nm.

### 2.20.3 RNA extraction using Qiagen RNeasy® minikit with RNAprotect bacteria reagent

Two volumes of RNAprotect bacteria reagent (1000 µl) was added to one volume of bacterial culture (500 µl) in an eppendorf tube (2 ml) and mixed by vortexing for 5 sec and then incubated at room temperature for 5 min. The suspension was then centrifuged for 10 min at 5000 x g. The supernatant was discarded and the pellet was resuspended in TE buffer (100 µl, supplied) containing lysozyme and Proteinase K (10-20 µl) and the mixture then vortexed for 10 sec. The solution was incubated at room temperature for 10 min, with vortexing every 2 min. RLT buffer (700 µl, supplied) was added to the solution and this was then vortexed vigorously for 5-10 sec. The suspension was transferred to a safe-lock tube (2 ml) containing acid-washed glass beads. The cells were disrupted by vortexing on ice for 5 min, followed by centrifugation for 10 min at a maximum speed of 20,000 x g. The supernatant was transferred into a new tube and ethanol (590 µl, 80%) was added. The mixture was agitated well by pipetting. The lysate was transferred to an RNeasy Mini spin column placed in a collection tube (2 ml, supplied) and then centrifuged for 15 sec at 8000 x g. The flow-through was discarded. Buffer RW1 (700µl, supplied) was added to the RNeasy spin column and the mixture centrifuged for 15 sec at 8000 x g in order to wash the spin column membrane. The RNeasy spin column was then placed into a new collection tube (2 ml) and Buffer RPE (500 µl, supplied) was added, followed by centrifugation for 15 sec at 8000 x g so as to wash the spin column membrane. The flow-through was discarded. Buffer RPE (500 µl, supplied) was added to the spin column and the mixture was centrifuged for 2 min at 8000 x g in order to wash the spin column membrane. The RNeasy spin column was placed in a new collection tube (1.5 ml, supplied) and RNase-free water (30 µl) was added and this was then centrifuged for 1 min at 8000 x g to elute the RNA. This step was repeated with a further 20 µl of RNase-free water and the final suspension was aliquoted and stored at -70 °C. Extracted RNA was quantified spectrophotometrically at 260/280 nm.

### 2.20.4 RNA extraction using TRI-reagent

RNA was isolated from exponentially growing bacterial cells. Aliquots of stationary phase *S. aureus* cultures were grown to exponential phase at 37 °C for 4 h. Cells were treated with an $MIC_{80}$ value of $AgNO_3$ (3.0 µg/ml) for 1 h. RNA extractions were carried out after relevant timepoint. Cells were harvested by centrifugation at 12,000 x g for 10 min at 4 °C. To the pellet, TRI-reagent (3.0 mls) and glass beads (0.5 g) were added. The mixture was vortexed vigorously and then incubated at room temperature for 15 min. The mixture was the distributed into sterile 1.5 ml tubes and centrifuged at 12,000 x g for 10 min at 4 °C. The pellets were discarded and chloroform (200 µl) was added to the supernatant. This mixture was vortexed vigorously and left to stand at room temperature for 10 min. It was subsequently centrifuged at 12,000 x g for 10 min at 4 °C in order to cause separation into two layers. The top layer was retained and to this 2-proponal (500 µl) was added. The tube was inverted several times and left to stand at room temperature for 10 min. The solution was centrifuged at 12,000 x g for 10 min at 4 °C. The supernatant was discarded. The pellet was washed with molecular grade ethanol (50 µl, 75% (v/v)) and the suspension then centrifuged at 7500 x g for 5 min at 4°C. The supernatant was removed, and the resulting pellet was allowed to air-dry before being resuspended in RNase-free water. The suspension was aliquoted and either stored at -70 °C or used immediately. Extracted RNA was quantified spectrophotometrically at 260/280 nm.

### 2.20.5 DNase treatment of RNA

In order to remove any contaminating DNA within the sample, DNase treatment was performed using a Deoxyribonuclease I (AMP-D1) kit. Reaction buffer (10 X, 1 µl, provided) and DNase I (1 µl, 1 unit/µl) were added to RNA (4 µg) and the sample was incubated at room temperature for 15 min. The enzyme activity was stopped by adding stop solution (1 µl, 50 mM EDTA, provided). Samples were then heated to 70 °C for 10 min and cooled on ice.

### 2.20.6 RNA electrophoresis

Prior to use, the gel rig was washed with hydrogen peroxide (2% v/v), rinsed with DEPC water and allowed to air-dry. RNA was visualised by running the extraction products on an agarose gel (1% (w/v)). Once the gel was hand-hot, formaldehyde was added (1.8 µl, 37% (v/v)) along with ethidium bromide (1 µl, 10 mg/ml) before pouring the gel. Prior to running, the gel was equilibrated in 1X FA running buffer for at least 30 min. RNA (4 µl) was added to 6X loading dye (1 µl) and formamide (6 µl) and the mixture then heated to 60 °C for 10-15 min before loading into the wells of the gel. The gel was run at 6 V/cm in 1X FA buffer. The gel was visualised using Syngene Geneflash.

### 2.20.7 cDNA synthesis

cDNA was synthesised using the Superscript III First-Strand Synthesis System for RT-PCR kit. RNA concentration was determined, and all samples contained equal amounts of RNA prior to cDNA synthesis. RNA was added to an RNA- and DNA-free tube and RNA-free water was added to bring the volume up to 8 µl. To this mixture, dNTP mix (1 µl, 10 mM, provided) and oligoDT's (1 µl, 50 µM, provided) were added. The solution was incubated at 65 °C for 5 min and then placed on ice for at least 1 min. A master mix was prepared according to the number of reactions required and 9 µl of this mix was added to each of the RNA/primer mixes. The combination was mixed gently, incubated at 42 °C for 2 min and held on ice. Superscript III RT (1 µl, 200 U/µl, provided) was added to each reaction tube and the mixture incubated as follows: 42 °C for 50 min, 70 °C for 5 min, and the mixture was then held on ice. To each tube, RNaseH (1 µl, supplied) was added and this was further incubated at 37 °C for 20 min. cDNA was aliquoted and stored at -20 °C.

### 2.20.8 Polymerase chain reaction (PCR)

Primers were dissolved in molecular grade water to give a stock solution of 100 µM and this was subsequently diluted to give a 10 µM working solution. Each PCR reaction tube (20 µl volume) contained cDNA (1 µg/µl), 10 X LA buffer (2 µl), DMSO (0.4 µl, molecular grade), dNTP mix (1 µl, 10 mM, promega), water (14.6

µl, molecular grade), forward primer (0.4 µl) (Table 2.3), reverse primer (0.4 µl) (Table 2.3) and AccuTaq™ LA DNA polymerase (0.2 µl). Solutions were mixed by pipetting and then immediately placed in the thermal cycler.

**Table 2.3:** Primers and RT-PCR cycle conditions.

| Gene | Primer | Sequence 5'-3' | PCR Cycle Conditions |
|---|---|---|---|
| DNA Gyrase[204] | gyrA-F | TGCTGAGTTAATGGAGGATATTG | 95 °C 5 min, [95 °C 30 sec, 50 °C 45 sec, 68 °C 45 sec] x 35 cycles, 68 °C 7 min. |
| | gyrA-R | CACGTGTAATACCACTCTTACC | |
| Superoxide Dismutase A[205] | SodA-F | CATAACACTTATGTWACTAAATTAAA | 95 °C 5 min, [95 °C 1 min, 55 °C 1 min, 68 °C 1 min] x 30 cycles, 68 °C 10 min. |
| | SodA-R | ATCTAAAGAACCCCATTGTTC | |
| Superoxide Dismutase M[206] | SodM-F | TTAATTCTCTTTAAAAGCGGGAAA | 95 °C 5 min, [95 °C 1 min, 62 °C 1 min, 68 °C 1 min] x 30 cycles, 68 °C 10 min. |
| | SodM-R | GGGACATTCATCAACTTTTATCAG | |

### 2.20.9 PCR product visualisation and quantification

The PCR product (4 µl) was run on a 1% agarose gel as detailed in Section 2.20.6.

### 2.20.10 Genomic DNA extraction

Cultures (50 ml) were grown to stationary phase overnight and harvested by centrifugation for 5 min at 1814 x g. The supernatant was discarded and the pellet was washed twice with PBS followed by EDTA (10 mM, pH 8). The pellet was then kept on ice for the remainder of the protocol. The pellet was resuspended in spheroplasting buffer (4 ml) along with acid-washed glass beads (5 g) and then the mixture was vortexed on ice for 5 min. Cells were harvested by centrifugation at

2056 x g for 5 min at 4 °C. Cells were resuspended in lysing buffer (4 mls), SDS (10%) and proteinase K (100 µl, 30 µg/µl). This combination was mixed by pipetting and then incubated at 65 °C for 30 min. An equal volume (4 mls) of phenol-chloroform-isoamyl alcohol mixture (25:24:1) was added and the mixture vortexed vigorously for 5 min on ice. The mixture was centrifuged at 17,400 x g for 15 min at 4 °C. The upper layer was transferred to a new tube and an equivalent volume of chloroform-isoamyl alcohol (24:1) was added and subsequently mixed by inversion. The mixture was centrifuged as before. The upper layer was transferred to a new tube and washing repeated until no white interphase layer remained. Two volumes of ice-cold ethanol (95% (v/v)) was added and the sample precipitated overnight at –20 °C. The sample was centrifuged as before. The recovered DNA pellet was washed with ice-cold ethanol (70% (v/v)). The ethanol was decanted off and the pellets allowed to air-dry. The pellets were resuspended in sterile water (4 mls) containing RNase (150 µl, 1 mg/µl) and then incubated at 37 °C for 30 min. Ice-cold ethanol (8 mls, 95% (v/v)) and ammonium acetate solution (3 M, pH 5.2) was added and the mixture stored at -20 °C overnight. The mixture was centrifuged as before and the pellet allowed to air-dry. The sample was resuspended in sterile distilled water (200 µl), aliquoted and stored at -20 °C.

## 2.21 SDS-PAGE Gel Electrophoresis

### 2.21.1 One-dimensional SDS-PAGE electrophoresis

Protein extraction was carried out as outlined in Section 2.18. Protein was precipitated by adding three times the volume of ice-cold acetone and storing the suspension at -20 ˚C overnight. The precipitated protein was collected by centrifugation (17,949 x g for 30 min at 4 ˚C). The acetone was removed and the pellet allowed to air-dry. Pellets were resuspended in 5X sample buffer (1 in 2 dilution of 10X sample buffer) and boiled for 2-3 min at 95 ˚C. Samples were loaded into the wells of a 12.5% separating gel with a 2.5% stacking gel, and immersed in 1X running buffer. The gels were electrophoresed initially at 80 V followed by 120 V once the protein had moved sufficiently through the gel. Protein bands were

revealed using either Coomassie or colloidal Coomassie staining solution, and destained using either destain or deionised water.

### 2.21.2 Two-dimensional SDS-PAGE electrophoresis

Protein extraction was carried out as outlined in Section 2.18. Protein was precipitated by adding three times the volume of ice-cold acetone and storing the suspensions at -20 ˚C overnight. The precipitated protein was collected by centrifugation (17,949 x g for 30 min at 4 ˚C). The acetone was removed and the pellet allowed to air-dry. Released proteins were resuspended in IEF buffer (250 µl) along with DTT (10 mmol), ampholytes (0.8%) and a few grains of molecular grade bromophenol blue. The solution was applied to a 13 cm Immobiline™ DryStrip pH 3-10, covered with pulse-1 cover fluid and iso-electric focusing was performed on an Ettan IPGphor II system using the following program:

1. Step 100 V 2 h
2. Step 500 V 1.5 h
3. Step 1000V 1 h
4. Step 2000 V 1 h
5. Step 4000 V 1 h
6. Step 6000 V 2 h
7. Step 8000 V 3 h
8. Step 500 V 4 h
9. Step 8000 V 3 h

Following iso-electric focusing, strips were equilibrated in reducing buffer for 10 min followed by equilibration in alkylation buffer for 10 min. Strips were placed on top of homogenous 12.5% SDS-PAGE gels. SDS-PAGE standards, low range, were boiled for 5 min in 2X sample buffer and loaded near to the positive end of the strip. Strips were overlaid with hand-warm agarose sealing solution. The gels were electrophoresed at 6 °C using a cooling system for 20 h at 100 V or until the bromophenol indication layer was at the bottom of the gel. Gels were fixed using a colloidal fixing solution for a minimum of 3 h and then washed three times with

deionised water before staining with colloidal staining solution for a period of several days. Gels were washed with deionised water to destain.

Protein was extracted on three separate occasions and gels were produced in triplicate per treatment and scanned on a HP Scanjet 5400C.

## 2.22 LC/MS Mass Spectrometry

The following procedures were adapted from the work of Shevchenko *et al*:[207]

### 2.22.1 Destaining gel pieces

Gels were washed twice in sterile water and protein spots of interest were removed and placed in sterile Eppendorf tubes containing a 1:1 (v/v) solution of ammonium bicarbonate (100.0 mM) : acetonitrile (100 µl) and incubated for 30 min with occasional vortexing. The liquid layer was removed and acetonitrile (500 µl) was added and left until the gel pieces became white and reduced in size. The liquid layer was again removed and the gel plugs were used in the next preparation step.

### 2.22.2 In-gel digestion

In-gel digestion was carried out using sequencing grade modified trypsin. A trypsin solution was prepared by adding ammonium bicarbonate (100 µl, 10 mM) containing acetonitrile (10% (v/v)) to the trypsin powder. This solution was aliquoted in 10 µl volumes into separate tubes. To one of these aliquots, ammonium bicarbonate (500 µl, 50 mM) was added. Approximately 40 µl of this resulting solution was added to each gel plug and the tubes were held at 4 ˚C for a minimum of 30 min. Gel pieces were held at 37 ˚C overnight.

### 2.22.3 Extraction of peptide digestion products

The trypsin solution was removed to another tube and extraction buffer (100 µl) was added to each tube and these were then incubated for 15 min at 37 ˚C in a shaker. This solution was removed and added to the tube containing the previously collected trypsin solution. The combined solutions were dried in a vacuum centrifuge overnight and stored at -20 ˚C.

### 2.22.4 LC/MS mass spectrometry

Dried peptides were resuspended in aqueous formic acid solution (20 µl, 0.1% (v/v)). The resuspended peptides were placed in a sonicator bath for 2 min and then centrifuged at 10,621 x g for 15 min at 4 ˚C. Samples were then centrifuged through spin filters for 2 min at 425 x g, transferred to sterile glass vials and analysed using BSA as external standards. The mass lists were generated using the search programme http://www.matrixscience.com and a Blast search was then carried out using the http://expasy.org/sprot/ search programme.

## 2.23 Statistical analysis

All experiments were performed on three separate occasions. Multiple comparisons of means were analysed using Fisher's least significant different test using PROC GLM of the SAS 9.1 statistical model. Differences were deemed significant with $p \leq 0.05$.

# Chapter 3

Chemical Synthesis and Characterisation

## 3.1 $[Ag_2(3,6,9\text{-tdda})].2H_2O$

$[Ag_2(3,6,9\text{-tdda})].2H_2O$ was synthesised using two different methods. The first, using a known concentration of 3,6,9-trioxaundecanedioic acid (3,6,9-tdda$H_2$) and NaOH, gave a product yield of 36% and the second, using the potassium salt, $K_2$(3,6,9-tdda), gave a yield of 73%. The complex was soluble in hot $H_2O$ and hot DMSO.

The IR spectrum of 3,6,9-tdda$H_2$ (Section 2.5.3) showed a broad O-H band (3444 $cm^{-1}$) and a characteristic C=O band for the carboxylic acid function (1736 $cm^{-1}$). Upon formation of the silver salt, $[Ag_2(3,6,9\text{-tdda})].2H_2O$, bands corresponding to asymmetric ($\upsilon_{(OCO)asym}$) and symmetric ($\upsilon_{(OCO)sym}$) stretches were observed (1612 $cm^{-1}$ and 1406 $cm^{-1}$, respectively) (Section 2.7.3). The separation between these two bands ($\Delta_{(OCO)}$ = 206 $cm^{-1}$) suggests an ionic interaction between the $tdda^{2-}$ anion and the metals (Fig. 3.1).[208]

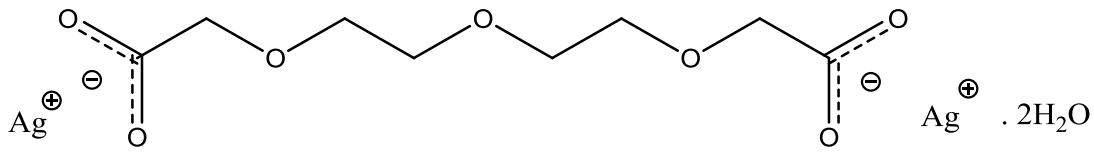


**Fig. 3.1:** Proposed structure for $[Ag_2(3,6,9\text{-tdda})].2H_2O$

The $^1H$ NMR spectrum of $[(Ag_2(3,6,9\text{-tdda})].2H_2O$ (Section 2.7.3) contained two singlets at 3.81 and 3.56 ppm (integral ratio 1:2), corresponding to the methylene groups of the $tdda^{2-}$ anion. The peak at 3.81 ppm corresponds to the $CH_2$ moieties close to the carboxylate function, whilst the peak at 3.56 ppm for the $CH_2$ moieties located between the ether oxygen atoms. As a consequence of the Ag(I) ions, these two peaks are shifted upfield compared to the free acid (4.13 and 3.65 ppm, respectively).

## 3.2 Characterisation of Bioglue Prepared in the Absence and in the Presence of Ag(I) Ions

### 3.2.1 Infrared spectroscopy

Bioglues (without added Ag(I) ions) were made by reacting BSA with GLA in a 4:1 ratio. The IR spectrum of BSA (Section 2.5.1) shows an intense band at 3312 $cm^{-1}$ which arises from the O-H and N-H stretching vibrations and also hydrogen-bonding interactions.[209] The IR spectrum of the supplied aqueous GLA (Section 2.5.2) shows a characteristic aldehyde band $\upsilon_{(C=O)}$ (1715 $cm^{-1}$) and, a broad band associated with the $\upsilon_{(O-H)}$ vibration (3424 $cm^{-1}$). Upon reacting GLA with BSA, the GLA aldehyde $\upsilon_{(C=O)}$ band disappears (Section 2.8.1) suggesting that crosslinking had occurred. It was noted that the IR spectrum of Bioglue closely resembled that of BSA.

Bioglues incorporating $AgNO_3$ and $[Ag_2(3,6,9\text{-tdda})].2H_2O$ were synthesised in triplicate using BSA, GLA and varying amounts of either $AgNO_3$ or $[Ag_2(3,6,9\text{-tdda})].2H_2O$. Again, the IR spectra of these Ag(I)-Bioglues were very similar in appearance to those of the BSA and Bioglue without added Ag(I). Ag(I) incorporation was further confirmed using atomic absorption spectroscopy (AAS) and Energy dispersive X-ray spectroscopy (EDX).

Reproducible Ag(I)-Bioglue formulations were obtained based on IR, atomic absorption, differential scanning calorimetry, scanning electron microscopy, swelling and drying studies, tensile testing and leaching studies. The BSA/GLA combination containing the highest quantity of added $AgNO_3$ (0.1 g) failed to produce a hydrogel (Fig. 3.2a), unlike the hydrogels formed using lower amounts of added Ag(I) ions (Fig. 3.2b-e). Thus, swelling studies were not carried out on the $AgNO_3$ (0.1 g) sample. In addition, the product obtained using the highest amount of $AgNO_3$ (0.1 g) failed to adhere to the wooden test pieces used to assess the glue-like properties of the Bioglues. The failure to form a hydrogel upon addition of $AgNO_3$ (0.1 g) may be due to the over-loading of the sample with Ag(I) ions, resulting in a product that is so extensively crosslinked with metal ions that most of the sites available for hydrogen-bonding molecules were effectively blocked.

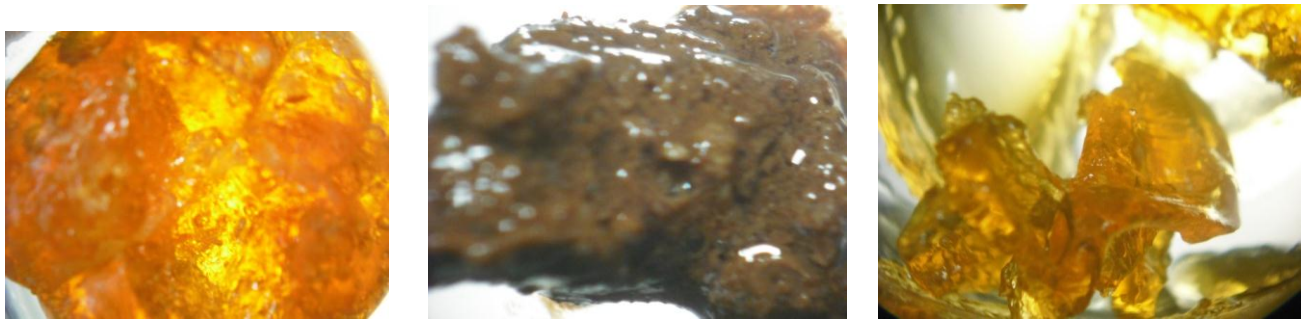

**(a)** **(b)** **(c)**

**(d)** **(e)** **(f)**

**Fig. 3.2:** Images of Bioglues prepared using (a) no Ag(I) ions, varying amounts of added $AgNO_3$: (b) 0.1 g, (c) 0.01 g, (d) 0.0001 g, [$Ag_2$(3,6,9-tdda)].2$H_2O$ (e) 0.01 g and (f) 0.00001 g.

### 3.2.2 Silver content

AAS was carried out to determine homogeneity of Ag(I) ions in the Ag(I)-Bioglues. Each Ag(I)-Bioglue sample was synthesised on three separate occasions and three separate portions of each sample were then analysed for % silver content (a total of nine readings per sample). Ag(I)-Bioglue formulated using the highest amount of added $AgNO_3$ (0.1 g) and the theoretical amount of silver content in this sample was 10.05%. The Ag(I)-Bioglue formulated with the lowest amount of added $AgNO_3$ (0.0001 g) had a theoretical amount of silver of 0.01%. It was also found that the Ag(I)-Bioglue made with the highest quantity of added $[Ag_2(3,6,9\text{-tdda})].2H_2O$ (0.01 g) had a theoretical silver content of 0.84%, whereas the lowest (0.00001 g) had an expected silver content of $8.6 \times 10^{-4}$%. For $AgNO_3$, the % Ag detected in the Ag(I)-Bioglue followed a stepwise reduction, corresponding to the decreased amount of added silver salt (0.1 g to 0.01 g added $AgNO_3$). However, this trend was not observed for the remaining formulations of $AgNO_3$-Bioglues or for the $[Ag_2(3,6,9\text{-tdda})].2H_2O$-Bioglues (Appendix II). This may be due to regions of these polymers having more silver content than others and resulting in a non-homogeneous distribution of the metal ion throughout the bulk sample.

### 3.2.3 Thermal analysis

Differential scanning calorimetry, a thermoanalytical technique which shows if a sample undergoes a temperature-induced physical transformation (e.g. a phase transition), was conducted on BSA (Fig. 3.3a-c), $AgNO_3$ (Fig. 3.4a), $[Ag_2(3,6,9\text{-tdda})].2H_2O$ (Fig. 3.4b), $AgNO_3$-Bioglues (Fig. 3.5b), $[Ag_2(3,6,9\text{-tdda})].2H_2O$-Bioglues (Fig. 3.5c) and a Bioglue made in the absence of any added Ag(I) salt (Fig. 3.5a). The DSC profile of the BSA protein alone (25-400 °C) showed two endothermic events at 72.70 °C and at 220.69 °C. Farahnaky *et al*[210] also reported two endothermic events for five commercial BSA samples which occurred between 35-60 °C and between 90-180 °C (Fig. 3.6). These researchers suggested that as the endothermic peak in the low temperature range is displaced by > 50 °C from the high temperature endotherm, this did not indicate that the peaks represented denaturation

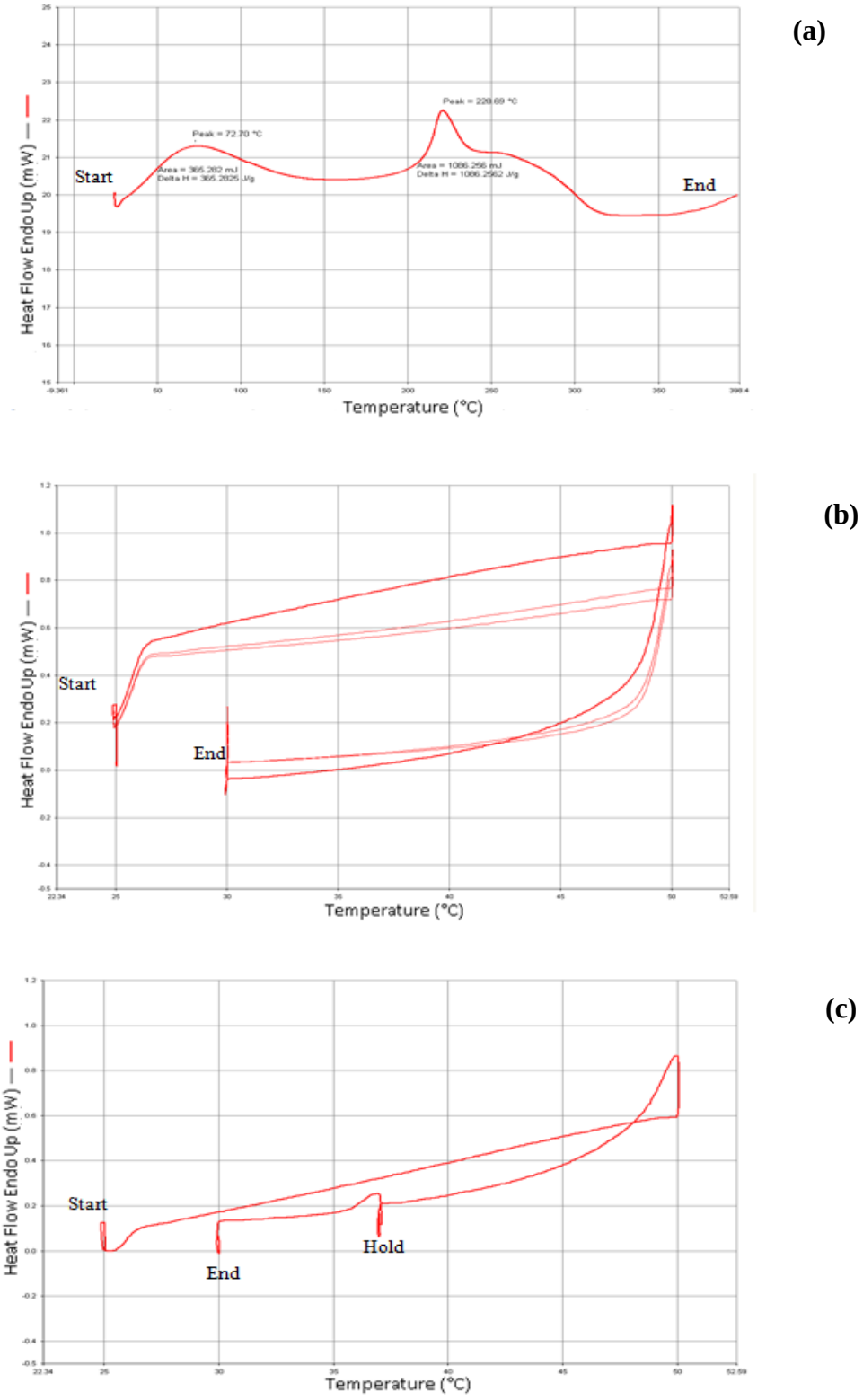


**Fig. 3.3:** DSC thermograms of (a) BSA (25-400 °C with increments of 50 °C), (b) BSA (25-50 °C with increments of 5 °C), (c) BSA (held at 37 °C with increments of 5 °C).

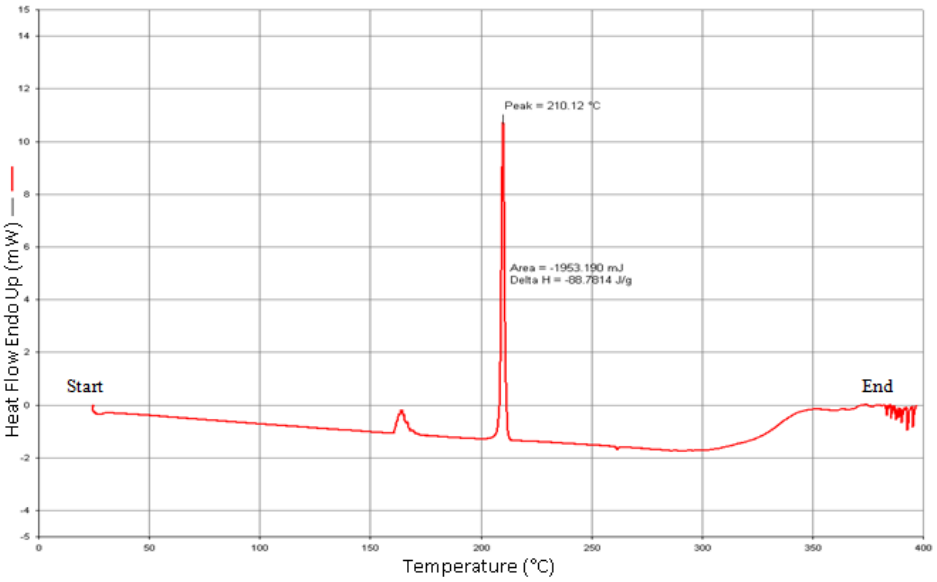


**(a)**

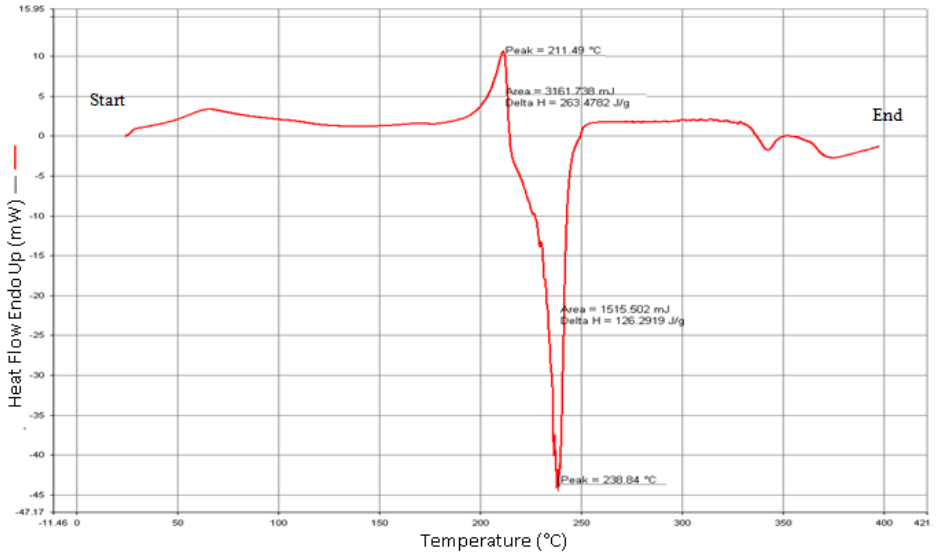


**(b)**

**Fig. 3.4:** DSC thermograms (25-400 °C with increments of 50 °C) of (a) $AgNO_3$ and (b) $[Ag_2(3,6,9\text{-tdda})].2H_2O$.

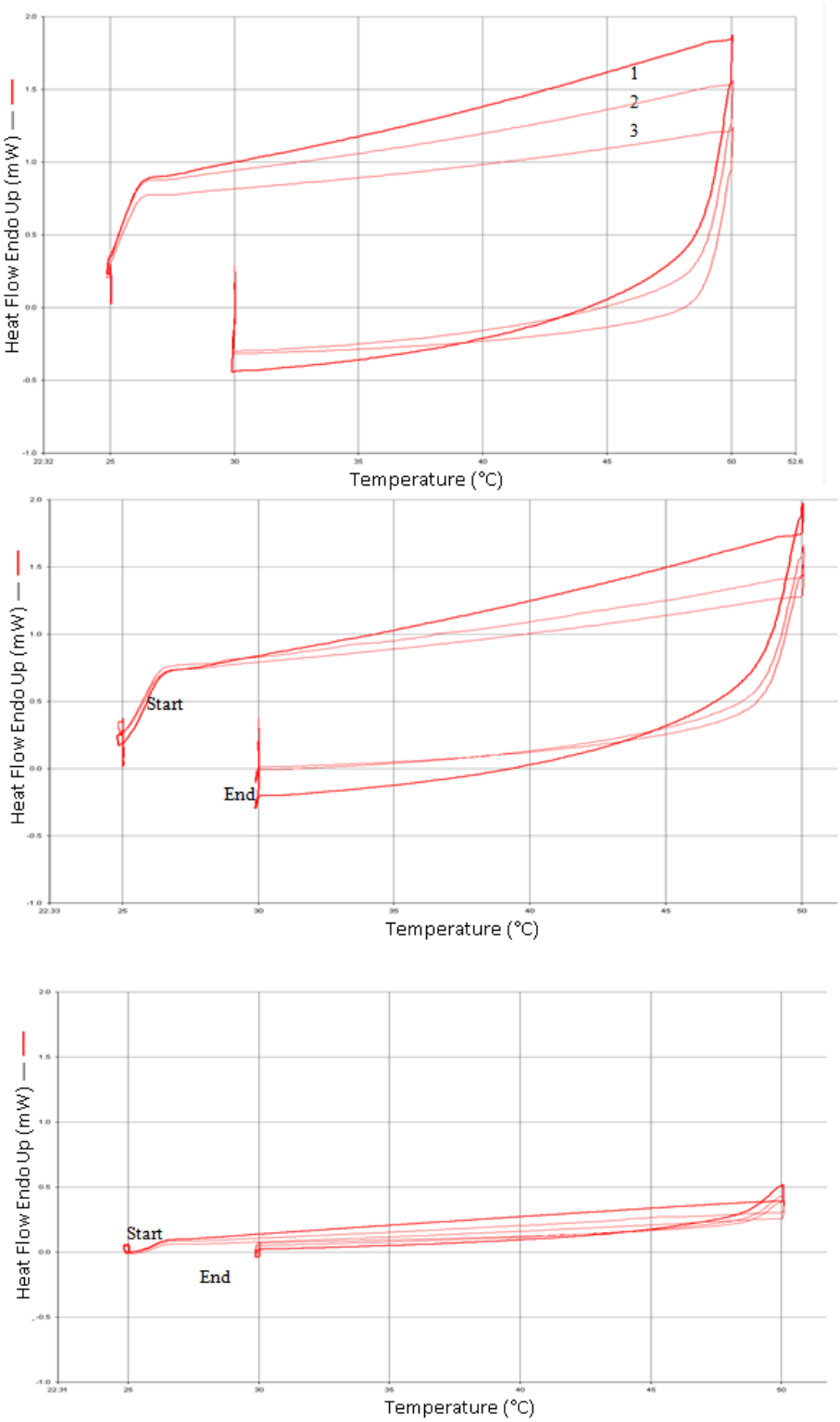


**Fig. 3.5:** DSC thermograms of Bioglue containing (a) no added Ag(I) ions, (b) added $AgNO_3$ (0.01 g) and (c) added $[Ag_2(3,6,9\text{-tdda})].2H_2O$ (0.01 g). Samples were heated from [25 °C → 50 °C → 30 °C with increments of 5 °C] and the cycle began again at 25 °C.

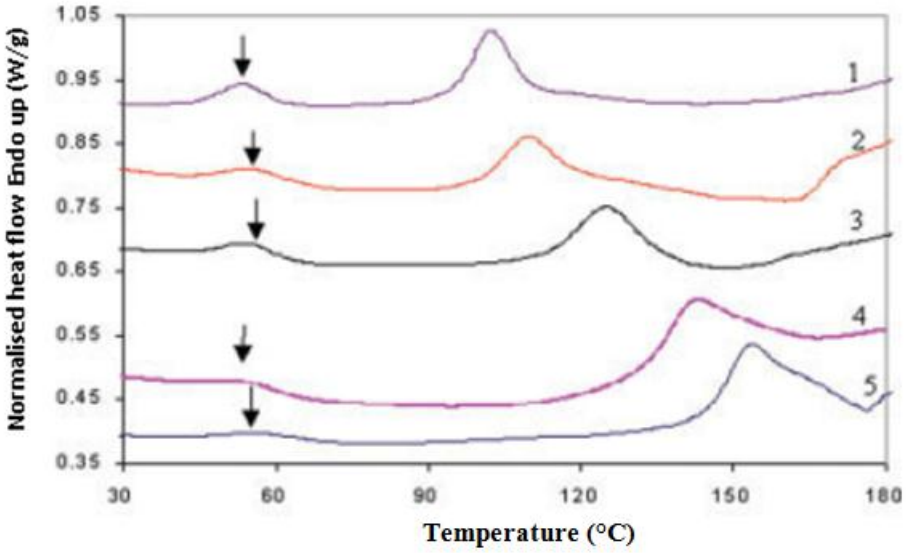


**Fig. 3.6:** DSC profiles of commercial BSA samples.[210]

1- BSA from Sigma (cat. No. A-7906)

2- BSA from Sigma (cat. No. A-0281)

3- BSA from ACROS (cat. No. 13473-0100)

4- BSA from Sigma (cat. No. A-2153)

5- BSA from Sigma (cat. No A-7906)

Moisture contents (% w/w) for BSA samples 1-5; 12.1, 8.6, 6.6, 5.1, and 3.7%, respectively (wet basis).

of the protein. Michnik *et al*[211] also reported a $T_m$ value of 70.1 °C although they did not observe a second endothermic peak due to the fact that a much smaller temperature range (20-100 °C) was used in their test. In the present studies, the DSC profile of BSA was also recorded over the temperature ranges 25-400 °C, 25-50 °C, and holding at 37 °C for 3 h, in order to determine the stability of the protein on its own (Fig. 3.3 (b and c)). No phase transitions were detected under these conditions.

The DSC thermogram of $AgNO_3$ (Fig. 3.4a) shows an endothermic event which is in relation to the melting of the compound (peak maximum 210.12 °C). This correlates to the literature value of 212 °C.[212] The DSC profile of $[Ag_2(3,6,9\text{-tdda})].2H_2O$ (Fig. 3.5b) showed a melting endothermic peak (211.49 °C) followed by an exothermic event in the range of 220-240 °C (peak maximum 238.84 °C). Logvinenko *et al*[213] observed a large exothermic event for silver(I) acetate, $CH_3COOAg$, between 170-280 °C. The authors postulated that this peak corresponds to decomposition of the carboxylate ligand and formation of metallic silver suggesting that the following reaction had taken place:[214]

$$2CH_3COOAg \longrightarrow 2Ag^0 + CH_3CO_2H + CO_2 + H_2 + C$$

To establish the DSC profile of vacuum dried Bioglue samples, the solids were heated from 25-50 ˚C, cooled back down to 30 ˚C and cycled again at [25 °C → 50 °C → 30 °C] etc. (without delay) a further two times (Fig. 3.5). The DSC profiles remained unchanged across the three cycles, suggesting that the Bioglues prepared in the absence and in the presence of added silver salt did not degrade within this temperature window. The IR spectrum of the samples were also recorded after they had been subjected to DSC scanning to further determine if the Bioglue samples were unchanged after the heating protocol (Fig. 3.7). No obvious changes in the IR spectral profiles of the Bioglue samples were evident suggesting that major structural changes did not occur upon heating to 50 °C (three times).

As an extension of these experiments, Bioglue samples were again heated to 50 ˚C but this time cooled to 37˚C and held at the latter temperature for 3 hrs. The reasoning behind this experiment was to assess if the Bioglue samples remained unaltered at body temperature for a prolonged time (Fig. 3.8). No phase transitions

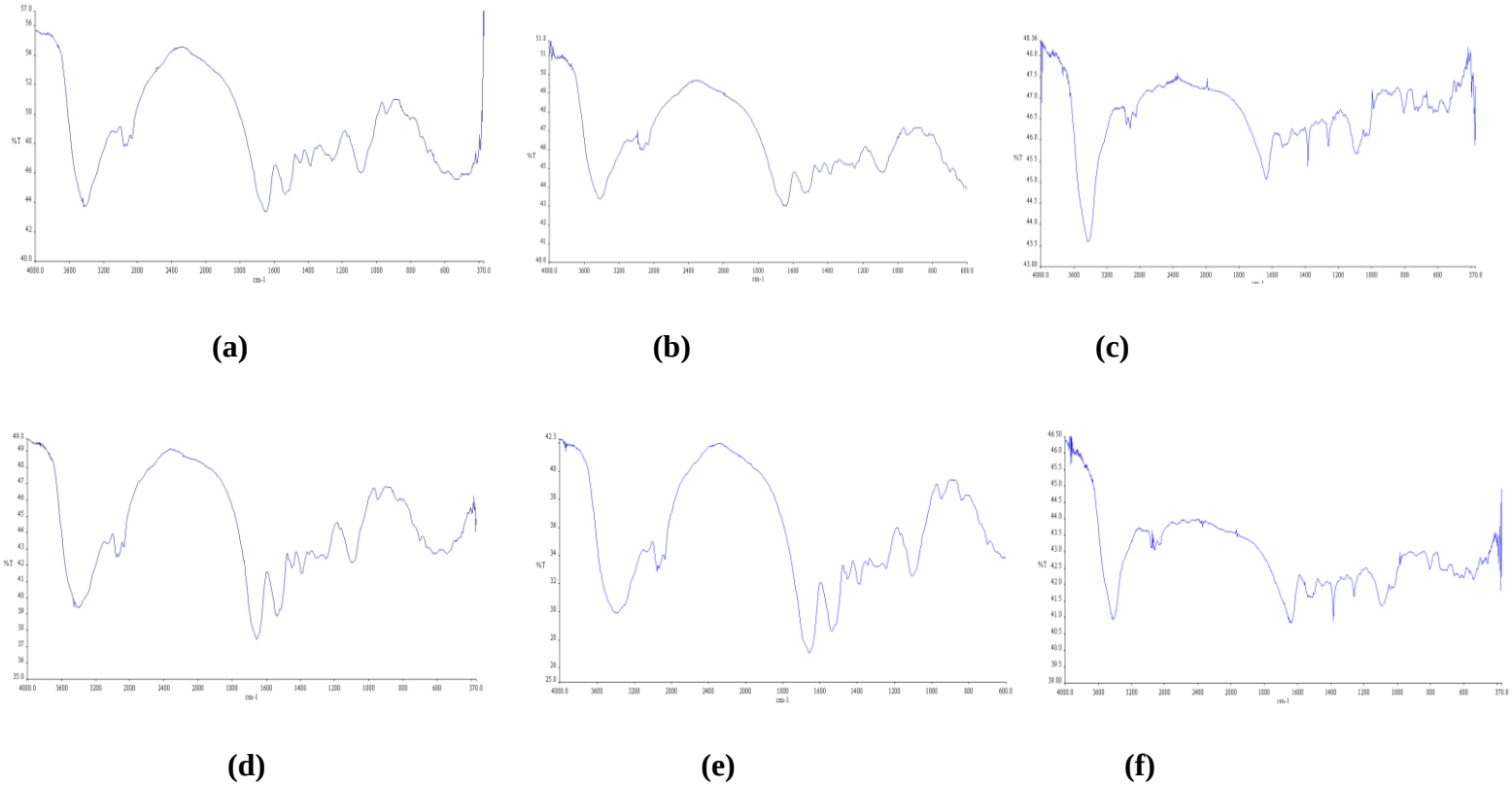


**Fig. 3.7:** Infrared spectra of (a) Bioglue with no added Ag(I) ions, (b) Bioglue with no added Ag(I) ions after DSC (cycled 3 times to 25-50 °C), (c) Bioglue with no added Ag(I) ions after DSC (held at 37 °C for 3 hours), (d) Bioglue with added $AgNO_3$ (0.01 g), (e) Bioglue with added $AgNO_3$ (0.01 g) after DSC (cycled 3 times to 25-50 °C) and (f) Bioglue with added $AgNO_3$ (0.01 g) after DSC (held at 37 °C for 3 hours).

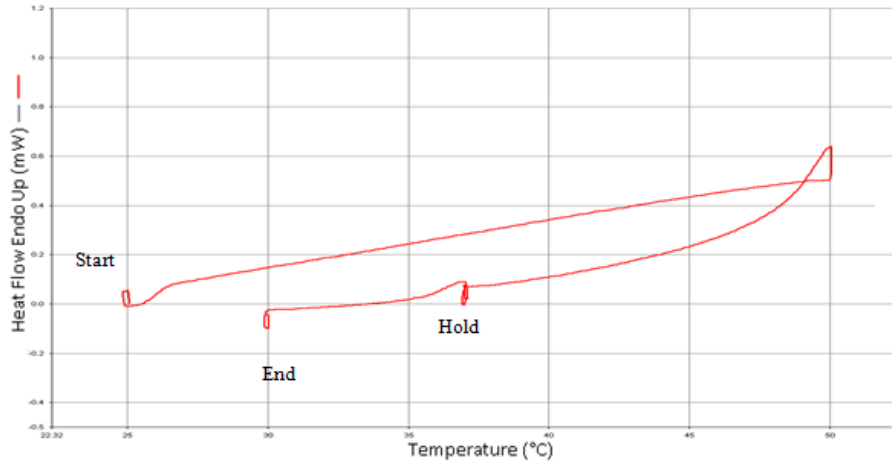


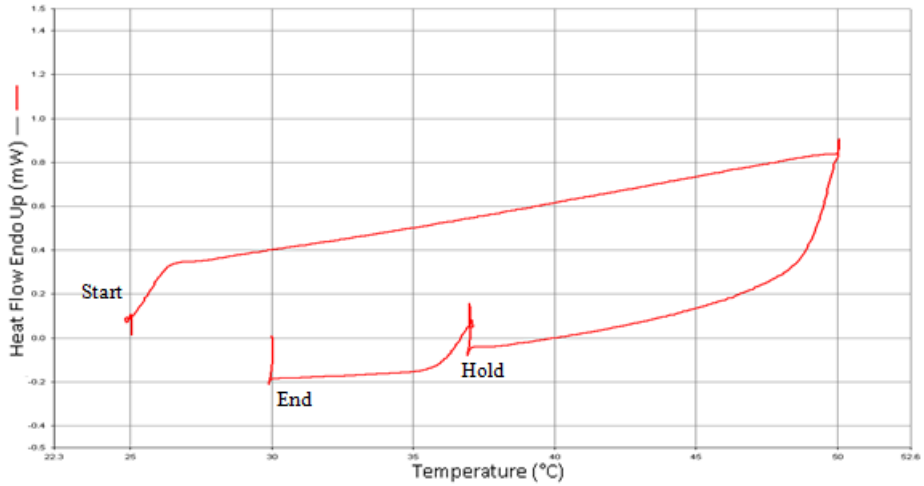


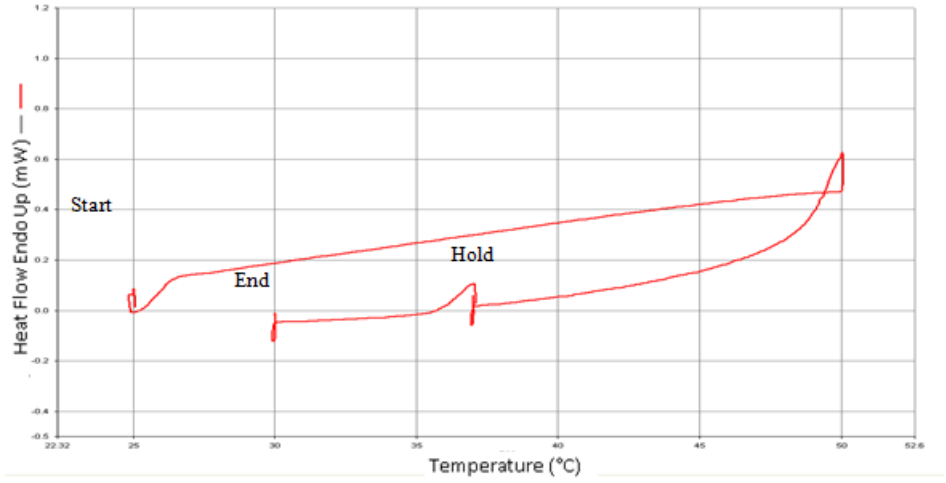


**Fig. 3.8:** DSC scans of Bioglues containing (a) no added Ag(I) ions, (b) added $AgNO_3$ (0.01 g) and (c) added $[Ag_2(3,6,9\text{-tdda})].2H_2O$ (0.01 g). Samples were heated from 25-50 °C with increments of 5 °C, cooled back down to 37 °C, held at this temperature for three hours, and then cooled to 30 °C.

were observed and the IR spectra remained unaltered (Fig. 3.7 (c and f)). These observations confirmed the thermal stability of the Bioglues at 37 °C over a 3 h period.

### 3.2.4 Surface morphologies

The surface morphology of the Bioglues was analysed using SEM in order to detect if any structural changes occurred when Ag(I) ions were included in the Bioglue formulation (Fig. 3.9). Bioglue without added $AgNO_3$ had a porous surface (Fig. 3.9a). This contrasted with the Bioglue containing added $AgNO_3$ (0.1 g), which appeared to have a rough surface (Fig. 3.9b). A ten-fold decrease in the amount of added $AgNO_3$ (0.01 g) gave a Ag(I)-Bioglue with a very smooth surface (Fig. 3.9c). At the lowest quantity of added $AgNO_3$ (0.0001 g) (Fig. 3.9d), the surface begins to appear porous once more and, unsurprisingly, resembles that of a Bioglue without added $AgNO_3$ (Fig. 3.9a).

Energy dispersive X-ray spectroscopy (EDX) was performed on the Bioglues to provide a qualitative elemental analysis of the sample (Fig. 3.10a). Three bands were observed between 2.98 and 3.35 KeV which are assigned to the $L_{\alpha}$, $L_{\beta 1}$ and $L_{\beta 2}$ lines, respectively, of silver.[215] Gold was also detected as this metal was used to sputter coat the samples prior to SEM and EDX analysis.

### 3.2.5 Swelling studies

Hydrogels by their nature are three-dimensional, cross-linked polymeric networks which have the ability to swell in water, and also in buffered or physiological solutions.[216,217] Swelling studies were carried out on the current Bioglue hydrogels in order to determine the maximum amount of water that the samples could absorb (Section 2.10) (Fig. 3.11 and 3.12). The swelling ratio was determined using the following equation:[199]

$$r = (m_f - m_i / m_i) \times 100\%$$

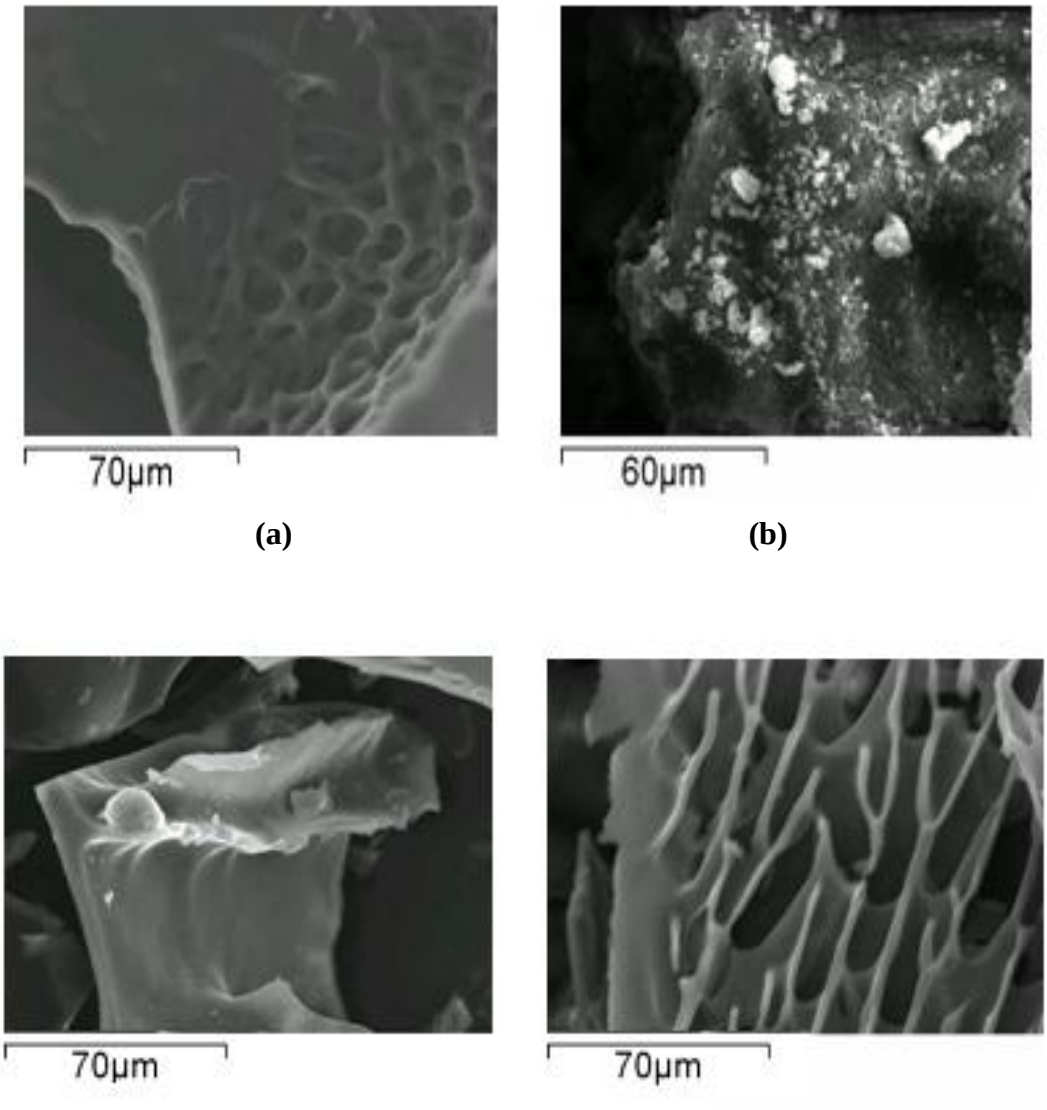


**Fig. 3.9:** SEM images of Bioglues (a) with no added $AgNO_3$, (b) added $AgNO_3$ (0.1 g), (c) with added $AgNO_3$ (0.01 g) and (d) added $AgNO_3$ (0.0001 g).

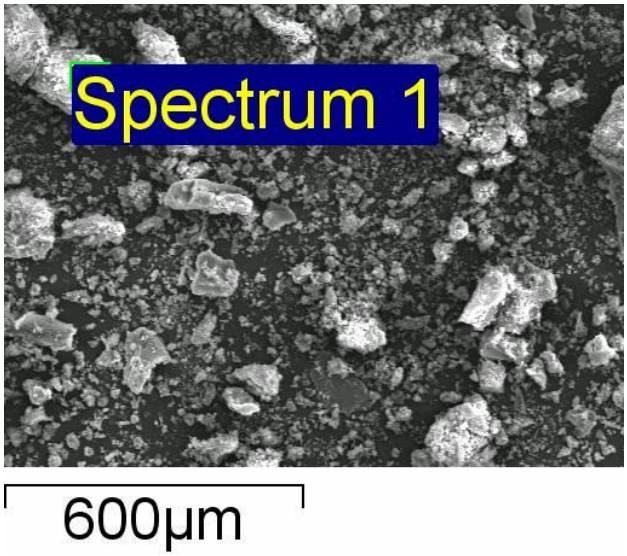


**(a)**

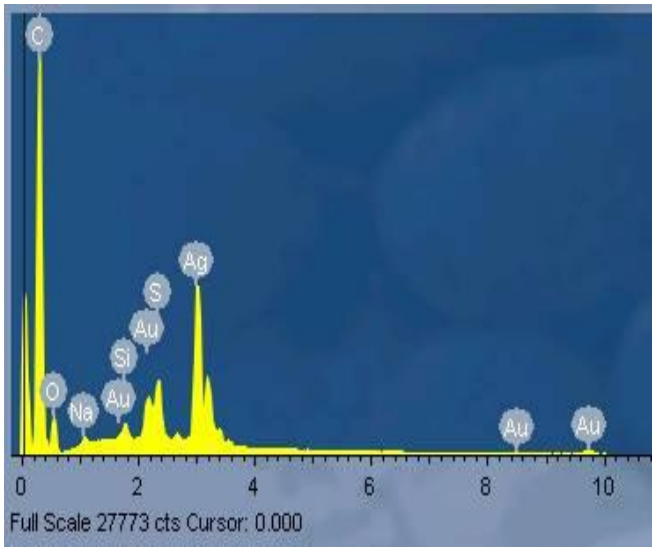


**(b)**

**Fig. 3.10:** (a) SEM image of Bioglue prepared with the highest amount of added $AgNO_3$ (0.1 g) and (b) the corresponding EDX spectrum.

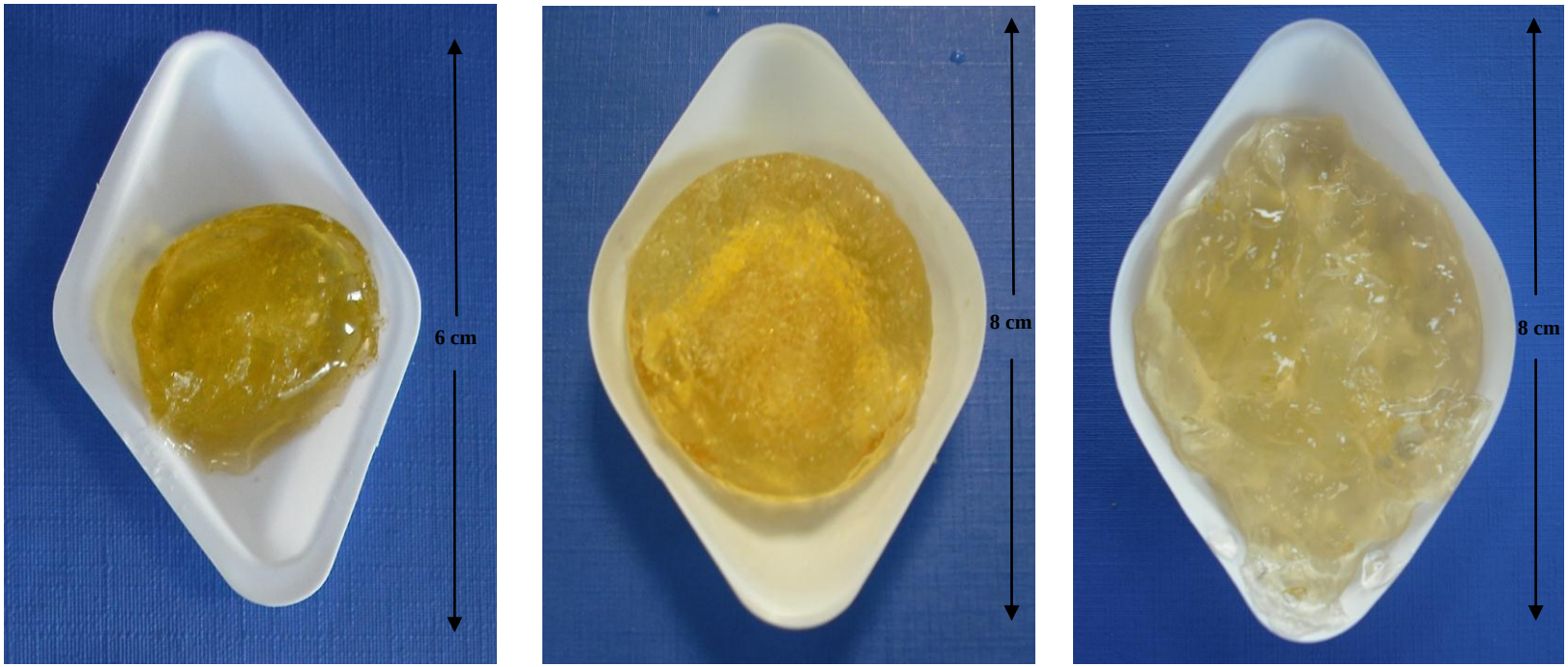


**(a)** **(b)** **(c)**

**Fig. 3.11:** Images depicting Biolue with no added Ag(I) ions at various stages of swelling studies (a) 0 h, (b) 24 h and (c) 120 h.

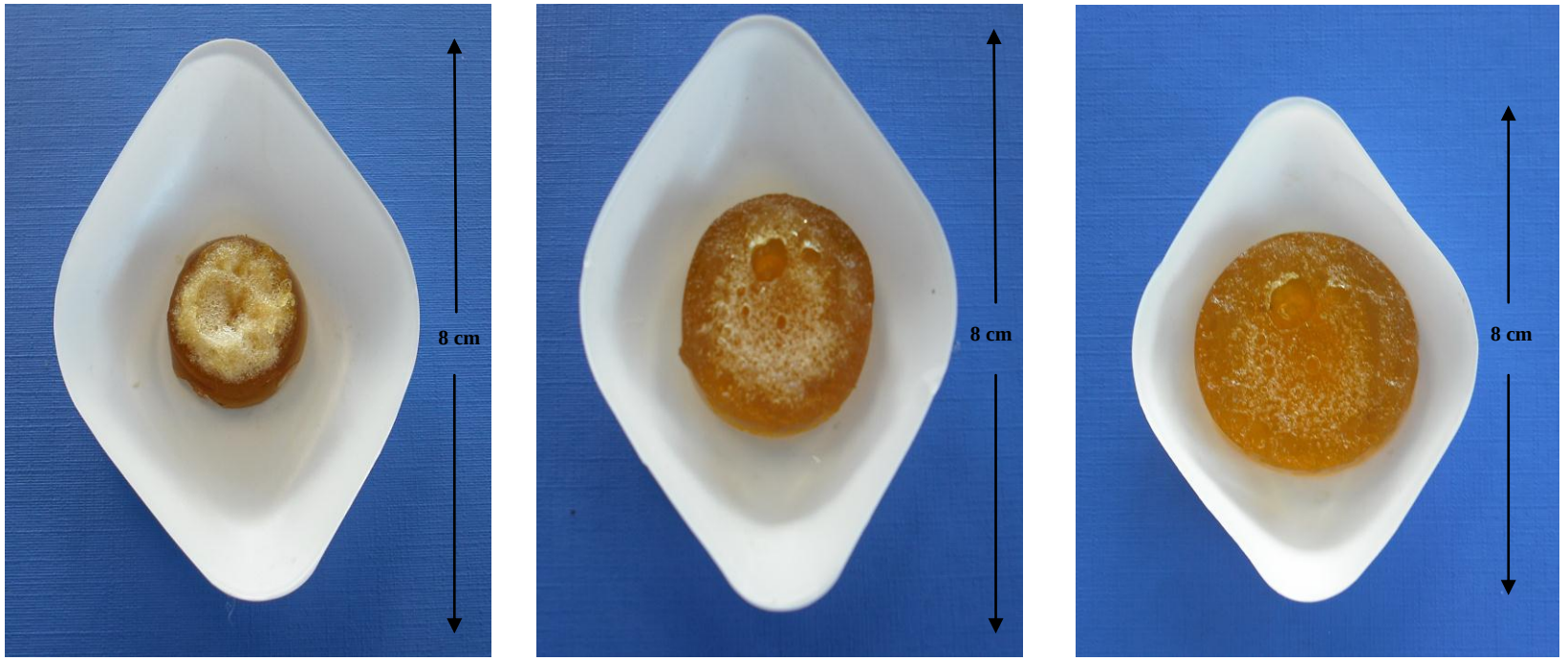


**(a)** **(b)** **(c)**

**Fig. 3.12:** Images depicting Bioglue with added $[Ag_2(3,6,9\text{-tdda})].2H_2O$ (0.01 g) at various stages of swelling studies (a) 0 h, (b) 24 h and (c) 120 h. Images of the Bioglue with added $AgNO_3$ (0.01g) over the same time period were very similar to those for the $[Ag_2(3,6,9\text{-tdda})].2H_2O$ Bioglue.

where r is the swelling ratio, $m_f$ is the final mass of the hydrogel after swelling and $m_i$ is the initial mass of the hydrogel sample. The Bioglue sample without Ag(I) ions reached a maximum weight (908% weight increase) after 48 h. The Bioglue containing added $AgNO_3$ (0.01 g) had a 117% weight increase over the same time period (Fig. 3.13).

Generally, for the $AgNO_3$-Bioglues, as the amount of added Ag(I) ions decreased the swelling ratio increased. A similar trend was also seen for the [$Ag_2$(3,6,9-tdda)].2$H_2O$-Bioglues (Fig. 3.14), where at the highest quantity of added [$Ag_2$(3,6,9-tdda)].2$H_2O$ (0.01 g) a 271% weight increase was observed, and at the lowest amount (0.00001 g) the weight increase was 945% after 48 h. Increasing the amount of added Ag(I) ion considerably reduces hydrogel swelling and also leads to a product whose glue-like adhesive properties are dramatically lessened. The structure of the Bioglue with the highest amount of added [$Ag_2$(3,6,9-tdda)].2$H_2O$ (0.01 g) is more rigid and retains its shape throughout the swelling studies (Fig. 3.12) in comparison to the Bioglue with little or no added Ag(I) ions (Fig. 3.11). This was also found for the $AgNO_3$-Bioglue (image not shown). Deen *et al*[218] found a similar trend for a poly(N-acryloyl-N'-ethylpiperazine) hydrogel, in which the swelling ratio decreased in the presence of added $Ni^{2+}$ ions. It was postulated that in the presence of the metal ion competition occurs between protonation and the formation of a metal-ligand complex which act as physical crosslinks within the gel network and thereby affects the elastic modulus of the gel which, in turn, reduces the swelling ratio.[218] Katime and Rodriguez[219] also found that increasing the amount of metal ion ($Cu^{2+}$) in a poly(acrylic acid-co-itaconic acid) hydrogel resulted in a decrease in the swelling of the hydrogel.

It was also found that the Bioglue (without added $AgNO_3$) degraded over the 120 h, and in particular after 24 h (Fig. 3.13), whereas the Ag(I)-Bioglues with the lower amounts of added $AgNO_3$ (0.001 g and 0.0001 g) started to degrade after 48 h. This may be due to hydrolysis of the imine bond and explains why breakdown of the Bioglue was observed.

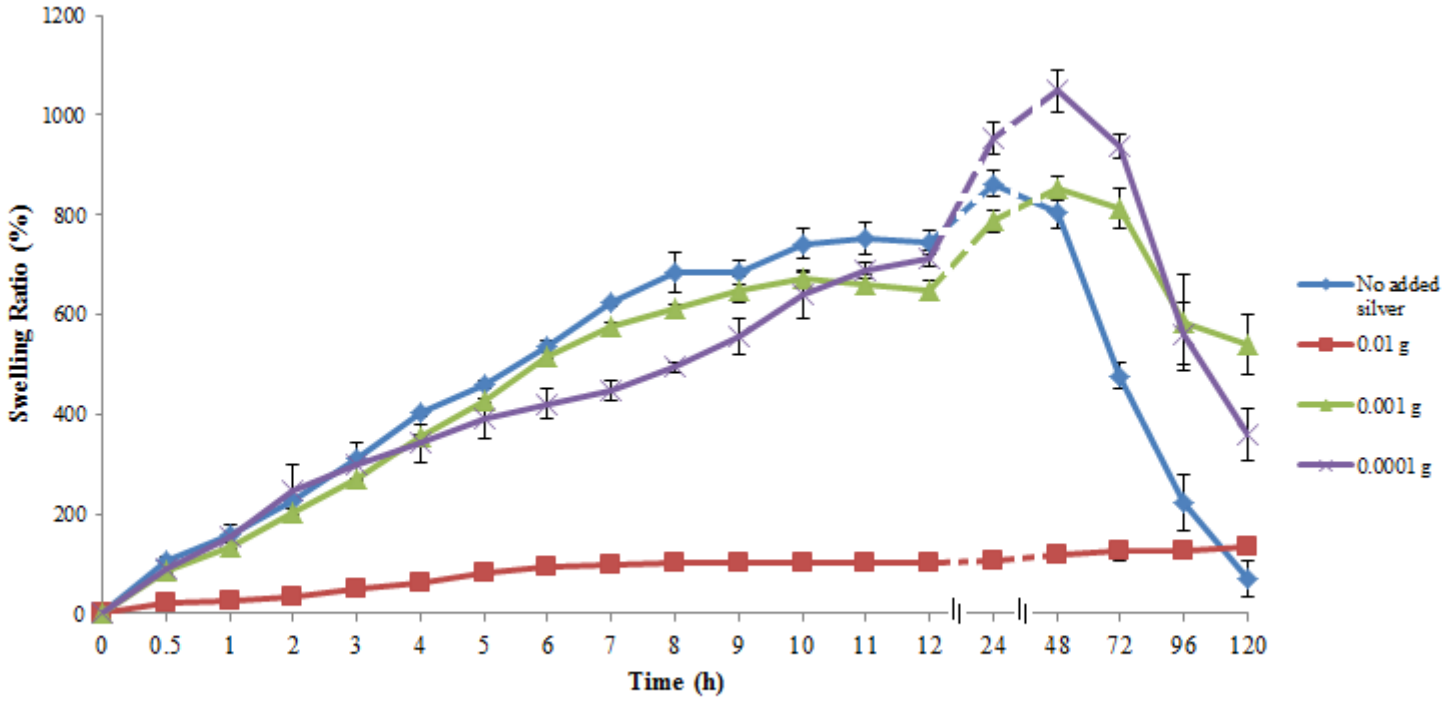


**Fig. 3.13:** Swelling studies for a Bioglue without added Ag(I) ions and for a series of $AgNO_3$-Bioglues (added $AgNO_3$ 0.01-0.0001 g). The experiments were repeated three times.

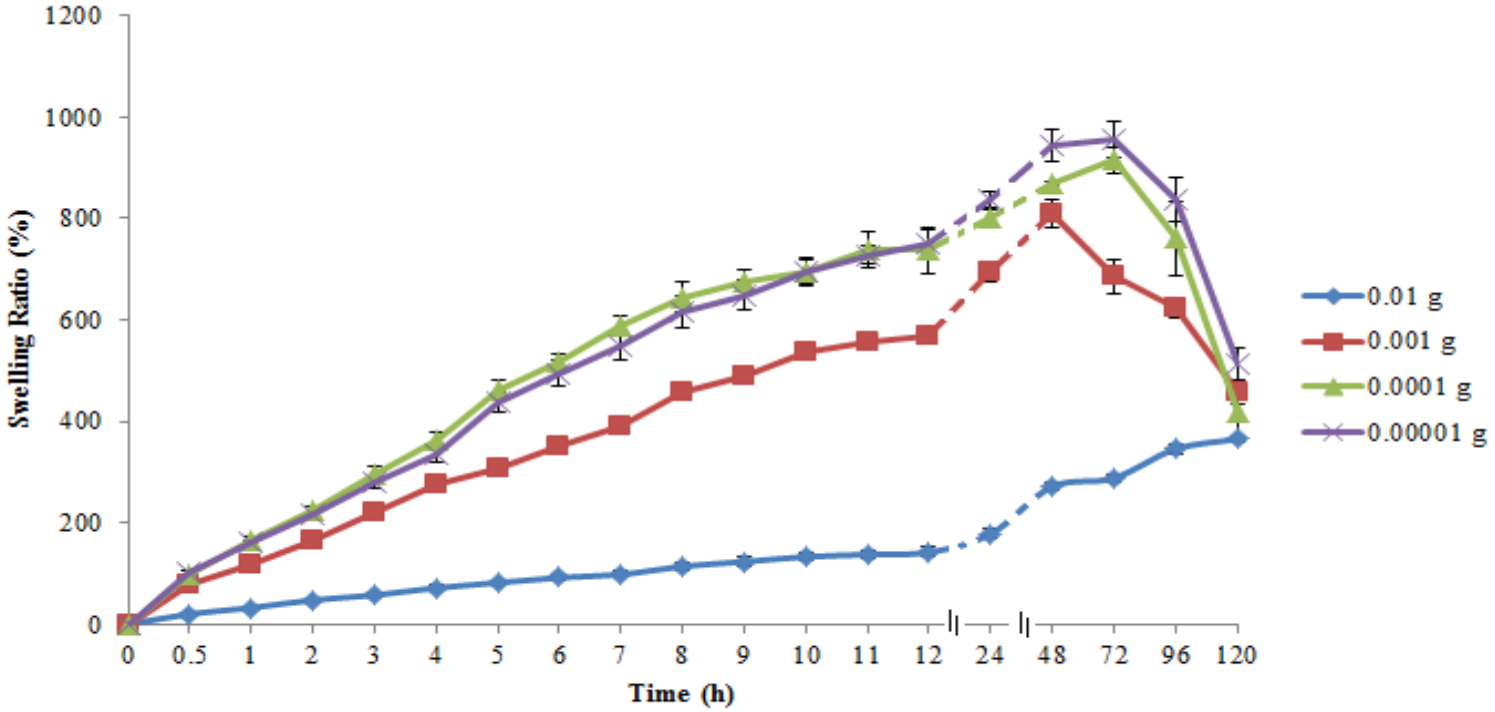


**Fig. 3.14:** Swelling studies for a series of Bioglues with $[Ag_2(3,6,9\text{-tdda})].2H_2O$ (0.01-0.00001 g). The experiments were repeated three times.

### 3.2.6 Mechanical testing

Mechanical testing studies were conducted in order to determine the tensile properties of the various Bioglues. The first series of tensile tests were carried out using strips of wood where Bioglue samples (15 µl) were applied to one surface of the wood before overlapping by 10 mm with the second piece of wood (Fig. 3.15a).[220] Samples of wood stuck together with Bioglue were left to stand overnight at room temperature before tensile testing was carried out. It was found that the maximum load required to break the test pieces was 136.25 ± 5.39 N for the Bioglue without added Ag(I) ions. The force decreased to 112.71 ± 10.56 N for the Ag(I)-Bioglue with the lowest amount of added $AgNO_3$ (0.0001 g), and a further decrease occurred for the Bioglue with the highest quantity of added $AgNO_3$ (0.01 g) (78.82 ± 6.86 N) (Fig. 3.16a).

The Young's modulus, which is an assessment of the stiffness of an elastic material, was also determined for the Bioglues (Fig. 3.17a). Bioglue without added Ag(I) ions had a Young's modulus of 293.46 ± 24.69 MPa. For the Bioglue containing the highest amount of added $AgNO_3$ (0.01 g) the Young's modulus was 334.47 ± 46.87 MPa and 269.65 ± 18.05 MPa for the Bioglue containing the lowest amount of added $AgNO_3$ (0.0001 g). These results imply that the presence of Ag(I) ions in the Bioglues does not alter the stiffness of the Bioglue.

Tensile testing was repeated using Bioglue bonded pig skin as this matrix has a close resemblance to human skin.[221] Initially, the majority of the fat layer was removed from the pig skin using a sterile scalpel. The second series of tensile tests were carried out using pig skin where Bioglue samples (100 µl) were applied to one surface of the skin before overlapping by 10 mm with the second piece of skin (Fig. 3.15b).[221] The sample was placed in a static incubator at 37 °C overnight to mimic body temperature before the tensile testing was carried out. The maximum load required to break apart the pieces of skin was 6.80 ± 1.22 N for the Bioglue without added $AgNO_3$, and this value decreased to 4.39 ± 0.38 N for the Bioglue with the highest amount of added $AgNO_3$ (0.01 g) (Fig. 3.16b). As the amount of $AgNO_3$ in the Bioglue decreased, the maximum load required for skin detachment also decreased. This contrasts with the results obtained with the glued wood pieces,

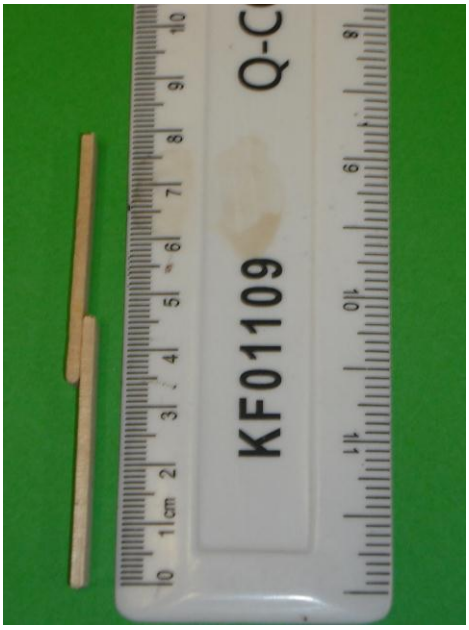


**(a)**

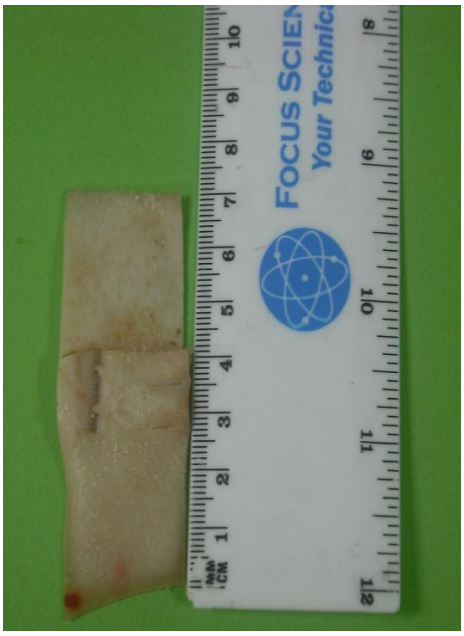


**(b)**

**Fig. 3.15:** Dimensions of (a) wood and (b) pig skin used in the present study.

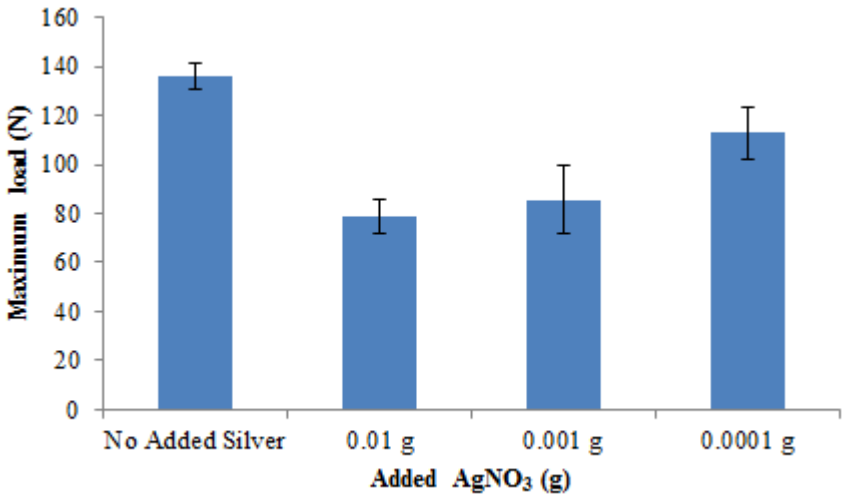


**(a)**

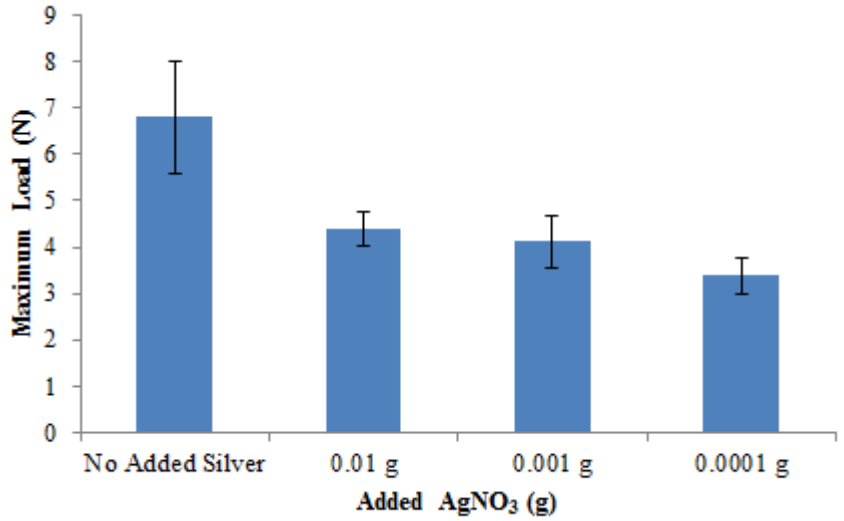


**(b)**

**Fig. 3.16:** Maximum load (N) required to break samples stuck together with Bioglue formulated with and without added $AgNO_3$: (a) bonded pieces of wood and (b) bonded pieces pig skin.

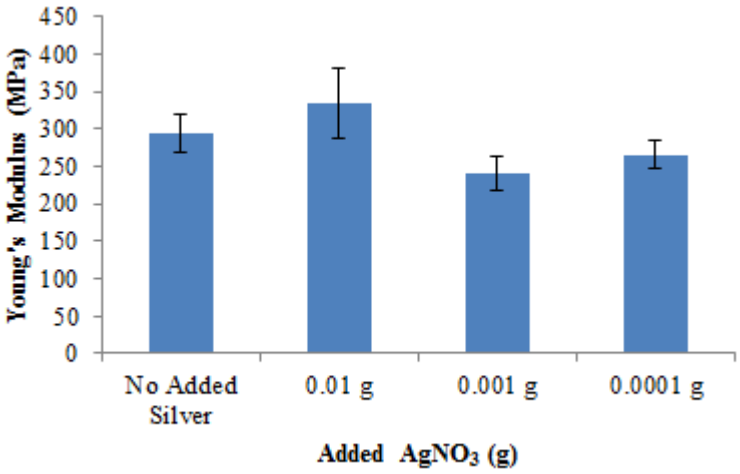


**(a)**

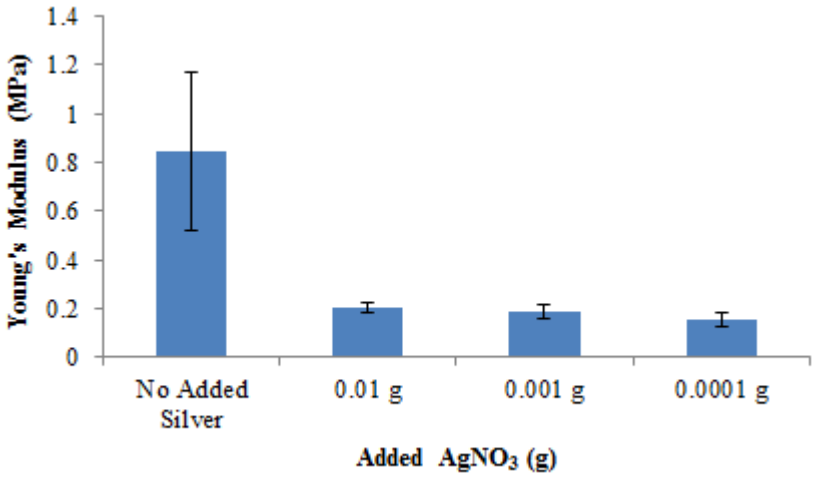


**(b)**

**Fig. 3.17:** Young's modulus (MPa) for samples stuck together with Bioglue samples formulated with and without added $AgNO_3$: (a) bonded pieces of wood and (b) bonded pieces of pig skin.

where the maximum load increased as the amount of added $AgNO_3$ decreased. The observed difference in the tensile testing trends between the wood and pig skin may be due to the fact that the wood is more porous than the pig skin and that the Bioglue seeps into the pores and creates a stronger bond between the glue and the material with the greatest porosity. This may also explain why the maximum load at the point of break was different for the wood and the pig skin. The difference in the elasticity of the material can be seen clearly in Fig. 3.17. Young's modulus for the pig skin adhered by Bioglue was found to be 0.85 ± 0.32 MPa for the Bioglue without added $AgNO_3$ and 0.20 ± 0.02 MPa for the Bioglue with the highest amount of added $AgNO_3$ (0.01 g) (Fig. 3.17b). At the lowest amounts of added $AgNO_3$ (0.0001 g) a small decrease in the Young's modulus was seen (0.16 ± 0.03 MPa). Subsequent increases in the amounts of added $AgNO_3$, (up to 0.01 g) did not cause significant further decreases in Young's modulus suggesting that increasing the amount of added $AgNO_3$ did not affect the elasticity of the Bioglue. In comparing the Bioglue without added Ag(I) ions a clear difference can be seen suggesting that the incorporation of Ag(I) ions into the Bioglue formulation does effect the elasticity of the Bioglue.

Issues concerning the effect that the elasticity of Bioglue may have on surrounding tissues have previously been raised. De Somer *et al*[64] used Bioglue and Tissucol Duo, a fibrin sealant, as controls in the comparison of the mechanical and chemical characteristics of an autologous glue. These researchers found that, in elasticity testing experiments, the maximum loads required to break apart the test pieces (aluminum blocks with a surface area of 25 $cm^2$ smeared with an even application of glue (2.1 ml)) were 322 ± 104 N for Bioglue and 144 ± 66 N for the canine autologous glue. Bioglue, in comparison to other adhesives, was found to be a rigid glue (relatively inelastic). Azadani *et al*[222] found that the Young's modulus of Bioglue was nearly 60 times greater than Crosseal, a fibrin sealant, and 30 times greater than Tisseel, another fibrin sealant and CoSeal, a synthetic glue consisting of polyethylene glycol macromers. For the successful use of a tissue adhesive, product limitations must be understood in order that the correct adhesive is chosen for a given circumstance.

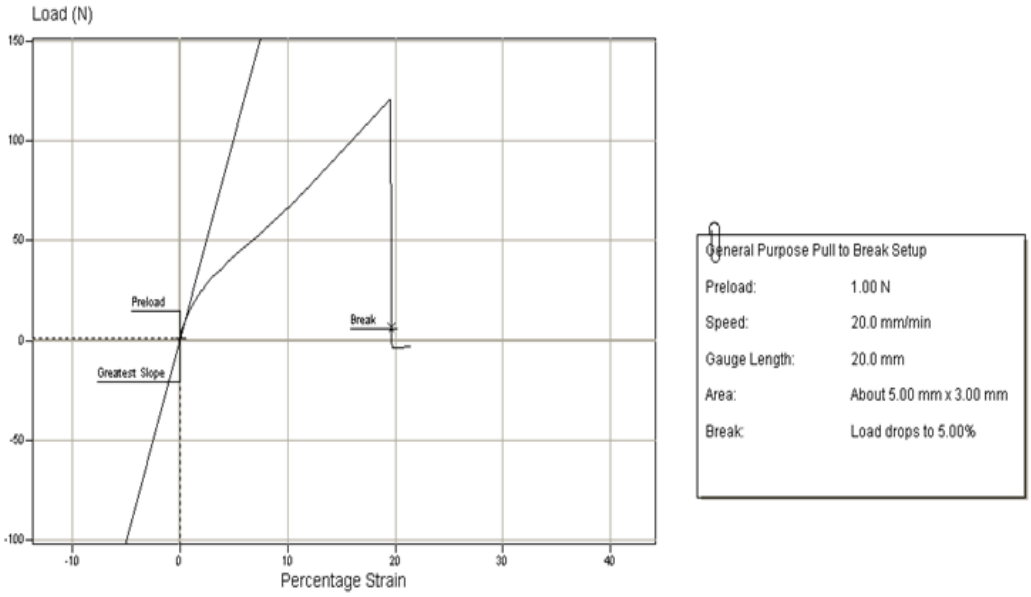


**(a)**

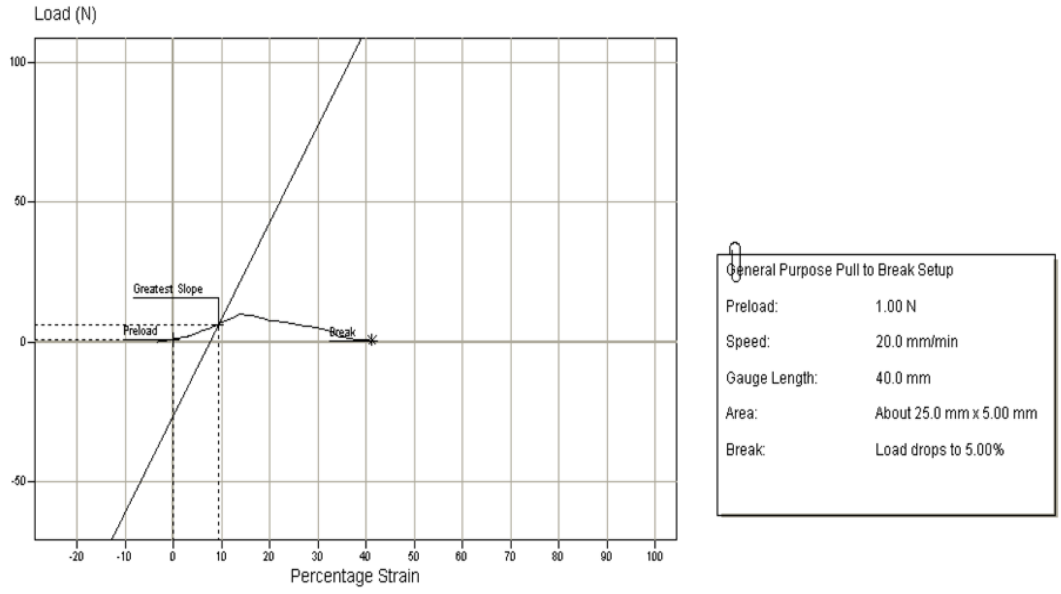


**(b)**

**Fig. 3.18:** Image depicting point of break for Bioglue-adhered surfaces without Ag(I) ions (a) wood and (b) pig skin.

### 3.2.7 Ag(I) leaching studies

Electrochemical analysis was carried out to determine the amount of Ag(I) ions that leached from $AgNO_3$-Bioglue samples over time. The dry mass of the $AgNO_3$-Bioglue (formulated using 0.01 g $AgNO_3$) was 0.50 g and contained 5.88 x $10^{-5}$ moles of Ag(I) ions. A portion (0.10 g, containing 1.17 x $10^{-5}$ moles Ag(I) ions) of this sample was used in the electrochemical cell that was employed in the leaching experiments. The supporting electrolyte (60 mls) was added to the cell and the amount of leached Ag(I) ions was determined at time intervals for up to 55 h (Fig. 3.19(a)). Over the first 10 h, there was rapid leaching of Ag(I) ions from the Bioglue into the supporting electrolyte. Leaching then slowed down and appeared to reach an equilibrium concentration value (*ca*. 6 x $10^{-5}$ M (Ag(I)). At the 55 h timepoint, approximately 30% of the original amount of Ag(I) ions in the Bioglue had leached into the supporting electrolyte. This experiment was carried out on two separate preparations of the $AgNO_3$-Bioglue (0.01 g $AgNO_3$) (see Appendix III Fig. 1 and 2) and it was found that there was a variance in the total amounts of Ag(I) ions leached from these two samples. This implies that there is not a homogenous distribution of the metal ion throughout the samples (as confirmed by earlier AA analysis of the samples). This electrochemical experiment was repeated for a $AgNO_3$-Bioglue a lower amount of added $AgNO_3$ (0.001 g) (contained 5.58 x $10^{-6}$ moles Ag(I) ions). A portion of this sample (0.1 g, containing 1.17 x $10^{-6}$ moles Ag(I) ions) was used in the leaching experiments. As with the previous sample, the supporting electrolyte (60 mls) was added to the cell and the amount of Ag(I) ions leached from the sample was monitored for up to 55 h (Fig. 3.19(b). Again, it was found that an equilibrium concentration value was reached after 55 h (*ca*. 6.5 x $10^{-6}$ M Ag(I) ions) and this corresponded to approximately 30% of the original amount of Ag(I) ions in the Bioglue sample.

These studies are important as they provide vital information on the rate at which Ag(I) ions leach from the samples and establish an antimicrobial environment. It can be seen from the graphs (Fig. 3.19) that the rate at which Ag(I) ions leach from the $AgNO_3$-Bioglues reach an equilibrium by 55-65 h. As most patients come into contact with microorganisms within the first few hours of admission to hospital and

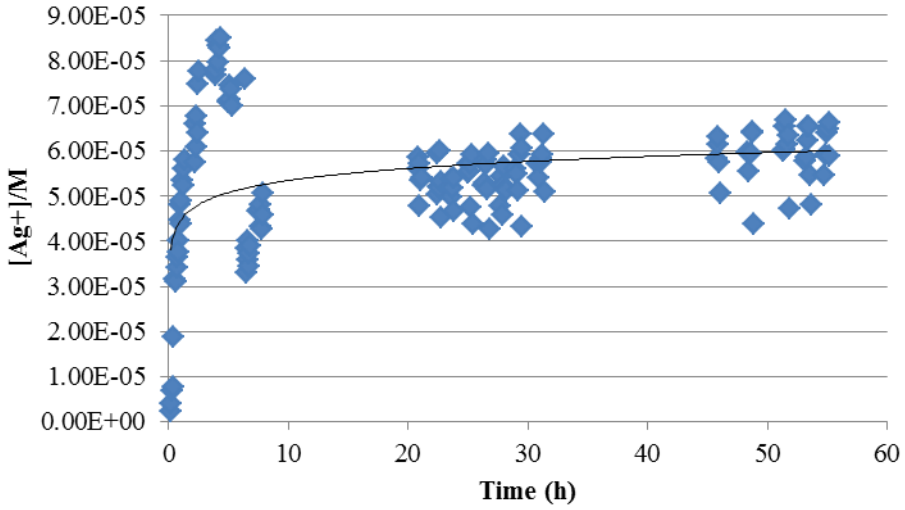


**(a)**

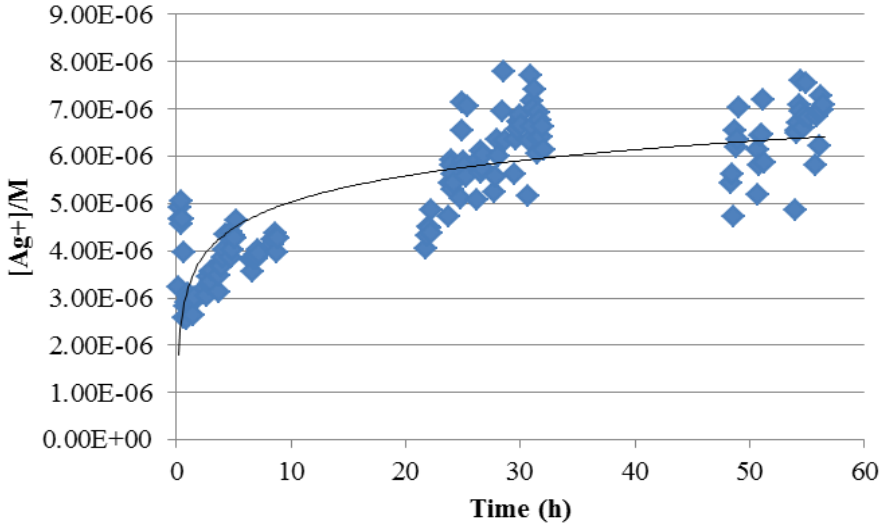


**(b)**

**Fig. 3.19:** Concentration of leached Ag(I) ions from $AgNO_3$-Bioglues (a) with 0.01 g added $AgNO_3$ and (b) with 0.001 g added $AgNO_3$.

infections become evident after 48 h,[223] the use of these $AgNO_3$-Bioglues may prevent such infections from occurring.

## 3.3 Reduction of Bioglues and the Synthesis of Ag(0) Nanoparticles

Aqueous solutions of two different reducing agents (sodium borohydride and sodium citrate) were used in an attempt to reduce the Ag(I) ion within the $AgNO_3$-Bioglue (0.01 g added $AgNO_3$) to Ag(0). It should be noted that sodium borohydride also has the ability to reduce imine functionalities formed upon the production of Bioglue from BSA and GLA. The Bioglue changed colour, from a golden-yellow to either a dark-brown or orange upon reduction with $NaBH_4$ (0.1 M and 0.01 M solutions, respectively) (Fig. 3.20) suggesting that the following chemical reaction had taken place:

$$2Ag^{+} + 2NaBH_4 + 6H_2O \longrightarrow 2Ag^{0} + 7H_2 + 2Na^{+} + 2B(OH)_3$$

Hydrogen gas may also be given off upon the reaction of sodium borohydride with water:

$$NaBH_4 + 4H_2O \longrightarrow NaB(OH)_4 + 4H_2$$

Bioglue without Ag(I) ions was also exposed to $NaBH_4$ solutions (0.1 M, 0.01 M and 0.001 M) and it was found that the Bioglue remained its usual golden-yellow colour.

Mohan *et al*[224] also found a colour change, (colourless to brown) for a $AgNO_3$-poly(acrylamide) hydrogel with aqueous $NaBH_4$ (0.1 M). In the present studies, UV-vis spectroscopy (Fig. 3.21) was carried out on the reaction supernatant of the reduced $AgNO_3$-Bioglue (0.01 g) to establish if nanoparticulate Ag(0) was present. The presence of a band with $\lambda_{max}$ = 276 nm suggesting that Ag(0) nanoparticles were not present in the supernatant (suspension of Ag(0) nanoparticles are expected to have a band with $\lambda_{max}$ = 400-500 nm).[224]

The surface morphology of the $NaBH_4$ reduced $AgNO_3$-Bioglue was analysed by SEM and it was found to be smooth in some areas but porous in others (Fig. 3.22). The hollow pores may be a result of escaping $H_2$ produced upon $NaBH_4$ reduction.

Silver detected by EDX studies showed three lines between 2.98 and 3.35 KeV ($L_{\alpha}$, $L_{\beta 1}$ and $L_{\beta 2}$ lines of silver).[215] Although Ag(0) nanoparticles were not detected either in the reaction supernatant or on the outer surface of the reduced Bioglue, it is still likely that Ag(0) nanoparticles (or micro-particles) were trapped within the Bioglue matrix (as suggested by the colour change of the reduced Bioglues shown in Fig. 3.20b).

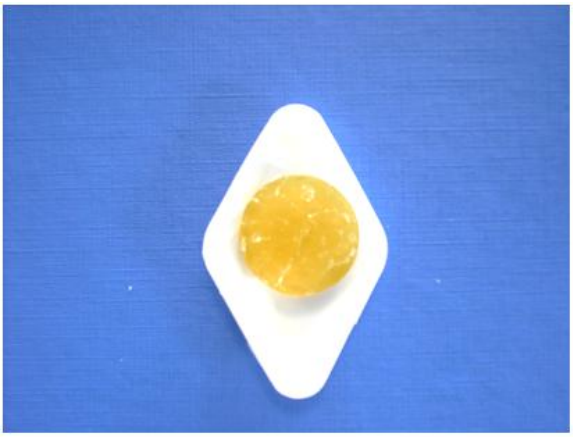

**(a)**

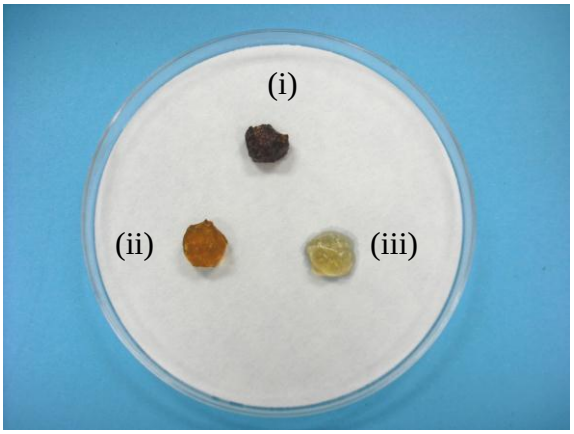


**(b)**

**Fig. 3.20:** Images depicting colours of $AgNO_3$-Bioglues (0.01 g $AgNO_3$) (a) before and (b) after reduction with (i) $NaBH_4$ (0.1 M), (ii) $NaBH_4$ (0.01 M) and (iii) $NaBH_4$ (0.001 M).

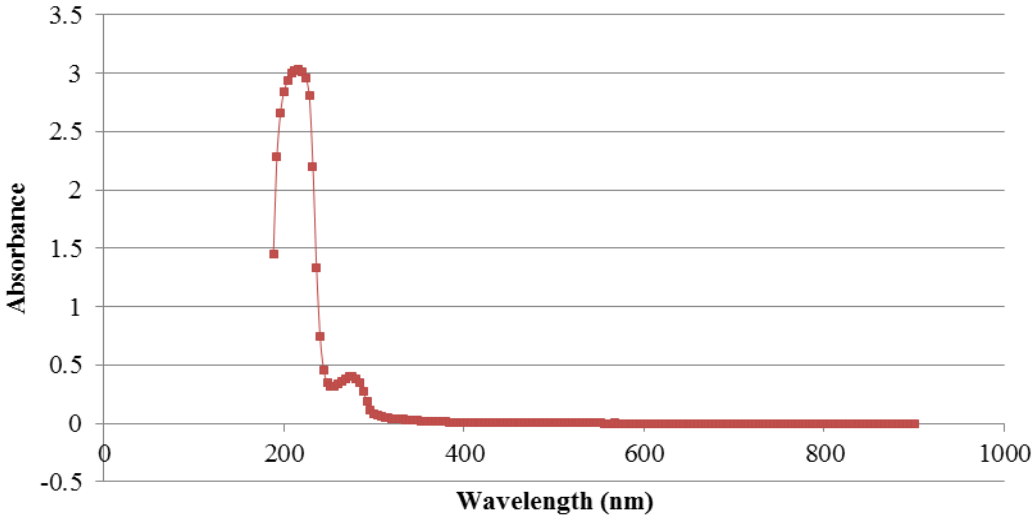


**Fig. 3.21:** UV-Vis spectrum of supernatant of $NaBH_4$ reduced $AgNO_3$-Bioglue (0.01 g $AgNO_3$).

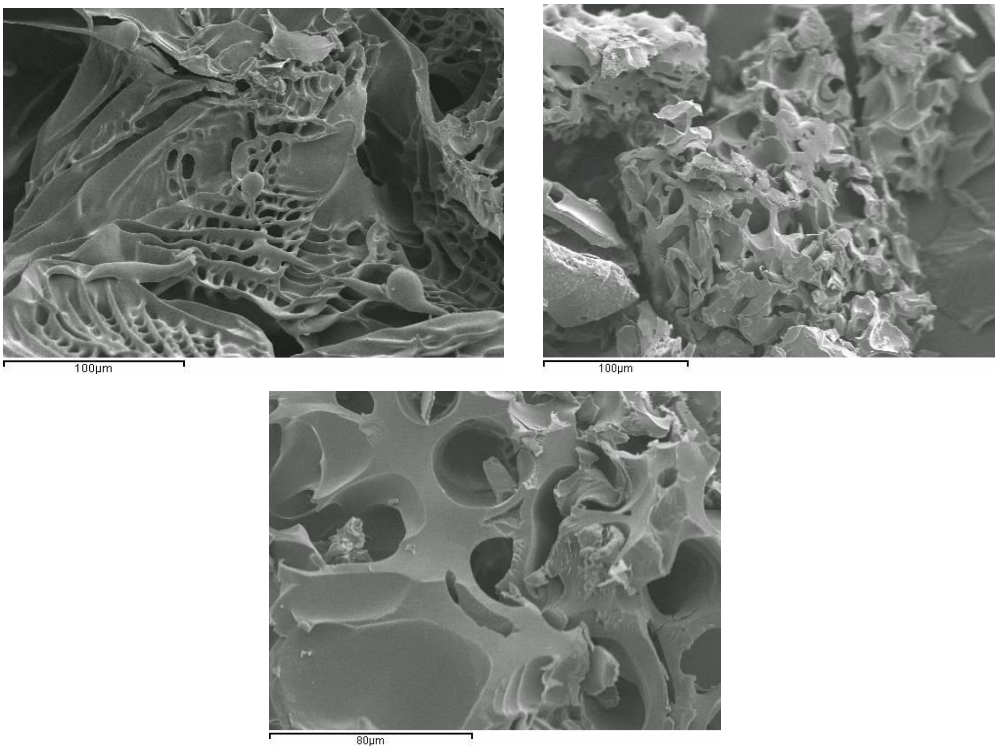


**Fig. 3.22:** Series of SEM images of different magnification for an $AgNO_3$-Bioglue (0.01 g $AgNO_3$) following reduction with aqueous $NaBH_4$ (0.01 M).

In a series of separate experiments, aqueous solutions of sodium citrate were employed in an attempt to reduce the $AgNO_3$-Bioglue (0.01 g of added $AgNO_3$). Three different experiments were performed (Section 2.11.2) in which the $AgNO_3$-Bioglue samples were exposed to either sodium citrate solution (1%, w/v) alone or to sodium citrate solution (1% w/v) + light, or to just light only. The reaction of sodium citrate and $Ag^+$ is given by the following equation:[225]

$$4Ag^+ + C_6H_5O_7Na_3 + 2H_2O \rightarrow 4Ag^0 + C_6H_5O_7H_3 + 3Na^+ + H^+ + O_2$$

The UV-vis spectra of the resulting supernatants from the three experiments outlined above showed only a peak with $\lambda_{max}$ = 276 nm (Fig. 3.23), again suggesting that Ag(0) nanoparticles were not present in the supernatant. The surface morphology of the reduced Bioglues were analysed by SEM (Fig. 3.24). The surface morphology was very smooth in comparison to the $NaBH_4$-reduced Bioglues. Silver was detected by EDX. Although Ag(0) nanoparticles were not detected in the supernatant or on the solid surface, it is again possible that Ag(0) nanoparticles (or micro-particles) were trapped within the matrix of the treated $AgNO_3$-Bioglue.

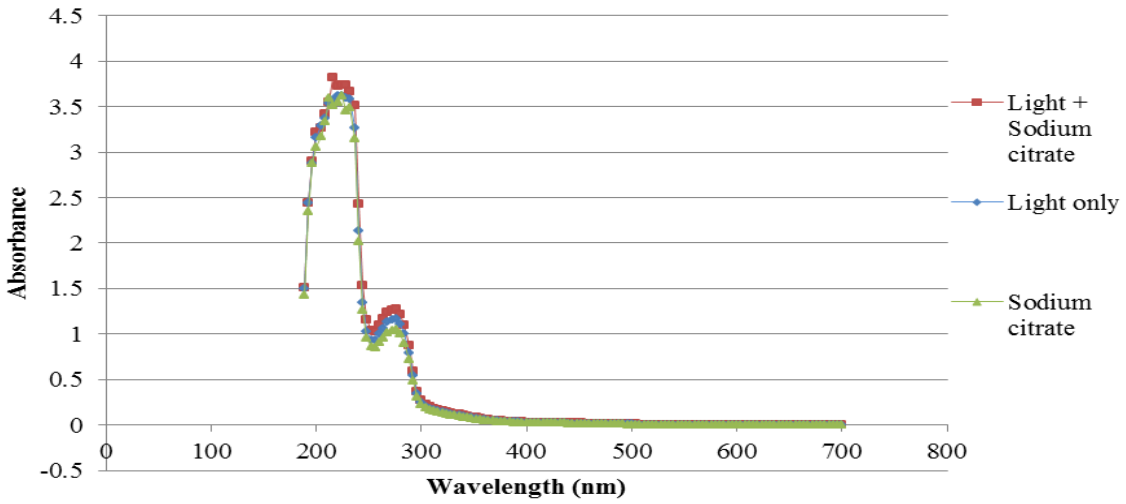


**Fig. 3.23:** UV-Vis spectrum of supernatant of reduced $AgNO_3$-Bioglue (0.01 g) with (a) sodium citrate (1%, w/v), (b) sodium citrate (1%, w/v) + light and (c) light only.

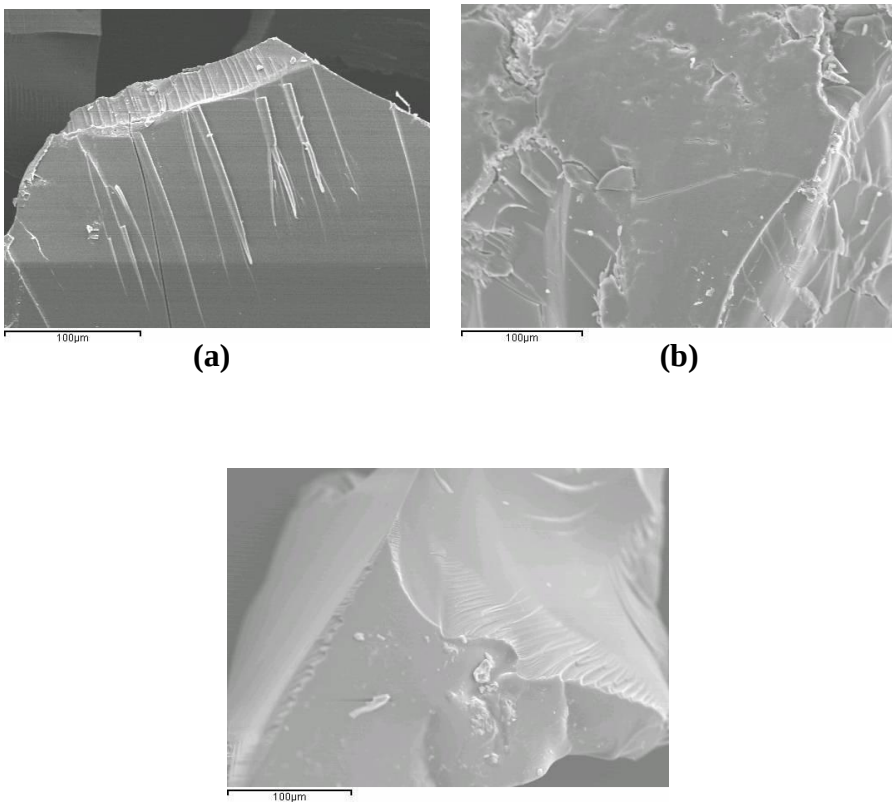


**(a)** **(b)**

**(c)**

**Fig. 3.24:** SEM images of reduced $AgNO_3$-Bioglue (0.01 g) with (a) sodium citrate (1%, w/v), (b) sodium citrate (1%, w/v) + light and (c) light only.

A number of experiments were conducted to investigate if a Bioglue (without added Ag(I) ions) would absorb Ag(0) nanoparticles from a reformed suspension of Ag(0) nanoparticles (Section 2.11.4). In the first instance, a suspension of Ag(0) nanoparticles was prepared using the established protocol[200] of reducing aqueous $AgNO_3$ with an aqueous solution of sodium citrate (1% w/v). The UV-visible spectrum of the resulting yellow/green suspension showed a broad band with $\lambda_{max}$ = 424 nm, characteristic of Ag(0) nanoparticle formation (Fig. 3.25a).[200] A Bioglue without added Ag(I) ions was prepared (in triplicate) and exposed to the previously synthesised Ag(0) nanoparticulate suspension for 120 h to allow sufficient time for any Ag(0) particles to diffuse into the Bioglue matrix. As there was no significant change in the absorption value of the 424 nm band after this time period (Fig. 3.25b) it was concluded that there had been no uptake of Ag(0) nanoparticles by the Bioglue.

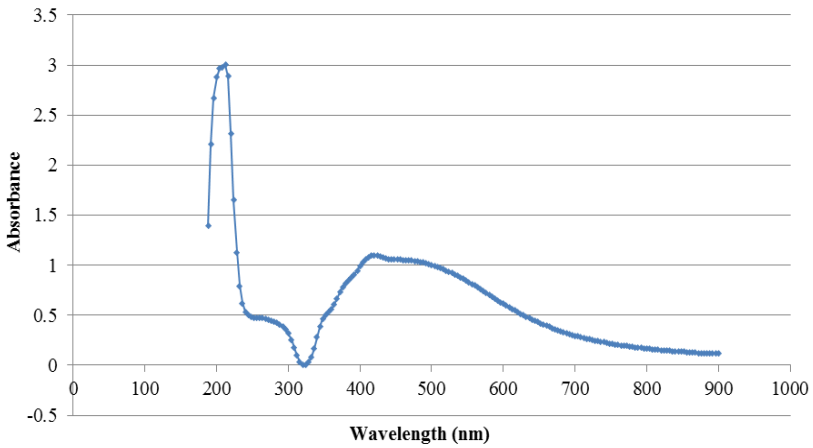


**(a)**

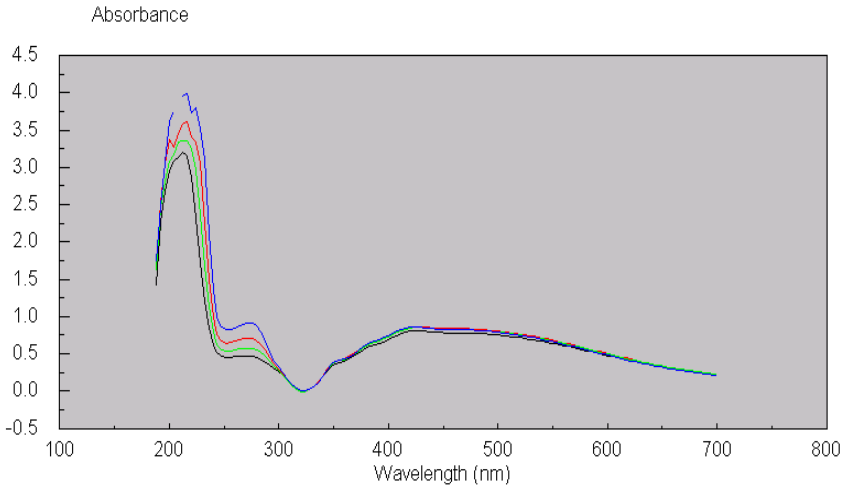


**(b)**

**Fig. 3.25:** (a) UV-Vis spectrum of Ag(0) nanoparticle suspension. The silver nanoparticles were prepared by reducing $AgNO_3$ (0.0314 g, 0.185 mmoles) with sodium citrate (1%, w/v) and (b) UV-Vis spectra of Bioglue (without added $AgNO_3$) in Ag(0) nanoparticle suspension. Black–6 h, green–24 h red–48 h, blue–120 h.

SEM and EDX were carried out on the Bioglue following exposure to the silver nanoparticles. The surface morphology of the Bioglue was found to be very porous (Fig. 3.26) which may explain why a decrease in the intensity of the UV-Vis spectra was not observed as the nanoparticles could diffuse easily in and also back out of the Bioglue. EDX did not detect any silver present in the Bioglue (Fig. 3.27).

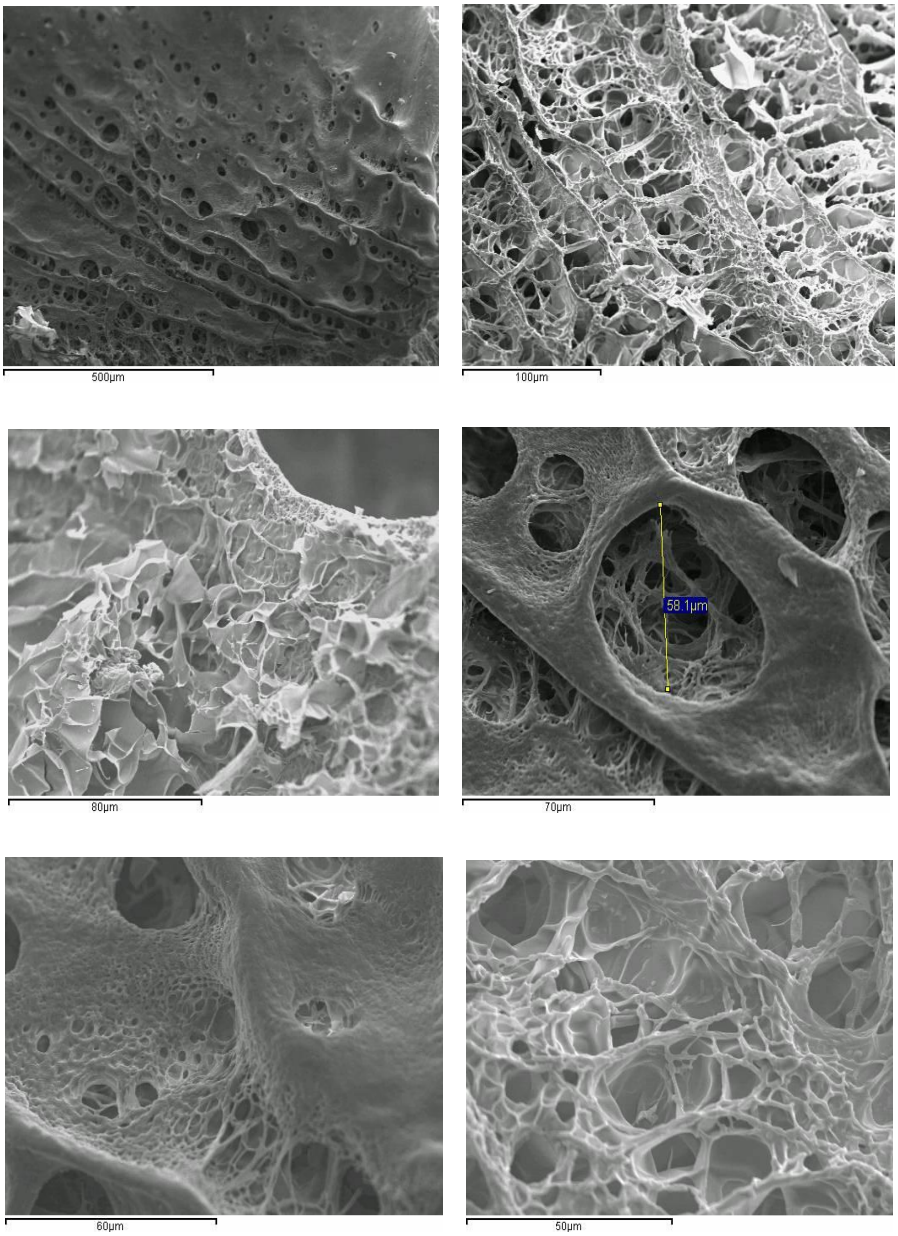


**Fig. 3.26:** SEM images of Bioglue without added $AgNO_3$ following immersion for 120 h in a Ag(0) nanoparticle suspension.

.

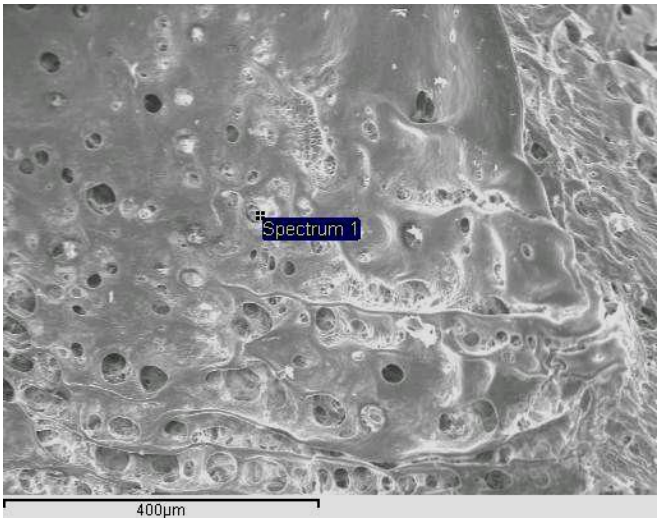


**(a)**

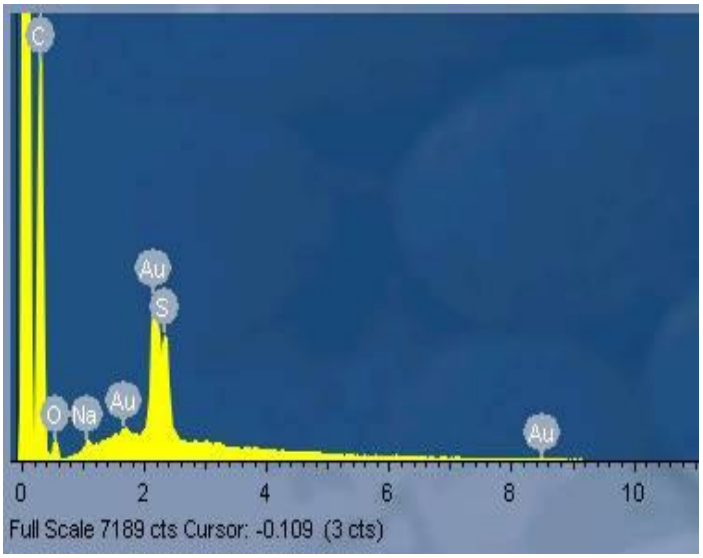


**(b)**

**Fig. 3.27**: (a) SEM image of Bioglue prepared in the absence of added $AgNO_3$ and (b) the corresponding EDX spectrum.

In correlation with the swelling studies, it was also found, Bioglue (without added $AgNO_3$) degraded over the 120 h period, and in particular after 24 h (Fig. 3.28). This was evident by the large increase in the 276 nm band over this time period which corresponds to the formation of BSA through hydrolysis of the imine bond in the Bioglue

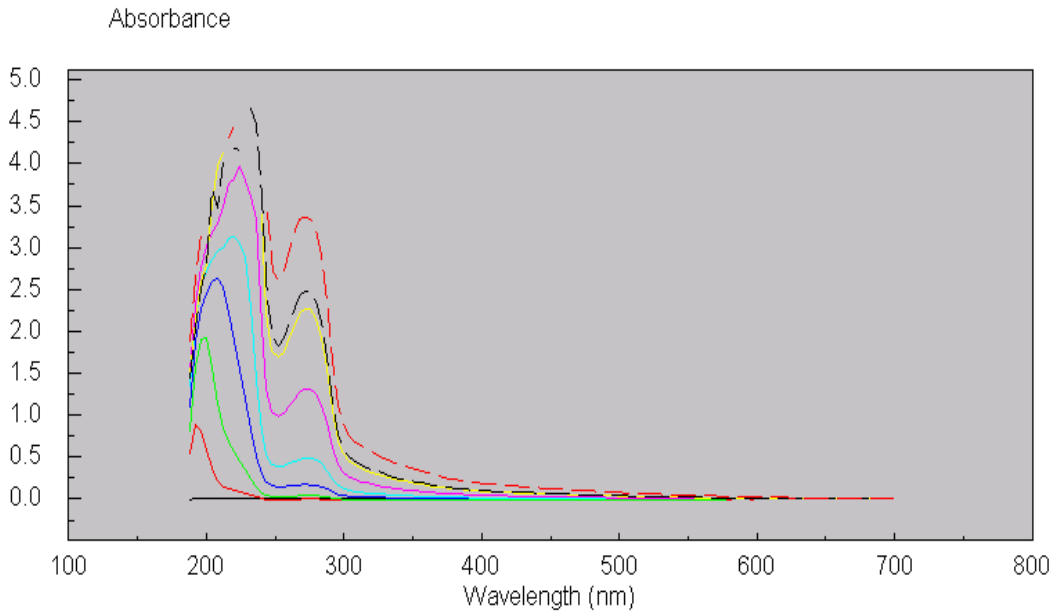


**Fig. 3.28:** UV-Vis absorption spectra of Bioglue (in the absence of Ag(I) ions) in deionised water over 120 h. Red-1 h, green-6 h, dark blue-12 h, light blue-24 h, pink-48 h, yellow-72 h, black (dashed)-96 h, red (dashed)-120 h.

## 3.4 Conclusion

Bioglues prepared in the absence and in the presence of a silver salt (up to 0.01 g of added $AgNO_3$ and $[Ag_2(3,6,9\text{-tdda})].2H_2O$ appear to be stable at temperatures up to 50 °C, have the ability to swell in a moist environment, have good adherence properties and Ag(I) ions progressively leach from the dried $AgNO_3$-Bioglues. $AgNO_3$-Bioglues are readily reduced by borohydride and citrate ions but Ag(0) nanoparticles are not formed. The properties of the Bioglues are important for medicinal purposes. Although the mechanical strength is lower in the Bioglues with added Ag(I) ions this may be a worthwhile compromise if the presence of Ag(I) ion over a 60 h period may seriously reduce or even totally inhibit any pathogenic microbial growth.

# Chapter 4

Antimicrobial Activity of Ag(I)-Bioglues

# 4.0 Introduction

The results presented in this Chapter aimed to determine the antimicrobial activity of $AgNO_3$- and $[Ag_2(3,6,9\text{-tdda})].2H_2O$-Bioglues against a range of Gram-negative and Gram-positive bacteria such as *Escherichia coli*, *Pseudomonas aeruginosa*, *Staphylococcus aureus*, *Methicillin-Resistant Staphylococcus aureus* (*M.R.S.A.*) and also the fungal pathogen, *Candida albicans*.

# 4.1 Antimicrobial disk diffusion assay with Ag(I)-containing Bioglues

The aim of these experiments was to determine the activity of the Ag(I)-containing Bioglues made using $AgNO_3$ and $[Ag_2(3,6,9\text{-tdda})].2H_2O$, against a range of Gram-negative (*P. aeruginosa* strains 27853, 10145 and *E. coli*) and Gram-positive bacteria (*S. aureus* (Fig. 4.1a) and *M.R.S.A.*) and also the fungal pathogen, *C. albicans* (Fig. 4.1b). The disk diffusion assay was carried out (Sections 2.16.1 and 2.16.2). After 24 h incubation at 37 °C, the area of the zone of inhibition (ZOI) (Fig. 4.1c) was measured. The ZOI data are summarised in Table 4.1 and Figs. 4.2 and 4.3.

Against the fungal pathogen, *C. albicans*, only direct inhibition (inhibition directly underneath the sample only, no ZOI detected) was observed for the Ag(I)-Bioglues. Only at the highest amount of added $AgNO_3$ (0.1 g) was a ZOI observed (100 $mm^2$).

Against the bacterial species, increasing the quantity of $AgNO_3$ in the formulation caused a progressive increase in the ZOI. In general, activity is greatest against Gram-negative bacteria and least against the resistant, Gram-positive strain, *M.R.S.A.* Percival *et al*[226] found a similar trend using a commercially available silver alginate wound dressing (AMS, Winsford, UK) prepared in 1 x 1 cm squares. This dressing had antimicrobial activity against a broad range of clinically isolated strains of fungi

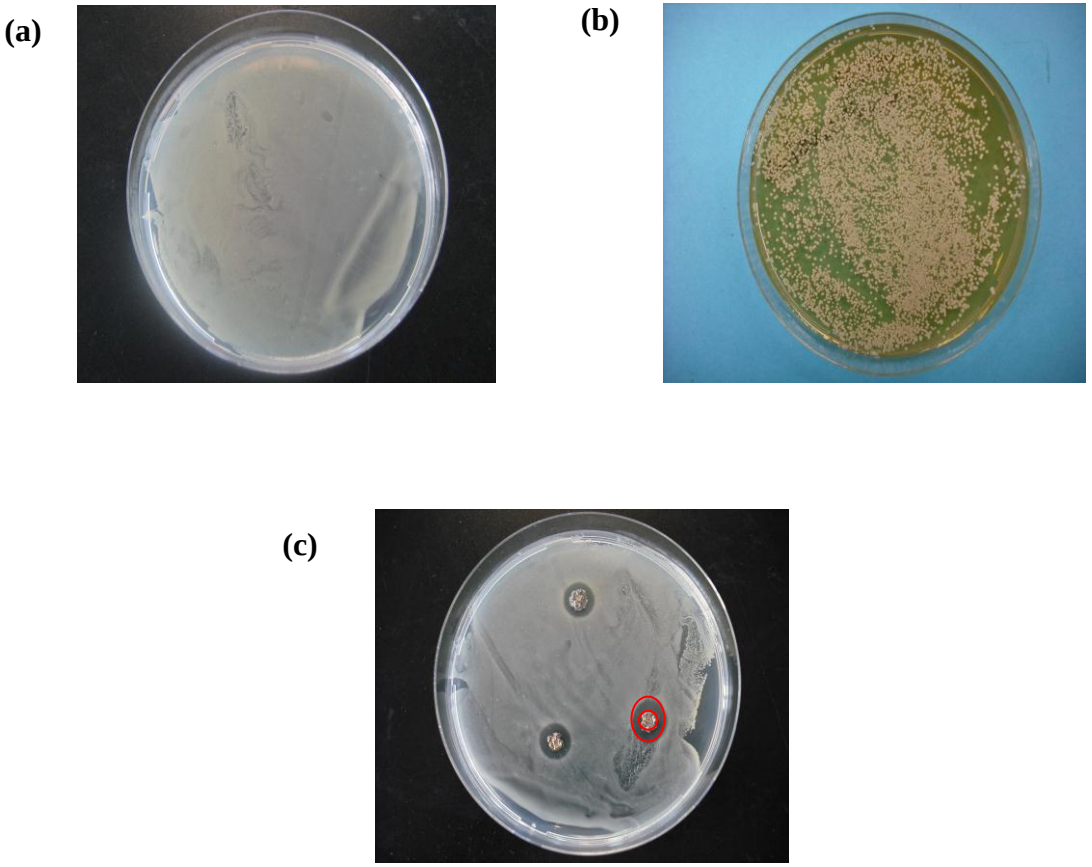


**Fig. 4.1:** Control plates of (a) *S. aureus*, (b) *C. albicans* and (c) image depicting zones of inhibition (ZOI) of $AgNO_3$-Bioglue (0.1 g) against *S. aureus*.

**Table 4.1:** Zones of inhibition (ZOI) for $AgNO_3$- and $[Ag_2(3,6,9\text{-tdda})].2H_2O$-Bioglues.

| **Ag(I)-Bioglue formulation (added $AgNO_3$ (g))** | ***C. albicans*** **($mm^2$)** | ***M.R.S.A.*** **($mm^2$)** | ***S. aureus*** **($mm^2$)** | ***E. coli*** **($mm^2$)** | ***P. aeruginosa 10145*** **($mm^2$)** | ***P. aeruginosa 27853*** **($mm^2$)** |
|---|---|---|---|---|---|---|
| 0.00001 | d.i. | 0 | 0 | 0 | 0 | 0 |
| 0.0001 | d.i. | 13 | 21 | 14 | 0 | 41 |
| 0.001 | d.i. | 23 | 26 | 35 | 38 | 38 |
| 0.01 | d.i. | 31 | 36 | 41 | 49 | 58 |
| 0.1 | 100 | 45 | 49 | 66 | 72 | 74 |
| **Ag(I)-Bioglue formulation (added $[Ag_2(3,6,9\text{-tdda})].2H_2O$)** | | | | | | |
| 0.0001 | 0 | 0 | 0 | 0 | 0 | 0 |
| 0.001 | d.i. | 18 | 31 | 36 | 14 | 27 |
| 0.01 | d.i. | 14 | 18 | 12 | 12 | 21 |

d.i. = direct inhibition

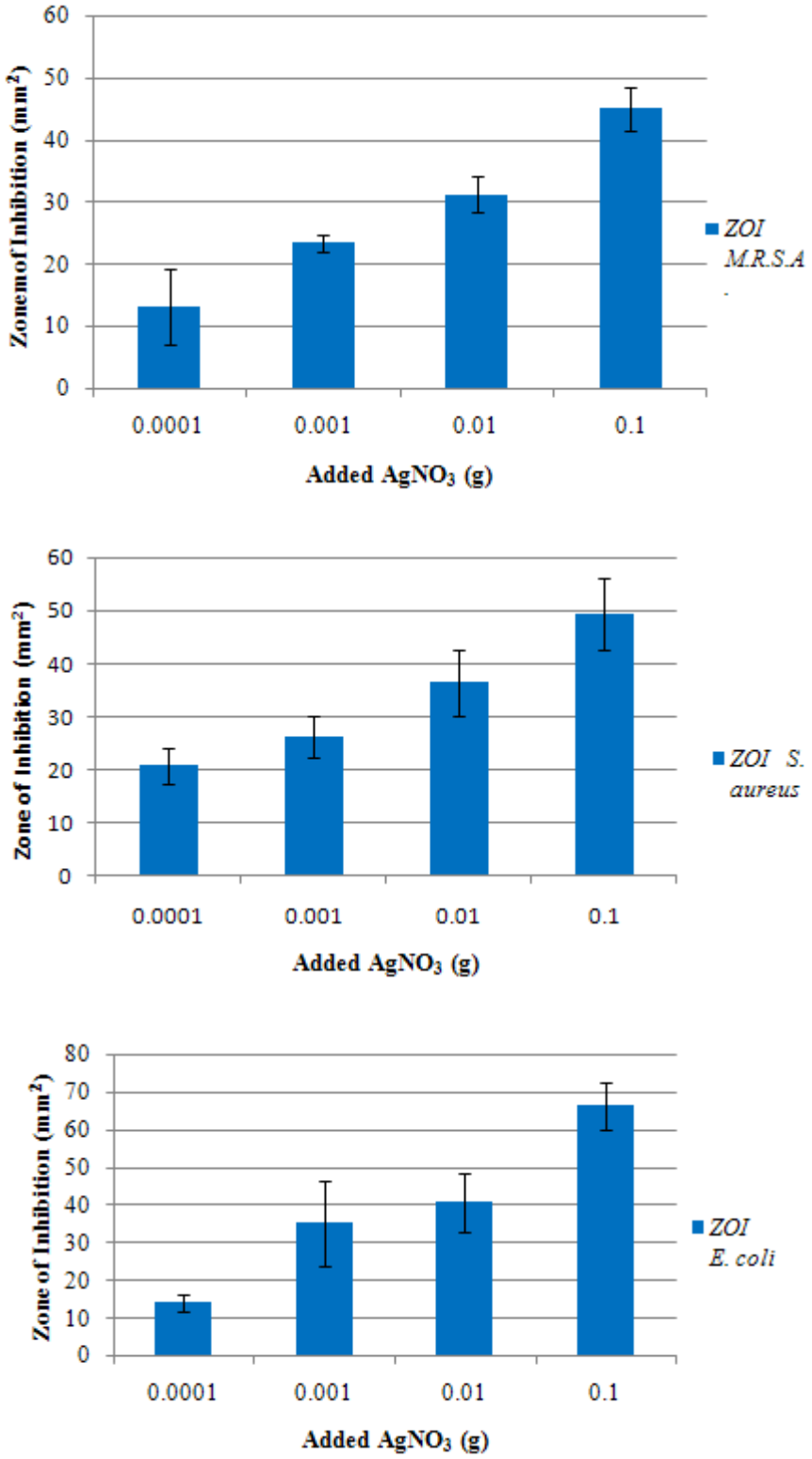


**Fig 4.2:** The effect of $AgNO_3$-Bioglues on zones of inhibition against (a) *M.R.S.A.* (b) *S. aureus* and (c) *E. coli*.

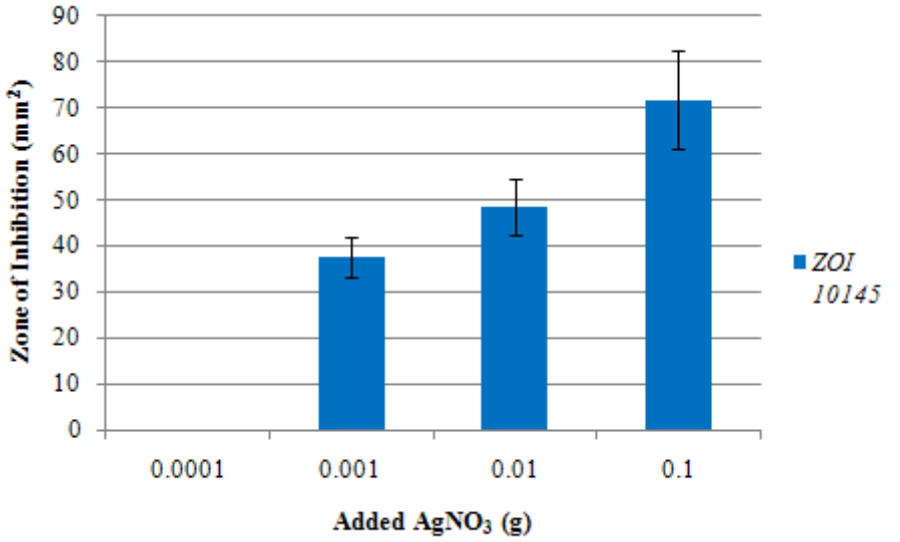


**(d)**

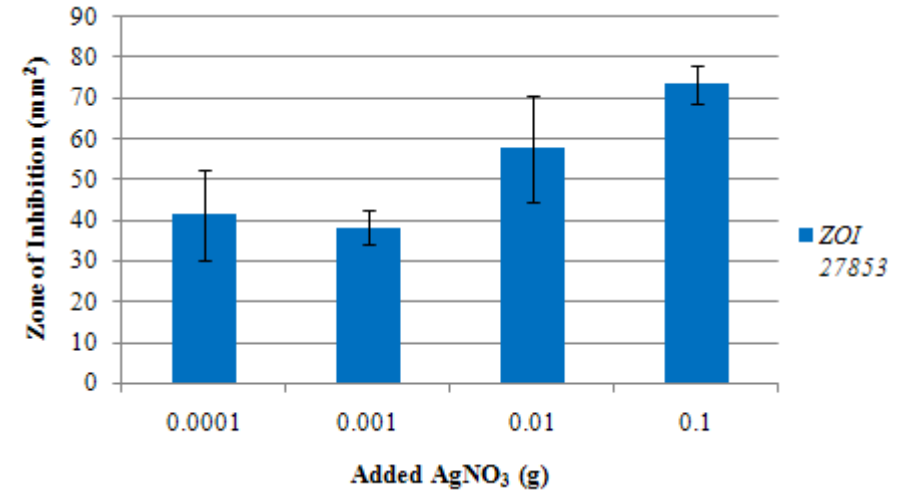


**(e)**

**Fig. 4.2 Contd:** The effect of $AgNO_3$-Bioglues on zones of inhibition against (d) *P. aeruginosa 10145* and (e) *P. aeruginosa 27853.*

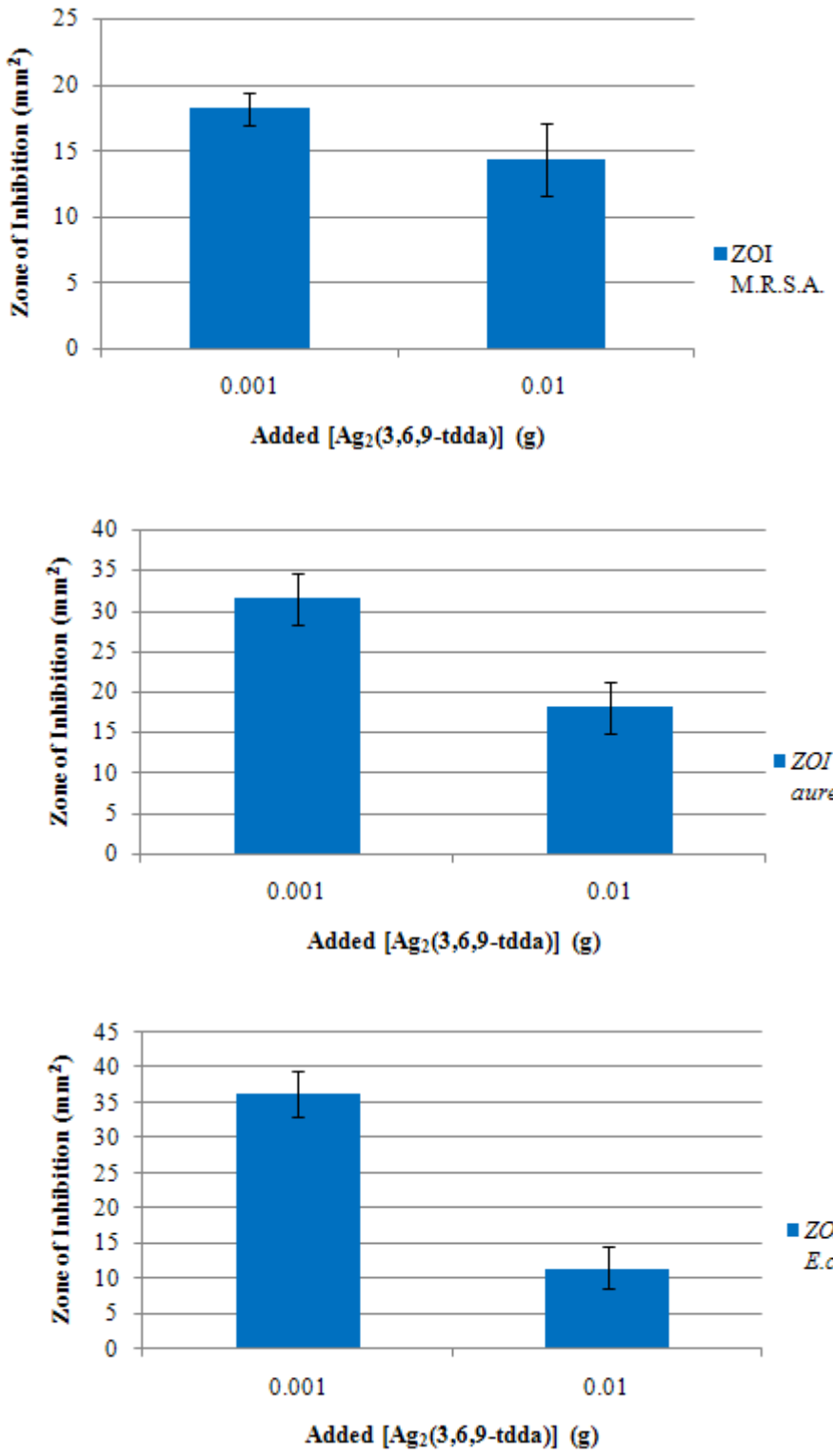


**Fig. 4.3:** The effect of $[Ag_2(3,6,9\text{-tdda})].2H_2O$-Bioglues against (a) *M.R.S.A.*, (b) S. *aureus* and (c) *E. coli*.

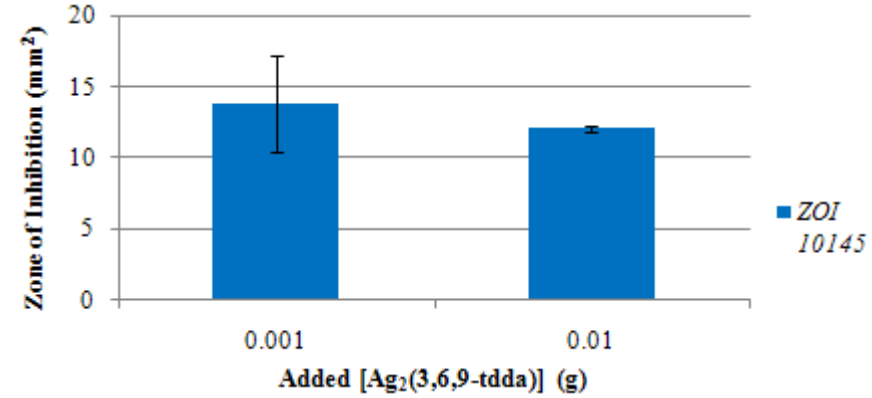


**(d)**

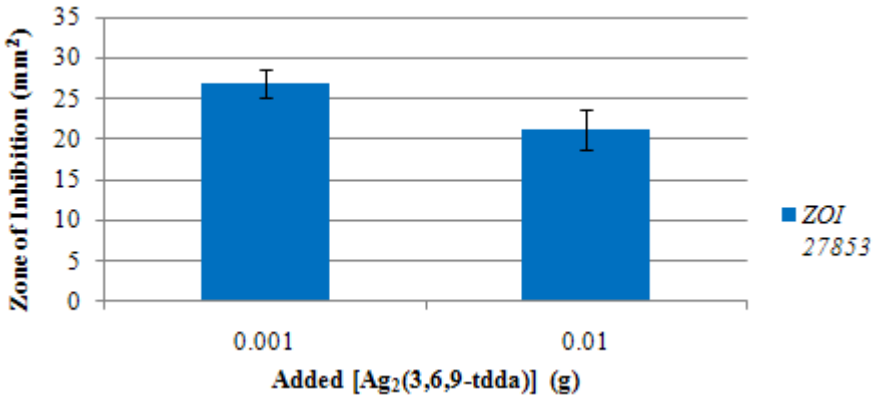


**(e)**

**Fig. 4.3 Contd:** The effect of [$Ag_2$(3,6,9-tdda)].2$H_2O$-Bioglues on zones of inhibition (d) *P. aeruginosa* 10145 and (e) *P. aeruginosa* 27853.

and bacteria in comparison to a non-silver gauze and a non-silver hydrofiber dressing (Convatec, Flintshire UK). Experiments revealed zones of inhibition of 7.2 $mm^2$ against *P. aeruginosa*, 3.8$mm^2$ against *E. coli*, 7.1 $mm^2$ against *S. aureus* and 5.3 $mm^2$ against *M.R.S.A.*, whereas no zones of inhibition were found for the non-silver gauze and dressing. The smaller ZOI for *E. coli* contrasts with that found in the present studies, and may be attributed to the use of a more virulent clinical isolate than the clinical strain used in the present study. Castellano *et al*[27] reported a similar trend to the one presented in this study, with the activity trend of a Silvercel dressing *P. aeruginosa* > *E. coli* > *S. aureus*.

In contrast to the trends observed with the present $AgNO_3$-Bioglues, increasing the amount of added $[Ag_2(3,6,9\text{-tdda})].2H_2O$ surprisingly lead to a decrease in activity. This was particularly noticeable for *E. coli* and *S. aureus*.

## 4.2 Conclusion

In conclusion, the $AgNO_3$- and $[Ag_2(3,6,9\text{-tdda})].2H_2O$-Bioglues both exhibit direct inhibition against *C. albicans*. The $AgNO_3$-Bioglues were more active against the bacterial strains than the $[Ag_2(3,6,9\text{-tdda})].2H_2O$-Bioglues.

# Chapter 5

Effect of Ag(I) Ions on Fungi and Bacteria

## 5.0 Introduction

It has previously been shown[174] that treating *C. albicans* with $AgClO_4$ induces an increase in SOD activity, with the maximum effect occurring after 1 h. Catalase (CAT) activity was increased by a factor of 10 fold when *C. albicans* was exposed to Ag(I) ions for 1 h.[174] In parallel, an increase in glutathione reductase (GLR) activity was also observed after an exposure time of 1 h.[174] These results suggested that the yeast was mounting a response to oxidative stress. This part of the research aimed to assess the effect of $AgNO_3$ on *S. aureus* and to determine whether or not an oxidative stress response was generated in response to exposure to Ag(I). The study sought to establish a possible mode(s) of action of the Ag(I) ion against the bacterium.

Oxidative stress is caused by a serious imbalance between the production of reactive oxygen species (ROS) and antioxidant defense (Scheme 1).[227] There are a number of antioxidant enzymes, such as superoxide dismutase (SOD), that catalyze the dismutation of radical anions (e.g. $O_2^{-\cdot}$)[228] which are involved in the generation of unstable and damaging species, such as hydroxyl radicals ($OH^{\cdot}$) and hydrogen peroxide ($H_2O_2$), which can lead to cytotoxicity.[229] Copper- and zinc-containing SODs are located mainly in the cytosol of animal cells, whilst manganese-SODs are found usually in the mitochondria of animal cells.[230] Reduced glutathione (GSH) is synthesised *de novo* from the amino acids glutamine, cysteine and glycine[231] and is responsible for maintaining the redox state within cells. GSH performs its antioxidant activity by scavenging radical species.[232] GSH peroxidase (GPx) detoxifies peroxidases, with GSH acting as an electron donor in the reduction reaction, producing GSSG as the oxidised end product. The reduction of GSSG back to GSH is catalysed by gluatathione reductase (GLR) and requires NADPH.[231] The FAD moiety of GLR is reduced by NADPH in the reduction half-reaction. In the oxidation half-reaction, the resulting dithiol reacts with the glutathione disulfide and the electron acceptor GSSG is reduced to two GSH at the active site of GLR.[227] Catalase (CAT), has the ability to break down hydrogen peroxide and has the advantage of not producing free radicals.[233] These reactions are summarised in Scheme 1.

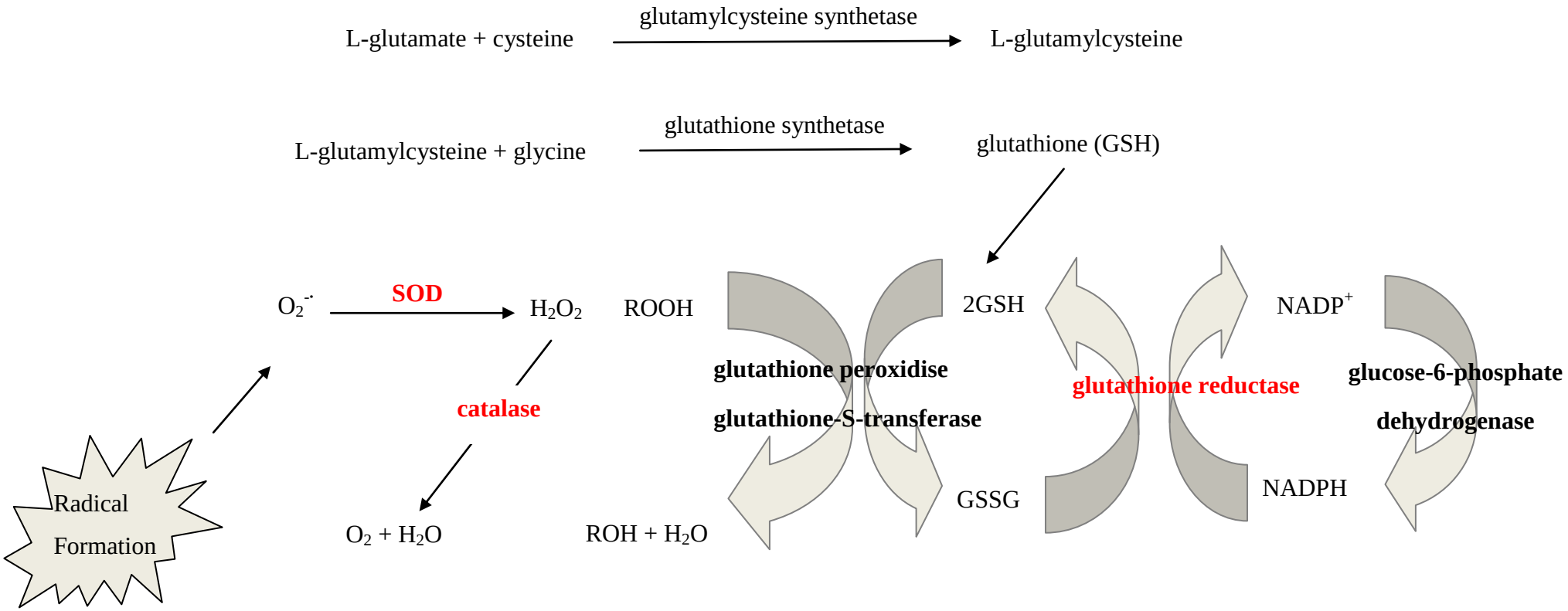


**Scheme 1:** Antioxidant defence mechanism of glutathione reductase, superoxide dismutase and catalase. Adapted from Tandoğan *et al.*[227]

## 5.1 Antimicrobial susceptibility testing with $AgNO_3$ and $[Ag_2(3,6,8\text{-tdda})].2H_2O$ (without Bioglue)

The aim of these experiments was to determine the *in vitro* susceptibility of the fungal pathogen, *C. albicans*, and the bacterial pathogens, *S. aureus* and *M.R.S.A.*, to the pure compounds, $AgNO_3$ and $[Ag_2(3,6,9\text{-tdda})].2H_2O$ (without Bioglue). After a 24 h incubation period at 37 °C, $OD_{600}$ readings were taken and the anti-fungal and anti-bacterial activities were measured (Sections 2.15.1 and 2.15.2). Growth was expressed as a percentage of untreated controls (Figs. 5.1-5.4).

$AgNO_3$ inhibited the growth of *C. albicans* in the concentration range of 6.25-100 µg/ml with an $MIC_{90}$ value of 6.3 µg/ml (36.8 µM) (Fig. 5.1 and Table 5.1). A similar trend was found for $[Ag_2(3,6,9\text{-tdda})].2H_2O$ (Fig. 5.2 and Table 5.1) where an $MIC_{90}$ value of 15.6 µg/ml (35.8 µM) was ascertained. In comparing activity based on Ag(I) content, $AgNO_3$ was more active than $[Ag_2(3,6,9\text{-tdda})].2H_2O$ against *C. albicans* ($MIC_{90}$ 36.8 and 71.6 µM Ag(I), respectively). Previous studies by Thati *et al*[180] showed that the anti-fungal activity against *C. albicans* increased upon complexation of the coumarin anion to an Ag(I) centre ($MIC_{80}$ 332 µM for coumarin carboxylic acid (CcaH) and 163 µM for [Ag(Cca)]) (Table 5.2). Rowan *et al*[179] established the $MIC_{100}$ value of $AgClO_4$ against *C. albicans* to be 1.4 µM. The di-silver(I) complex, $[Ag_2(NH_3)_2(salH)_2]$, tested by Coyle *et al*,[234] had excellent activity against *C. albicans* ($MIC_{100}$ of 0.5 µM).

$AgNO_3$ and $[Ag_2(3,6,9\text{-tdda})].2H_2O$ inhibited the growth of the bacterial species, *S. aureus* and *M.R.S.A.* (Figs. 5.3, 5.4 and Table 5.1). Whereas $AgNO_3$ was equally active against both species ($MIC_{80}$ ca. 3.0 µg/ml (17.7 µM)), $[Ag_2(3,6,9\text{-tdda})].2H_2O$ was more effective against *S. aureus* ($MIC_{80}$ ca. 3.9 µg/ml (17.9 µM)) than *M.R.S.A.* ($MIC_{80}$ 31.3 µg/ml (143.5 µM)). When comparing activities based on Ag(I) content, $AgNO_3$ and $[Ag_2(3,6,9\text{-tdda})].2H_2O$ had similar activities against *S. aureus* ($MIC_{80}$ 17.7 and 17.9 µM, respectively). However, a large difference in activity against *M.R.S.A.* was observed between the two Ag(I) compounds, with $AgNO_3$ being more effective than $[Ag_2(3,6,9\text{-tdda})].2H_2O$ ($MIC_{80}$ values of 17.7 and 143.5 µM, respectively).

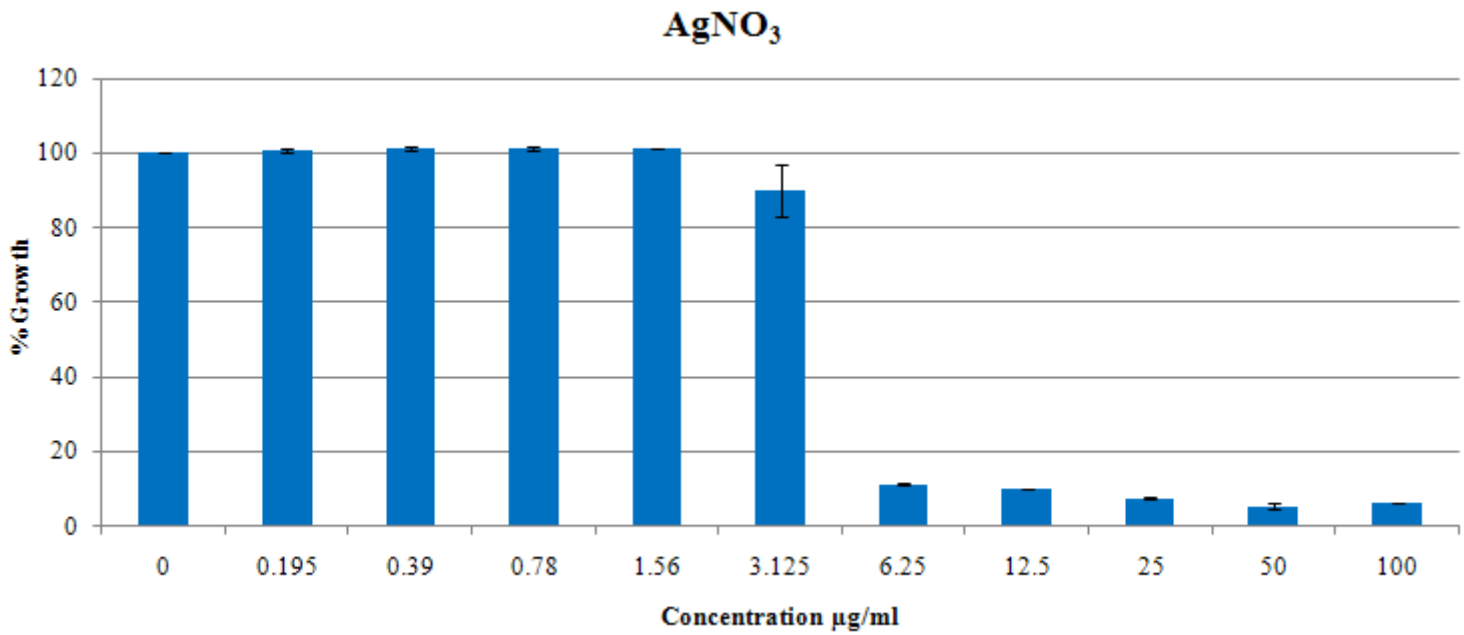


**Fig. 5.1:** Susceptibility of *C. albicans* to $AgNO_3$. The anti-fungal activity of $AgNO_3$ against *C. albicans* was determined using the microdilution assay (Section 2.17.1). Results are presented as a percentage of the control growth.

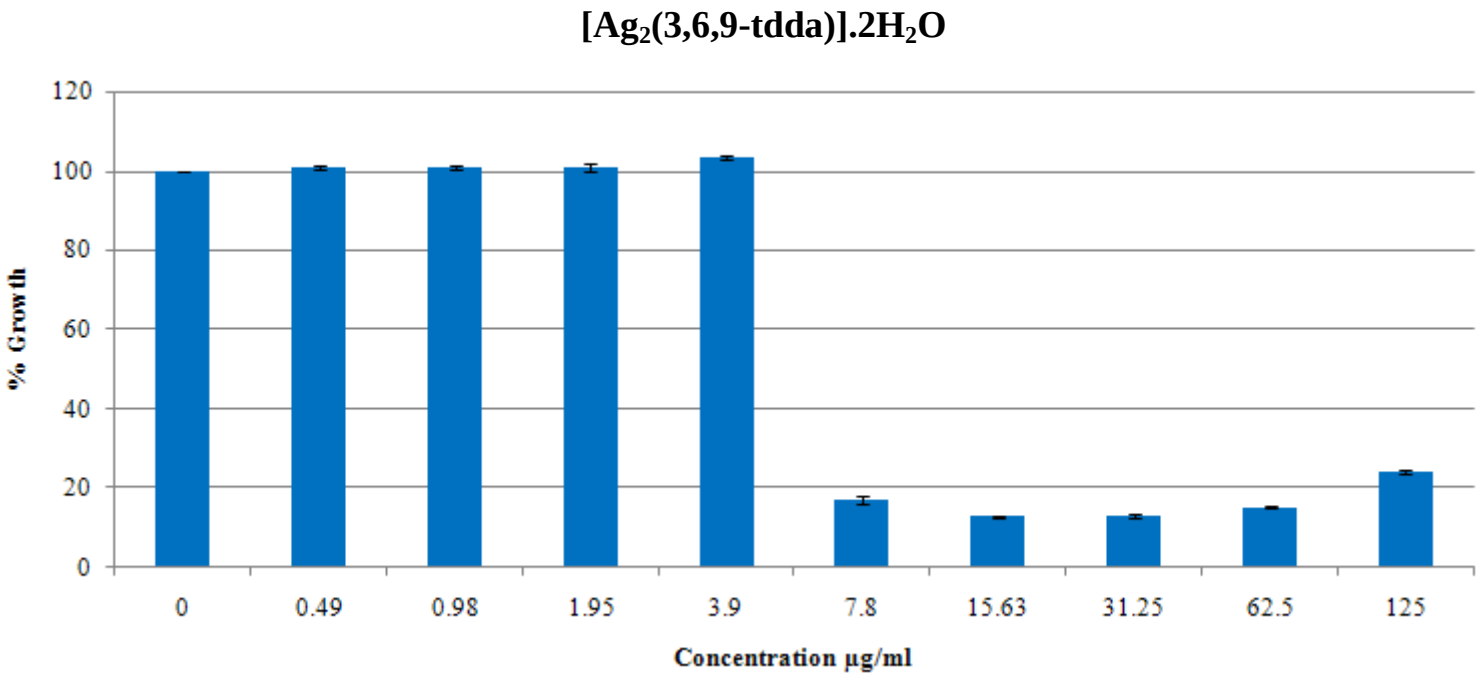


**Fig. 5.2:** Susceptibility of *C. albicans* to $[Ag_2(3,6,9\text{-tdda})].2H_2O$. The anti-fungal activity of $[Ag_2(3,6,9\text{-tdda})].2H_2O$ against *C. albicans* was determined using the microdilution assay (Section 2.17.1). Results are presented as a percentage of the control growth.

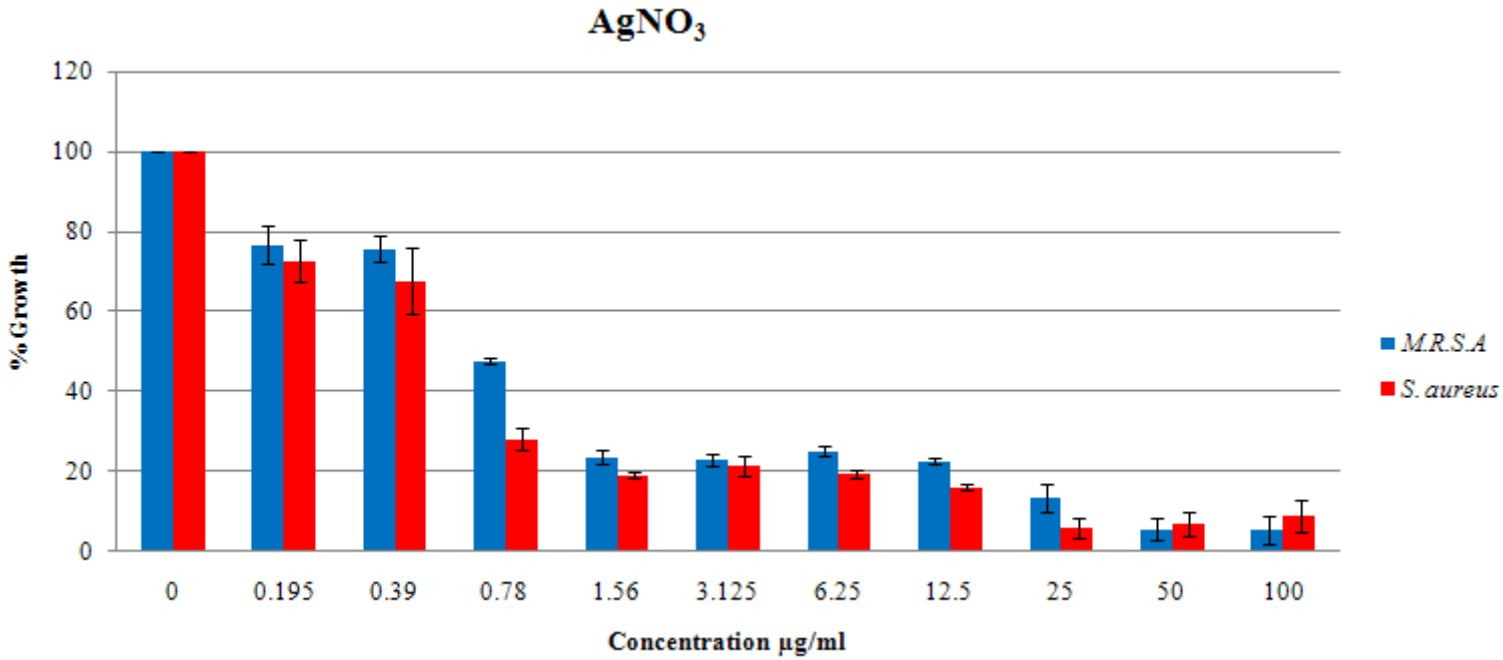


**Fig. 5.3:** Susceptibility of *M.R.S.A.* and *S. aureus* to $AgNO_3$. The anti-bacterial activity of $AgNO_3$ against *M.R.S.A.* and *S. aureus* was determined using the microdilution assay (Section 2.17.2). Results are presented as a percentage of the control growth.

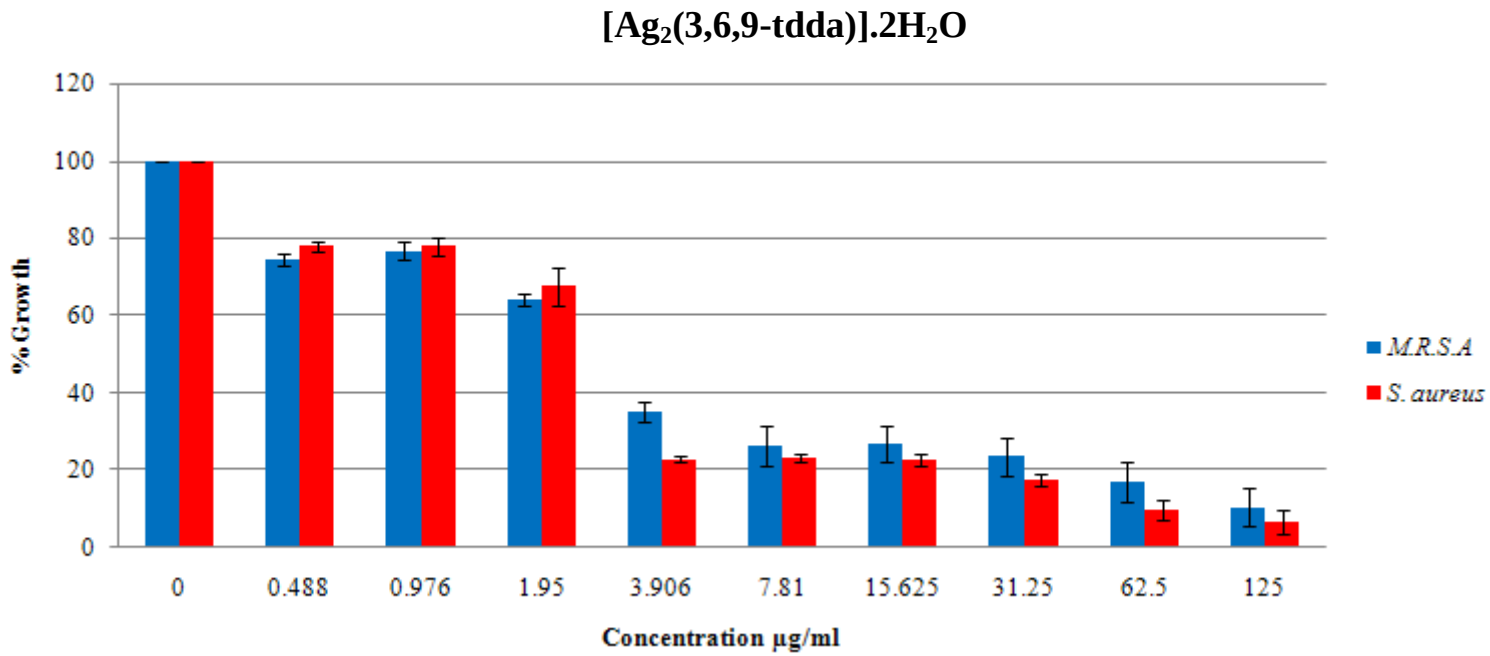


**Fig. 5.4:** Susceptibility of *M.R.S.A.* and *S. aureus* to [$Ag_2$(3,6,9-tdda)].2$H_2O$. The anti-bacterial activity of [$Ag_2$(3,6,9-tdda)]

.2$H_2O$ against *M.R.S.A.* and *S. aureus* was determined using the microdilution assay (Section 2.17.2). Results are presented as a percentage of the control growth.

**Table 5.1:** Minimum inhibitory concentrations ($MIC_{80}$, *$MIC_{90}$) of $AgNO_3$ and $[Ag_2(3,6,9\text{-tdda})].2H_2O$ against *C. albicans*, *S. aureus* and *M.R.S.A.* in the present study.

| **Organism** | **$AgNO_3$** | | | **$[Ag_2(3,6,9\text{-tdda})].2H_2O$** | | |
|---|---|---|---|---|---|---|
| | **$MIC_{80}$ (µg/ml)** | **$MIC_{80}$ (µM)** | **$MIC_{80}$ (µM $Ag^+$)** | **$MIC_{80}$ (µg/ml)** | **$MIC_{80}$ (µM)** | **$MIC_{80}$ (µM $Ag^+$)** |
| ***C. albicans*** | 6.3* | 36.8 | 36.8 | 15.6* | 35.8 | 71.6 |
| ***S. aureus*** | 3.0 | 17.7 | 17.7 | 3.9 | 8.9 | 17.9 |
| ***M.R.S.A.*** | 3.0 | 17.7 | 17.7 | 31.3 | 71.8 | 143.5 |

**Table 5.2:** Minimum inhibitory concentrations (MICs) of various compounds tested against *C. albicans*, *S. aureus* and *M.R.S.A.* References superscripted.

| **Compounds Tested** | ***C. albicans*** **(µM)** | ***M.R.S.A.*** **(µM)** | ***S. aureus*** **(µM)** |
|---|---|---|---|
| $AgNO_3$ | $MIC_{80}$ 66.8 [235] | $MIC_{80}$ 123.9 [235] | $MIC_{80}$ 69.5 [235] |
| | $MIC_{100}$ 1.8 [179] | $MIC_{50}$ 36.8 [179] | |
| $AgClO_4{\cdot}H_2O$ | $MIC_{100}$ 1.4 [179] | $MIC_{50}$ 43.4 [179] | |
| CcaH | $MIC_{80}$ 331.6 [180] | $MIC_{80}$ > 2500 [235] | $MIC_{80}$ > 2500 [235] |
| [Ag(Cca)] | $MIC_{80}$ 163 [180] | $MIC_{80}$ 0.6 [235] | $MIC_{80}$ 71. 9[235] |
| $[Ag_2(NH_3)_2(SalH)_2]$ | $MIC_{100}$ 0.5 [234] | $MIC_{50}$ 17.2 [179] | |

CcaH = Coumarin carboxylic acid ($SalH_2$) = Salicylic acid

Creaven *et al*[235] reported the $MIC_{80}$ values of $AgNO_3$ against *S. aureus* and *M.R.S.A.* to be 69.5 µM and 123.9 µM, respectively (Table 5.2). These somewhat large $MIC_{80}$ values may be attributed to the fact that both of the strains used in their study were clinical isolates, which can be more virulent than the strains used in the present study. The present results show that $[Ag_2(3,6,9\text{-tdda})].2H_2O$ is slightly more active than $AgNO_3$ against *C. albicans* and *S. aureus*, whereas $AgNO_3$ is substantially more active against *M.R.S.A.*

## 5.2 Assessment of the Oxidative Stress Response of *S. aureus* and $AgNO_3$

### 5.2.1 Assessment of superoxide dismutase activity in $H_2O_2$-treated and $AgNO_3$-treated *S. aureus* cells

The activity of the superoxide dismutase enzymes was determined in cells following treatment with either $H_2O_2$ (the positive control, 0.5 mM), $AgNO_3$ (3.0 µg/ml) or no treatment (negative control) for 15, 30 and 60 min. The SOD activity was measured (Section 2.19.2) and the results are presented in Fig. 5.5. For cells which were exposed for 15 min to $H_2O_2$ and $AgNO_3$, the SOD activity increased by 1.7 ± 0.2 and 1.9 ± 0.02 fold, respectively, relative to the control. An increase in SOD activity was also observed at 30 min (1.9 ± 0.1 fold in $H_2O_2$-treated cells) with the most significant increase in activity being found for $AgNO_3$-treated cells (3.8 ± 0.4 fold increase ($p< 0.001$)). At the 60 min timepoint, a decrease in activity was observed compared to the control (0.8 ± 0.16 fold) to 0.4 ± 0.05 fold in the $H_2O_2$-treated cells. In contrast there was a large increase (2.6 ±0.25 fold) for the $AgNO_3$-treated cells ($p< 0.01$). It is interesting to note that the SOD activity decreased dramatically from the 30 min to the 60 min timepoint in $H_2O_2$-treated cells, which was chosen as the positive control. It is known that *S. aureus* has the ability to produce a single, major catalase, KatA,[236] which might explain why a decrease in activity was observed for the $H_2O_2$-treated cells. The longer the *S. aureus* cells were exposed to $H_2O_2$, the less SOD activity was detected as *S. aureus* had the ability to disproportionate $H_2O_2$

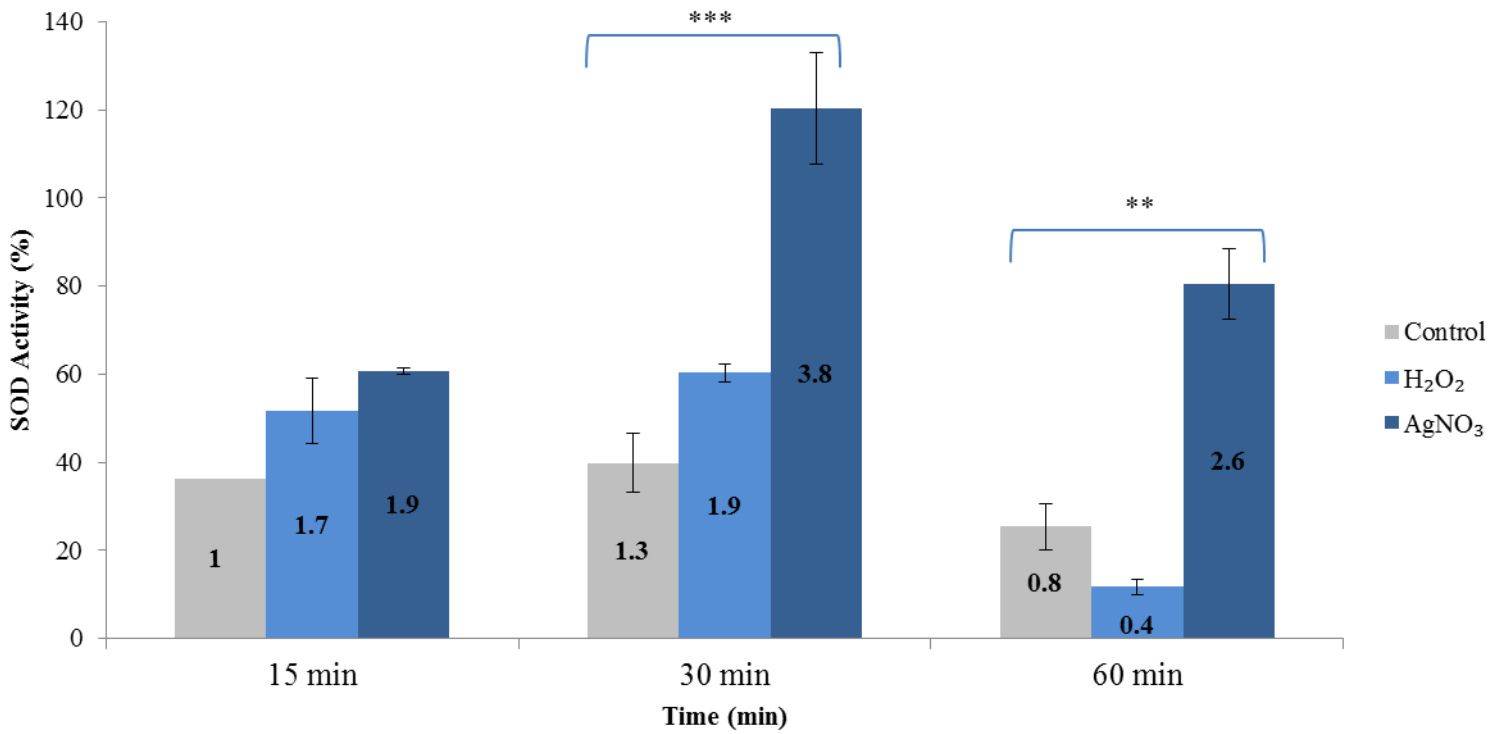


**Fig. 5.5:** Superoxide dismutase activity in *S. aureus* cells treated with $H_2O_2$ and $AgNO_3$. *S. aureus* cells were treated with the $MIC_{80}$ value of $AgNO_3$ for 15, 30 and 60 min. Cells were also exposed to $H_2O_2$ for the relevant time-points and protein was extracted from the cells (Section 2.18) and superoxide dismutase activity assessed (Section 2.19.2). Results are presented as % SOD activity along the x-axis and as fold changes in the bar chart. Differences in activity were deemed statistically significant at $p < 0.05$(*), $p < 0.01$ (**) and $p < 0.001$ (***).

using its own KatA catalase. Therefore, oxidative stress was not induced and so greater levels of SOD were not detected. In relation to $AgNO_3$ exposure, oxidative stress was induced at both 30 and 60 min, with the greatest increase in activity observed at 30 min.

### 5.2.2 Assessment of catalase activity in $H_2O_2$-treated and $AgNO_3$-treated *S. aureus* cells

Catalase activity was measured (Section 2.19.3) in cells exposed to $AgNO_3$ (3.0 µg/ml), $H_2O_2$ (positive control, 0.5 mM) or no treatment (negative control) for 15, 30 and 60 min (Fig. 5.6). After 15 min an increase was observed from 1.0 fold in the negative control cells to 1.7 ± 0.13 fold and 1.3 ± 0.19 fold in $H_2O_2$-treated cells and $AgNO_3$-treated cells, respectively. At 30 min, there was an increase of 1.7 ± 0.2 fold in control cells and a slight increase of 1.4 ± 0.1 fold in $H_2O_2$-treated cells. The most significant increase in catalase activity was observed with the $AgNO_3$-treated cells at 30 min (4.1 ± 0.4 fold ($p<0.01$)). The 60 min timepoint remained significantly higher in the $AgNO_3$-treated cells (1.2 ± 0.2 fold in negative control cells to 3.3 ± 0.5 fold). However, this represented a decrease in activity when compared to the 30 min timepoint.

It was also observed that a fold decrease in the $H_2O_2$-treated cells occurred (1.7 ± 0.13 fold at 15 min to 1.4 ± 0.06 fold at 30 min and finally to 1.2 ± 0.05 fold at 60 min). As already mentioned in relation to the SOD assay results, the minor decreases in catalase activity found for the $H_2O_2$-treated cells might be attributed to the presence of KatA, which could break down the $H_2O_2$ before the catalase activity was measured.

### 5.2.3 Assessment of glutathione reductase activity in $H_2O_2$-treated and $AgNO_3$-treated *S. aureus* cells

The aim of these experiments was to determine if *S. aureus* cells demonstrated an oxidative stress response as a result of exposure to Ag(I) ions. Normally, cells

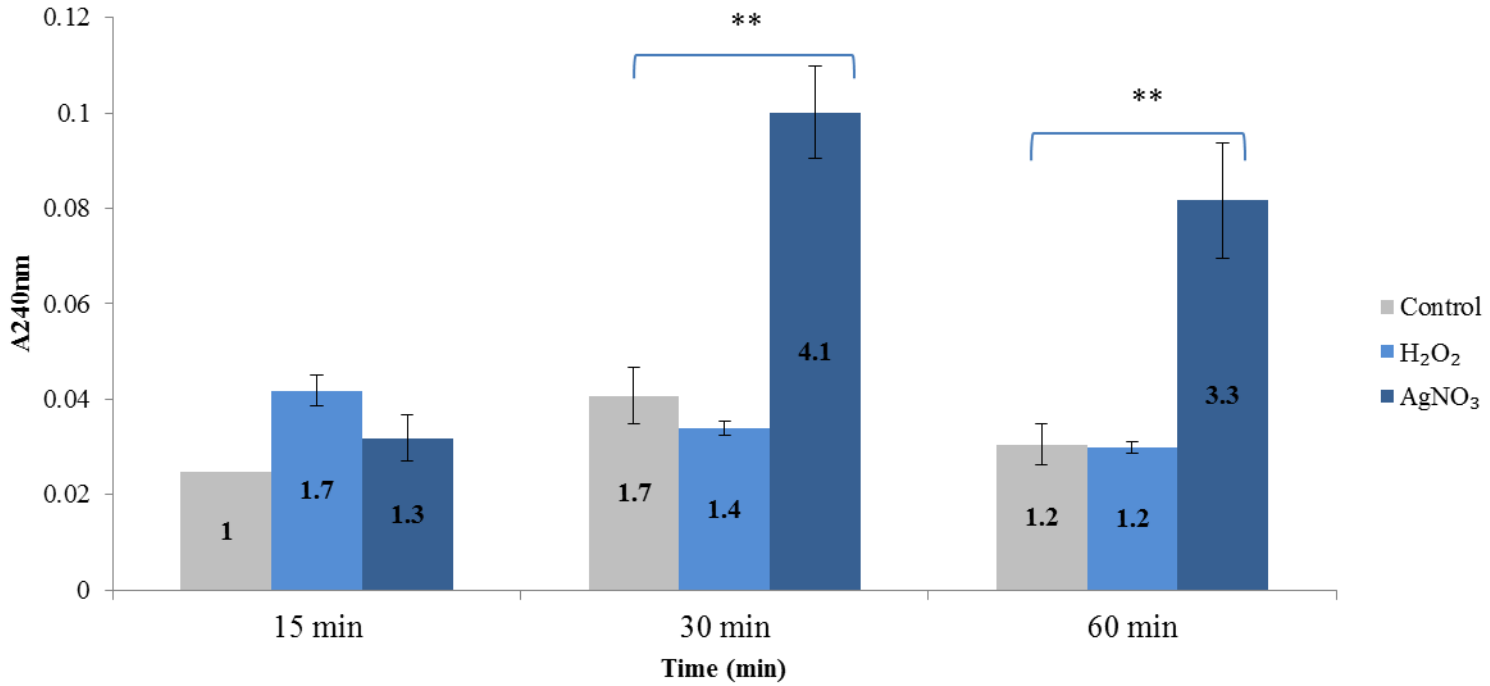


**Fig. 5.6:** Catalase activity in *S. aureus* cells treated with $H_2O_2$ and $AgNO_3$. *S. aureus* cells were treated with the $MIC_{80}$ value of $AgNO_3$ for 15, 30 and 60 min. Cells were also exposed to $H_2O_2$ for the relevant time-points and protein was extracted from the cells (Section 2.18) and catalase activity was assessed (2.19.3). Results are presented as absorbance along the x-axis and as fold changes in the bar chart. Differences in activity were deemed statistically significant at $p < 0.05$ (*), $p < 0.01$ (**) and $p < 0.001$ (***).

respond by increasing the activity of antioxidant enzymes in order to deal with this stress. *S. aureus* cells were exposed to $AgNO_3$ at the $MIC_{80}$ concentration (3.0 µg/ml) for 15, 30 and 60 min. Hydrogen peroxide (0.5 mM) was used as a positive control and no treatment as a negative control. The GLR activity was assessed (Section 2.19.1) and the results are presented in Fig. 5.7. When cells were exposed to $H_2O_2$ and $AgNO_3$ for 15 min, the GLR activity increased from 1.0 fold in the negative control to 1.2 ± 0.1 fold in the $H_2O_2$-treated cells and decreased to 0.6 ± 0.2 fold for the $AgNO_3$-treated cells. At the 30 min timepoint, the GLR activity increased to 1.2 ± 0.5 fold in the $H_2O_2$-treated cells and also increased to 1.6 ± 0.4 fold in the $AgNO_3$-treated cells. Finally, at the 60 min timepoint, there was an increase in activity to 1.3 ± 0.1 fold in the $AgNO_3$-treated cells. Even though an increase in activity for $AgNO_3$-treated cells was observed at both the 30 and 60 min timepoints, these changes were not deemed to be statistically significant ($p > 0.05$).

As GSH is known to chelate Cu(II) ions,[230] it is possible that it is also chelating the Ag(I) ions through its carboxylate and amine groups thus inhibiting the antioxidant defense properties of the GSH. Similar results were found when Ag(0) nanoparticles were used on eukaryotic cells.[12] Another possibility may be the interaction of Ag(I) ions with the glutathione reductase enzyme. Cardosa *et al*[237] suggested that the transfer of electrons from the NADPH to the FAD moiety of GLR results in making the oxidised thiol groups at the active site more prone to interact with Fe(II) ions, rendering the glutathione reductase inactive.

## 5.3 Evaluation of *S. aureus* RNA Extraction Methods

The aim of this part of the research work was to determine if specific genes in *S. aureus* encoding for SOD enzymes were differentially expressed as a result of exposure to $AgNO_3$. Most organisms produce enzymes such as superoxide dismutase and catalase to deal with the harmful effects of reactive oxygen species. *S. aureus* contains two genes, *sodA* and *sodM*, which encode for SOD and are important for the viability of the organism when it is experiencing stressful conditions.[206] The *sodA* gene encodes for the manganese-dependent SOD, which inactivates harmful

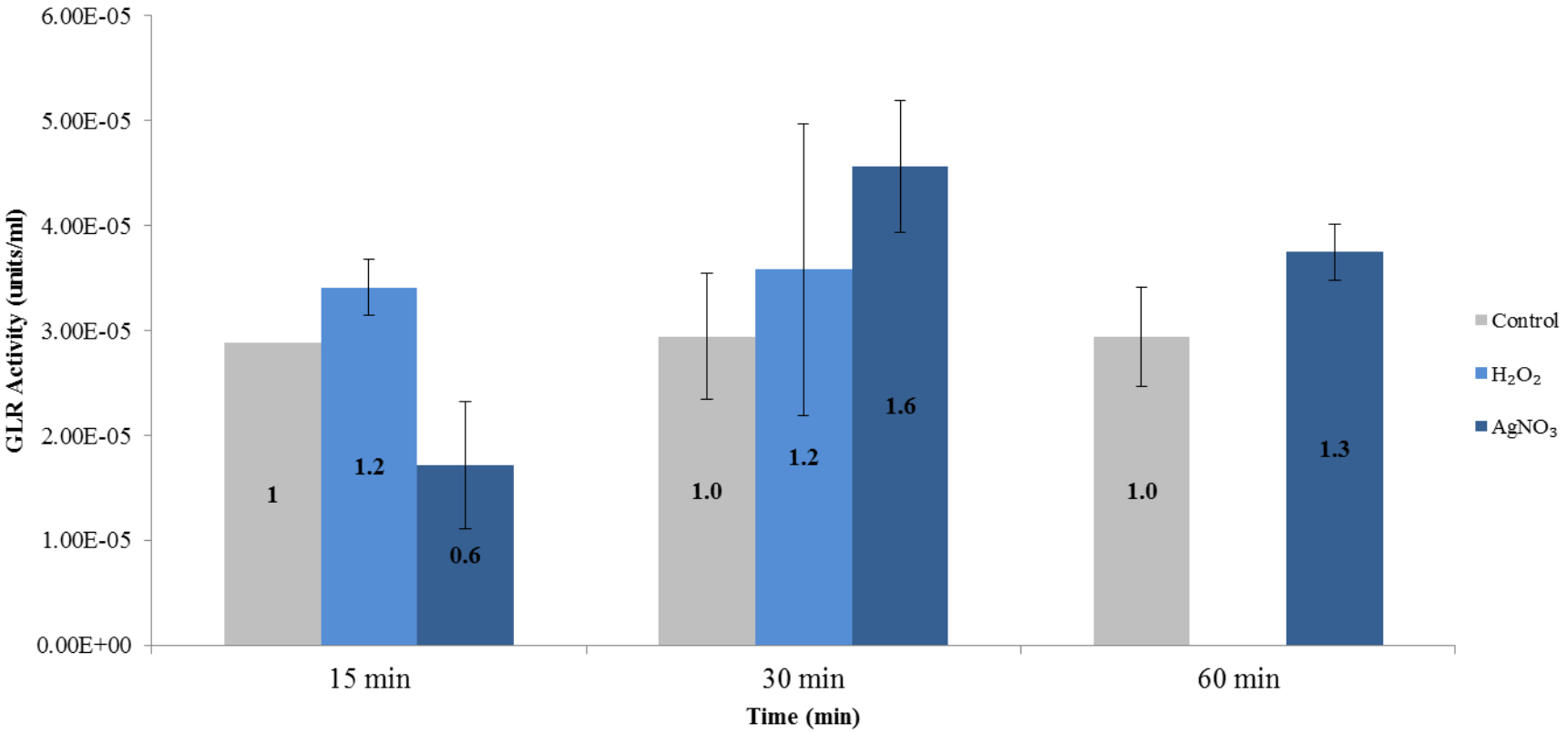


**Fig. 5.7:** Glutathione reductase activity in *S. aureus* cells treated with $H_2O_2$ and $AgNO_3$. *S. aureus* cells were treated with the $MIC_{80}$ values of $AgNO_3$ for 15, 30 and 60 min. Cells were also exposed to $H_2O_2$ for the relevant time-points and protein was extracted from the cells (Section 2.18) and glutathione reductase activity was assessed (Section 2.19.1). Results are presented as GLR activity along the x-axis and as fold changes in the bar chart. Differences in activity were deemed statistically significant at $p < 0.05$(*), $p < 0.01$ (**) and $p < 0.001$ (***).

superoxide radicals[205] and protect the cells from oxidative stress. The metal requirement for *sodM* has been suggested to also be manganese.[238] The gene encoding for DNA gyraseA (a housekeeping gene) was also assessed and this was used as a positive control.

Following RNA extraction, samples were analysed for purity using RNA electrophoresis (Section 2.20.6), and the samples were also analysed at $OD_{260/280nm}$. A variety of RNA extraction procedures (Section 2.20) were used in an attempt to recover the nucleic acid in sufficient quantity and quality but none were successful. A brief overview of the unsuccessful extraction methods is given below and reasons for their failure are offered.

RNA electrophoretic analysis of *S. aureus* samples was carried out using each of the following extraction methods: a) Qiagen kit RNeasy® minikit, b) Qiagen RNeasy® minikit with RNAprotect bacteria reagent, and c) Tri reagent (Appendix IV, Fig. 1). Bands were observed using the Tri reagent method. Following RNA extraction, DNase treatment was carried out, after which cDNA synthesis was also performed. The extraction protocol using the Tri reagent provided the best quality RNA, with $OD_{260/280nm}$ readings in the range 1.7-2.2 which is slightly out of the range expected ($OD_{260/280nm}$ 1.9-2.1).[239] Synthesised cDNA was also assessed spectrophotometrically ($OD_{260/280nm}$) prior to RT-PCR analysis.

RT-PCR was first performed using the housekeeping gene, DNA gyrase (*gyrA*), and no bands indicating a PCR product were observed (Appendix IV, Fig. 2a). It was then decided to try another primer set to determine if either the cDNA or the primers were the cause of no PCR product being recovered. The next set of primers tested was SodA and again no PCR product bands were observed (Appendix IV, Fig. 2b). Following this, a genomic DNA extraction protocol was carried out followed by PCR analysis using the SodA primer set. If bands were observed then the problem was due to the cDNA, and if no bands were observed then the problem could be attributed to the primers. The PCR product was visualised on a 1% agarose gel and again no bands were observed, suggesting that the primers were the cause (Appendix IV, Fig. 3a). However, when the synthesised cDNA was run on an agarose gel no

bands were observed suggesting that the RNA precursor was not of a high enough quality to proceed to the PCR analysis (Appendix IV, Fig. 3b).

Previous research has been carried out to assess the gene expression in *S. aureus* cells.[113,205,206,240] However, Gram-positive cocci are one of the most difficult to disrupt[241] and may have contributed to the problem associated with our inability to extract RNA from *S. aureus* cells. This may be due to the fact that staphylococci and other Gram-positive bacteria have a rigid cell wall which is thicker (15-80 nm) in comparison to Gram-negative bacteria (10 nm)[242] which, in turn, makes it more difficult to lyse.[243] This may explain the low quantity of RNA obtained. The general instability of mRNA also adds to the problem and this is due to the presence of a hydroxyl group on the pentose ring of the RNA, making it more susceptible to hydrolysis and therefore less stable than DNA.[244] For most bacteria, mRNA has a half-life between 0.5-50 min and an average half-life of 3 min.[245] This short half-life explains why gene expression is much more difficult to determine in prokaryotes than eukaryotes. As numerous extraction methods resulted in poor yields of RNA and no PCR product, it was decided not to proceed any further with this line of research.

## 5.4 Conclusion

In conclusion, the results presented in this Chapter suggest that exposure of *S. aureus* to $AgNO_3$, at a concentration of 3.0 µg/ml, causes a significant increase in the activity of two detoxifying enzymes (SOD and CAT), which become upregulated in an effort by the cells to minimise the damage caused by exposure to the Ag(I) ion. The elevation in enzymatic activity of SOD and CAT at 30 min is evidence of a response to oxidative stress, but the decline in activity by 60 min suggest a loss in cell function or even cell death. Furthermore, exposure to $AgNO_3$ also caused an increase in the amount of amino acid leakage from the cells, suggesting that the cell membrane integrity was compromised. These findings demonstrate the antimicrobial activity of $AgNO_3$ and assist in elucidating the modes of action.

# Chapter 6

Proteomic Analysis of the Response of *Staphylococcus aureus* to $AgNO_3$

## Overview of protein analysis

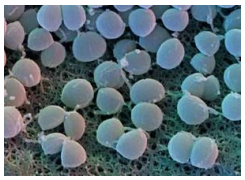

*S. aureus* cells

$AgNO_3$

Released extracellular protein

Internal

Extracted protein

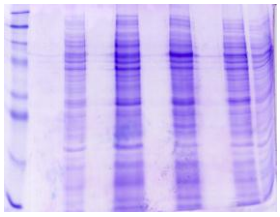

1-D Electrophoresis

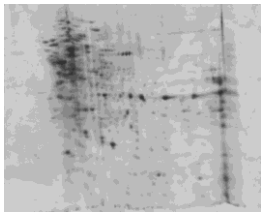

2-D Electrophoresis

Spots excised

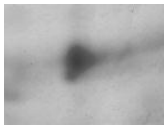

Mass Spec

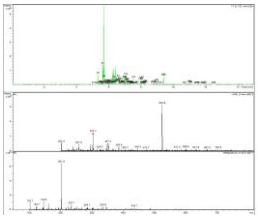

Identification of proteins and function

(Software)

# 6.0 Introduction

The results presented in this Chapter set out to further establish possible mode(s) of action of $AgNO_3$ against *S. aureus* cells through the assessment of amino acid leakage and proteomic analysis following exposure to Ag(I) ions.

## 6.1 Assessment of amino acid leakage from *S. aureus* cells as a result of exposure to $AgNO_3$

It has been suggested that the release of amino acids from the bacterial cell could be due to damage to the membrane integrity.[246] It was decided to use a ninhydrin calorimetric assay to determine amino acid leakage from untreated cells (negative control) and cells exposed to either DMSO (positive control) or $AgNO_3$ (3.0 µg/ml) for 1, 2, 4 and 24 h (Section 2.19.4). The results were determined by reference to a standard curve of known amino acid concentration. As shown in Fig. 6.1, treating cells with 10% DMSO led to significant amino acid leakage at all timepoints ($p < 0.001$). This was to be expected, as DMSO is known to alter membrane permeability[246] and was therefore employed as the positive control. Specifically, it was found that, in relation to the negative control in which 34 ± 2.9 µg/ml of amino acid leakage was detected, 60 ± 3.8 µg/ml of amino acid was detected at the 1 h timepoint in DMSO-treated cells ($p < 0.001$). This increased from 55 ± 1.9 µg/ml (negative control) to 69 ± 3.2 µg/ml after 2 h DMSO treatment, and from 47 ± 2.6 µg/ml (negative control) to 71 ± 1.0 µg/ml in the case of the 4 h DMSO treatment. After 24 h DMSO treatment, an increase from 48 ± 3.0 µg/ml in the negative control to 65 ± 2.3 µg/ml was observed.

For cells treated with $AgNO_3$, a minor increase in amino acid leakage was observed at the 1 h timepoint (38 ± 1.2 µg/ml) compared to the negative control. By 2 h, no statistical difference was observed between the $AgNO_3$-treated and the control cells. After 4 h treatment, an increase from 47 ± 2.6 µg/ml in the negative control to 58 ± 2.1 µg/ml in the $AgNO_3$-treated cells ($p < 0.001$) was observed. At the 24 h

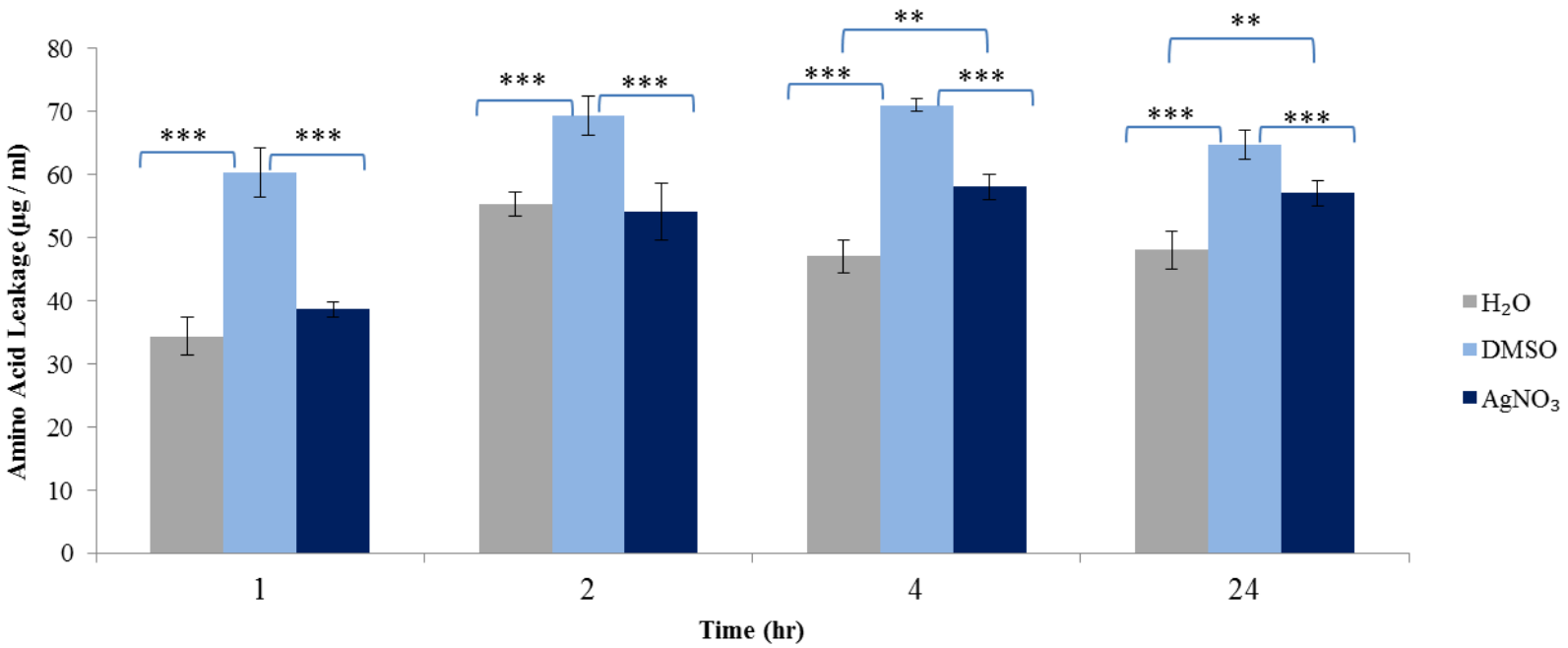


**Fig. 6.1:** Effect of $AgNO_3$ on amino acid leakage from *S. aureus* cells. The leakage of amino acids from *S. aureus* cells, which had been exposed to the $MIC_{80}$ value of $AgNO_3$ for 1, 2, 4 or 24 h, was assessed using the method described in Section 2.19.4. Differences in activity were deemed statistically significant at $p < 0.05$ (*), $p < 0.01$ (**) and $p < 0.001$ (***).

timepoint, an increase from 48 ± 3 µg/ml in the negative control to 57 ± 2.0 µg/ml amino acids leaked from $AgNO_3$-treated cells ($p< 0.01$).

Thus, treatment with DMSO resulted in the greatest leakage of amino acids. The maximum amount of amino acid leakage for $AgNO_3$-treated cells occurred at 4 h (58 µg/ml of amino acids). The quantity of amino acids released from the cell had plateaued by the 4 h timepoint as no further increase was observed by 24 h, suggesting that at this time the cells had reached the maximum leakage stage. Research into the effect of Ag(0) nanoparticles on *S. aureus* cells was conducted by Mirzajani *et al*[247] who showed that the metal atoms interact with the peptidoglycan layer and lead to the formation of pits. It was found that the Ag(0) nanoparticles increased the amount of muramic acid, a major component of the peptidoglycan layer. Similar studies into the effect of Ag(0) nanoparticles on the Gram-negative bacterium, *E. coli*, showed an increase in the amount of reducing sugars and proteins released from the cells upon treatment with Ag(0) atoms.[248] Kim *et al*[249] suggested that exposure of *C. albicans* to Ag(0) nanoparticles promoted an antifungal effect through disruption of the cell membrane structure. This effect was assessed by measuring the release of glucose and trehalose. The Ag(0) nanoparticles induced 30.3 µg/mg of glucose and trehalose release in comparison to the release of 6.8 µg/mg in the untreated control cells. The results of the present studies suggest that Ag(I) ions do affect the membrane permeability of the *S. aureus* cells as a statistically significant increase in amino acid leakage from the cell was observed.

## 6.2 Proteomic analysis of the proteins released by *S. aureus* following exposure to $AgNO_3$

Following the assessment of changes in the enzymatic function and membrane permeability of *S. aureus* cells, it was decided to further investigate the response of *S. aureus* to $AgNO_3$ using proteomic analysis involving one- and two-dimensional SDS-PAGE (Summarised in Section 6.0). *S. aureus* cells were exposed to the $MIC_{80}$ value of $AgNO_3$ (3.0 µg/ml) for 2 h. Protein was extracted from $AgNO_3$-treated and untreated *S. aureus* cells for comparison (Section 2.18), separated by 1-D

electrophoresis (Section 2.21.1) and visualised using Coomassie blue (Section 2.3). Protein expression in treated and untreated cells is illustrated in Fig. 6.2. It is evident from this gel that administering $AgNO_3$ has an effect on the protein leakage in relation to the control, particularly at 2 h.

For 2-D SDS-PAGE, protein was first separated by isoelectric focusing and secondly by molecular weight (Section 2.21.2) (Fig. 6.3-6.4). Protein was visualised using colloidal Coomassie (Section 2.3). Following the visualisation of protein, spot intensities were analysed using ImageQuant 5.0 software and changes in protein expression were evaluated relative to the control. The spots of interest were excised, washed and trypsin digested (Section 2.22) and LC/MS analysis was then carried out to determine the identity and function of these proteins. The extracellular leaked proteins which had changed significantly in their fold expression (Tables 6.1-6.4) were identified following LC/MS analysis and their biochemical functions were established using MASCOT and Uniprot software programmes.

A total of 30 leaked proteins were identified (Tables 6.1-6.4). Of these, 17 were involved in metabolism (Table 6.1), 6 were involved in virulence (Table 6.2), 4 in the stress response of *S. aureus* (Table 6.3) and 3 were uncharacterised proteins (Table 6.4). Proteins which were involved in metabolism included (a) the tricarboxylic acid cycle enzymes; malate:quinone oxidoreductase (Spot 1), acetate kinase (Spot 4) and succinyl Coenzyme A synthetase (Spot 7), (b) the glycolytic enzyme; phosphoglycerate mutase (Spot 10), (c) proteins involved in translation; 30S ribosomal protein (Spot 8), 50S ribosomal protein L25 (Spot 9) and 50S ribosomal protein L31 (Spot 17), (d) protein biosynthesis enzymes; translation elongation factor Tu (Spot 11) and elongation factor G (Spot 16), (e) other metabolic processes; glycerol phosphate lipoteichoic acid synthetase (Spot 2), serine hydroxymethyltransferase (Spot 3), aminoacyltransferase FemB FemB protein (Spot 5), lipase (Spot 6), 2-C-methyl-D- erythritol 4-phosphate cytidylyltransferase (Spot 12), 3-hexulose-6-phosphate synthetase (Spot 13), glutamine amidotransferase subunit PdxT (Spot 14) and uracil phosphoribosyltransferase (Spot 15) (Table 6.1). There were also significant changes in fold expression of proteins involved in the virulence of *S. aureus* (Table 6.2) such as leukocidin F (Spot 18), transcriptional repressor CodY (Spot 19), ABC transporter (Spot 20), alpha-hemolysin (Spot 21),

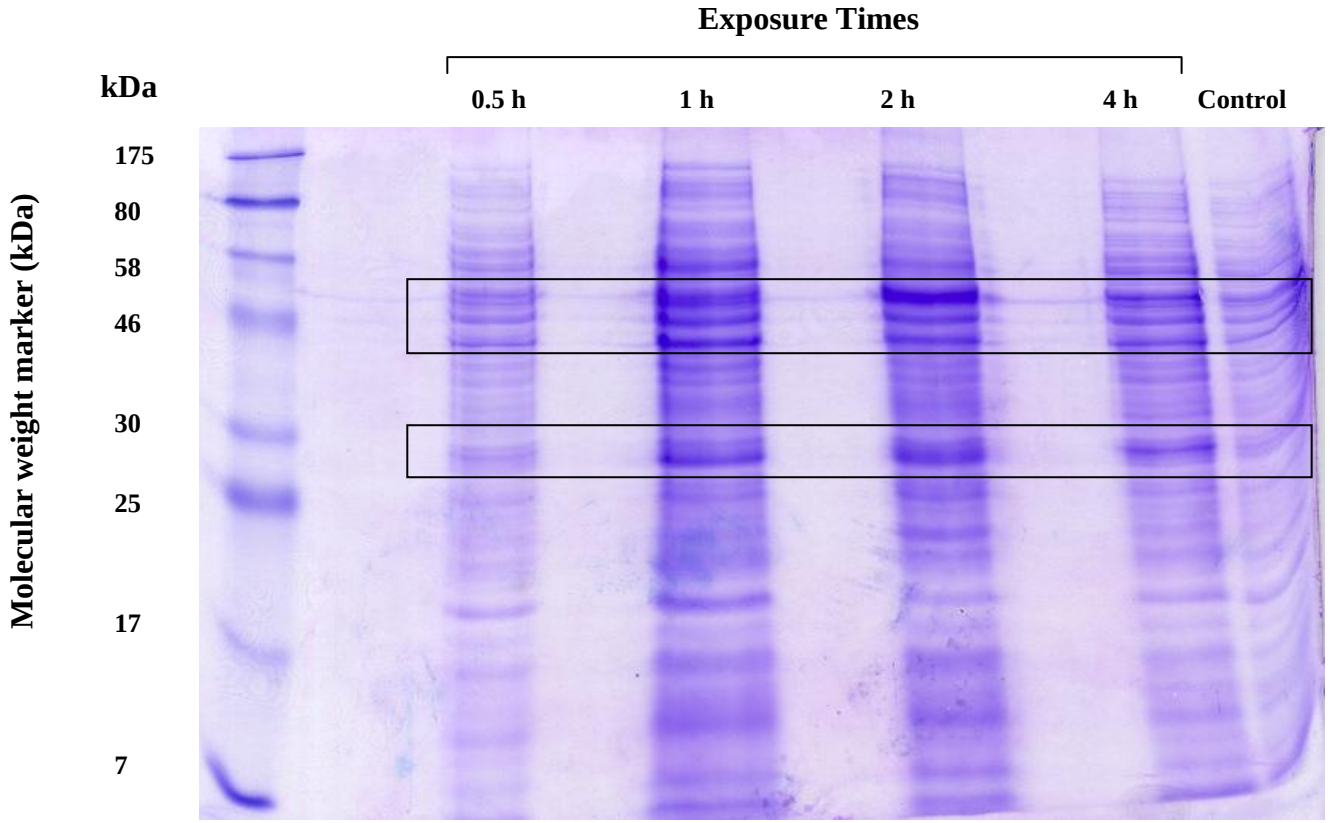


**Fig. 6.2:** One-Dimensional SDS-PAGE analysis of proteins leaked from *S. aureus* cells. Protein was extracted using mild sonication (Section 2.18) and separated by 1-D SDS PAGE (Section 2.21.1). Protein bands (highlighted) appear to be altered in expression as a result of $AgNO_3$ treatment at various times in relation to the control (no $AgNO_3$ added).

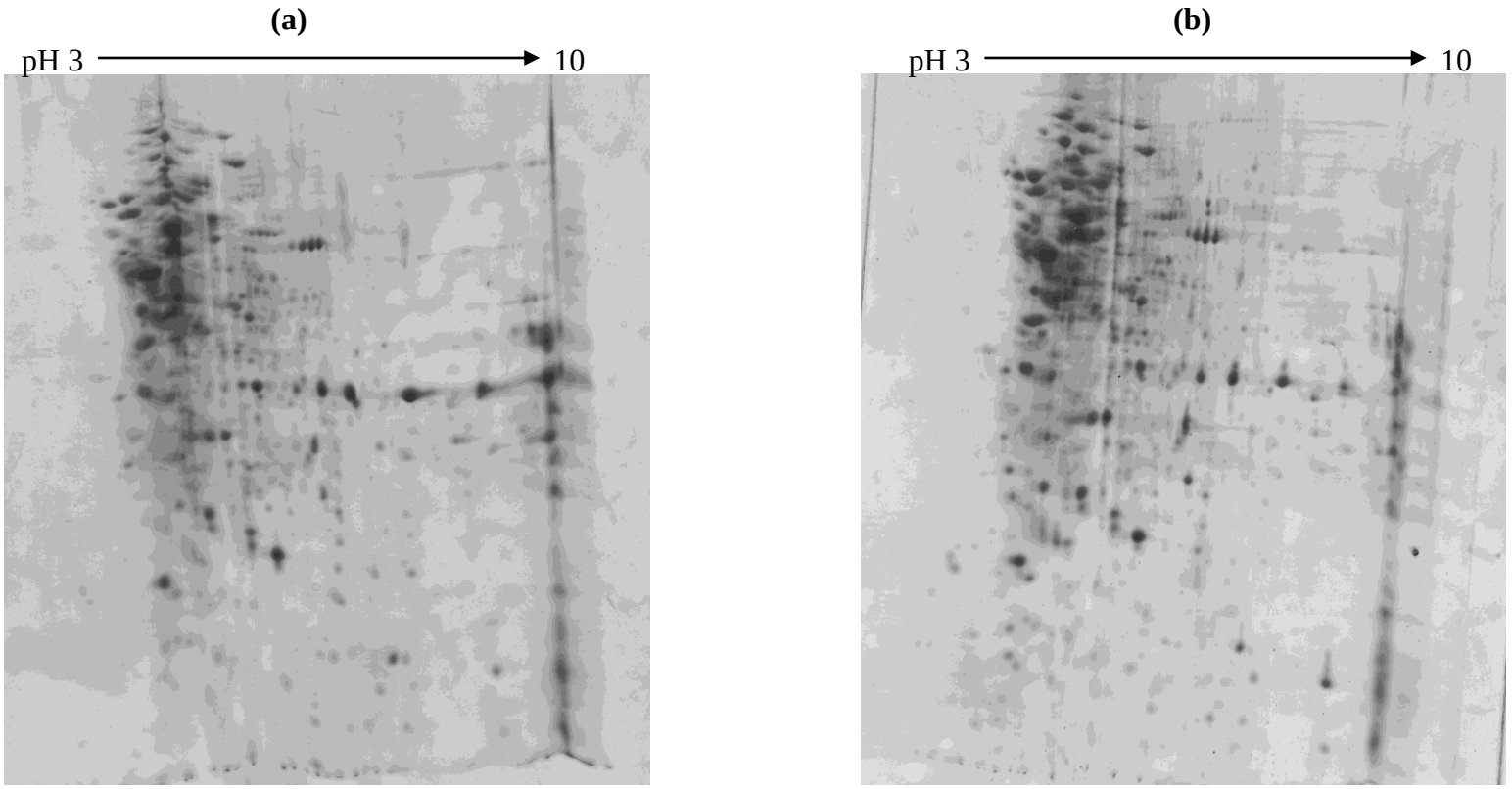


**Fig. 6.3:** Two-Dimensional SDS-PAGE analysis of proteins leaked from *S. aureus* cells. Protein was extracted using mild sonication (Section 2.18) and separated by 2-D SDS PAGE (Section 2.21.2). (a) Control cells (untreated) and (b) cells incubated for 2 h with $AgNO_3$ (3.0 µg/ml)

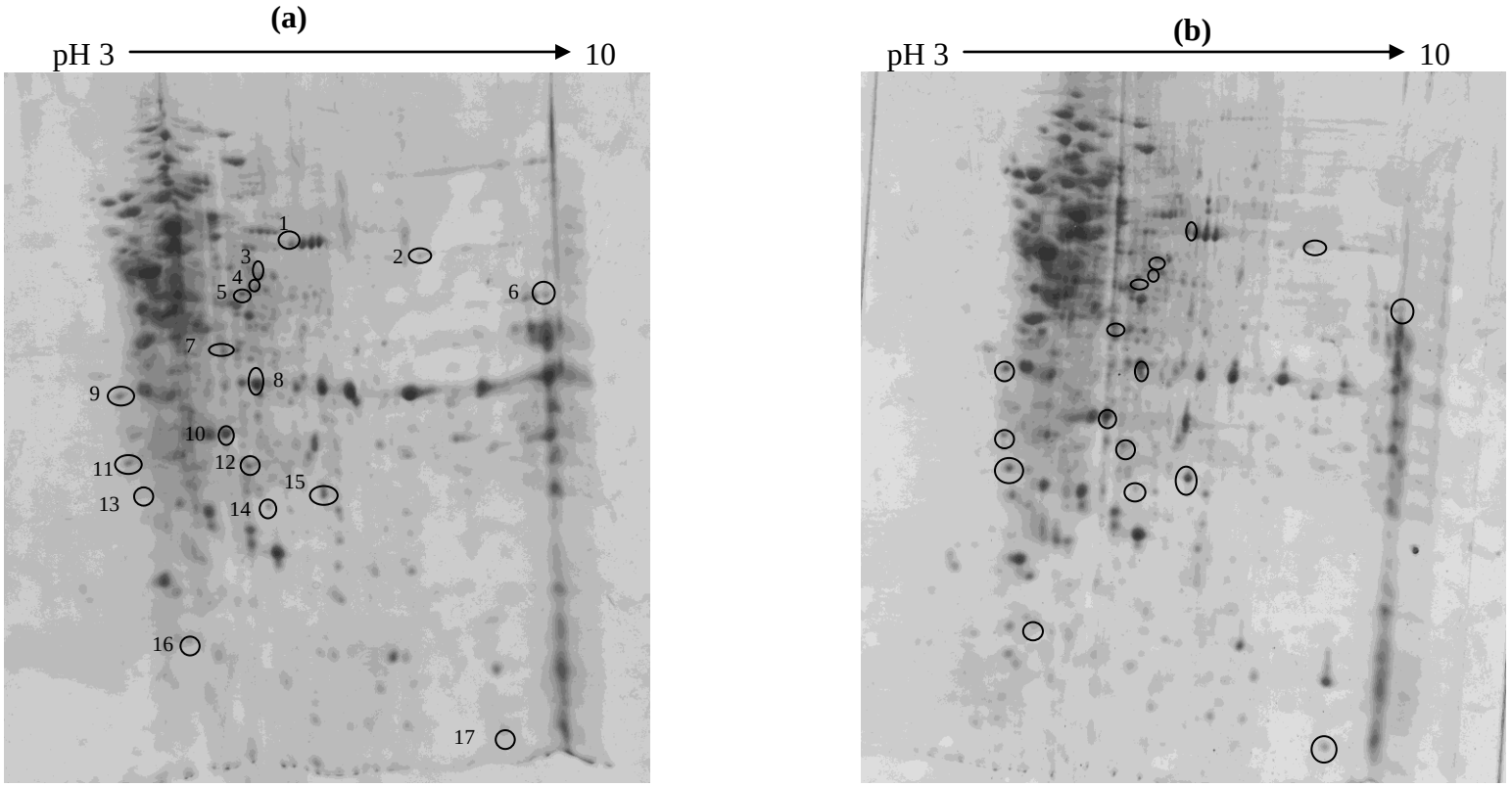


**Fig. 6.4:** Two-Dimensional SDS-PAGE analysis of metabolic proteins leaked from *S. aureus* cells. Protein was extracted using mild sonication (Section 2.18) and separated by 2-D SDS PAGE (Section 2.21.2). (a) Control cells (untreated) and (b) cells incubated for 2 h with $AgNO_3$ (3.0 µg/ml).

**Table 6.1:** Identification of proteins involved in metabolic processes associated with *S. aureus* cells.

| Spot No. | Accession No. | Protein | Function | Mass (kDa) | Score | pI | % Coverage | Fold Difference |
|---|---|---|---|---|---|---|---|---|
| 1 | Q6G669 | Malate:quinone oxidoreductase 2 | Tricarboxylic acid cycle | 56138 | 957 | 6.12 | 47% | - 3.1 |
| 2 | Q99VQ4 | Glycerol phosphate lipoteichoic acid synthase | Cell wall biogenesis | 74353 | 395 | 9.04 | 15% | - 1.7 |
| 3 | C5PZ99 | Serine hydroxymethyltransferase | Metabolic process | 45299 | 517 | 5.72 | 27% | + 2.0 |
| 4 | C8MFH1 | Acetate kinase | Tricarboxylic acid cycle | 44074 | 1081 | 5.58 | 61% | + 2.1 |
| 5 | P0A0A8 | Aminoacyltransferase femB FemB protein | Formation of the pentaglycine interpeptide bridge | 49761 | 376 | 5.44 | 16% | - 1.6 |
| 6 | Q6GJZ6 | Lipase | Triglyceride lipase activity | 44344 | 390 | 8.95 | 20% | + 2.4 |

**Table 6.1:** Continued.

| Spot No. | Accession No. | Protein | Function | Mass (kDa) | Score | pI | % Coverage | Fold Difference |
|---|---|---|---|---|---|---|---|---|
| 7 | P99070 | Succinyl-CoA synthetase | Tricarboxylic acid cycle | 31754 | 377 | 5.47 | 27% | + 1.6 |
| 8 | P66545 | 30S ribosomal protein S2 | Translation | 29134 | 647 | 5.44 | 47% | + 1.6 |
| 9 | Q7A1s4 | 50S ribosomal protein L25/general stress protein | Translation | 23773 | 464 | 4.39 | 34% | + 1.7 |
| 10 | D2UHN7 | Phosphoglycerate mutase | Glycolysis | 26722 | 898 | 5.14 | 78% | + 2.1 |
| 11 | C8MB74 | Translation elongation factor Tu | Protein biosynthesis | 43135 | 573 | 4.77 | 38% | - 1.6 |
| 12 | Q2G1C0 | 2-C-methyl-D-erythritol 4-phosphate cytidylyltransferase | Nucleotidyl-transferase | 26698 | 449 | 5.42 | 46% | + 1.5 |

**Table 6.1:** Continued.

| Spot No. | Accession No. | Protein | Function | Mass (kDa) | Score | pI | % Coverage | Fold Difference |
|---|---|---|---|---|---|---|---|---|
| 13 | D0K9M2 | 3-hexulose-6-phosphate synthase | Carbohydrate metabolic process | 22422 | 620 | 4.61 | 64% | - 1.8 |
| 14 | Q7A1R6 | Glutamine amidotransferase subunit PdxT | Hydrolysis of glutamine to glutamate and ammonia | 20733 | 693 | 5.69 | 61% | + 2.3 |
| 15 | P67397 | Uracil phosphoribosyltransferase | Glycosyltransferase | 23093 | 652 | 6.08 | 65% | + 1.5 |
| 16 | P68791 | Elongation factor G | Protein biosynthesis | 76854 | 365 | 4.8 | 14% | + 1.8 |
| 17 | P66197 | 50S ribosomal protein L31 type B | Translation | 9717 | 166 | 8.04 | 61% | + 1.7 |

bifunctional autolysin (Spot 22) and signal transduction protein TRAP (Spot 23). The proteins involved in the stress response of *S. aureus* all showed increases in release upon exposure to $AgNO_3$ (Table 6.3). These proteins included a putative universal stress response protein (Spot 24), methionine sulfoxide reductase A (Spot 25), alkaline shock protein 23 (Spot 26) and transcription repressor of class III stress genes-like protein (Spot 27). Finally, there were three proteins with a significant fold change whose identity and function remains unknown (Table 6.4).

Acetate kinase (Spot 4) and succinyl CoA synthetase (Spot 7) are two enzymes involved in the tricarboxylic acid cycle (Appendix VI). This cycle involves the initial conversion of pyruvate (the product of glycolysis) into acetyl CoA and, through a series of steps, it is converted to oxaloacetate. Acetate kinase catalyses the first reaction in the conversion of acetate to acetyl CoA, where acetate is converted to acetyl phosphate, whereas the second reaction is mediated by phosphotransacetylase.[250] Succinyl CoA synthetase is involved in the cycle at a later stage in which it catalyses the transformation of succinyl CoA to succinate.[251] This cycle results in the production of two molecules of ATP, carbon dioxide and also the reduction of $NAD^+$ to NADH. It was found that these proteins were increased in abundance by 2.1 fold and 1.6 fold, respectively, suggesting that *S. aureus* cells are trying to increase cellular respiration as a result of $AgNO_3$ exposure.

Glycolysis is one of the major metabolic pathways which produces energy needed to fuel all other cellular processes (Appendix V). It can be divided into two parts; firstly, the energy investment phase and secondly, the energy pay-off phase. In the first phase, energy is consumed in the process of converting glucose to triose phosphates whilst in the second phase energy is gained in the form of ATP production.[252] Phosphoglycerate mutase (Spot 10) was found to have increased in expression by 2.1 fold. Sigdel *et al*[253] also found that this protein was increased due to Zn(II) ion exposure in *E. coli* cells. This protein is also involved in the energy pay-off phase and is responsible for the interconversion of 3-phosphoglycerate and 2-phosphoglycerate within the glycolysis pathway.[254]

The virulence of *S. aureus* can be attributed to the expression of adhesins and also to the secretion of toxins.[255] Alpha hemolysin is one of the main pore-forming toxins of

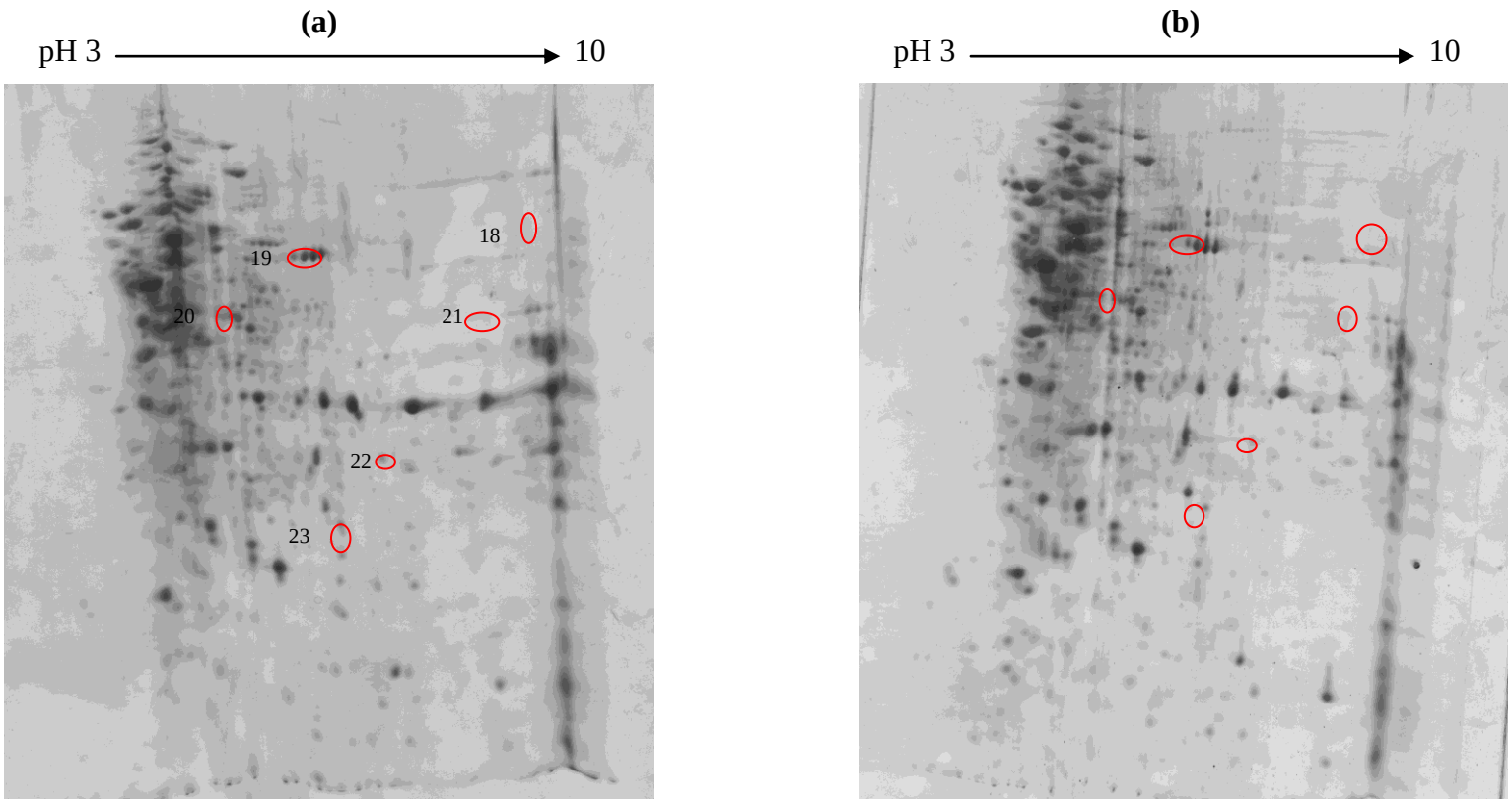


**Fig. 6.5:** Two-Dimensional SDS-PAGE analysis of virulence proteins leaked from *S. aureus* cells. Protein was extracted using mild sonication (Section 2.18) and separated by 2-D SDS PAGE (Section 2.21.2). (a) Control cells (untreated) and (b) cells incubated for 2 h with $AgNO_3$ (3.0 µg/ml).

**Table 6.2:** Identification of proteins involved in the virulence of *S. aureus*.

| Spot No. | Accession No. | Protein | Function | Mass (kDa) | Score | pI | % Coverage | Fold Difference |
|---|---|---|---|---|---|---|---|---|
| 18 | Q53747 | Leucocidin F | Cytolysis in other organism pathogenesis | 36986 | 98 | 9.12 | 7% | - 1.5 |
| 19 | P63845 | Transcriptional repressor CodY | Transcription regulation | 28737 | 532 | 5.87 | 56% | + 1.6 |
| 20 | Q5HIU3 | ABC transporter | ATP-binding | 31575 | 609 | 5.25 | 41% | + 1.7 |
| 21 | P09616 | Alpha-hemolysin | Pore formation | 33227 | 633 | 7.94 | 49% | - 2.1 |
| 22 | P0Z5Z8 | Bifunctional autolysin | Cellular cell wall organization | 62644 | 219 | 9.29 | 10% | - 1.7 |
| 23 | Q7A4W3 | Signal transduction protein TRAP | Major regulator of staphylococcal pathogenesis | 19594 | 187 | 6.12 | 37% | + 3.1 |

*S. aureus* and integrates into a target cell membrane forming a cylindrical heptamer. This leads to pore formation and allows the efflux of cellular contents and the influx of $Na^+$ and $Ca^{2+}$ into the cell causing osmotic swelling and resulting in cell rupture.[142] Proteomic analysis identified a 2.1 fold decrease in expression of alpha hemolysin (Spot 21), suggesting that, at the $MIC_{80}$ value, $AgNO_3$ reduces the expression of an *S. aureus* virulence factor. Bernardo *et al*[255] also found that the abundance of secreted exoproteins, such as alpha- and beta-hemolysin, were reduced in *S. aureus* cells after exposure to the antibiotic, linezolid. Another virulence factor which was found to be increased in expression was the signal transduction protein, TRAP (target of RNAIII-activating protein) (Spot 23). *S. aureus* TRAP is known to play a key role in regulating the pathogenesis of *S. aureus* by controlling a range of virulence factors.[256] It has been suggested that RNAIII allows *S. aureus* to adhere to host cells when they are in a low density. The bacterial cells then express toxins in the late exponential growth phase, thus allowing the organism to establish an infection.[257] It has also been shown that without the expression or the phosphorylation of TRAP, virulence factors, such as hemolysins, are not expressed.[258] Korem *et al*[258] have also shown that cells which are defective in the expression or the phosphorylation of TRAP do not adhere as strongly *in vitro* to plastic polymers or mammalian host cells and fail to form biofilms *in vivo*. The expression TRAP was found to have increased by 3.1 fold, suggesting that *S. aureus* cells are responding by upregulating virulence factors to combat $AgNO_3$ exposure.

As already mentioned, organisms defend against ROS using a range of antioxidant enzymes such as SOD, catalase and glutathione. In spite of these antioxidant mechanisms cellular damage can still occur. This is where methionine sulfoxide reductase A (MsrA) can intervene and function as a repair enzyme.[259] The Msr enzyme family are made up of MsrA and MsrB which reduce *S*-MetO and *R*-MetO, respectively, back to methionine.[260] The proteins involved in the stress response of *S. aureus* were all found to be up-regulated (1.2-2.9 fold) upon $AgNO_3$ treatment. Methionine sulphoxide reductase A (Spot 25) was the protein most induced, with a 2.9 fold increase in abundance. Singh *et al*[261] also found that this protein was induced upon exposure of *S. aureus* cells to the antibiotic, oxacillin. The identification of these proteins confirm that S. aureus cells are experiencing stress as

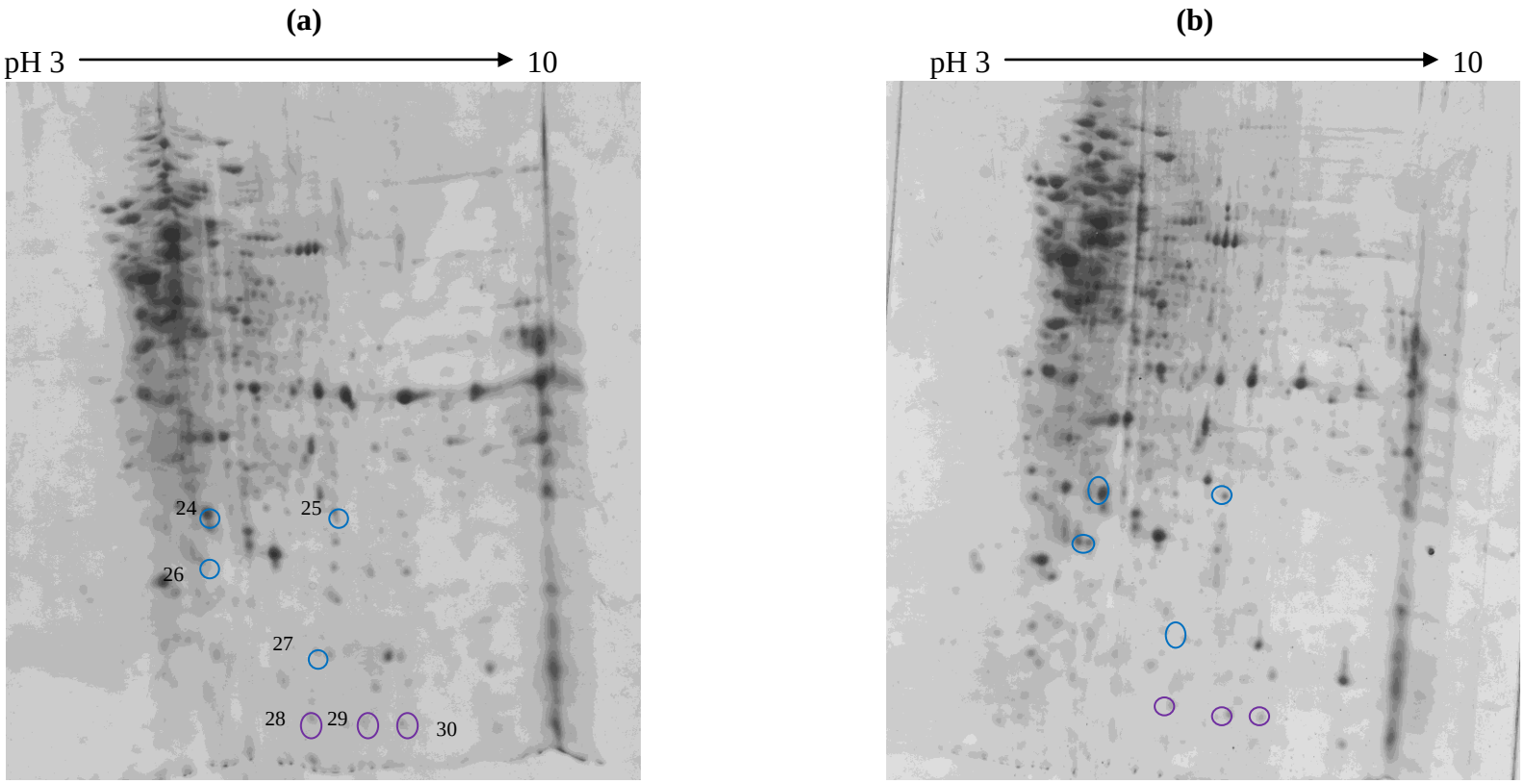


**Fig. 6.6:** Two-Dimensional SDS-PAGE analysis of proteins leaked from *S. aureus* cells involved in stress response (blue) and unknown function (purple). Protein was extracted using sonication (Section 2.18) and separated by 2-D SDS PAGE (Section 2.21.2). (a) Control cells (untreated) and (b) cells incubated for 2 h with $AgNO_3$ (3.0 µg/ml)

**Table 6.3:** Identification of proteins involved in the stress response of *S. aureus*.

| Spot No. | Accession No. | Protein | Function | Mass (kDa) | Score | pI | % Coverage | Fold Difference |
|---|---|---|---|---|---|---|---|---|
| 24 | Q2FXL6 | Putative universal stress protein | Response to stress | 18522 | 639 | 5.60 | 69% | + 1.2 |
| 25 | P65446 | Methionine sulfoxide reductase A | Repair enzyme | 20749 | 254 | 6.37 | 35% | + 2.9 |
| 26 | P0A0P7 | Alkaline shock protein 23 | Alkaline pH tolerance | 19180 | 466 | 5.13 | 55% | + 2.8 |
| 27 | Q7A1R4 | Transcription repressor of class III stress genes-like protein | Stress response | 17888 | 467 | 5.93 | 52% | + 1.6 |

**Table 6.4:** Identification of proteins of unknown function

| Spot No. | Accession No. | Protein | Function | Mass (kDa) | Score | pI | % Coverage | Fold Difference |
|---|---|---|---|---|---|---|---|---|
| 28 | Q99UP3 | Hypothetical protein SAV1225 | Function unknown | 13435 | 365 | 5.78 | 72% | + 1.5 |
| 29 | Q2FW79 | UPF0457 protein SAOUHSC_02425 | Belongs to the uncharacterised protein (UPF0457) family | 10000 | 152 | 6.07 | 51% | + 1.5 |
| 30 | Q99TW8 | Hypothetical protein SAV1525 | Putative uncharacterised protein | 13323 | 316 | 6.84 | 65% | - 1.6 |

as a result of $AgNO_3$ exposure, and this correlates with the earlier oxidative stress response found using the SOD and CAT assays (Chapter 5).

## 6.3 Proteomic analysis of the effect of $AgNO_3$ on *S. aureus* intracellular protein expression

Following the analysis of the extracellular proteins released from *S. aureus* cells it was decided to examine the intracellular proteins which may have changed in expression as a result of $AgNO_3$ exposure. This was determined using one- and two-dimensional SDS-PAGE. *S. aureus* cells were exposed to the $MIC_{80}$ value of $AgNO_3$ (3.0 µg/ml) for either 1 or 4 h. Protein was extracted using the glass beads method (Section 2.18), separated by 1-D electrophoresis (Section 2.21.1) and visualised using Coomassie blue (Section 2.3). Protein expression in treated and untreated bacterial cells is illustrated in Fig. 6.6. It is evident from this gel that treatment with $AgNO_3$ has an effect on the protein expression (in relation to the control) and it was decided to focus attention on the protein expression at 1 and 4 h.

Glass beads were used as a more robust method of protein extraction to ensure that the cells were totally lysed and the intracellular content released. 2-D SDS-PAGE analysis was performed and protein was visualised using colloidal Coomassie (Section 2.3). Following the visualisation of protein spots, spot intensities were analysed using Progenesis SameSpot™ software and changes in expression were evaluated relative to the control. The spots of interest were excised, washed and trypsin digested (Section 2.22) and LC/MS analysis was carried out to determine the identity and function of these proteins. Listed in Table 6.5 are the identified intracellular proteins found following LC/MS analysis with their functions were identified using MASCOT and Uniprot software programmes. Protein expression in untreated *S. aureus* cells (control cells) in comparison the $AgNO_3$-treated cells for 1 and 4 h is shown in Fig. 6.7 and the reference image for Progenesis is shown in Fig. 6.8.

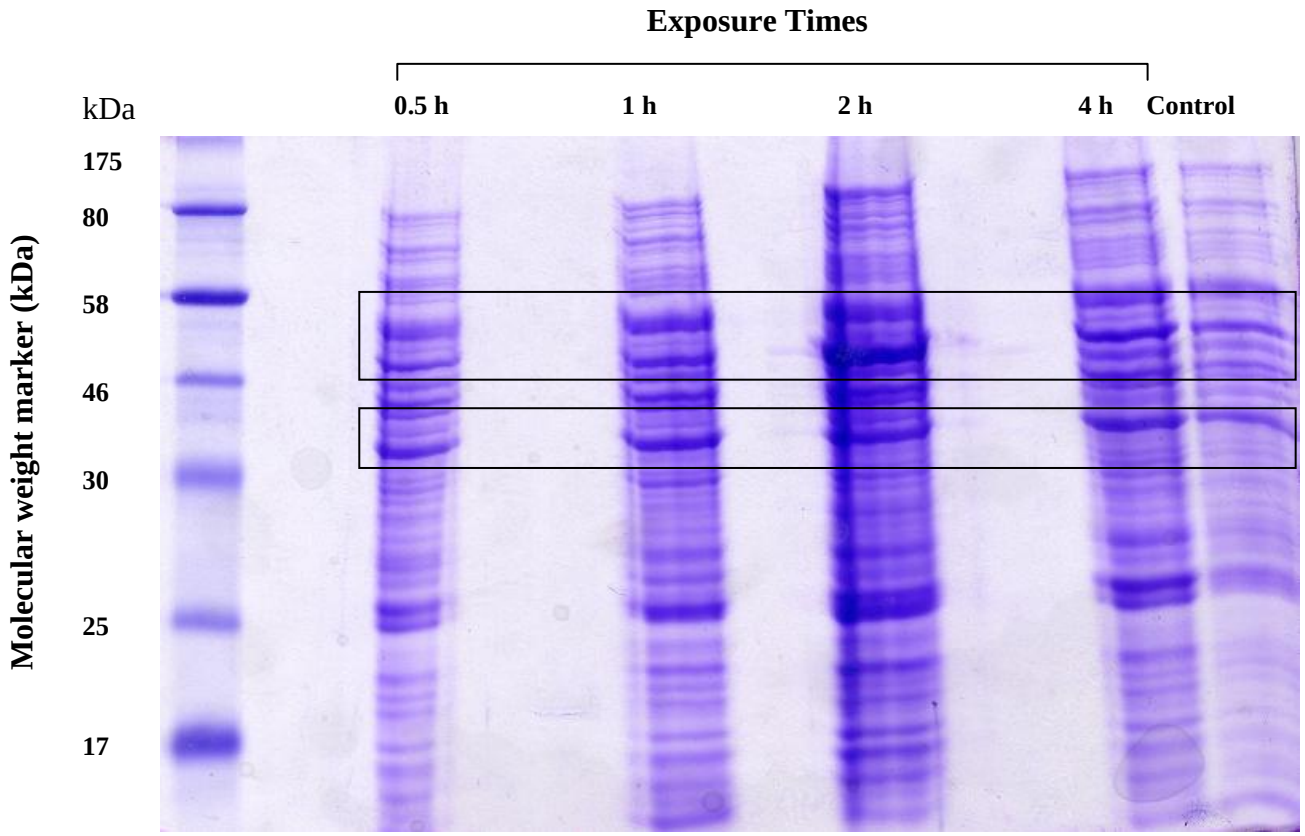


**Fig. 6.6:** One-Dimensional SDS-PAGE analysis of intracellular proteins from *S. aureus* cells. Protein was extracted using the glass beads method (Section 2.18) and separated by 1-D SDS PAGE (Section 2.21.1). Protein bands highlighted appear to be altered in expression as a result of $AgNO_3$ treatment at various times in relation to the control.

In total, 12 spots were identified (Table 6.5). $AgNO_3$ induced an increase in the expression of proteins after 1 h treatment. Of these, 9 proteins were identified to be involved in metabolism, 2 were involved in virulence and 1 in the stress response of *S. aureus*. The metabolic proteins included elongation factors Ts, Tu and G (spot 236, 155 and 78, respectively), ornithine carbamoyltransferase (spot 237), hypothetical protein EF0177 (spot 217), dihydrolipoamide dehydrogenase (Spot 147), fructose-bisphosphate aldolase (spot 314), 30S ribosomal protein S3 (spot 333) and triosephosphate isomerase (spot 340).

Protein biosynthesis is one of the essential processes of living cells and is the driving force behind the growth and development of all organisms, with the protein elongation cycle being one of the main steps.[262] Elongation factors play an important role in the translation stage of protein biosynthesis, i.e. the progressive addition of amino acids to the growing polypeptide chain. The elongation factors are involved in the addition of amino acids in the elongation stage of this process. The elongation factors, Ts, Tu and G, followed a similar trend with expression increases peaking at 1 h (4.1, 2.3 and 1.3 fold, respectively) and decreasing in expression by 4 h (2.1, 1.1 and -3.2 fold, respectively). Each of the elongation factors have a specific role, with elongation factor Tu (EF-Tu) being activated upon exchange of GDP for GTP[263] and responsible for the transportation of the aminoacyl-tRNA to the ribosome.[262] The exchange of GDP for GTP is carried out by the elongation factor Ts (EF-Ts), which is a nucleotide exchange factor.[264] The last of the elongation factors, EF-G, is involved in the translocation of tRNA and mRNA by one codon on the ribosome.[265] The increase in expression of these elongation factors at 1 h suggests that the *S. aureus* cells are responding to $AgNO_3$ treatment by increasing protein biosynthesis. However, this effect is lost by 4 h as a decrease in expression is observed, suggesting cell death. Kaakoush *et al*[266] also found that the elongation factors Tu and G of *Campylobacter jejuni* were upregulated as a result of exposure to Cd(II) ions, suggesting that additional protein biosynthesis occurs in response to metal ion exposure.

A number of the identified proteins were involved in cellular respiration in either the glycolytic pathway or the tricarboxylic acid pathway (Appendices IV and V,

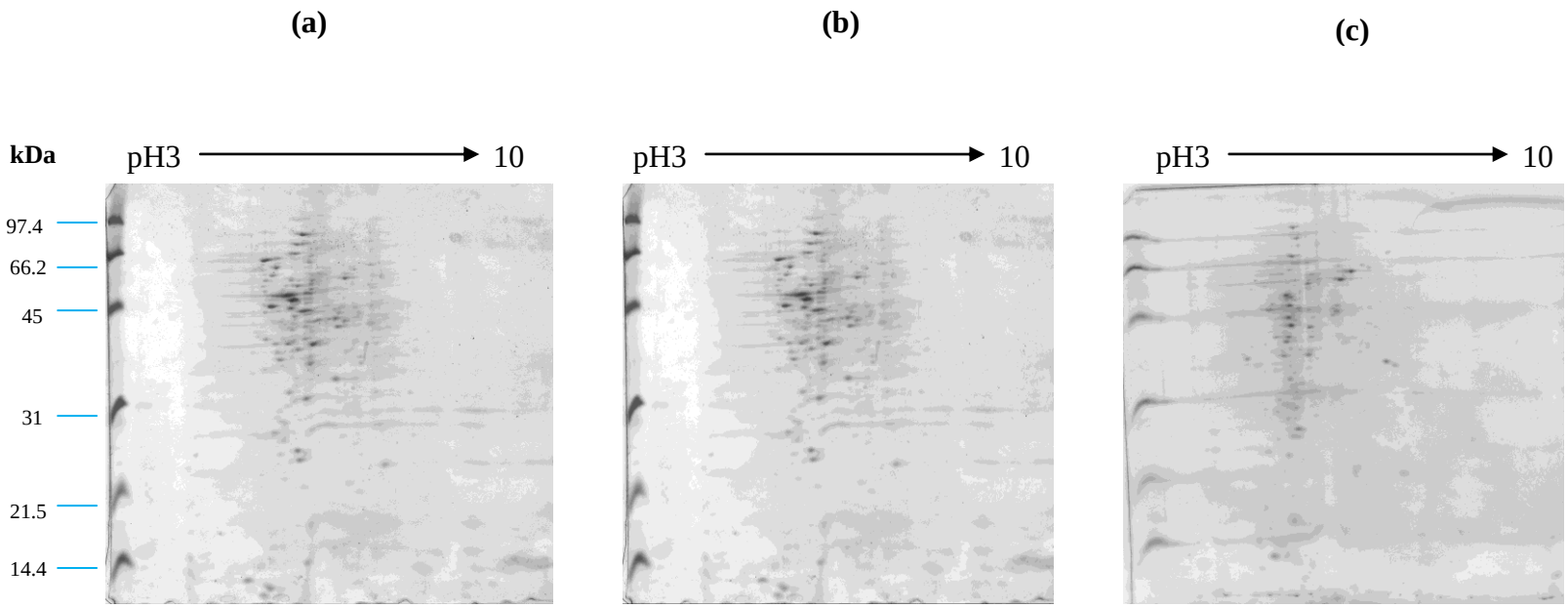


**Fig. 6.7:** Two-Dimensional SDS-PAGE analysis of *S. aureus* cells treated with $MIC_{80}$ $AgNO_3$. Protein was extracted using the glass beads method (Section 2.18) and separated by 2-D SDS PAGE (Section 2.21.2). (a) Control cells (untreated), cells incubated in $AgNO_3$ (3 µg/ml) for (b) 1 h and (c) 4 h.

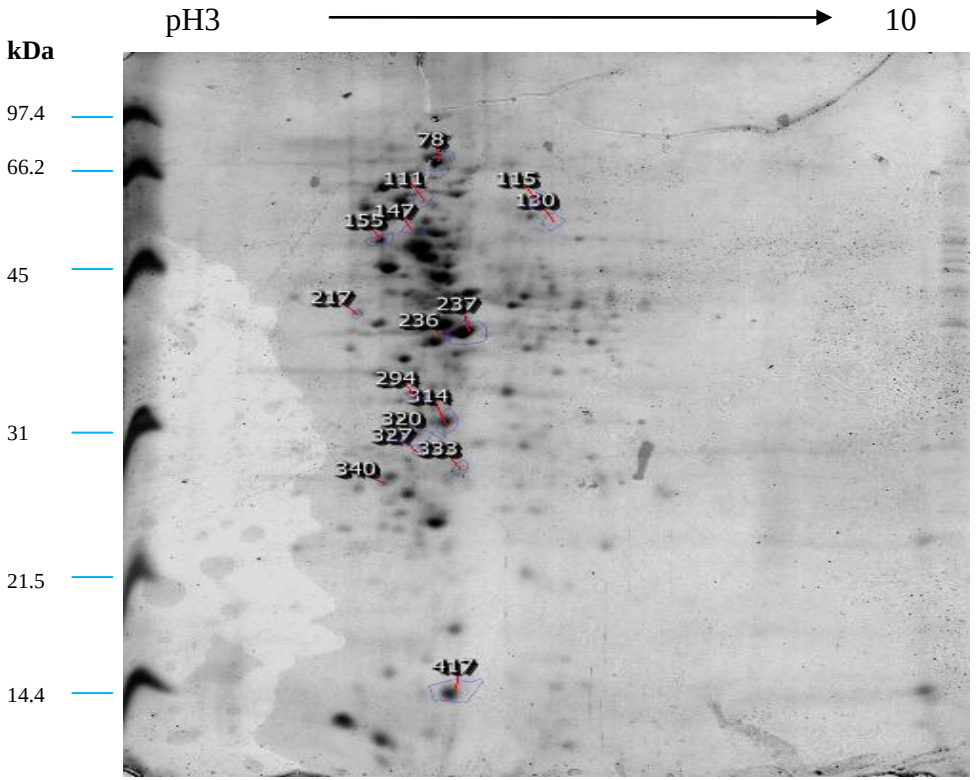


**Fig. 6.8:** Progenesis SameSpot™ software reference image. Protein spots were analysed for fold changes in comparison to untreated cells. Protein spots were extracted for identification using LC/MS (Section 2.22).

**Table 6.5:** Summary of *S. aureus* intracellular proteins identified using LC/MS.

| Spot No. | Accession No. | Protein | Function | Mass (kDa) | Score | % Coverage | pI | Fold Changes | | |
|---|---|---|---|---|---|---|---|---|---|---|
| | | | | | | | | 0 h | 1 h | 4 h |
| 111 | NP_814413 | Oligoendopeptidase F | Proteolysis | 69025 | 260 | 10% | 4.85 | 1 | 1.1 | 1.5 |
| 236 | NP_816048 | Elongation factor Ts | Protein biosynthesis | 32113 | 335 | 43% | 4.87 | 1 | 4.1 | 2.1 |
| 237 | ZP_05425197 | Ornithine carbamoyltransferase | Transferase activity | 38135 | 1126 | 74% | 5.02 | 1 | 1.7 | - 1.6 |
| 217 | NP_813980 | Hypothetical protein EF0177 | Lipid binding | 37784 | 930 | 65% | 4.88 | 1 | 1.9 | - 1.6 |
| 155 | NP_371072 | Elongation factor Tu | Protein biosynthesis | 43135 | 281 | 15% | 4.74 | 1 | 2.3 | 1.0 |
| 314 | NP_814897 | Fructose-bisphosphate aldolase | Fructose 1,6-bisphosphate metabolic process | 31025 | 387 | 33% | 4.86 | 1 | 1.4 | - 1.6 |
| 147 | NP_815077 | Dihydrolipoamide dehydrogenase | Flavin adenine dinucleotide binding | 49229 | 683 | 45% | 4.95 | 1 | 2.3 | - 1.1 |

**Table 6.5:** Continued.

| Spot No. | Accession No. | Protein | Function | Mass (kDa) | Score | % Coverage | pI | Fold Changes | | |
|---|---|---|---|---|---|---|---|---|---|---|
| | | | | | | | | 0 h | 1 h | 4 h |
| 333 | NP_814010 | 30S ribosomal protein S3 | Translation | 24355 | 221 | 23% | 9.80 | 1 | 2.0 | - 1.1 |
| 78 | NP_371071 | Elongation factor G | Protein biosynthesis | 76854 | 362 | 16% | 4.80 | 1 | 1.3 | - 3.2 |
| 340 | NP_815638 | Triosephosphate isomerase | Glycolysis | 27130 | 324 | 39% | 4.63 | 1 | 1.9 | - 1.3 |
| 294 | YP_002559945 | ABC transporter | ATP-binding | 29096 | 404 | 25% | 4.85 | 1 | 1.5 | 2.7 |
| 417 | 1FU0_A | Chain A, Crystal Structure Analysis Of The Phospho-Serine 46 Hpr | Phosphotransferase system | 9210 | 98 | 13% | 5.00 | 1 | 1.7 | 1.0 |

respectively). The metabolic proteins, fructose-bisphosphate aldolase and triosephosphate isomerase, are involved in the glycolysis pathway, which is a major source of energy for cells and which involves the metabolism of glucose. Fructose-bisphosphate aldolase is involved in step four of the glycolysis pathway, in which fructose-1,6-bisphosphate is cleaved into the two 3-carbon sugars, dihydroxyacetone phosphate and glyceraldehyde-3-phosphate.[267] It is in the next step of the glycolytic pathway that triosephosphate isomerase is responsible for the interconversion of these two sugars.[268] It was found that both of these proteins were increased in expression (1.4 fold for fructose-bisphosphate aldolase and 1.9 fold for triosephosphate isomerase) at 1 h and decreased in expression at 4 h (fructose-bisphosphate aldolase by 1.6 fold and triosephosphate isomerase decreased by 1.3 fold, both in relation to the control). The dihydrolipoamide dehydrogenase protein was increased in expression by 2.3 fold at 1 h, but this decreased by 1.1 fold at 4 h. This latter protein is the third enzyme involved in the pyruvate dehydrogenase complex. The enzyme converts pyruvate, the product of glycolysis, into acetyl-CoA which is then used in the tricarboxylic acid cycle[269] for cellular respiration and therefore linking the two processes of glycolysis and the tricarboxylic acid cycle.[270] These observations suggest that *S. aureus* cells are responding to $AgNO_3$ exposure by increasing cellular respiration. Fructose-bisphosphate aldolase has previously been reported to be increased in expression in caspofungin-treated *C. albicans* cells, where it was postulated to be contributing to a stronger immune response.[271] Triosephosphate isomerase and dihydrolipoamide dehydrogenase were both found to be up-regulated following exposure to Cd(II) ions, suggesting that these cations have a significant impact upon carbohydrate metabolism in *C. albicans* cells.[272]

The bacterial ribosome (70S) is made up of two subunits; a small subunit (30S) and a larger subunit (50S). The 30S subunit itself is made up of 21 proteins and a single strand of RNA[273] of around 1500 nucleotides (which corresponds to a 16S sedimentation coefficient).[274] The larger subunit (50S) is made up of 34 proteins and 2 strands of RNA which correspond to a 23S and a 5S sedimentation coefficient.[273] It is only when the 30S and 50S subunits attach to an mRNA molecule that a functional ribosome is formed and this subsequently plays an important role in the translation of a protein. The 30S ribosomal subunit is central to the selection of a start site on

the mRNA which is a critical phase of the initiation process of translation.[274] In the current study, the 30S ribosomal protein, S3, was found to have increased in expression by 2.0 fold at 1 h and decreased by 1.1 fold at 4 h. This suggests that the *S. aureus* cells are increasing protein biosynthesis as a result of $AgNO_3$ exposure.

The proteins involved in the virulence of *S. aureus* include an ABC (ATP binding cassette) transporter protein (spot 294) and also the protein, phosphoserine 46 Hpr (spot 417). The ABC transporter protein is one of the largest classes of transporters which, by their nature, are responsible for mediating the movement of small molecules, ions and even macromolecules across membranes.[275] ABC transporters are involved in many processes such as the uptake of nutrients, energy generation and cell signalling.[276] They have also been implicated in the removal of waste products, xenobiotic protection and bacterial immunity and virulence.[277] *S. aureus* cells respond to $AgNO_3$ treatment by significantly increasing the expression of this ABC transporter at 1 and 4 h (1.5 fold and 2.7 fold, respectively), suggesting that the cells are attempting to prevent the entry of $AgNO_3$ into the cell or the efflux of metabolites. Bacteria have developed mechanisms to decrease the residence time of toxic materials in the cell by effluxing them from the cell across the cytoplasmic membrane.[277] ABC transporters have received considerable attention due to their contribution to the resistance of cells to antibiotics and has led to the development of synthetic inhibitors whose function is to prevent the interference of these transporters with administered drugs.[278]

The phosphoserine 46 HPr, plays an important role in the carbon catabolite repression system, which is a regulatory mechanism to help bacteria make efficient use of the available carbon sources, of which glucose is the most preferred.[279] As bacteria can be exposed to a variety of carbon sources in their natural habitat, this mechanism allows for selective uptake and the metabolism of carbon sources which will encourage the most rapid growth of the organism.[280] As bacteria aim to gain access to nutrients, the HPr protein contributes to the pathogenicity of *S. aureus*. The phosphorylation of HPr is catalysed by HPrK kinase which is triggered by the availability of fructose-1,6-bisphosphate.[279] This is interesting to note, as

phosphoserine 46 HPr was increased by 1.7 fold at 1 h and the expression of fructose-1,6-bisphosphate was also found to be increased (as previously discussed).

Oligoendopeptidase F (spot 111) is implicated in the stress response of *S. aureus* and is involved in proteolysis, which allows for the controlled degradation of proteins.[281] Proteolysis is an essential process and is required for quality control and also for the regulatory response to environmental stimuli.[282] Proteolysis has been implicated in many processes such as regulation of the cell cycle, stress response and also apoptosis. Proteases have been known to contribute to the ability of an organism to withstand stressful conditions, such as oxidative stress.[283] It is interesting to note that this protein was found to be increased by 1.5 fold in expression at 4 h after $AgNO_3$ treatment, suggesting that the *S. aureus* cells are trying to withstand the stressful environment. Oligoendopeptidase F is suspected to also contribute to the virulence of this organism since Group A *Streptococci* has been shown to evade the host immune response by disrupting the recruitment of phagocytic cells through the action of a serine endopeptidase.[284]

As was found in the case of the extracellular leaked proteins, a protein of unknown function was also significantly changed in expression. The hypothetical protein, EF-177, was increased in expression by 1.9 fold at 1 h and reduced by 1.6 fold at 4 h (in relation to the control).

## 6.4 Conclusion

In conclusion, it has been discovered that when *S. aureus* cells were exposed to $AgNO_3$ there were significant fold changes (increases and decreases) in extracellular leaked proteins and also the expression of intracellular proteins, such as metabolic proteins, proteins involved in virulence and also those implicated in the stress response of the bacterium. For the extracellular proteins, at the 2 h timepoint, 12 metabolic proteins, 3 virulence proteins and all 4 stress response proteins were increased in abundance, whereas 5 metabolic proteins and 3 virulence proteins were decreased. For the intracellular proteins, at the 1 h timepoint, 9 metabolic proteins were increased in expression, but by 4 h they had decreased. These findings suggest

that the cells are responding to administered $AgNO_3$ by increasing the expression of proteins involved in essential cellular processes such as translation (which is involved in protein biosynthesis), glycolysis and the tricarboxylic acid cycle, which results in the production of ATP and is essential for metabolism within the cell. Ultimately, in the case of the intracellular proteins, the cells were unable to maintain this protective response after 4 h of exposure to $AgNO_3$. It is interesting to note that of the proteins involved in virulence, the ABC transporter was identified amongst both the extracellular leaked proteins and the intracellular proteins. This ABC protein was increased in expression at all timepoints, suggesting that the organism was mounting an efflux response in an attempt to remove toxins from the cell as a result of $AgNO_3$ exposure. The results presented in this Chapter demonstrate the impact of $AgNO_3$ on essential cellular processes in *S. aureus* cells up to 4 h. The study also revealed the response of *S. aureus* to this antimicrobial agent at a proteomic level.

# Conclusion

# 7.0 Concluding Remarks

The main aims of this research were (i) to synthesise a surgical Bioglue incorporating Ag(I) ions in order to prevent the occurrence of nosocomial infections, and (ii) to determine a possible mode(s) of action of the Ag(I) ion against *Staphylococcus aureus*.

Clinically used Bioglue hydrogel, prepared by reacting bovine serum albumin with glutaraldehyde, is very susceptible to colonization by pathogenic microbes. Addition of specific amounts of Ag(I) ions to the albumin/aldehyde mixture gives an Ag(I)-Bioglue that offers protection against fungal and bacterial growth.

Bioglue hydrogel samples prepared in the absence and in the presence of the Ag(I) ions (from $AgNO_3$ and $[Ag_2(3,6,9\text{-tdda})].2H_2O$), were thermally stable and had reversible swelling properties in the presence of water. As the amount of added Ag(I) ions in the Bioglue formulation decreased the swelling ratio in water increased. The Ag(I) ions crosslink the gel network giving a more rigid structure and limit the amount of hydrogen-bonding sites available for water molecules to access and cause swelling. After 24-48 h, Bioglue without Ag(I) ions and Bioglues containing very small amounts of Ag(I) ions start to break down due to hydrolysis. Bioglues without added Ag(I) ions have a very porous surface morphology, whilst the addition of Ag(I) ions into the formulation gives a product with a smoother surface due to the formation of a more rigid structure.

Adherence of wood and pigskin samples bonded together with Bioglue decreases as the amount of added Ag(I) ions in the formulation increases. Elasticity of the Bioglue is also inversely proportional to the quantity of added Ag(I) ions. Leaching of Ag(I) ions from the $AgNO_3$-Bioglues occurred rapidly over the first 10 h and steadily reached an equilibrium after 55 h.

Bioglue samples containing $AgNO_3$ (0.01 g) could be reduced using sodium borohydride and sodium citrate. However, no Ag(0) nanoparticles were detected using either UV-Visible spectroscopy or SEM analysis. Exposing Bioglue (without

Ag(I) ions) to Ag(0) nanoparticles does not lead to uptake of Ag(0) into the Bioglue matrix.

Ag(I)-Bioglues inhibit the growth of the fungal pathogen, *Candida albicans*, and they also exhibit potent activity against the bacterial species, *Pseudomonas aeruginosa*, *Escherichia coli*, *Staphylococcus aureus* and *Methicillin-Resistant Staphylococcus aureus*. Bioglues formulated using $AgNO_3$ exhibited superior anti-bacterial activity than those made from $[Ag_2(3,6,9\text{-tdda})].2H_2O$. Based on Ag(I) ion content, $AgNO_3$ was more active than $[Ag_2(3,6,9\text{-tdda})].2H_2O$ against *Candida albicans* (36.8 µM and 71.6 µM Ag(I), respectively). $AgNO_3$ and $[Ag_2(3,6,9\text{-tdda})].2H_2O$ were equally active against *S. aureus* ($MIC_{80}$ *ca.* 18 µM) and $AgNO_3$ was more effective against *M.R.S.A.* than $[Ag_2(3,6,9\text{-tdda})].2H_2O$ ($MIC_{80}$ 17.7 µM and 143.5 µM, respectively).

Exposing *S. aureus* cells to a $MIC_{80}$ value of $AgNO_3$ results in an increase in activity of the antioxidant enzymes superoxide dismutase, catalase and, to a lesser extent, glutathione reductase, after a 30 min exposure time. This activity subsequently decreases after 60 min due to the loss of cell viability. Furthermore, exposing these bacterial cells to $AgNO_3$ results in an increase in the amount of amino acid leakage from the cells, suggesting that Ag(I) ions affect membrane permeability. In addition, proteomic analysis revealed that *S. aureus* cells exposed to $AgNO_3$ resulted in an increase in expression of a number of proteins involved in the stress response of the organism and as the bacterium attempts to mount a protective response. This is evident by the increase in expression of virulent and essential metabolic proteins. Exposure of *S. aureus* to $AgNO_3$ causes a short-term protective response within the organism but ultimately these defense strategies are overwhelmed and the cells die.

The exposure of patients to harmful microorganisms within the first few hours of admission to hospital makes these Ag(I)-Bioglues an attractive option. They have the ability to prevent such an infection, due to the rapid availability of bioactive Ag(I) ions within these crucial first few hours and also provide a steady accessibility of Ag(I) ions over a 55 h period. The reduction in adherence and elasticity properties of the Ag(I)-Bioglue may be a worthwhile compromise for the availability of antimicrobial Ag(I) ions.

# Appendix

# Appendix I: Mass Spectra for $[Ag_2(3,6,9\text{-tdda}].2H_2O$

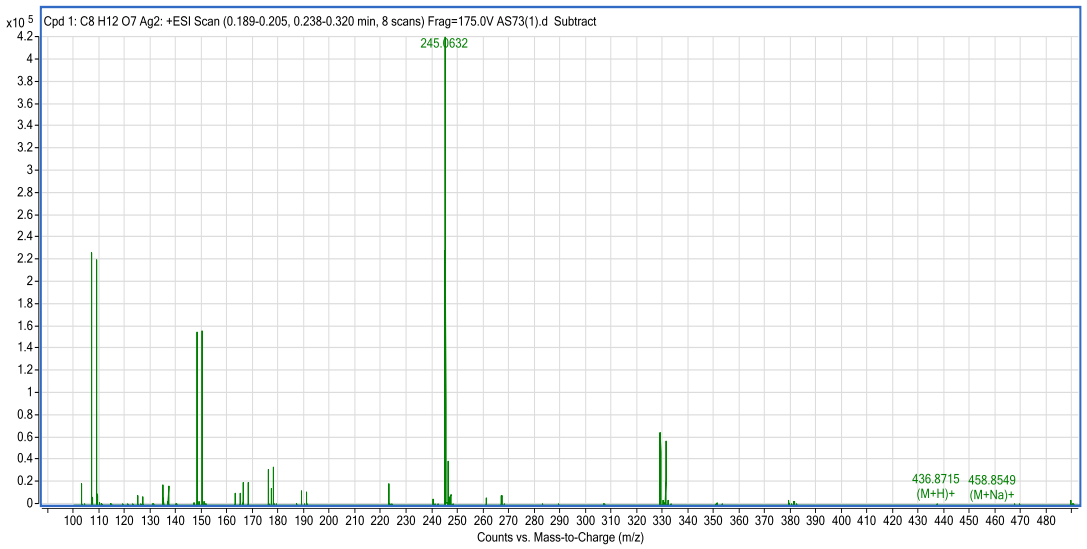


**(a)**

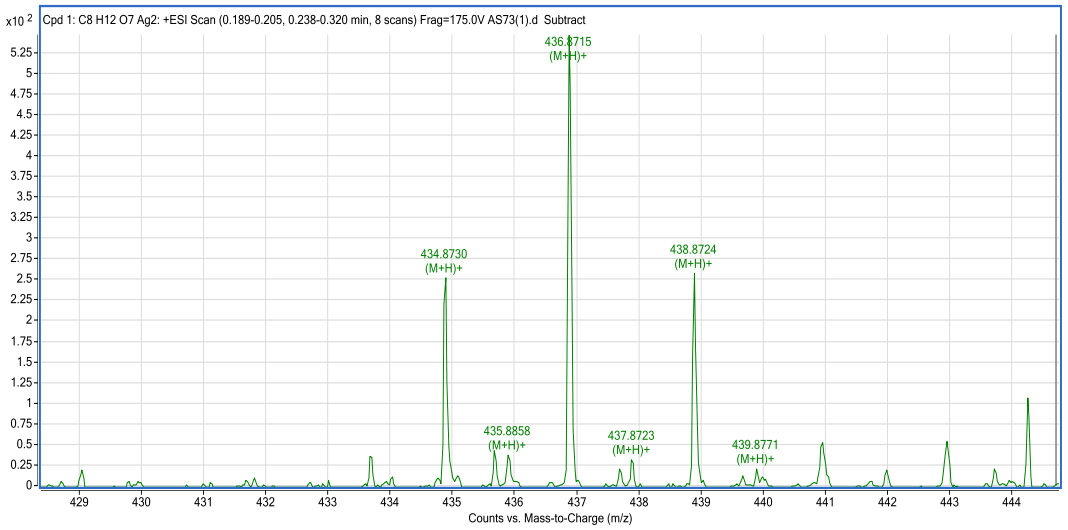


**(b)**

**Fig. 1:** Mass spectra for $[Ag_2(3,6,9\text{-tdda})].2H_2O$: (a) complete mass spectrum indicating 3,6,9-tdda$H_2$ + $Na^+$ fragment (245.06 g $mol^{-1}$) and (b) mass spectrum indicating isotopes of $[Ag_2(3,6,9\text{-tdda}) + H]^+$ (434.87, 436.87 and 438.87 g $mol^{-1}$).

# Appendix II: Atomic Absorption Spectroscopy Data

**Table 1:** Atomic Absorption Spectroscopy data for $AgNO_3$-Bioglue (0.1 g).

| | **Sample (1) (%)** | **Sample (2) (%)** | **Sample (3) (%)** |
|---|---|---|---|
| **Run 1** | 10.56 | 13.31 | 14.28 |
| **Run 2** | 11.99 | 10.44 | 12.28 |
| **Run 3** | 10.75 | 9.91 | 10.97 |

**Table 2:** Atomic Absorption Spectroscopy data for $AgNO_3$-Bioglue (0.01 g).

| | **Sample (1) (%)** | **Sample (2) (%)** | **Sample (3) (%)** |
|---|---|---|---|
| **Run 1** | 1.77 | 1.89 | 3.29 |
| **Run 2** | 1.50 | 1.37 | 1.24 |
| **Run 3** | 1.36 | 1.22 | 1.09 |

**Table 3:** Atomic Absorption Spectroscopy data for $AgNO_3$-Bioglue (0.001 g).

| | **Sample (1) (%)** | **Sample (2) (%)** | **Sample (3) (%)** |
|---|---|---|---|
| **Run 1** | 1.04 | 1.07 | 0.90 |
| **Run 2** | 0.35 | 0.34 | 0.29 |
| **Run 3** | 0.24 | 0.24 | 0.22 |

**Table 4:** Atomic Absorption Spectroscopy data for $AgNO_3$-Bioglue (0.0001 g).

| | **Sample (1) (%)** | **Sample (2) (%)** | **Sample (3) (%)** |
|---|---|---|---|
| **Run 1** | 0.23 | 0.26 | 0.31 |
| **Run 2** | 0.40 | 0.29 | 0.19 |
| **Run 3** | 0.14 | 0.13 | 0.21 |

**Table 5:** Atomic Absorption Spectroscopy data for $[Ag_2(3,6,9\text{-tdda})].2H_2O$-Bioglue (0.01 g).

| | **Sample (1) (%)** | **Sample (2) (%)** | **Sample (3) (%)** |
|---|---|---|---|
| **Run 1** | 1.10 | 1.35 | 1.08 |
| **Run 2** | 1.18 | 1.13 | 1.29 |
| **Run 3** | 0.77 | 0.88 | 0.93 |

**Table 6:** Atomic Absorption Spectroscopy data for $[Ag_2(3,6,9\text{-tdda})].2H_2O$-Bioglue (0.001 g).

| | **Sample (1) (%)** | **Sample (2) (%)** | **Sample (3) (%)** |
|---|---|---|---|
| **Run 1** | 0.51 | 0.54 | 0.47 |
| **Run 2** | 0.23 | 0.31 | 0.36 |
| **Run 3** | 0.15 | 0.16 | 0.15 |

**Table 7:** Atomic Absorption Spectroscopy data for $[Ag_2(3,6,9\text{-tdda})].2H_2O$-Bioglue (0.0001 g).

| | **Sample (1) (%)** | **Sample (2) (%)** | **Sample (3) (%)** |
|---|---|---|---|
| **Run 1** | 0.09 | 0.48 | 0.53 |
| **Run 2** | 0.31 | 0.26 | 0.36 |
| **Run 3** | 0.09 | 0.06 | 0.12 |

**Table 8:** Atomic Absorption Spectroscopy data for $[Ag_2(3,6,9\text{-tdda})].2H_2O$-Bioglue (0.00001 g).

| | **Sample (1) (%)** | **Sample (2) (%)** | **Sample (3) (%)** |
|---|---|---|---|
| **Run 1** | 0.41 | 0.65 | 0.56 |
| **Run 2** | 0.26 | 0.22 | 0.19 |
| **Run 3** | 0.16 | 0.19 | 0.21 |

# Appendix III: Ag(I) Leaching Studies

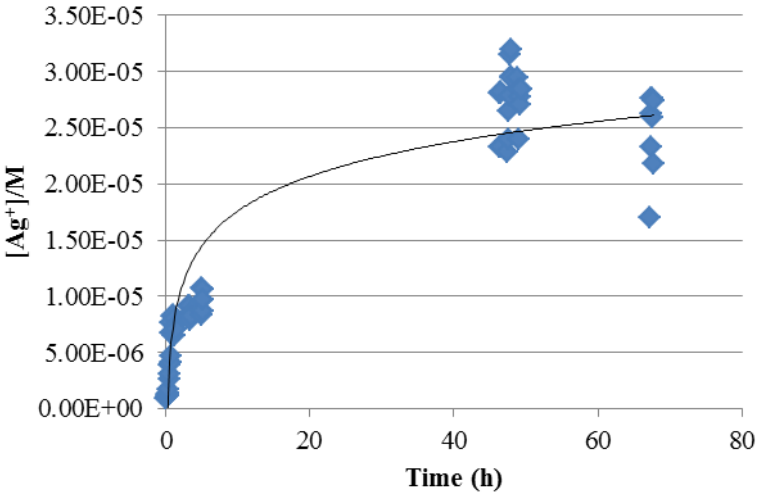


**(a)**

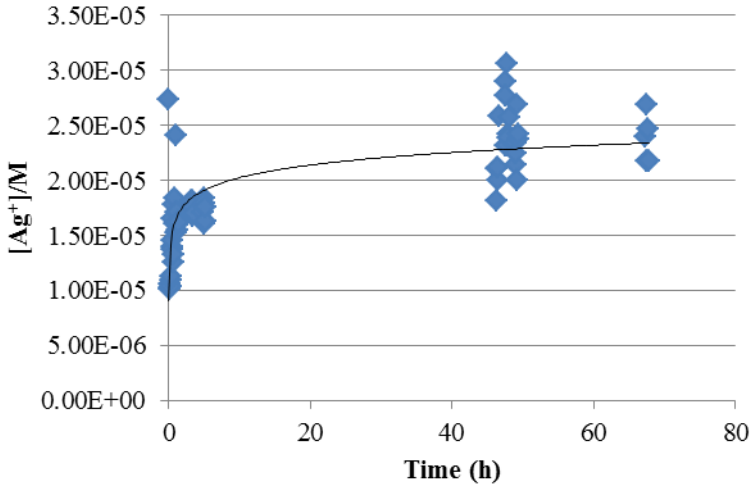


**(b)**

**Fig. 1:** Initial study to determine concentration of leached silver from Bioglue (0.01 g added $AgNO_3$) calculated by (a) peak height (Ip) and (b) charge.

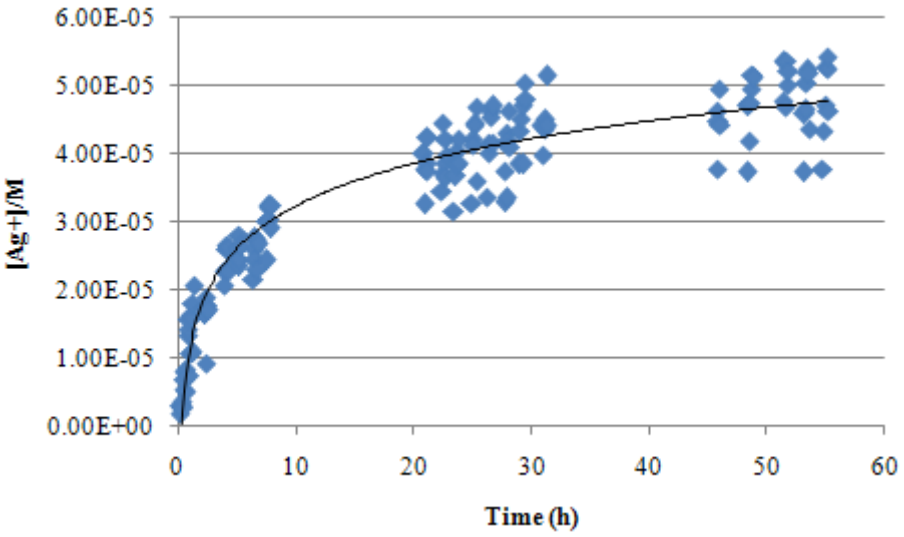


**(a)**

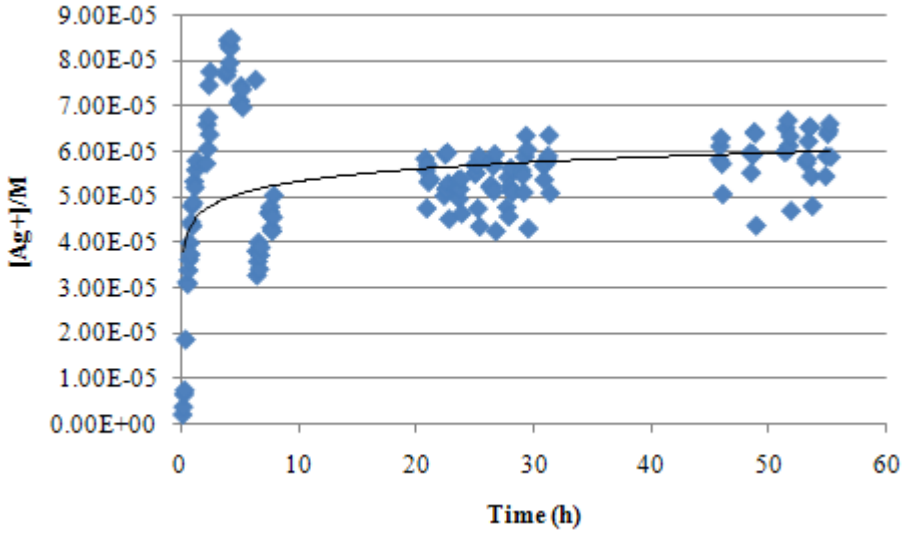


**(b)**

**Fig. 2:** Concentration of leached silver from Bioglue (0.01 g added $AgNO_3$) calculated by (a) peak height (Ip) and (b) charge.

## Appendix IV: Molecular Biology Images

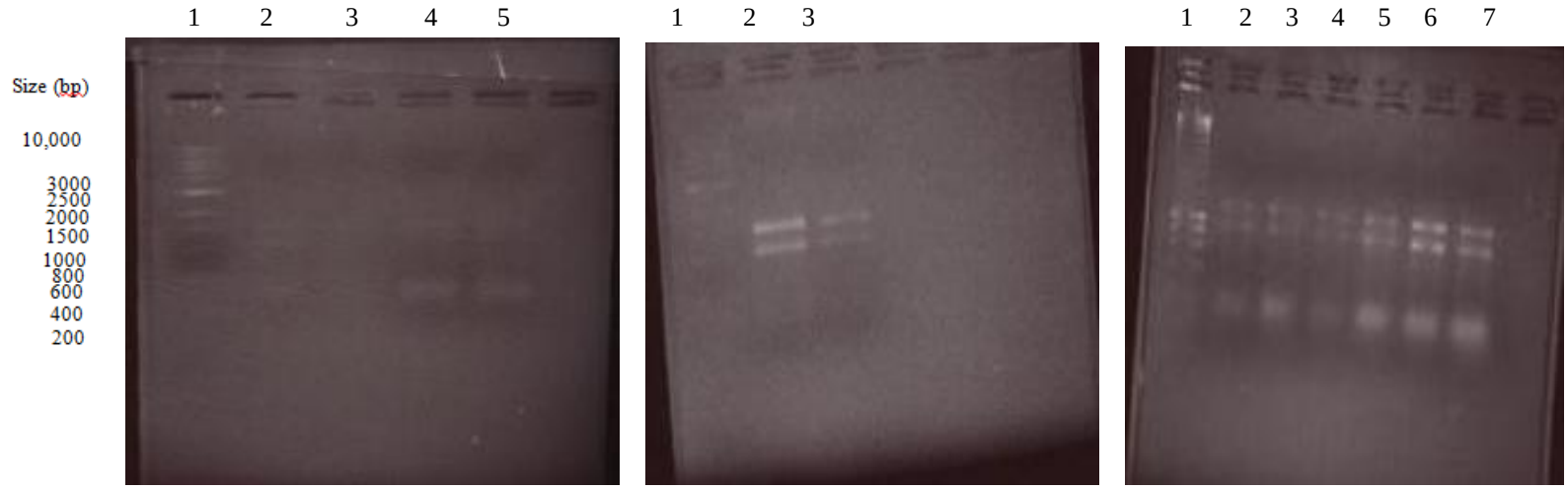


**(a)** **(b)** **(c)**

**Fig. 1:** RNA gel electrophoresis using various RNA extraction methods (a) Qiagen RNeasy® minikit (b) Qiagen RNeasy® minikit and RNAprotect bacteria reagent and (c) Tri Reagent

(a) Lane 1; Molecular weight marker, Lane 2; Untreated *S. aureus* cells, Lane 3; $AgNO_3$ treated cells, Lane 4; Duplicate of untreated *S. aureus* cells and Lane 5; Duplicate of $AgNO_3$ treated cells (b) Lane 1; Molecular weight marker, Lane 2; Untreated *S. aureus* cells and Lane 3; $AgNO_3$ treated *S. aureus* cells (c) Lane 1; Molecular weight marker, Lane 2-4; Untreated *S. aureus* cells and Lanes 5-7; $AgNO_3$ treated *S. aureus* cells

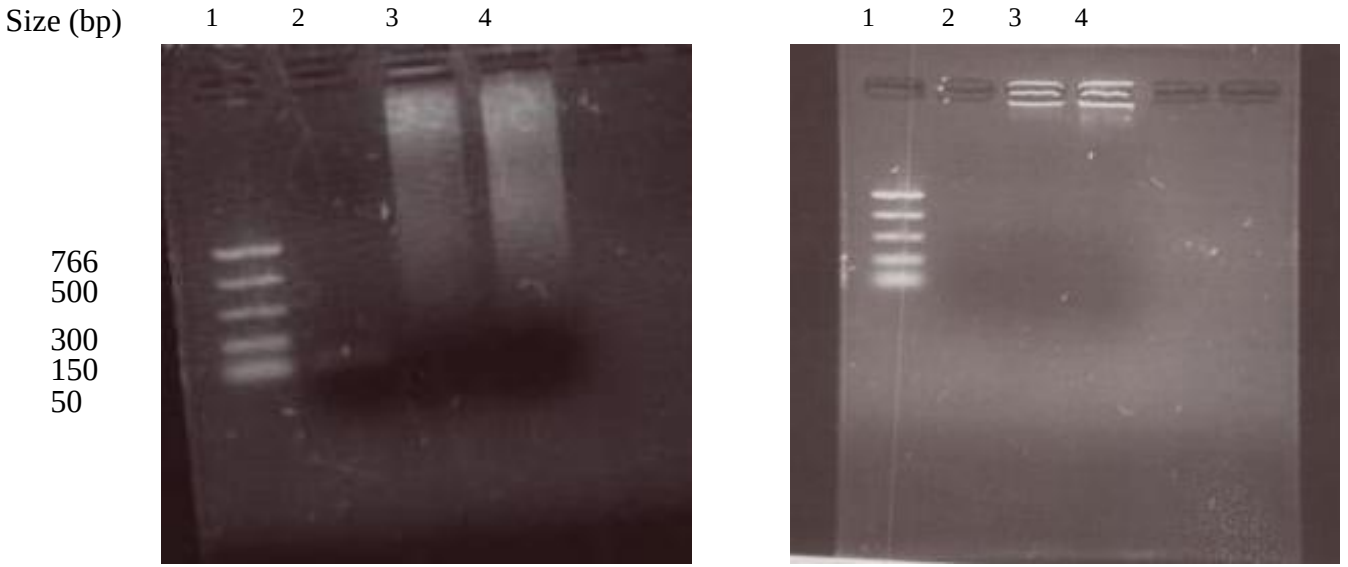


**Fig. 2:** PCR product visualisation of (a) gyrA primer set and (b) SodA primer set.

(a) Lane 1; Molecular weight marker, Lane 2; Blank, Lane 3; Untreated *S. aureus* cells and Lane 4; $AgNO_3$ treated cells and (b) Lane 1; Molecular weight marker, Lane 2; Blank, Lane 3; Untreated *S. aureus* cells and Lane 4; $AgNO_3$ treated cells

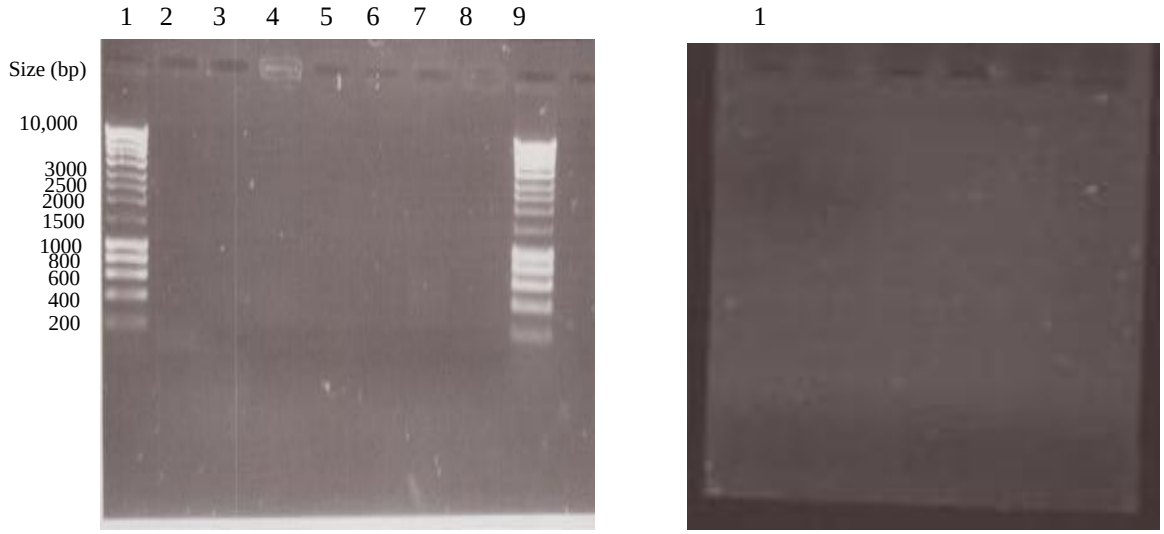


**Fig. 3:** Image depicting (a) PCR product using genomic DNA and (b) cDNA on a 1% agarose gel

(a) Lane 1 and 9; Molecular weight marker, Lanes 2-4; Untreated *S. aureus* cells and Lanes 5-7; $AgNO_3$ treated *S. aureus* cells and (b) Lane 1; cDNA

# Appendix V: Glycolysis

## Energy Investment Phase

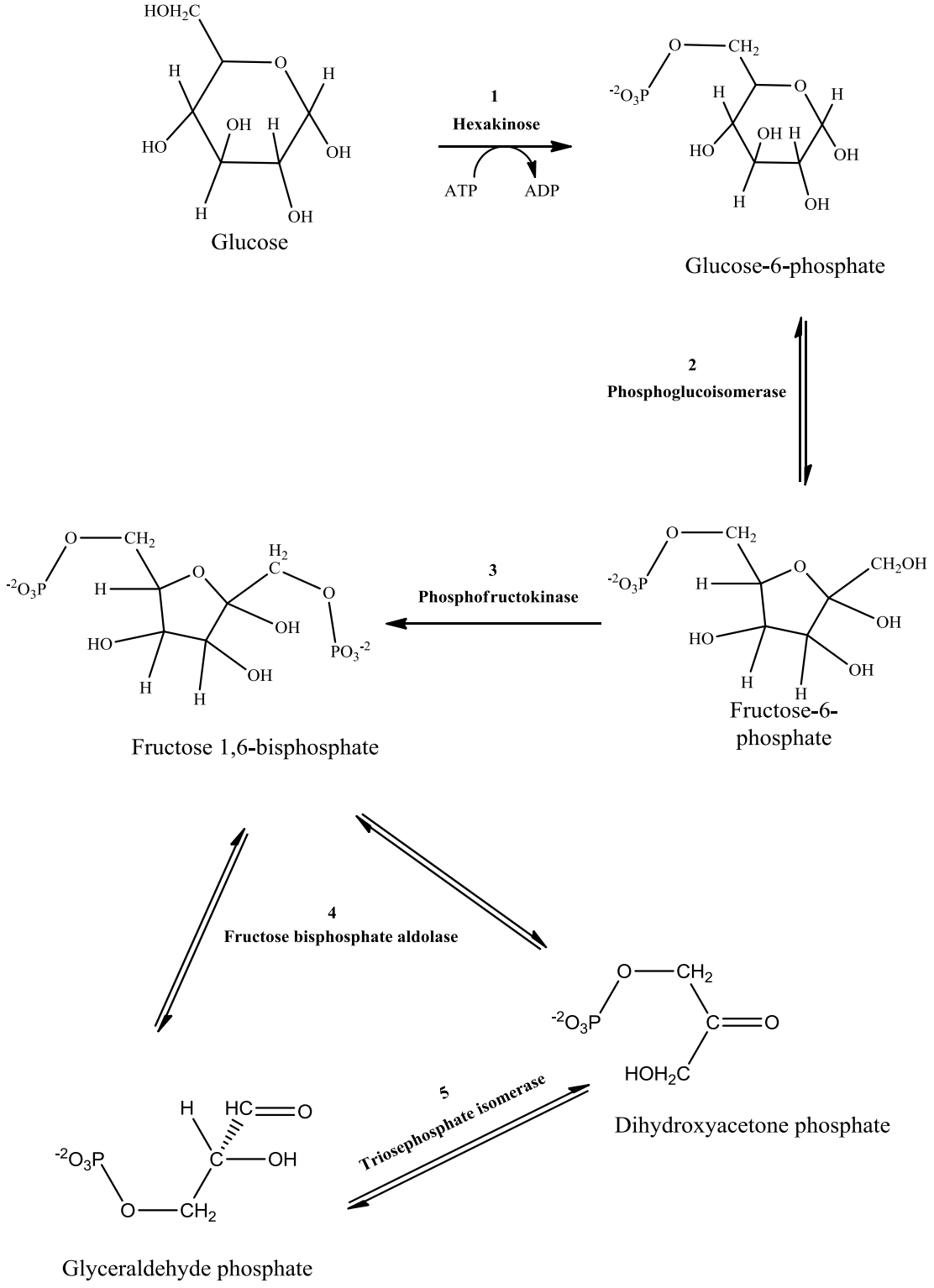

## Energy Pay-off Phase

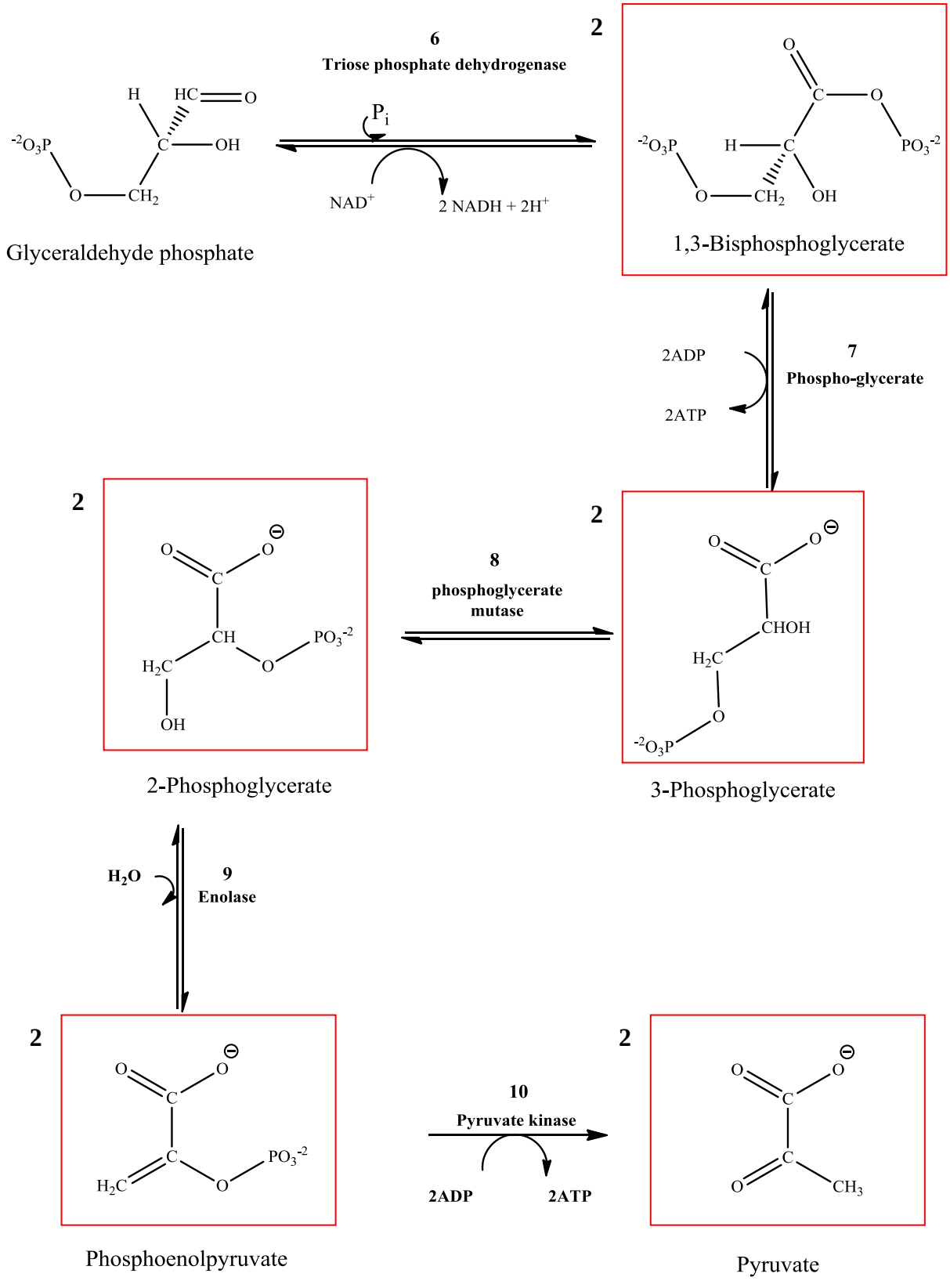

| | |
|---|---|
| ATP – Adenosine triphosphate | $P_i$ – Inorganic phosphate $H_2PO_4$ |
| ADP – Adenosine diphosphate | $NAD^+$ – Nicotinamide adenine dinucleotide |
| GTP – Guanine triphosphate | ⇌ Reversible |
| GDP – Guanine diphosphate | → Irreversible |

# Appendix VI: Tricarboxylic Acid Cycle

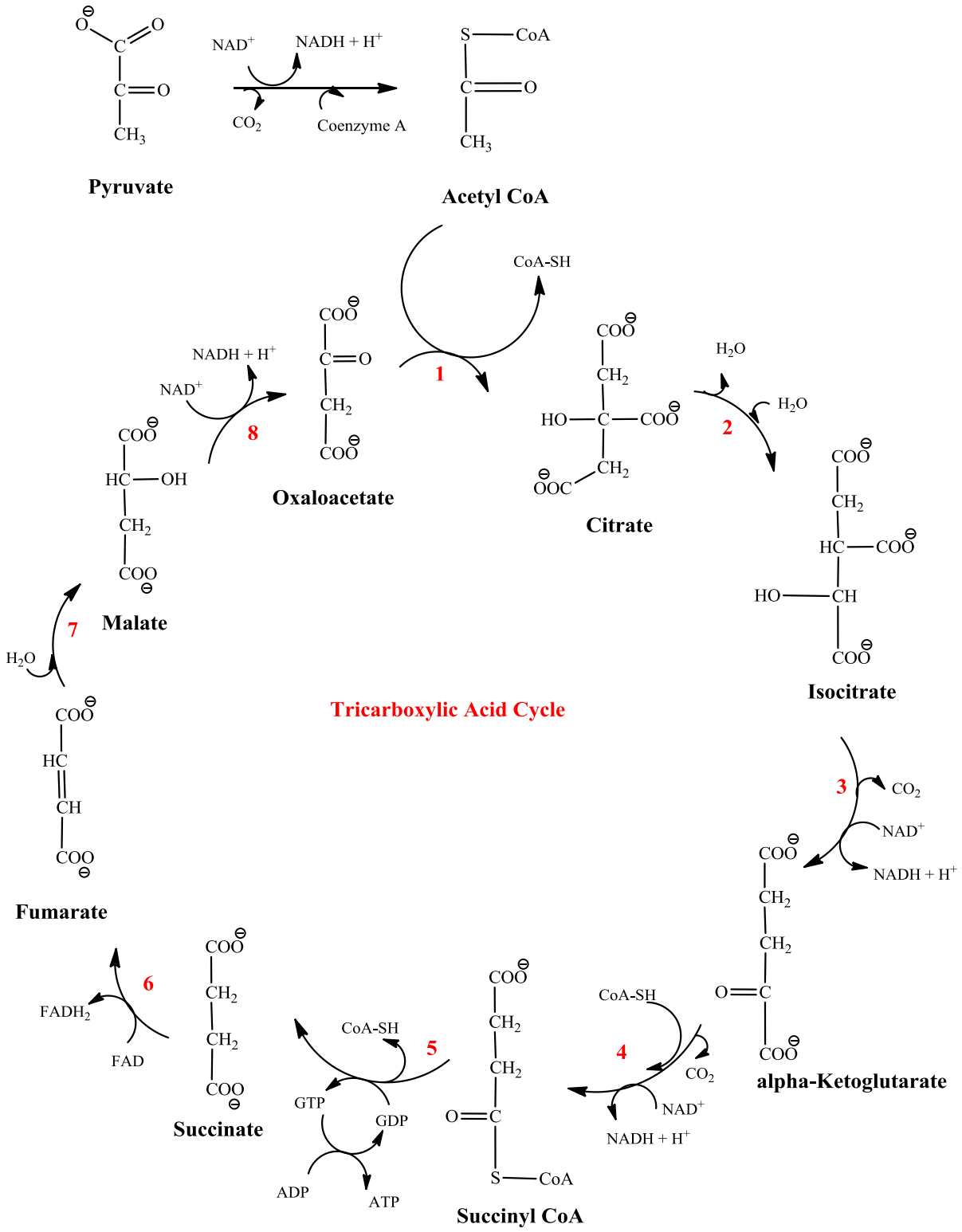

## Overview of Cellular Respiration

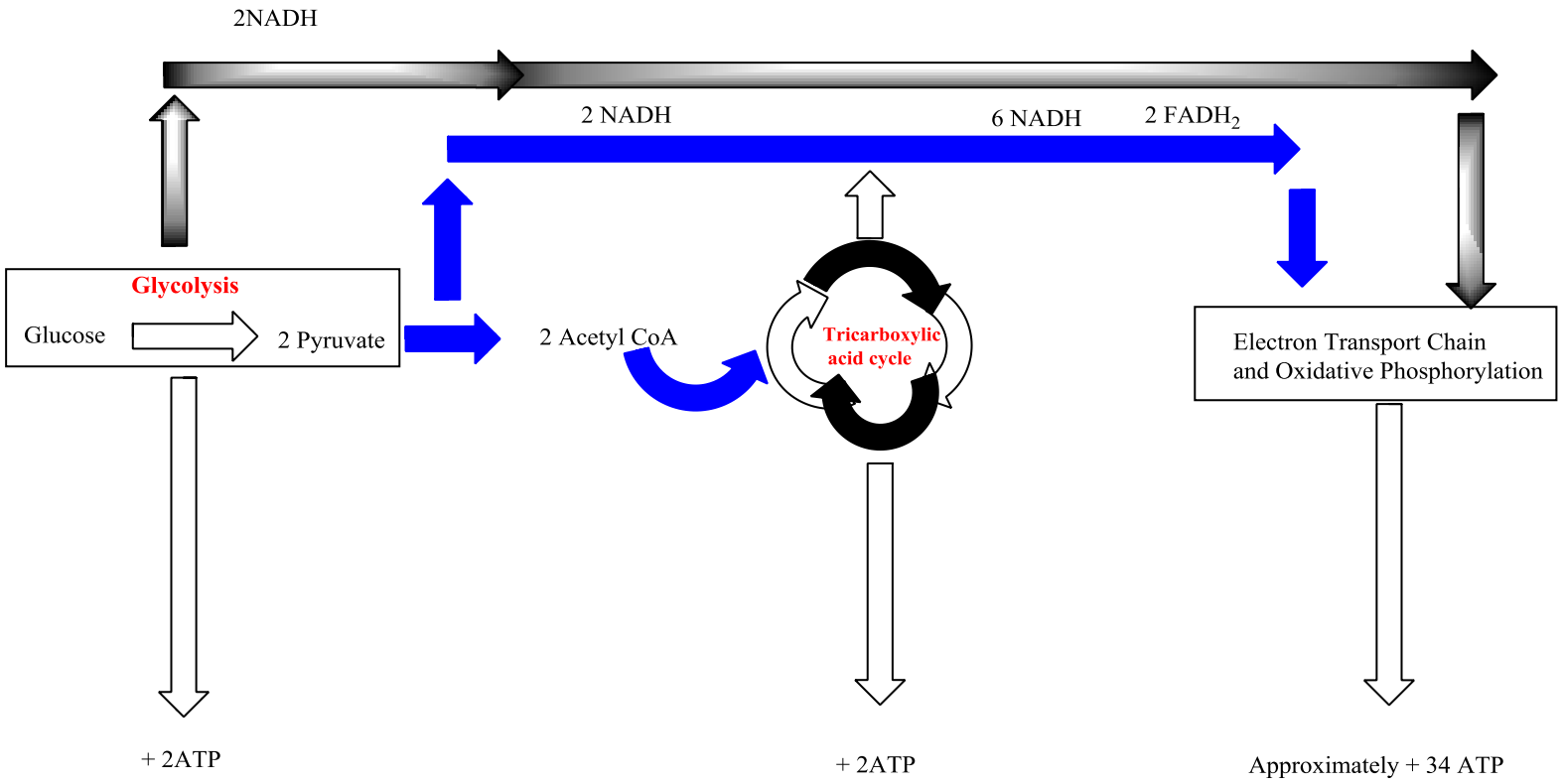

## References


(1) Lansdown, A. B. G. *Silver in Healthcare: Its Antimicrobial Efficacy and Safety in Use*; Royal Society of Chemistry, **2010**.
(2) King, B. R.; *Encyclopedia of inorganic chemistry*; 2nd Edition ed.; John Wiley and Sons: **2005**.
(3) Greenwood, N. N.; Earnshaw, A. In *Chemistry of the Elements*; Pergamon Press Ltd.: Great Britain, **1984**.
(4) Wilberg, N.; Holleman, A. F. *Inorganic Chemistry*; illustrated ed., **2001**.
(5) http://www.mii.org/Minerals/photosilver.html Date accessed, 15/09/2011.
(6) Cotton, F. A.; Wilkinson, G.; *Advanced inorganic chemistry*; 5th Edition ed.; John Wiley and Sons: **1988**.
(7) Xie, J.; Lee, J. Y.; Wang, D. I. C.; Ting, Y. P. Silver nanoplates: From biological to biomimetic synthesis; *Acs Nano* **2007**, *1*, 429.
(8) Johnston, H. J.; Hutchison, G.; Christensen, F. M.; Peters, S.; Hankin, S.; Stone, V. A review of the in vivo and in vitro toxicity of silver and gold particulates: Particle attributes and biological mechanisms responsible for the observed toxicity; *Critical Reviews in Toxicology* **2010**, *40*, 328.
(9) Pulit, J.; Banach, M.; Kowalski, Z. Nanosilver- Making difficult decisions; *Ecological Chemistry and Engineering S-Chemia I Inzynieria Ekologiczna S* **2011**, *18*, 185.
(10) Ahamed, M.; AlSalhi, M. S.; Siddiqui, M. K. J. Silver nanoparticle applications and human health; *Clinica Chimica Acta* **2010**, *411*, 1841.
(11) Wijnhoven, S. W. P.; Peijnenburg, W. J. G. M.; Herberts, C. A.; Hagens, W. I.; Oomen, A. G.; Heugens, E. H. W.; Roszek, B.; Bisschops, J.; Gosens, I.; Van de Meent, D.; Dekkers, S.; De Jong, W. H.; Van Zijverden, M.; Sips, A. J. A. M.; Geertsma, R. E. Nano-silver - a review of available data and knowledge gaps in human and environmental risk assessment; *Nanotoxicology* **2009**, *3*, 109.
(12) Marambio-Jones, C.; Hoek, E. M. V. A review of the antibacterial effects of silver nanomaterials and potential implications for human health and the environment; *Journal of Nanoparticle Research* **2010**, *12*, 1531.
(13) Ravindran, A.; Singh, A.; Raichur, A. M.; Chandrasekaran, N.; Mukherjee, A. Studies on interaction of colloidal Ag nanoparticles with Bovine Serum Albumin (BSA); *Colloids and Surfaces B: Biointerfaces* **2010**, *76*, 32.
(14) Rai, M.; Yadav, A.; Gade, A. Silver nanoparticles as a new generation of antimicrobials; *Biotechnology Advances* **2009**, *27*, 76.
(15) Silver, S. Bacterial silver resistance: molecular biology and uses and misuses of silver compounds; *Fems Microbiology Reviews* **2003**, *27*, 341.
(16) Lansdown, A. B. G. Critical observations on the neurotoxicity of silver; *Critical Reviews in Toxicology* **2007**, *37*, 237.
(17) Wan, A. T.; Conyers, R. A. J.; Coombs, C. J.; Masterton, J. P. Determination of silver in blood, urine and tissues of volunteers and burn patients; *Clinical Chemistry* **1991**, *37*, 1683.
(18) Lansdown, A. B. G. Silver in health care: antimicrobial effects and safety in use; *Current problems in dermatology* **2006**, *33*, 17.

(19)Lansdown, A. B. G. A pharmacological and toxicological profile of silver as an antimicrobial agent in medical devices; *Advances in pharmacological sciences* **2010**, *2010*, 910686.
(20)Leaper, D. J. Silver dressings: their role in wound management; *International wound journal* **2006**, *3*, 282.
(21)Slawson, R. M.; Lee, H.; Trevors, J. T. Bacterial interactions with silver; *Biology of Metals* **1990**, *3*, 151.
(22)Lansdown, A. B. G. Silver. I: Its antibacterial properties and mechanism of action; *Journal Wound Care* **2002**, *11*, 125.
(23)Wells, T. N. C.; Scully, P.; Paravicini, G.; Proudfoot, A. E. I.; Payton, M. A. Mechanism of irreversible inactivation of phosphomannose isomerases by silver ions and flamazine *Biochemistry* **1995**, *34*, 7896.
(24) Atiyeh, B. S.; Costagliola, M.; Hayek, S. N.; Dibo, S. A. Effect of silver on burn wound infection control and healing: Review of the literature; *Burns* **2007**, *33*, 139.
(25) Schaller, U. C.; Klauss, V. Is Crede's prophylaxis for ophthalmia neonatorum still valid?; *Bulletin of the World Health Organization* **2001**, *79*, 262.
(26) Klasen, H. J. A historical review of the use of silver in the treatment of burns. II. Renewed interest for silver; *Burns* **2000**, *26*, 131.
(27) Castellano, J. J.; Shafii, S. M.; Ko, F.; Donate, G.; Wright, T. E.; Mannari, R. J.; Payne, W. G.; Smith, D. J.; Robson, M. C. Comparative evaluation of silver-containing antimicrobial dressings and drugs; *International Wound Journal* **2007**, *4*, 114.
(28) Lansdown; G, A. B. *Silver in Healthcare It's Antimicrobial Efficacy and Safety in Use*; The Royal Society of Chemistry **2010**; Vol. Issues in Toxicology No 6.
(29) Fox, C. L.; Modak, S. M. Mechanism of silver sulfadiazine action on burn wound infections; *Antimicrobial Agents and Chemotherapy* **1974**, *5*, 582.
(30) Silver, S.; Phung, L. T.; Silver, G. Silver as biocides in burn and wound dressings and bacterial resistance to silver compounds; *Journal of Industrial Microbiology & Biotechnology* **2006**, *33*, 627.
(31) Wright, J. B.; Lam, K.; Burrell, R. E. Wound management in an era of increasing bacterial antibiotic resistance: A role for topical silver treatment; *American Journal of Infection Control* **1998**, *26*, 572.
(32) Melaiye, A.; Youngs, W. J. Silver and its application as an antimicrobial agent; *Expert Opinion on Therapeutic Patents* **2005**, *15*, 125.
(33) Fung, M. C.; Bowen, D. L. Silver products for medical indications: Risk-benefit assessment; *Journal of Toxicology-Clinical Toxicology* **1996**, *34*, 119.
(34) Kwon, H. B.; Lee, J. H.; Lee, S. H.; Lee, A. Y.; Choi, J. S.; Ahn, Y. S. A case of argyria following colloidal silver ingestion; *Annals of Dermatology* **2009**, *21*, 308.
(35) White, J. M. L.; Powell, A. M.; Brady, K.; Russell-Jones, R. Severe generalized argyria secondary to ingestion of colloidal silver protein; *Clinical and Experimental Dermatology* **2003**, *28*, 254.
(36)Jacobs, R. Argyria: my life story; *Clinics in Dermatology* **2006**, *24*, 66.
(37)Cloete, T. E. Resistance mechanisms of bacteria to antimicrobial compounds; *International Biodeterioration & Biodegradation* **2003**, *51*, 277.
(38)Neu, H. C. The crisis in antibiotic-resistance; *Science* **1992**, *257*, 1064.

(39)McHugh, G. L.; Moellering, R. C.; Hopkins, C. C.; Swartz, M. N. *Salmonella typhimurium* resistant to silver nitrate, chloramphenicol, and ampicillin - new threat in burns units; *Lancet* **1975**, *1*, 235.
(40)Woods, E. J.; Cochrane, C. A.; Percival, S. L. Prevalence of silver resistance genes in bacteria isolated from human and horse wounds; *Veterinary Microbiology* **2009**, *138*, 325.
(41)Percival, S. L.; Bowler, P. G.; Russell, D. Bacterial resistance to silver in wound care; *Journal of Hospital Infection* **2005**, *60*, 1.
(42)Chopra, I. The increasing use of silver-based products as antimicrobial agents: a useful development or a cause for concern?; *Journal of Antimicrobial Chemotherapy* **2007**, *59*, 587.
(43)Gupta, A.; Phung, L. T.; Taylor, D. E.; Silver, S. Diversity of silver resistance genes in IncH incompatibility group plasmids; *Microbiology-Sgm* **2001**, *147*, 3393.
(44)Silver, S.; Gupta, A.; Matsui, K.; Lo, J.-F. Resistance to Ag(I) cations in bacteria: Environments, genes and proteins; *Metal-Based Drugs* **1999**, *6*, 315.
(45)Gupta, A.; Silver, S. Molecular genetics - Silver as a biocide: Will resistance become a problem?; *Nature Biotechnology* **1998**, *16*, 888.
(46)Gupta, A.; Matsui, K.; Lo, J. F.; Silver, S. Molecular basis for resistance to silver cations in Salmonella; *Nature Medicine* **1999**, *5*, 183.
(47)Nies, D. H. Efflux-mediated heavy metal resistance in prokaryotes; *Fems Microbiology Reviews* **2003**, *27*, 313.
(48)Solioz, M.; Odermatt, A. Copper and silver transport by CopB-ATPase in membrane-vesicles of *Enterococcus hirae*; *Journal of Biological Chemistry* **1995**, *270*, 9217.
(49)Peppas, N. A.; Bures, P.; Leobandung, W.; Ichikawa, H. Hydrogels in pharmaceutical formulations; *European Journal of Pharmaceutics and Biopharmaceutics* **2000**, *50*, 27.
(50)Ganji, F.; Vasheghani-Farahani, E. Hydrogels in controlled drug delivery systems; *Iranian Polymer Journal* **2009**, *18*, 63.
(51)Allan S, H. Hydrogels for biomedical applications; *Advanced Drug Delivery Reviews* **2002**, *54*, 3.
(52)Nair, L. S.; Laurencin, C. T. Biodegradable polymers as biomaterials; *Progress in Polymer Science* **2007**, *32*, 762.
(53)Slaughter, B. V.; Khurshid, S. S.; Fisher, O. Z.; Khademhosseini, A.; Peppas, N. A. Hydrogels in regenerative medicine; *Advanced Materials* **2009**, *21*, 3307.
(54)Mano, J. F.; Silva, G. A.; Azevedo, H. S.; Malafaya, P. B.; Sousa, R. A.; Silva, S. S.; Boesel, L. F.; Oliveira, J. M.; Santos, T. C.; Marques, A. P.; Neves, N. M.; Reis, R. L. Natural origin biodegradable systems in tissue engineering and regenerative medicine: present status and some moving trends; *Journal of the Royal Society Interface* **2007**, *4*, 999.
(55)Berger, J.; Reist, M.; Mayer, J. M.; Felt, O.; Peppas, N. A.; Gurny, R. Structure and interactions in covalently and ionically crosslinked chitosan hydrogels for biomedical applications; *European Journal of Pharmaceutics and Biopharmaceutics* **2004**, *57*, 19.
(56)Omidian, H.; Park, K. Swelling agents and devices in oral drug delivery; *Journal of Drug Delivery Science and Technology* **2008**, *18*, 83.

(57)Peppas, N. A.; Hilt, J. Z.; Khademhosseini, A.; Langer, R. Hydrogels in biology and medicine: From molecular principles to bionanotechnology; *Advanced Materials* **2006**, *18*, 1345.
(58)Duarte, A. P.; Coelho, J. F.; Bordado, J. C.; Cidade, M. T.; Gil, M. H. Surgical adhesives: Systematic review of the main types and development forecast; *Progress in Polymer Science* **2012**, *37*, 1031.
(59) Spotnitz, W. D.; Burks, S. Hemostats, sealants, and adhesives II: update as well as how and when to use the components of the surgical toolbox; *Clinical and Applied Thrombosis-Hemostasis* **2010**, *16*, 497.
(60)Doraiswamy, N. V.; Baig, H.; Hammett, S.; Hutton, M. Which tissue adhesive for wounds; *Injury-International Journal of the Care of the Injured* **2003**, *34*, 564.
(61)Paez, J. M. G.; Herrero, E. J.; Rocha, A.; Maestro, M.; Castillo-Olivares, J. L. Comparative study of the mechanical behaviour of a cyanoacrylate and a bioadhesive; *Journal of Materials Science-Materials in Medicine* **2004**, *15*, 109.
(62)Thompson, D. F.; Davis, T. W. The addition of antibiotics to fibrin glue; *Southern Medical Journal* **1997**, *90*, 681.
(63)Ryou, M.; Thompson, C. C. Tissue Adhesives: A Review; *Techniques in Gastrointestinal Endoscopy* **2006**, *8*, 33.
(64)De Somer, F.; Delanghe, J.; Somers, P.; Debrouwere, M.; Van Nooten, G. Mechanical and chemical characteristics of an autologous glue; *Journal of Biomedical Materials Research Part A* **2008**, *86A*, 1106.
(65)Bruns, T. B.; Worthington, J. M. Using tissue adhesive for wound repair: A practical guide to Dermabond; *American Family Physician* **2000**, *61*, 1383.
(66) Reece, T. B.; Maxey, T. S.; Kron, I. L. A prospectus on tissue adhesives; *American Journal of Surgery* **2001**, *182*, 40S.
(67)Hidas, G.; Kastin, A.; Mullerad, M.; Shental, J.; Moskovitz, B.; Nativ, O. Sutureless nephron-sparing surgery: Use of albumin glutaraldehyde tissue adhesive (BioGlue); *Urology* **2006**, *67*, 697.
(68)de la Portilla, F.; Rada, R.; Leon, E.; Cisneros, N.; Hugo Maldonado, V.; Espinosa, E. Evaluation of the use of BioGlue (R) in the treatment of high anal fistulas: Preliminary results of a pilot study; *Diseases of the Colon & Rectum* **2007**, *50*, 218.
(69)Passage, J.; Jalah, H.; Tam, R. K. W.; Harrocks, S.; O'Brien, M. F. BioGlue surgical adhesive - An appraisal of its indications in cardiac surgery; *Annals of Thoracic Surgery* **2002**, *74*, 432.
(70)Van Belleghem, Y.; Forsyth, R. G.; Narine, K.; Moerman, A.; Taeymans, Y.; Van Nooten, G. J. Bovine glue (BioGlue) is catabolized by enzymatic reaction in the vascular dog model; *Annals of Thoracic Surgery* **2004**, *77*, 2177.
(71)Campbell, N.; Reece, J.; Mitchell, L. *Biology*; Jim Green, **1999**.
(72)Patrick, G. L.; *An Introduction to Medicinal Chemistry*; Second Edition ed.; Oxford University Press: **2001**.
(73)Brown, T. A.; *Genomes*, 2nd edition ed.; Oxford: Wiley-Liss: **2002**.
(74) Friedli, G.-L., PhD Thesis; Interaction of deamidated soluble wheat protein (SWP) with other foods and metals.University of Surrey, **1996**.
(75)Wu, L.-Z.; Ma, B.-L.; Zou, D.-W.; Tie, Z.-X.; Wang, J.; Wang, W. Influence of metal ions on folding pathway and conformational stability of bovine serum albumin; *Journal of Molecular Structure* **2008**, *877*, 44.

(76) Stewart, A. J.; Blindauer, C. A.; Berezenko, S.; Sleep, D.; Tooth, D.; Sadler, P. J. Role of Tyr84 in controlling the reactivity of Cys34 of human albumin; *Febs Journal* **2005**, *272*, 353.
(77) Sokolowska, M.; Pawlas, K.; Bal, W. Effect of common buffers and heterocyclic ligands on the binding of Cu(II) at the multimetal binding site in human serum albumin; *Bioinorganic Chemistry and Applications* **2010**, *2010*, 1.
(78) Sadler, P. J.; Tucker, A. Proton NMR-studies of bovine serum albumin - assignment of spin systems; *European Journal of Biochemistry* **1992**, *205*, 631.
(79) Sadler, P. J.; Tucker, A.; Viles, J. H. Involvement of a lysine residue in the N-terminal $Ni^{2+}$ and $Cu^{2+}$ binding site of serum albumins comparison with $Co^{2+}$, $Cd^{2+}$ and $Al^{3+}$; *European Journal of Biochemistry* **1994**, *220*, 193.
(80) Ghuman, J.; Zunszain, P. A.; Petitpas, I.; Bhattacharya, A. A.; Otagiri, M.; Curry, S. Structural basis of the drug-binding specificity of human serum albumin; *Journal of Molecular Biology* **2005**, *353*, 38.
(81) Curry, S.; Mandelkow, H.; Brick, P.; Franks, N. Crystal structure of human serum albumin complexed with fatty acid reveals an asymmetric distribution of binding sites; *Nature Structural Biology* **1998**, *5*, 827.
(82) Vetri, V.; Librizzi, F.; Leone, M.; Militello, V. Thermal aggregation of bovine serum albumin at different pH: comparison with human serum albumin; *European Biophysics Journal with Biophysics Letters* **2007**, *36*, 717.
(83) Roche, M.; Rondeau, P.; Singh, N. R.; Tarnus, E.; Bourdon, E. The antioxidant properties of serum albumin; *Febs Letters* **2008**, *582*, 1783.
(84) Carter, D. C.; Ho, J. X. Structure of serum-albumin; *Advances in Protein Chemistry* **1994**, *45*, 153.
(85) Ostojic, S.; Dragutinovic, V.; Kicanovic, M.; Simonovic, B. R. A DSC study of zinc binding to bovine serum albumin (BSA); *Journal of the Serbian Chemical Society* **2007**, *72*, 331.
(86) Wetzel, R.; Becker, M.; Behlke, J.; Billwitz, H.; Bohm, S.; Ebert, B.; Hamann, H.; Krumbiegel, J.; Lassmann, G. Temperature behaviour of human-serum albumin; *European Journal of Biochemistry* **1980**, *104*, 469.
(87) Laurie, O.; Oakes, J. Thermally denatured proteins - spin label studies of reversal of thermal aggregation of bovine serum-albumin BSA; *Journal of the Chemical Society-Faraday Transactions I* **1976**, *72*, 2681.
(88) Oakes, J. Thermally denatured proteins - nuclear magnetic resonance, binding isotherm and chemical modification studies of thermally denatured bovine serum albumin; *Journal of the Chemical Society-Faraday Transactions I* **1976**, *72*, 228.
(89) Kun, R.; Szekeres, M.; Dekany, I. Isothermal titration calorimetric studies of the pH induced conformational changes of bovine serum albumin; *Journal of Thermal Analysis and Calorimetry* **2009**, *96*, 1009.
(90) Michnik, A.; Michalik, K.; Drzazga, Z. Stability of bovine serum albumin at different pH; *Journal of Thermal Analysis and Calorimetry* **2005**, *80*, 399.
(91) Sadler, P. J.; Tucker, A. pH-induced structural transitions of bovine serum albumin - histidine pKa values and unfolding of the N-terminus during N to F transition; *European Journal of Biochemistry* **1993**, *212*, 811.
(92) Fasano, M.; Curry, S.; Terreno, E.; Galliano, M.; Fanali, G.; Narciso, P.; Notari, S.; Ascenzi, P. The extraordinary ligand binding properties of human serum albumin; *Iubmb Life* **2005**, *57*, 787.

(93) Oettl, K.; Stauber, R. E. Physiological and pathological changes in the redox state of human serum albumin critically influence its binding properties; *British Journal of Pharmacology* **2007**, *151*, 580.
(94) Stewart, A. J.; Blindauer, C. A.; Berezenko, S.; Sleep, D.; Sadler, P. J. Interdomain zinc site on human albumin; *Proceedings of the National Academy of Sciences of the United States of America* **2003**, *100*, 3701.
(95) Lu, J.; Stewart, A. J.; Sadler, P. J.; Pinheiro, T. J. T.; Blindauer, C. A. Albumin as a zinc carrier: properties of its high-affinity zinc-binding site; *Biochemical Society Transactions* **2008**, *36*, 1317.
(96) Shahabadi, N.; Maghsudi, M.; Ahmadipour, Z. Study on the interaction of silver(I) complex with bovine serum albumin by spectroscopic techniques; *Spectrochimica acta. Part A, Molecular and biomolecular spectroscopy* **2012**, *92*, 184.
(97) Migneault, I.; Dartiguenave, C.; Bertrand, M. J.; Waldron, K. C. Glutaraldehyde: behavior in aqueous solution, reaction with proteins, and application to enzyme crosslinking; *Biotechniques* **2004**, *37*, 790.
(98) Russell, A. D. Gluteraldehyde - current status and uses *Infection Control and Hospital Epidemiology* **1994**, *15*, 724.
(99) Wine, Y.; Cohen-Hadar, N.; Freeman, A.; Frolow, F. Elucidation of the mechanism and end products of glutaraldehyde crosslinking reaction by X-ray structure analysis; *Biotechnology and Bioengineering* **2007**, *98*, 711.
(100) Wade, L. G. *Organic Chemistry*; 4th Edition ed.; Prentice Hall International, **1999**.
(101) LeMaire, S. A.; Ochoa, L. N.; Conklin, L. D.; Schmittling, Z. C.; Undar, A.; Clubb, F. J., Jr.; Wang, X. L.; Coselli, J. S.; Fraser, C. D., Jr. Nerve and conduction tissue injury caused by contact with BioGlue; *Journal of Surgical Research* **2007**, *143*, 286.
(102) http://www.youtube.com/watch?v=fHZw4OyT9lc, Date accessed, 20/07/2011.
(103) Raanani, E.; Latter, D. A.; Errett, L. E.; Bonneau, D. B.; Leclerc, Y.; Salasidis, G. C. Use of "BioGlue" in aortic surgical repair; *The Annals of Thoracic Surgery* **2001**, *72*, 638.
(104) LeMaire, S. A.; Schmittling, Z. C.; Coselli, J. S.; Undar, A.; Deady, B. A.; Clubb, F. J.; Fraser, C. D. BioGlue surgical adhesive impairs aortic growth and causes anastomotic strictures; *Annals of Thoracic Surgery* **2002**, *73*, 1500.
(105) Furst, W.; Banerjee, A. Release of glutaraldehyde from an albumin-glutaraldehyde tissue adhesive causes significant in vitro and in vivo toxicity; *Annals of Thoracic Surgery* **2005**, *79*, 1522.
(106) Ngaage, D. L.; Edwards, W. D.; Bell, M. R.; Sundt, T. M. A cautionary note regarding long-term sequelae of biologic glue; *Journal of Thoracic and Cardiovascular Surgery* **2005**, *129*, 937.
(107) Pasic, M.; Unbehaun, A.; Drews, T.; Hetzer, R. Late wound healing problems after use of BioGlue® for apical hemostasis during transapical aortic valve implantation; *Interactive CardioVascular and Thoracic Surgery* **2011**, *13*, 532.
(108) Elefteriades, J. "How I do it: utilization of high-pressure sealants in aortic reconstruction"; *Journal of Cardiothoracic Surgery* **2009**, *4*, 27.

(109) Yuen, T.; Kaye, A. H. Persistence of Bioglue(R) in spinal dural repair; *Journal of Clinical Neuroscience* **2005**, *12*, 100.
(110) Hewitt, C. W.; Marra, S. W.; Kann, B. R.; Tran, H. S.; Puc, M. M.; Chrzanowski, F. A.; Tran, J. L. V.; Lenz, S. D.; Cilley, J. H.; Simonetti, V. A.; DelRossi, A. J. BioGlue surgical adhesive for thoracic aortic repair during coagulopathy: Efficacy and histopathology; *Annals of Thoracic Surgery* **2001**, *71*, 1609.
(111) Gaberel, T.; Borgey, F.; Thibon, P.; Lesteven, C.; Lecoutour, X.; Emery, E. Surgical site infection associated with the use of bovine serum albumine-glutaraldehyde surgical adhesive (BioGlueA (R)) in cranial surgery: a case-control study; *Acta Neurochirurgica* **2011**, *153*, 156.
(112) http://www.accessdata.fda.gov/cdrh_docs/pdf/P010003b.pdf Date accessed, 24/09/2011.
(113) Clements, M. O.; Watson, S. P.; Foster, S. J. Characterization of the major superoxide dismutase of *Staphylococcus aureus* and its role in starvation survival, stress resistance, and pathogenicity; *Journal of Bacteriology* **1999**, *181*, 3898.
(114) http://www.clinicalwebcasts.com/pdfs/Treaht_critcare_Web.pdf Date accessed, 30/09/2011.
(115) Kirby, J. T.; Mutnick, A. H.; Jones, R. N.; Biedenbach, D. J.; Pfaller, M. A.; Grp, S. P. Geographic variations in garenoxacin (BMS284756) activity tested against pathogens associated with skin and soft tissue infections: report from the SENTRY Antimicrobial Surveillance Program (2000); *Diagnostic Microbiology and Infectious Disease* **2002**, *43*, 303.
(116) Plano, L. R. W. *Staphylococcus aureus* exfoliative toxins: How they cause disease; *Journal of Investigative Dermatology* **2004**, *122*, 1070.
(117) http://www.niaid.nih.gov/topics/antimicrobialResistance/Pages/aureusBacteria.aspx Date accessed, 29/09/2011.
(118) http://www.woundsinternational.com/article.php?articleid=8915&page=1, Date accessed, 30/09/2011.
(119) Skinner, D.; Keefer, C. S. Significance of bacteremia caused by *Staphylococcus aureus*; *Archives of Internal Medicine* **1941**, *68*, 851.
(120) Deurenberg, R. H.; Stobberingh, E. E. The evolution of *Staphylococcus aureus*; *Infection, Genetics and Evolution* **2008**, *8*, 747.
(121) García-Lara, J.; Masalha, M.; Foster, S. J. *Staphylococcus aureus*: the search for novel targets; *Drug Discovery Today* **2005**, *10*, 643.
(122) http://www.hpsc.ie/hpsc/A-Z/MicrobiologyAntimicrobialResistance/EuropeanAntimicrobialResistanceSurveillanceSystemEarss/ReferenceandEducationalResourceMaterial/SaureusMrsa/LatestSaureusMrsadata/File, Date accessed, 29/09/2011.
(123) http://www.irishpatients.ie/storage/Mrsa%20Report%20Final1.pdf Date accessed, 30/09/2011.
(124) Collins, J.; Rudkin, J.; Recker, M.; Pozzi, C.; O'Gara, J. P.; Massey, R. C. Offsetting virulence and antibiotic resistance costs by *MRSA*; *Isme Journal* **2010**, *4*, 577.
(125) Foster, T. J. Colonization and infection of the human host by staphylococci: adhesion, survival and immune evasion; *Veterinary Dermatology* **2009**, *20*, 456.

(126) Sutter, D. E.; Summers, A. M.; Keys, C. E.; Taylor, K. L.; Frasch, C. E.; Braun, L. E.; Fattom, A. I.; Bash, M. C. Capsular serotype of *Staphylococcus aureus* in the era of community-acquired *MRSA*; *Fems Immunology and Medical Microbiology* **2011**, *63*, 16.
(127) Lowy, F. D. Medical progress - *Staphylococcus aureus* infections; *New England Journal of Medicine* **1998**, *339*, 520.
(128) Joh, D.; Wann, E. R.; Kreikemeyer, B.; Speziale, P.; Hook, M. Role of fibronectin-binding MSCRAMMs in bacterial adherence and entry into mammalian cells; *Matrix Biology* **1999**, *18*, 211.
(129) Rivera, J.; Vannakambadi, G.; Hook, M.; Speziale, P. Fibrinogen-binding proteins of Gram-positive bacteria; *Thrombosis and Haemostasis* **2007**, *98*, 503.
(130) Chavakis, T.; Wiechmann, K.; Preissner, K. T.; Herrmann, M. *Staphylococcus aureus* interactions with the endothelium - The role of bacterial "Secretable Expanded Repertoire Adhesive Molecules" (SERAM) in disturbing host defense systems; *Thrombosis and Haemostasis* **2005**, *94*, 278.
(131) Pizarro-Cerda, J.; Cossart, P. Bacterial adhesion and entry into host cells; *Cell* **2006**, *124*, 715.
(132) Ozeri, V.; Rosenshine, I.; Ben-Ze'ev, A.; Bokoch, G. M.; Jou, T. S.; Hanski, E. De novo formation of focal complex-like structures in host cells by invading s*treptococci*; *Molecular Microbiology* **2001**, *41*, 561.
(133) Agerer, F.; Lux, S.; Michel, A.; Rohde, M.; Ohlsen, K.; Hauck, C. R. Cellular invasion by *Staphylococcus aureus* reveals a functional link between focal adhesion kinase and cortactin in integrin-mediated internalisation; *Journal of Cell Science* **2005**, *118*, 2189.
(134) Foster, T. J.; Hook, M. Surface protein adhesins of *Staphylococcus aureus*; *Trends in Microbiology* **1998**, *6*, 484.
(135) Kline, K. A.; Falker, S.; Dahlberg, S.; Normark, S.; Henriques-Normark, B. Bacterial Adhesins in Host-Microbe Interactions; *Cell Host & Microbe* **2009**, *5*, 580.
(136) von Eiff, C.; Becker, K.; Machka, K.; Stammer, H.; Peters, G.; Study, G. Nasal carriage as a source of *Staphylococcus aureus* bacteremia; *New England Journal of Medicine* **2001**, *344*, 11.
(137) Vandaux P; Francois P; Lew D; F, W. *Infections Associated with indwelling devices*; 3rd Edition ed.; ASM Press: Washington DC, **2000**.
(138) Iwatsuki, K.; Yamasaki, O.; Morizane, S.; Oono, T. Staphylococcal cutaneous infections: Invasion, evasion and aggression; *Journal of Dermatological Science* **2006**, *42*, 203.
(139) Kong, K. F.; Vuong, C.; Otto, M. *Staphylococcus* quorum sensing in biofilm formation and infection; *International Journal of Medical Microbiology* **2006**, *296*, 133.
(140) Fuqua, W. C.; Winans, S. C.; Greenberg, E. P. Qurum sensing in bacteria - the LuxR-LuxI family of cell density - responsive transcriptional regulators; *Journal of Bacteriology* **1994**, *176*, 269.
(141) Goerke, C.; Wolz, C. Regulatory and genomic plasticity of *Staphylococcus aureus* during persistent colonization and infection; *International Journal of Medical Microbiology* **2004**, *294*, 195.
(142) Dinges, M. M.; Orwin, P. M.; Schlievert, P. M. Exotoxins of *Staphylococcus aureus*; *Clinical Microbiology Reviews* **2000**, *13*, 16.

(143) Menestrina, G.; Dalla Serra, M.; Comai, M.; Coraiola, M.; Viero, G.; Werner, S.; Colin, D. A.; Monteil, H.; Prevost, G. Ion channels and bacterial infection: the case of beta-barrel pore-forming protein toxins of *Staphylococcus aureus*; *Febs Letters* **2003**, *552*, 54.
(144) Montoya, M.; Gouaux, E. beta-barrel membrane protein folding and structure viewed through the lens of alpha-hemolysin; *Biochimica Et Biophysica Acta-Biomembranes* **2003**, *1609*, 19.
(145) Gouaux, E.; Hobaugh, M.; Song, L. Z. alpha-Hemolysin, gamma-hemolysin, and leukocidin from *Staphylococcus aureus*: Distant in sequence but similar in structure; *Protein Science* **1997**, *6*, 2631.
(146) Boyle-Vavra, S.; Daum, R. S. Community-acquired *methicillin-resistant Staphylococcus aureus*: the role of Panton-Valentine Leukocidin; *Laboratory Investigation* **2007**, *87*, 3.
(147) Zetola, N.; Francis, J. S.; Nuermberger, E. L.; Bishai, W. R. Community-acquired *meticillin-resistant Staphylococcus aureus*: an emerging threat; *Lancet Infectious Diseases* **2005**, *5*, 275.
(148) Foster, T. J. Immune evasion by Staphylococci; *Nature Reviews Microbiology* **2005**, *3*, 948.
(149) Lo, W.-T.; Wang, C.-C. Panton-Valentine leukocidin in the pathogenesis of community-associated *methicillin-resistant Staphylococcus aureus* infection; *Pediatrics and Neonatology* **2011**, *52*, 59.
(150) Edwards-Jones, V. Toxic shock syndrome: Causes in people with burn wounds; *Wounds UK* **2006**, *2*, 66.
(151) Balaban, N.; Rasooly, A. Staphylococcal enterotoxins; *International Journal of Food Microbiology* **2000**, *61*, 1.
(152) Miller, L. S.; Cho, J. S. Immunity against *Staphylococcus aureus* cutaneous infections; *Nature Reviews Immunology* **2011**, *11*, 505.
(153) Janeway, C.; Travers, P.; Walport, M.; Shlomchik, M. *Immunobiology; the immune system in health and disease*; fourth edition ed.; Garland science publishing: New York, **2005**.
(154) Kumar, A.; Tassopoulos, A. M.; Li, Q.; Yu, F. S. X. *Staphylococcus aureus* protein A induced inflammatory response in human corneal epithelial cells; *Biochemical and Biophysical Research Communications* **2007**, *354*, 955.
(155) Backert, S.; Konig, W. Interplay of bacterial toxins with host defence: Molecular mechanisms of immunomodulatory signalling; *International Journal of Medical Microbiology* **2005**, *295*, 519.
(156) Anwar, S.; Prince, L. R.; Foster, S. J.; Whyte, M. K. B.; Sabroe, I. The rise and rise of *Staphylococcus aureus*: laughing in the face of granulocytes; *Clinical and Experimental Immunology* **2009**, *157*, 216.
(157) Fournier, B.; Philpott, D. J. Recognition of *Staphylococcus aureus* by the innate immune system; *Clinical Microbiology Reviews* **2005**, *18*, 521.
(158) Putman, M.; van Veen, H. W.; Konings, W. N. Molecular properties of bacterial multidrug transporters; *Microbiology and Molecular Biology Reviews* **2000**, *64*, 672.
(159) Hiramatsu, K.; Cui, L.; Kuroda, M.; Ito, T. The emergence and evolution of *methicillin-resistant Staphylococcus aureus*; *Trends in Microbiology* **2001**, *9*, 486.
(160) Marquez, B. Bacterial efflux systems and efflux pumps inhibitors; *Biochimie* **2005**, *87*, 1137.

(161) Kumar, A.; Schweizer, H. P. Bacterial resistance to antibiotics: Active efflux and reduced uptake; *Advanced Drug Delivery Reviews* **2005**, *57*, 1486.
(162) Wright, J. S.; Jin, R.; Novick, R. P. Transient interference with staphylococcal quorum sensing blocks abscess formation; *Proceedings of the National Academy of Sciences of the United States of America* **2005**, *102*, 1691.
(163) Gotz, F. Staphylococci in colonization and disease: prospective targets for drugs and vaccines; *Current Opinion in Microbiology* **2004**, *7*, 477.
(164) Kokai-Kun, J. F.; Walsh, S. M.; Chanturiya, T.; Mond, J. J. Lysostaphin cream eradicates *Staphylococcus aureus* nasal colonization in a cotton rat model; *Antimicrobial Agents and Chemotherapy* **2003**, *47*, 1589.
(165) Josefsson, E.; Hartford, O.; O'Brien, L.; Patti, J. M.; Foster, T. Protection against experimental *Staphylococcus aureus* arthritis by vaccination with clumping factor A, a novel virulence determinant; *Journal of Infectious Diseases* **2001**, *184*, 1572.
(166) Rivas, J. M.; Speziale, P.; Patti, J. M.; Hook, M. MSCRAMM - Targeted vaccines and immunotherapy for staphylococcal infection; *Current Opinion in Drug Discovery & Development* **2004**, *7*, 223.
(167) Nilsson, I. M.; Patti, J. M.; Bremell, T.; Hook, M.; Tarkowski, A. Vaccination with a recombinant fragment of collagen adhesin provides protection against *Staphylococcus aureus*-mediated septic death; *Journal of Clinical Investigation* **1998**, *101*, 2640.
(168) Edwards-Jones, V. Antimicrobial and barrier effects of silver against *methicillin-resistant Staphylococcus aureus*; *Journal of wound care* **2006**, *15*, 285.
(169) Rattanaruengsrikul, V.; Pimpha, N.; Supaphol, P. In vitro efficacy and toxicology evaluation of silver nanoparticle-loaded gelatin hydrogel pads as antibacterial wound dressings; *Journal of Applied Polymer Science* **2012**, *124*, 1668.
(170) Coia, J. E. Clinical, microbiological and epidemiological aspects of *Escherichia coli* O157 infection; *FEMS Immunology and Medical Microbiology* **1998**, *20*, 1.
(171) Kerr, K. G.; Snelling, A. M. *Pseudomonas aeruginosa*: a formidable and ever-present adversary; *Journal of Hospital Infection* **2009**, *73*, 338.
(172) Breidenstein, E. B. M.; de la Fuente-Nunez, C.; Hancock, R. E. W. *Pseudomonas aeruginosa*: all roads lead to resistance; *Trends in Microbiology* **2011**, *19*, 419.
(173) Rowan, R.; Moran, C.; McCann, M.; Kavanagh, K. Use of Galleria mellonella larvae to evaluate the in vivo anti-fungal activity of $[Ag_2(mal)(phen)_3]$; *Biometals* **2009**, *22*, 461.
(174) Rowan, R.; McCann, M.; Kavanagh, K. Analysis of the response of *Candida albicans* cells to Silver(I); *Medical Mycology* **2010**, *48*, 498.
(175) Kavanagh, K. *Fungi; Biology and applications* John Wiley and Sons, **2005**.
(176) Coyle, B.; Kavanagh, K.; McCann, M.; Devereux, M.; Geraghty, M. Mode of anti-fungal activity of 1,10-phenanthroline and its Cu(II), Mn(II) and Ag(I) complexes; *Biometals* **2003**, *16*, 321.
(177) McCann, M.; Coyle, B.; McKay, S.; McCormack, P.; Kavanagh, K.; Devereux, M.; McKee, V.; Kinsella, P.; O'Connor, R.; Clynes, M. Synthesis and X-ray crystal structure of $[Ag(phendio)_2]ClO_4$ (phendio=1,10-

phenanthroline-5,6-dione) and its effects on fungal and mammalian cells; *Biometals* **2004**, *17*, 635.
(178) Eshwika, A.; Coyle, B.; Devereux, M.; McCann, M.; Kavanagh, K. Metal complexes of 1,10-phenanthroline-5,6-dione alter the susceptibility of the yeast *Candida albicans* to amphotericin B and miconazole; *Biometals* **2004**, *17*, 415.
(179) Rowan, R.; Tallon, T.; Sheahan, A. M.; Curran, R.; McCann, M.; Kavanagh, K.; Devereux, M.; McKee, V. 'Silver bullets' in antimicrobial chemotherapy: Synthesis, characterisation and biological screening of some new Ag(I)-containing imidazole complexes; *Polyhedron* **2006**, *25*, 1771.
(180) Thati, B.; Noble, A.; Rowan, R.; Creaven, B. S.; Walsh, M.; McCann, M.; Egan, D.; Kavanagh, K. Mechanism of action of coumarin and silver(I)-coumarin complexes against the pathogenic yeast *Candida albicans*; *Toxicology in Vitro* **2007**, *21*, 801.
(181) Stevens, M. P. *Polymer Chemistry, An Introduction*; 2nd ed.; Oxford University Press: New York, **1990**.
(182) Stuart, P. *Polymer Analysis*; John Wiley and Sons, Ltd., **2002**.
(183) http://www.instron.co.uk/wa/glossary/Tensile-Testing.aspx, Date accessed, 13/1/2012.
(184) http://www.msm.cam.ac.uk/phase-trans/2002/Thermal2.pdf, Date accessed, 24/01/2012.
(185) http://www.colby.edu/chemistry/PChem/lab/DiffScanningCal.pdf, Date accessed, 24/01/2012.
(186) http://www.pslc.ws/mactest/level5.htm, Date accessed, 24/01/2012.
(187) Tyers, M.; Mann, M. From genomics to proteomics; *Nature* **2003**, *422*, 193.
(188) Roe, S. *Protein purification techniques: a practical approach*; Oxford University Press, 2001.
(189) Speers, A. E.; Wu, C. C. Proteomics of integral membrane proteins-theory and application; *Chemical Reviews* **2007**, *107*, 3687.
(190) http://iitb.vlab.co.in/?sub=41&brch=118&sim=375&cnt=1, Date accessed, 21.2.2012.
(191) http://www.aesociety.org/areas/pdfs/Garfin_1DE_WebArticle9-07.pdf, Date accessed, 21.2.2012.
(192) Skoog, D. A. *Fundamentals of analytical chemistry*; Thomson-Brooks/Cole, **2004**.
(193) http://www.asdlib.org/onlineArticles/ecourseware/Kelly_Potentiometry/PDF-15-Ref&AuxElec.pdf, Date accessed, 22.2.2012.
(194) Skoog, D. A.; Holler, F. J.; Nieman, T. A. *Principles of instrumental analysis*; Saunders College Pub., **1998**.
(195) Colleran, J. J., PhD thesis; Electrochemistry of the organic molecule methylene blue, Trinity College Dublin, **2007**.
(196) Southampton Electrochemistry, G. *Instrumental methods in electrochemistry*; E. Horwood, **1985**.
(197) Bard, A. J.; Faulkner, L. R. *Electrochemical methods: fundamentals and applications*; Wiley, **2001**.
(198) Perone, S. P. Application of stripping analysis to determination of silver(I) using graphite electrodes; *Analytical Chemistry* **1963**, *35*, 2091.

(199) Butler, M. F.; Clark, A. H.; Adams, S. Swelling and mechanical properties of biopolymer hydrogels containing chitosan and bovine serum albumin; *Biomacromolecules* **2006**, *7*, 2961.
(200) Liu, R.; Sun, F.; Zhang, L.; Zong, W.; Zhao, X.; Wang, L.; Wu, R.; Hao, X. Evaluation on the toxicity of nanoAg to bovine serum albumin; *Science of the Total Environment* **2009**, *407*, 4184.
(201) Foster, J. G.; Hess, J. L. Responses of superoxide dismutase and glutathione reductase activities of cotton leaf tissue exposed to an atmosphere enriched in oxygen; *Plant Physiology* **1980**, *66*, 482.
(202) Ghosh, A.; Ghosh, J. J. Release of intracellular constituents of *Candida albicans* in presence of polyene antibiotics; *Annals of biochemistry and experimental medicine* **1963**, *23*, 611.
(203) Friedman, M. Applications of the ninhydrin reaction for analysis of amino acids, peptides, and proteins to agricultural and biomedical sciences; *Journal of Agricultural and Food Chemistry* **2004**, *52*, 385.
(204) Mertz, P. M.; Cardenas, T. C. P.; Snyder, R. V.; Kinney, M. A.; Davis, S. C.; Plano, L. R. W. *Staphylococcus aureus* virulence factors associated with infected skin lesions - Influence on the local immune response; *Archives of Dermatology* **2007**, *143*, 1259.
(205) Heikens, E.; Fleer, A.; Paauw, A.; Florijn, A.; Fluit, A. C. Comparison of genotypic and phenotypic methods for species-level identification of clinical isolates of coagulase-negative staphylococci; *Journal of Clinical Microbiology* **2005**, *43*, 2286.
(206) Valderas, M. W.; Gatson, J. W.; Wreyford, N.; Hart, M. E. The superoxide dismutase gene *sodM* is unique to *Staphylococcus aureus*: Absence of *sodM* in coagulase-negative staphylococci; *Journal of Bacteriology* **2002**, *184*, 2465.
(207) Shevchenko, A.; Tomas, H.; Havlis, J.; Olsen, J. V.; Mann, M. In-gel digestion for mass spectrometric characterization of proteins and proteomes; *Nature Protocols* **2006**, *1*, 2856.
(208) Nakamoto, K. *Infrared and Raman Spectra of Inorganic and Coordination Compounds: Theory and applications in inorganic chemistry*; 6th ed.; Wiley and Sons, **2009**.
(209) Grdadolink, J.; Marechal, Y. Bovine serum albumin observed by infrared spectrometry. I. Methodology, structural investigation, and water uptake; *Biopolymers* **2001**, *62*, 40.
(210) Farahnaky, A.; Badii, F.; Farhat, I. A.; Mitchell, J. R.; Hill, S. E. Enthalpy relaxation of bovine serum albumin and implications for its storage in the glassy state; *Biopolymers* **2005**, *78*, 69.
(211) Michnik, A. Thermal stability of bovine serum albumin DSC study; *Journal of Thermal Analysis and Calorimetry* **2003**, *71*, 509.
(212) Company, C. R. *CRC Handbook of Chemistry and Physics*; CRC Press, **1978**.
(213) Logvinenko, V.; Polunina, O.; Mikhailov, Y.; Mikhailov, K.; Bokhonov, B. Study of thermal decomposition of silver acetate; *Journal of Thermal Analysis and Calorimetry* **2007**, *90*, 813.
(214) Uvarov, N. F.; Burleva, L. P.; Mizen, M. B.; Whitcomb, D. R.; Zou, C. Conductivity of long-chain silver carboxylates and their thermal decomposition products; *Solid State Ionics* **1998**, *107*, 31.
(215) http://xdb.lbl.gov, Date accessed, 16/04/2012.

(216) Tada, D.; Tanabe, T.; Tachibana, A.; Yamauchi, K. Drug release from hydrogel containing albumin as crosslinker; *Journal of Bioscience and Bioengineering* **2005**, *100*, 551.
(217) Hoare, T. R.; Kohane, D. S. Hydrogels in drug delivery: Progress and challenges; *Polymer* **2008**, *49*, 1993.
(218) Deen, G. R. Swelling behavior and metal-ion uptake capacity of pH-responsive hydrogels of poly(N-acryloyl-N'-ethylpiperazine); *Journal of Dispersion Science and Technology* **2010**, *31*, 1673.
(219) Katime, I.; Rodriguez, E. Absorption of metal ions and swelling properties of poly(acrylic acid-CO-itaconic acid) hydrogels; *Journal of Macromolecular Science-Pure and Applied Chemistry* **2001**, *38*, 543.
(220) Berchane, N. S.; Andrews, M. J.; Kerr, S.; Slater, N. K. H.; Jebrail, F. F. On the mechanical properties of bovine serum albumin (BSA) adhesives; *Journal of Materials Science-Materials in Medicine* **2008**, *19*, 1831.
(221) Lim, J.; Hong, J.; Chen, W. W.; Weerasooriya, T. Mechanical response of pig skin under dynamic tensile loading; *International Journal of Impact Engineering* **2011**, *38*, 130.
(222) Azadani, A. N.; Matthews, P. B.; Ge, L.; Shen, Y.; Jhun, C. S.; Guy, T. S.; Tseng, E. E. Mechanical properties of surgical glues used in aortic root replacement; *Annals of Thoracic Surgery* **2009**, *87*, 1154.
(223) http://emedicine.medscape.com/article/967022-overview, Date accessed, 03/04/2012.
(224) Mohan, Y. M.; Vimala, K.; Thomas, V.; Varaprasad, K.; Sreedhar, B.; Bajpai, S. K.; Raju, K. M. Controlling of silver nanoparticles structure by hydrogel networks; *Journal of Colloid and Interface Science* **2010**, *342*, 73.
(225) Sileikaite, A.; Prosycevas, I.; Puiso, J.; Juraitis, A.; Guobiene, A. Analysis of silver nanoparticles produced by chemical reduction of silver salt solution; *Materials Science (Medziagotyra)* **2006**, *12*, 287.
(226) Percival, S. L.; Slone, W.; Linton, S.; Okel, T.; Corum, L.; Thomas, J. G. The antimicrobial efficacy of a silver alginate dressing against a broad spectrum of clinically relevant wound isolates; *International Wound Journal* **2011**, *8*, 237.
(227) Tandogan, B.; Ulusu, N. N. Kinetic mechanism and molecular properties of glutathione reductase; *FABAD Journal of Pharmaceutical Sciences* **2006**, *31*, 182.
(228) Kelly, J.; Rowan, R.; McCann, M.; Kavanagh, K. Exposure to caspofungin activates Cap and Hog pathways in *Candida albicans*; *Medical Mycology* **2009**, *47*, 697.
(229) Sorci, G.; Faivre, B. Inflammation and oxidative stress in vertebrate host-parasite systems; *Philosophical Transactions of the Royal Society B-Biological Sciences* **2009**, *364*, 71.
(230) Halliwell, B.; Gutteridge, J. M. C. *Free radicals in biology and medicine*; 3rd ed.; Oxford Science Publications, **1999**.
(231) Townsend, D. M.; Tew, K. D.; Tapiero, H. The importance of glutathione in human disease; *Biomedicine & Pharmacotherapy* **2003**, *57*, 145.
(232) Cortese-Krott, M. M.; Suschek, C. V.; Wetzel, W.; Kroncke, K. D.; Kolb-Bachofen, V. Nitric oxide-mediated protection of endothelial cells from hydrogen peroxide is mediated by intracellular zinc and glutathione; *American Journal of Physiology-Cell Physiology* **2009**, *296*, C811.

(233) Wu, M.; Lin, Z. H.; Wolfbeis, O. S. Determination of the activity of catalase using a europium(III)-tetracycline-derived fluorescent substrate; *Analytical Biochemistry* **2003**, *320*, 129.
(234) Coyle, B.; McCann, M.; Kavanagh, K.; Devereux, M.; McKee, V.; Kayal, N.; Egan, D.; Deegan, C.; Finn, G. J. Synthesis, X-ray crystal structure, anti-fungal and anti-cancer activity of $[Ag_2(NH_3)_2(salH)_2]$ ($salH_2$= salicylic acid); *Journal of Inorganic Biochemistry* **2004**, *98*, 1361.
(235) Creaven, B. S.; Egan, D. A.; Kavanagh, K.; McCann, M.; Noble, A.; Thati, B.; Walsh, M. Synthesis, characterization and antimicrobial activity of a series of substituted coumarin-3-carboxylatosilver(I) complexes; *Inorganica Chimica Acta* **2006**, *359*, 3976.
(236) Clements, M. O.; Foster, S. J. Stress resistance in *Staphylococcus aureus*; *Trends in Microbiology* **1999**, *7*, 458.
(237) Cardoso, L. A.; Ferreira, S. T.; Hermes-Lima, M. Reductive inactivation of yeast glutathione reductase by Fe(II) and NADPH; *Comparative Biochemistry and Physiology - Part A: Molecular & Integrative Physiology* **2008**, *151*, 313.
(238) Karavolos, M. H.; Horsburgh, M. J.; Ingham, E.; Foster, S. J. Role and regulation of the superoxide dismutases of *Staphylococcus aureus*; *Microbiology-Sgm* **2003**, *149*, 2749.
(239) Tomkins, K., PhD thesis; A molecular and proteomic investigation of the *in vitro* and *in vivo* anti-microbial efficacy of novel silver(I)-coumarin compounds. Institute of Technology, Tallaght, **2011**.
(240) Ballal, A.; Manna, A. C. Regulation of Superoxide Dismutase (*sod*) Genes by SarA in *Staphylococcus aureus*; *Journal of Bacteriology* **2009**, *191*, 3301.
(241) Sissons, C. H.; Hancock, E. M.; Perinpanayagam, H. E. R.; Cutress, T. W. A procedure for urease and protein extraction from staphylococci; *Journal of Applied Bacteriology* **1989**, *67*, 433.
(242) http://textbookofbacteriology.net/themicrobialworld/Structure.html, Date accessed, 30/01/2012.
(243) Sohail, M. A simple and rapid method for preparing genomic DNA from Gram-positive bacteria; *Molecular Biotechnology* **1998**, *10*, 191.
(244) Wang, S.; Kool, E. T. Origins of the large differences in stability of DNA and RNA helixes: C-5 methyl and 2'-hydroxyl effects; *Biochemistry* **1995**, *34*, 4125.
(245) Takayama, K.; Kjelleberg, S. A. The role of RNA stability during bacterial stress responses and starvation; *Environmental Microbiology* **2000**, *2*, 355.
(246) Reeves, E. P.; Murphy, T.; Daly, P.; Kavanagh, K. Amphotericin B enhances the synthesis and release of the immunosuppressive agent gliotoxin from the pulmonary pathogen *Aspergillus fumigatus*; *Journal of Medical Microbiology* **2004**, *53*, 719.
(247) Mirzajani, F.; Ghassempour, A.; Aliahmadi, A.; Esmaeili, M. A. Antibacterial effect of silver nanoparticles on *Staphylococcus aureus*; *Research in Microbiology* **2011**, *162*, 542.
(248) Li, W. R.; Xie, X. B.; Shi, Q. S.; Zeng, H. Y.; Ou-Yang, Y. S.; Chen, Y. B. Antibacterial activity and mechanism of silver nanoparticles on *Escherichia coli*; *Applied Microbiology and Biotechnology* **2010**, *85*, 1115.

(249) Kim, K. J.; Sung, W. S.; Suh, B. K.; Moon, S. K.; Choi, J. S.; Kim, J.; Lee, D. G. Antifungal activity and mode of action of silver nano-particles on *Candida albicans*; *Biometals* **2009**, *22*, 235.
(250) Cozzone, A. J. Regulation of acetate metabolism by protein phosphorylation in enteric bacteria; *Annual Review of Microbiology* **1998**, *52*, 127.
(251) Przybyla-Zawislak, B.; Dennis, R. A.; Zakharkin, S. O.; McCammon, M. T. Genes of succinyl-CoA ligase from *Saccharomyces cerevisiae*; *European Journal of Biochemistry* **1998**, *258*, 736.
(252) Commichau, F. M.; Rothe, F. M.; Herzberg, C.; Wagner, E.; Hellwig, D.; Lehnik-Habrink, M.; Hammer, E.; Voelker, U.; Stuelke, J. Novel activities of glycolytic enzymes in *Bacillus subtilis*; *Molecular & Cellular Proteomics* **2009**, *8*, 1350.
(253) Sigdel, T. K.; Cilliers, R.; Gursahaney, P. R.; Thompson, P.; Easton, J. A.; Crowder, M. W. Probing the adaptive response of *Escherichia coli* to extracellular Zn(II); *Biometals* **2006**, *19*, 461.
(254) Jedrzejas, M. J. Structure, function, and evolution of phosphoglycerate mutases: comparison with fructose-2,6-bisphosphatase, acid phosphatase, and alkaline phosphatase; *Progress in Biophysics & Molecular Biology* **2000**, *73*, 263.
(255) Bernardo, K.; Pakulat, N.; Fleer, S.; Schnaith, A.; Utermohlen, O.; Krut, O.; Muller, S.; Kronke, M. Subinhibitory concentrations of linezolid reduce *Staphylococcus aureus* virulence factor expression; *Antimicrobial Agents and Chemotherapy* **2004**, *48*, 546.
(256) Balaban, N.; Goldkorn, T.; Nhan, R. T.; Dang, L. B.; Scott, S.; Ridgley, R. M.; Rasooly, A.; Wright, S. C.; Larrick, J. W.; Rasooly, R.; Carlson, J. R. Autoinducer of virulence as a target for vaccine and therapy against *Staphylococcus aureus*; *Science* **1998**, *280*, 438.
(257) Balaban, N.; Goldkorn, T.; Gov, Y.; Hirshberg, M.; Koyfman, N.; Matthews, H. R.; Nhan, R. T.; Singh, B.; Uziel, O. Regulation of *Staphylococcus aureus* pathogenesis via target of RNAIII-activating protein (TRAP); *Journal of Biological Chemistry* **2001**, *276*, 2658.
(258) Korem, M.; Gov, Y.; Kiran, M. D.; Balaban, N. Transcriptional profiling of target of RNAIII-activating protein, a master regulator of staphylococcal virulence; *Infection and Immunity* **2005**, *73*, 6220.
(259) Ezraty, B.; Aussel, L.; Barras, F. Methionine sulfoxide reductases in prokaryotes; *Biochimica Et Biophysica Acta-Proteins and Proteomics* **2005**, *1703*, 221.
(260) Moskovitz, J. Roles of methionine suldfoxide reductases in antioxidant defense, protein regulation and survival; *Current Pharmaceutical Design* **2005**, *11*, 1451.
(261) Singh, V. K.; Jayaswal, R. K.; Wilkinson, B. J. Cell wall-active antibiotic induced proteins of *Staphylococcus aureus* identified using a proteomic approach; *Fems Microbiology Letters* **2001**, *199*, 79.
(262) Berisio, R.; Ruggiero, A.; Vitagliano, L. Elongation factors EFIA and EF-Tu: Their role in translation and beyond; *Israel Journal of Chemistry* **2010**, *50*, 71.
(263) Abel, K.; Jurnak, F. A complex profile of protein elongation: Translating chemical energy into molecular movement; *Structure* **1996**, *4*, 229.

(264) Andersen, G. R.; Nissen, P.; Nyborg, J. Elongation factors in protein biosynthesis; *Trends in Biochemical Sciences* **2003**, *28*, 434.
(265) Gao, Y.-G.; Selmer, M.; Dunham, C. M.; Weixlbaumer, A.; Kelley, A. C.; Ramakrishnan, V. The structure of the ribosome with elongation factor G trapped in the posttranslocational state; *Science* **2009**, *326*, 694.
(266) Kaakoush, N. O.; Raftery, M.; Mendz, G. L. Molecular responses of *Campylobacter jejuni* to cadmium stress; *FEBS Journal* **2008**, *275*, 5021.
(267) Berry, A.; Marshall, K. E. Identification of zinc-binding ligands in the class-II fructose-1,6-bisphosphate aldolase of *Escherichia coli*; *Febs Letters* **1993**, *318*, 11.
(268) Wierenga, R. K. The TIM-barrel fold: a versatile framework for efficient enzymes; *Febs Letters* **2001**, *492*, 193.
(269) de Kok, A.; Hengeveld, A. F.; Martin, A.; Westphal, A. H. The pyruvate dehydrogenase multi-enzyme complex from Gram-negative bacteria; *Biochimica et Biophysica Acta (BBA) - Protein Structure and Molecular Enzymology* **1998**, *1385*, 353.
(270) Smolle, M.; Prior, A. E.; Brown, A. E.; Cooper, A.; Byron, O.; Lindsay, J. G. A new level of architectural complexity in the human pyruvate dehydrogenase complex; *Journal of Biological Chemistry* **2006**, *281*, 19772.
(271) Kelly, J.; Kavanagh, K. Proteomic analysis of proteins released from growth-arrested *Candida albicans* following exposure to caspofungin; *Medical Mycology* **2010**, *48*, 598.
(272) Yin, Z.; Stead, D.; Walker, J.; Selway, L.; Smith, D. A.; Brown, A. J. P.; Quinn, J. A proteomic analysis of the salt, cadmium and peroxide stress responses in *Candida albicans* and the role of the Hog1 stress-activated MAPK in regulating the stress-induced proteome; *Proteomics* **2009**, *9*, 4686.
(273) Sykes, M. T.; Williamson, J. R. A complex assembly landscape for the 30S ribosomal subunit: *Annual Review of Biophysics*, **2009**, *38*, 197.
(274) Simonetti, A.; Marzi, S.; Jenner, L.; Myasnikov, A.; Romby, P.; Yusupova, G.; Klaholz, B. P.; Yusupov, M. A structural view of translation initiation in bacteria; *Cellular and Molecular Life Sciences* **2009**, *66*, 423.
(275) Rees, D. C.; Johnson, E.; Lewinson, O. ABC transporters: the power to change; *Nature Reviews Molecular Cell Biology* **2009**, *10*, 218.
(276) Linton, K. J. Structure and function of ABC transporters; *Physiology* **2007**, *22*, 122.
(277) Lubelski, J.; Konings, W. N.; Driessen, A. J. M. Distribution and physiology of ABC-Type transporters contributing to multidrug resistance in bacteria; *Microbiology and Molecular Biology Reviews* **2007**, *71*, 463.
(278) Borst, P.; Elferink, R. O. Mammalian ABC transporters in health and disease; *Annual Review of Biochemistry* **2002**, *71*, 537.
(279) Gorke, B.; Stulke, J. Carbon catabolite repression in bacteria: many ways to make the most out of nutrients; *Nature reviews. Microbiology* **2008**, *6*, 613.
(280) Singh, K. D.; Schmalisch, M. H.; Stulke, J.; Gorke, B. Carbon catabolite repression in *Bacillus subtilis*: quantitative analysis of repression exerted by different carbon sources; *Journal of Bacteriology* **2008**, *190*, 7275.
(281) Jenal, U.; Hengge-Aronis, R. Regulation by proteolysis in bacterial cells; *Current Opinion in Microbiology* **2003**, *6*, 163.

(282) Jain, R.; Chan, M. K. Support for a potential role of *E. coli* oligopeptidase A in protein degradation; *Biochemical and Biophysical Research Communications* **2007**, *359*, 486.
(283) Ingmer, H.; Brondsted, L. Proteases in bacterial pathogenesis; *Research in Microbiology* **2009**, *160*, 704.
(284) Voyich, J. M.; Musser, J. M.; DeLeo, F. R. Streptococcus pyogenes and human neutrophils: a paradigm for evasion of innate host defense by bacterial pathogens; *Microbes and Infection* **2004**, *6*, 1117.